DFT-Studien zum mechanistischen Verständnis und zur rationalen Entwicklung homogenkatalytischer Reaktionen

vom Fachbereich Chemie der Technischen Universität Kaiserslautern zur Verleihung des akademischen Grades 'Doktor der Naturwissenschaften' genehmigte

DISSERTATION

D 386

vorgelegt von

Dipl.-Chem. Andreas Fromm

angefertigt im Arbeitskreis von

Prof. Dr. Lukas J. Gooßen

Kaiserslautern, 2015

Datum der wissenschaftlichen Aussprache: 16.01.2015

Die vorliegende Arbeit wurde im Zeitraum von Juli 2008 bis November 2014 im Arbeitskreis von Prof. Dr. Lukas J. Gooßen am Fachbereich Chemie der Technischen Universität Kaiserslautern angefertigt.

Promotionskommission

Vorsitzender:	Prof. Dr. Werner R. Thiel
Berichterstatter:	Prof. Dr. Lukas J. Gooßen
Berichterstatter:	Prof. Dr. Christoph van Wüllen

Datum der wissenschaftlichen Aussprache: 16.01.2015

Eidesstattliche Erklärung

Hiermit versichere ich, dass ich die vorliegende Arbeit eigenständig verfasst und keine anderen als die angegebenen Quellen und Hilfsmittel verwendet, sowie Literaturzitate kenntlich gemacht habe. Kooperationsprojekte sind ausdrücklich als solche gekennzeichnet und die Mitarbeiter genannt. Die Arbeit liegt weder in gleicher noch in ähnlicher Form in einem anderen Prüfungsverfahren vor.

Kaiserslautern, den 20.01.2015

A. Fromm

Andreas Fromm

Mein herzlicher Dank gebührt Herrn Prof. Dr. Lukas J. Gooßen für die Aufnahme in seinen Arbeitskreis, die interessanten und abwechslungsreichen Aufgabenstellungen, die großen Freiräume bei der Bearbeitung der Themen und das entgegengebrachte Vertrauen.

Herrn Prof. Dr. Christoph van Wüllen danke ich für seine stete Diskussionsbereitschaft und die vielen hilfreichen Ratschläge zu DFT-Rechnungen und Gaussian, für die großzügige Bereitstellung von Rechenkapazitäten auf seinen Linux-Clustern sowie für das Erstellen des Zweitgutachtens.

Herrn Prof. Dr. Werner R. Thiel danke ich für seine Hilfe bei DFT-Rechnungen, für die Bereitstellung von Liganden und für die Übernahme des Prüfungsvorsitzes.

Weiter gilt mein Dank allen aktuellen und ehemaligen Mitarbeitern des Arbeitskreises Gooßen. Ich danke Dr. Ana Alcalde, Dr. Matthias Arndt, Sabrina Baader, Roman Bauer, Bilguun Bayarmagnai, Dr. Sukalyan Bhadra, Agostino Biafora, Dr. Mathieu Blanchot, Annette Buba, Dr. Florence Collet, Dr. Filipe Costa, Dr. Grégory Danoun, Dr. Wojciech Dzik, Benjamin Erb, Benjamin Exner, Thomas Fett, Dr. Matthias Grünberg, Dagmar Hackenberger, Dr. Liangbin Huang, Leopoldo Schöller Izquierda, Fan Jia, Dr. Kevin Jouvin, Dr. Dmitry Katayev, Christian Kerner, Prof. Dr. Bilal Khan, Dr. Thomas Knauber, Prof. Dr. Debasis Koley, Thilo Krause, Dr. Paul Lange, Dr. Christophe Linder, Dr. Patrizia Mamone, Christian Matheis, Julian Menges, Dr. Dominik Ohlmann, Dr. Christoph Oppel, Kai Pfister, Patricia Podsiadly, Eugen Risto, Prof. Dr. Nuria Rodriguez, Dr. Felix Rudolphi, Martin Rudzki, Dr. Kifah Salih, Nicolas Servely, Dr. Bingrui Song, Dr. Corneliu Stanciu, Jie Tang, Dr. Stefano Tartaggia, Stefania Trita, Dr. Minyan Wang, Philip Weber, Timo Wendling und Dr. Bettina Zimmermann für die gute Arbeitsatmosphäre und die Unterstützung in allen Phasen meiner Arbeit. Besonders hervorheben möchte ich Matthias Arndt, Annette Buba, Dagmar Hackenberger, Christian Kerner, Patrizia Mamone, Martin Rudzki und Bettina Zimmermann, die mir in dieser Zeit zu guten Freunden geworden sind.

Meinen Koautoren Prof. Dr. Dr. Gereon Niedner-Schatteburg, Prof. Dr. Christoph van Wüllen, Dr. Matthias Arndt, Dr. Matthias Grünberg, Dagmar Hackenberger, Prof. Dr. Bilal Khan, Dr. Paul Lange, Dr. Christophe Linder, Dr. Patrizia Mamone, Dr. Fabian Menges, Prof. Dr. Nuria Rodriguez und Dr. Kifah Salih danke ich für die angenehme und produktive Zusammenarbeit bei den gemeinsamen Kooperationsprojekten.

Den Mitarbeitern des Arbeitskreises van Wüllen, insbesondere Dr. Markus Mang, sowie den Mitarbeitern des Regionalen Hochschulrechenzentrums Kaiserslautern Dr. Tonnis Pool und Hans-Josef Schummer danke ich für ihre stete Hilfsbereitschaft bei allen Problemen mit den Linux-Clustern und mit Gaussian.

Den Mitarbeitern des RHRK Claudia Baltes, Thomas Esselen, Andreas Forster, Ralph Hagl, Ralf Hellriegel, Dr. Markus Hillenbrand, Christian Krick, Heiko Krupp, Maurice Massar, Nils Meurisch, Thorsten Michels, Christian Müller, Henri Schmidt und Philipp Zimmer danke ich für ihre Unterstützung beim Lösen von Computerproblemen aller Art.

Den Sekretärinnen der organischen Chemie und des Dekanats Edit Müller, Susanne Zeigner und Heike Schramm danke ich für ihre Hilfe bei allen organisatorischen Angelegenheiten.

Dr. Marc Prosenc, Matthias Tombers und Carolin Braun danke ich für die Organisation diverser Veranstaltungen im Rahmen des Transregio-Sonderforschungsbereichs SFB/TRR 88 “3MET”.

Dem Jungchemikerforum, der Jongliergruppe des Hochschulsports, der Fachschaft Mathematik und der DLRG Ortsgruppe Kaiserslautern danke ich für schöne Gestaltung verschiedenster Aktivitäten.

Für finanzielle Unterstützung danke ich der Stipendienstiftung des Landes Rheinland-Pfalz, der Deutschen Forschungsgemeinschaft (GO 853/5-2), dem Transregio-Sonderforschungsbereich SFB/TRR 88 “3MET”, dem Landesforschungszentrum OPTIMAS, dem Forschungsschwerpunkt NanoKat, der Gesellschaft Deutscher Chemiker e. V. sowie den Unternehmen Saltigo GmbH, Umicore AG & Co. KG und Mettler-Toledo GmbH.

Dr. Käthe Gooßen danke ich für das Korrekturlesen von Manuskripten sowie Matthias Ernst und Dagmar Hackenberger für das Korrekturlesen dieser Arbeit.

Meiner Familie, vor allem meinen Eltern Ulrike und Klaus, meiner Schwester Christine und meinen Paten Manfred und Jürgen sowie all meinen Freunden, insbesondere Matthias Ernst, Andreas Gebhard, Christian Rieder und Marcus Weber, danke ich sehr herzlich für ihre Unterstützung und ihren Rückhalt während meiner gesamten Promotion.

Veröffentlichungen

Einige Ergebnisse dieser Arbeit wurden bereits in folgenden Publikationen veröffentlicht:

5. A. Fromm, C. van Wüllen, D. Hackenberger, L. J. Gooßen, *J. Am. Chem. Soc.* **2014**, *136*, 10007−10023: *Mechanism of Cu/Pd-Catalyzed Decarboxylative Cross-Couplings: A DFT Investigation*.

4. P. Mamone, M. F. Grünberg, A. Fromm, B. A. Khan, L. J. Gooßen, *Org. Lett.* **2012**, *14*, 3716−3719: *[Pd(μ-Br)(P^tBu_3)]$_2$ as a Highly Active Isomerization Catalyst: Synthesis of Enol Esters from Allylic Esters*.

3. M. Arndt, K. S. M. Salih, A. Fromm, L. J. Goossen, F. Menges, G. Niedner-Schatteburg, *J. Am. Chem. Soc.* **2011**, *133*, 7428−7449: *Mechanistic Investigation of the Ru-Catalyzed Hydroamidation of Terminal Alkynes*.

2. L. J. Gooßen, N. Rodríguez, C. Linder, P. P. Lange, A. Fromm, *ChemCatChem* **2010**, *2*, 430−442: *Comparative Study of Copper- and Silver-Catalyzed Protodecarboxylations of Carboxylic Acids*.

1. L. J. Gooßen, C. Linder, N. Rodríguez, P. P. Lange, A. Fromm, *Chem. Commun.* **2009**, 7173−7175: *Silver-Catalysed Protodecarboxylation of Carboxylic Acids*.

Nummerierung der Verbindungen und Strukturen

Die große Anzahl der in dieser Arbeit bezeichneten Verbindungen und Strukturen, vor allem die der Intermediate in Katalysezyklen, erschwert eine durchgehende Nummerierung, die dem Leser dienen soll, die Verbindungen und Strukturen aus Schemata eindeutig und übersichtlich zuzuordnen. Deshalb erfolgt die Nummerierung der Verbindungen und Strukturen für jedes Kapitel separat.

Die Bezeichnung setzt sich hierbei aus der Nummer des Kapitels der zweiten Gliederungsebene gefolgt von einem Bindestrich und einer fortlaufenden Nummer zusammen, beispielsweise **3.1-1** für Verbindung **1** in Kapitel 3.1. Daher kommt es vor, dass eine Verbindung in verschiedenen Kapiteln unterschiedliche Nummern trägt. Zum Beispiel besitzt Kohlendioxid in Kapitel 3.1 die Nummer **3.1-5** und in Kapitel 3.2 die Nummer **3.2-3**.

Struktur der Dissertation

Die vorliegende Dissertation umfasst vier große Themengebiete, die Kupfer- und Silber-katalysierte Protodecarboxylierung von Carbonsäuren, die Kupfer/Palladium-katalysierte decarboxylierende Kreuzkupplung, die Ruthenium-katalysierte Hydroamidierung terminaler Alkine sowie die Palladium-katalysierte Synthese von Enolestern aus Allylestern.

Die kumulative Dissertation enthält fünf englische Originaltexte eigener wissenschaftlicher Veröffentlichungen, deren Inhalt in kurzen deutschsprachigen Passagen wiedergegeben wird. Bei den gemeinsam bearbeiteten Kooperationsprojekten wird die Aufgabenverteilung unter den einzelnen Koautoren jeweils ausführlich dargelegt.

Die auf Seite i im Kapitel Veröffentlichungen aufgelisteten Publikationen werden in dieser Arbeit mit *ChemComm*, *ChemCatChem*, *JACS* 2011, *OrgLett* und *JACS* 2014 bezeichnet.

Auf einen Anhang wird bei dieser Dissertation verzichtet. Alle Daten sind in den entsprechenden 'supporting informations' zu den jeweiligen Publikationen zu finden:

ChemComm	http://www.rsc.org/suppdata/cc/b9/b912509d/b912509d.pdf
ChemCatChem	http://onlinelibrary.wiley.com/doi/10.1002/cctc.200900277/suppinfo
JACS 2011	http://pubs.acs.org/doi/suppl/10.1021/ja111389r
OrgLett	http://pubs.acs.org/doi/suppl/10.1021/ol301563g
JACS 2014	http://pubs.acs.org/doi/suppl/10.1021/ja503295x

Abkürzungsverzeichnis

B3LYP	Dichtefunktional: Becke 3-Parameter (Austausch), Lee, Yang und Parr (Korrelation)
BLYP	Dichtefunktional: Becke (Austausch), Lee, Yang und Parr (Korrelation)
BVWN	Dichtefunktional: Becke (Austausch), Vosko, Wilk und Nusair (Korrelation)
CC	Coupled cluster
CID	Collision-induced dissociation
cod	1,5-Cyclooctadien
COSMO	Conductor-like screening solvation model
COSY	Correlation spectroscopy
CPCM	Conductor-like polarizable continuum model
CPU	Central processing unit
dcypm	Bis-(dicyclohexylphosphino)-methan
DFT	Dichtefunktionaltheorie
DMAP	4-(Dimethylamino)-pyridin
DOI	Digital object identifier
ECP	Effective core potential
ESI	Electrospray ionization
G2	Gaussian-2 Molekülsatz
GGA	Generalized gradient approximation
HF	Hartree-Fock
HK	Hohenberg-Kohn
HMQC	Heteronuclear multiple-quantum correlation
IR	Infrarot
IRC	Intrinsic reaction coordinate
Kat	Katalysator
KS	Kohn-Sham
LDA	Local density approximation
LNE	Largest negative error
LPE	Largest positive error
MAD	Mean absolute deviation
met	Methallyl
MO	Molekülorbital

MPI	Message passing interface
MP*n*	Møller-Plesset Störungstheorie *n*-ter Ordnung
MS	Mass spectrometry
NMP	*N*-Methyl-2-pyrrolidon
NMR	Nuclear magnetic resonance
PES	Potential energy surface
QCI	Quadratic configuration interaction
SCF	Self-consistent field
SD	Standard deviation
SLYP	Dichtefunktional: Slater (Austausch), Lee, Yang und Parr (Korrelation)
SMP	Symmetric multiprocessing
SPE	Single point energy
STQN	Synchronous transit-guided quasi-Newton
SVWN	Dichtefunktional: Slater (Austausch), Vosko, Wilk und Nusair (Korrelation)
Tf	Triflyl
TOF	Turnover frequency
TON	Turnover number

Inhaltsverzeichnis

1 Einleitung

1.1 Methodenentwicklung in der organischen Chemie

Die Methodenentwicklung, welche in der organischen Chemie seit jeher eine Schlüsseldisziplin darstellt, verfolgt hauptsächlich zwei Ziele. Zum einen versucht sie, neue Reaktionswege zu bisher unzugänglichen Zielverbindungen zu erschließen, zum anderen Synthesen von bekannten Produkten zu verbessern.[1] Letzteres kann durch die Entwicklung alternativer Syntheserouten ausgehend von anderen Ausgangsstoffen oder durch die Steigerung der Effizienz bestehender Prozesse geschehen.[2–5]

Auf diese Weise werden immer mehr Zielverbindungen in wenigeren und sichereren Schritten, in höheren Ausbeuten mit geringerer Abfallproduktion verfügbar. Dabei gehen die Synthesen von breit verfügbaren Basischemikalien und zunehmend auch von nachwachsenden Rohstoffen aus. Es stellt sich nun die Frage, ob es eine Möglichkeit gibt, wie die hohen Anforderungen an chemische Reaktionen, wie funktionelle Gruppentoleranz, hohe Selektivität, Nachhaltigkeit durch Vermeidung von Neben- und Abfallprodukten sowie hohe Wirtschaftlichkeit, erfüllt werden können. Ein Ansatzpunkt, um diese Frage zu beantworten, ist der Einsatz der Katalyse in der Methodenentwicklung in der organischen Chemie.[6,7]

1.2 Katalyse

Nachdem Davy 1817 erstmalig einen katalytischen Vorgang beschrieb[8] und Berzelius 1835 den Begriff der Katalyse einführte,[9] definierte Ostwald 1894 einen Katalysator:[10] „Somit ist ein Katalysator ein Stoff, welcher die Geschwindigkeit einer chemischen Reaktion ändert, ohne seinerseits in den Endprodukten dieser Reaktion zu erscheinen.“ Der Katalysator ändert folglich nicht die Lage des chemischen Gleichgewichts, sondern nur die Geschwindigkeit seiner Einstellung.

Ein Katalysator vermittelt eine chemische Reaktion, indem er die Eduktmoleküle nacheinander zu den Produktmolekülen umsetzt. Dabei durchläuft der Katalysator bei jeder Umsetzung einen Zyklus, aus dem er jeweils unverändert hervorgeht und somit selbst nicht verbraucht wird. Eine wichtige Kennzahl eines Katalysators ist das Verhältnis aus Stoffmenge an Produkt, die pro Stoffmenge an Katalysator erzeugt werden kann, welches als katalytische Produktivität (engl. 'turnover number', TON) bezeichnet wird. Eine weitere bedeutende

Kenngröße ist die Anzahl der Umsetzungen pro Zeiteinheit, welche Wechselzahl (engl. 'turnover frequency', TOF) genannt wird und ein Maß für die katalytische Effizienz darstellt.

Im Vergleich zur unkatalysierten Reaktion eröffnet der Einsatz von Katalysatoren alternative Reaktionspfade. Dies hat zwei Konsequenzen. Zum einen können mit Katalysator andere Produkte aus denselben Edukten gebildet werden als ohne Katalysator, oder die Produktselektivität einer Reaktion kann geändert werden. Zum anderen sind die Aktivierungsbarrieren eines alternativen Reaktionspfades meist niedriger, was zu höheren 'turnover frequencies' und damit höheren Reaktionsgeschwindigkeiten führt.[11] Somit können meist auch unreaktivere Reaktanden eingesetzt werden, was ohne Katalysator oft nicht möglich ist, oder die Reaktionstemperatur kann reduziert werden.

Das Gebiet der Katalyse lässt sich in die drei Teilgebiete homogene Katalyse,[12] heterogene Katalyse[13,14] und Biokatalyse[15–17] unterteilen. Bei der homogenen Katalyse befinden sich Edukte und Katalysator in derselben Phase, meist im flüssigen Medium. Wichtige Unterklassen sind die Übergangsmetallkatalyse,[18] bei welcher durch Liganden koordinierte Übergangsmetalle den Katalysator darstellen und die Organokatalyse,[19,20] bei welcher der Katalysator ein kleines, metallfreies organisches Molekül ist. Bei der heterogenen Katalyse befinden sich Edukte und Katalysator in unterschiedlichen Phasen. In der Regel handelt es sich um einen Festphasenkatalysator an dem die Edukte in flüssiger oder gasförmiger Phase reagieren, häufig bei höheren Temperaturen und Drücken. In der Biokatalyse stellen Enzyme den Katalysator dar. Oft besteht dieser aus Proteinen und setzt die Edukte in wässriger Lösung um.

Die große Bedeutung der Katalyse zeigt sich durch die Vergabe etlicher Nobelpreise auf diesem Gebiet. Für seine Pionierarbeiten zur Katalyse wurde Ostwald 1909 der Nobelpreis für Chemie verliehen.[21] Weitere Erfinder katalytischer Reaktionen wurden ebenfalls mit dem Nobelpreis für Chemie geehrt, darunter Ziegler und Natta 1963 für Polymerisations-katalysatoren,[22] Fischer und Wilkinson 1973 für sogenannte Sandwich-Katalysatoren,[23] Knowles, Noyori und Sharpless 2001 für enantioselektive Katalysen,[24] Chauvin, Grubbs und Schrock 2005 für Metathesekatalysatoren[25] sowie Heck, Negishi und Suzuki 2010 für Palladium-katalysierte Kreuzkupplungsreaktionen (Schema 1).[26]

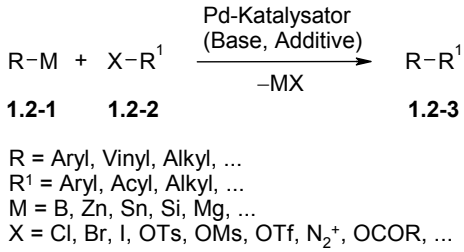

Schema 1. *Palladium-katalysierte Kreuzkupplungsreaktionen*.

Die enorme Relevanz der Katalyse zeigt sich weiterhin durch die vielfältige Anwendung katalytischer Prozesse in industriellem Maßstab. Heutzutage wird bei schätzungsweise 80–90% der großindustriellen Synthesen in mindestens einem Reaktionsschritt ein Katalysator eingesetzt.[27–29] Die Tendenz dabei ist steigend. Jährlich werden Produkte im Wert von mehr als 400 Mrd. Euro unter dem Einsatz von Katalysatoren hergestellt (Stand 2008).[12] Dabei beträgt das ständig wachsende jährliche Marktvolumen der Katalysatoren ca. 25 Mrd. Euro.[30] Die bedeutendsten katalytischen Verfahren sind die Synthese von Ammoniak aus den Elementen (Haber-Bosch-Verfahren, 1913), die Oxidation von Ammoniak zu Stickstoffmonoxid (Ostwald-Verfahren, 1915), die Kraftstofferzeugung aus Kohlenmonoxid und Wasserstoff (Fischer-Tropsch-Synthese, 1938), die Polymersynthese (Ziegler-Natta-Verfahren, 1955), die Acetaldehydsynthese durch Oxidation von Ethylen (Wacker-Verfahren, 1960) und die Synthese höhere Alkene (SHOP-Prozess, 1977).[31]

In den letzten Jahrzehnten wurden etliche katalytische Reaktionen entwickelt, um nicht nur Basischemikalien, sondern auch komplexe chemische Verbindungen aufzubauen,[32–35] darunter pharmakologische Wirkstoffe, Pflanzenschutzmittel, Duft- und Aromastoffe sowie andere Feinchemikalien. Die Entwicklung neuer katalytischer Transformationen ist jedoch alles andere als trivial, da die Reaktionsmechanismen komplexer katalytischer Reaktionen oft wenig verstanden sind, so dass Erklärungen und Vorhersagen von Reaktionsergebnissen meist schwierig sind. Häufig existieren mehrere vernetzte Katalysezyklen mit ähnlichen Aktivierungsbarrieren, so dass geringe Änderungen der Reaktionsbedingungen zu großen Änderungen der Reaktionsverläufe führen.[36] Es stellt sich somit die Frage, ob es eine Möglichkeit für eine zielgerichtete Methodenentwicklung in der organischen Chemie gibt. Die Antwort auf diese Frage ist die rationale Katalysatorentwicklung mit Hilfe von DFT-Rechnungen.

1.3 Rationale Katalysatorentwicklung mit Hilfe von DFT-Rechnungen

Die rationale Katalysatorentwicklung unter Einsatz von DFT-Rechnungen stellt eine attraktive Alternative zur klassischen Katalysatorentwicklung mit Hilfe des sogenannten Katalysatorscreenings dar. Beim Screening werden verschiedene Reaktionsparameter nacheinander systematisch variiert, bis die optimalen Reaktionsbedingungen gefunden sind. Speziell im Bereich der Übergangsmetallkatalyse ist dieses Vorgehen aufgrund der großen Anzahl an Metallen, Liganden und Additive sehr erfolgreich.[37] Es lässt sich jedoch nur dann effektiv anwenden, wenn alle benötigten Chemikalien verfügbar und nur einfache Arbeitstechniken erforderlich sind. Müssen beispielsweise die Startmaterialien synthetisiert und viele Lösungsmittel getrocknet werden und muss beispielsweise unter Luft- und Feuchtigkeitsausschluss gearbeitet werden, so führt dies zu einem erhöhten Zeit- und Arbeitsaufwand. Speziell, wenn für jedes einzelne Screening-Experiment ein maßgeschneiderter Ligand synthetisiert werden muss, bricht die Effektivität des Screenings drastisch ein. Daher ist als Alternative zum Screening eine rationale Katalysatorentwicklung von großer Bedeutung.[38]

Die rationale Entwicklung neuer, katalytischer Synthesemethoden lässt sich mit Hilfe von DFT (Dichtefunktionaltheorie)-Rechnungen bewerkstelligen. Hierbei muss zunächst der Reaktionsmechanismus der betrachteten Reaktion aufgeklärt werden. Anschließend können durch Betrachtung des geschwindigkeitsbestimmenden Schritts Voraussagen für effizientere Katalysatoren getroffen werden. Das Vorgehen bei dieser Methode wird im Folgenden ausführlich geschildert.

Um zu einem detaillierten Verständnis des Reaktionsmechanismus zu gelangen, wird zunächst mit Hilfe von DFT-Rechnungen das Energieprofil des Katalysezyklus der betrachteten Reaktion berechnet. Dazu werden Geometrien und Energien aller Edukte, Produkte, Katalysatoren, Intermediate und Übergangszustände berechnet. Für viele Spezies müssen dabei mehrere Isomere, meistens Konformere (Rotamere), aber auch Konfigurationsisomere oder Konstitutionsisomere berechnet und miteinander verglichen werden. Durch sogenannte IRC (engl. 'intrinsic reaction coordinate')-Rechnung (für Details siehe Kapitel 5.3.2, Seite 106) wird dann festgestellt, welche Überganszustände die verschiedenen Intermediate miteinander verbinden. Die so identifizierten Reaktionspfade werden dann miteinander verglichen, und der energetisch günstigste Katalysezyklus wird

aufgestellt. Nun kann der geschwindigkeitsbestimmende Schritt identifiziert werden. Er stellt den langsamsten Elementarschritt mit der höchsten Aktivierungsbarriere in der Katalyse dar.

Um nun Voraussagen zur Entwicklung eines effizienteren Katalysators zu machen, ist im Wesentlichen der geschwindigkeitsbestimmende Schritt von Bedeutung, denn eine Beschleunigung eines anderen Elementarschritts würde nicht die Zeit zum Durchlaufen eines Katalysezyklus verkürzen und damit nicht die Wechselzahl, welche ein Maß für die Katalysatoreffizienz ist, erhöhen.

Die freie Aktivierungsenthalpie $\Delta G^{\ddagger}$ des geschwindigkeitsbestimmenden Schritts wird nun mit anderen Metallen oder Liganden berechnet. In diesem virtuellen Screening werden dann über die Eyring-Gleichung[39]

$$k = \frac{k_{\mathrm{B}} T}{h} e^{-\frac{\Delta G^{\ddagger}}{RT}}$$

die absoluten Geschwindigkeitskonstanten k für die jeweiligen Metall/Ligand-Kombinationen berechnet. Die Division durch die absolute Geschwindigkeitskonstante des ursprünglichen Katalysatorsystems liefert die relativen Geschwindigkeitskonstanten. Letztere ist dann für das ursprünglichen Katalysatorsystems genau Eins. Relative Geschwindigkeitskonstanten größer als Eins lassen auf effizientere Katalysatorsysteme für die betrachtete Reaktion schließen, die größte relative Geschwindigkeitskonstante auf den effizientesten.

Auf diese Weise lassen sich neue effizientere Katalysatoren identifizieren, die dann synthetisiert und in der Katalyse getestet werden können. Die Reaktionen sollten im Optimalfall mit um die berechneten Faktoren gesteigerte Reaktionsgeschwindigkeiten ablaufen oder eine Absenkung der Temperatur unter Erhalt der Katalysatoraktivität tolerieren. Diese Absenkung kann nach einer Faustregel grob abgeschätzt werden, die besagt, dass sich die Geschwindigkeit einer Reaktion verdoppelt, wenn die Temperatur um 10 °C erhöht wird. Beispielsweise sollte eine berechnete relative Geschwindigkeitskonstante von zwei folglich eine Temperaturabsenkung um 10 °C ermöglichen, eine von vier eine Temperaturabsenkung um 20 °C.

Ein im Vergleich zur Eyring-Theorie recht neuer Ansatz zur Abschätzung der katalytischen Effizienz von Katalysatorsystemen ist das von Amatore und Jutand vorgestellte 'energetic span'-Modell,[40] welches von Kozuch und Shaik noch weiterentwickelt wurde.[41] Es besagt,

dass die größtmögliche Reaktionsgeschwindigkeit und damit die höchste 'turnover frequency' des Katalysezyklus bei der niedrigsten freien Enthalpiespanne vorliegt, welche die Differenz der freien Enthalpien zwischen dem höchsten Übergangszustand und dem niedrigsten Intermediat des gesamten Katalysezyklus darstellt. Für eine rationale Katalysatorentwicklung nach diesem Konzept müssten nicht die am geschwindigkeitsbestimmenden Schritt beteiligten Spezies, sondern der höchste Übergangszustand und das niedrigste Intermediat des Katalysezyklus mit anderen Metall/Ligand-Kombinationen berechnet werden. Eine geringere freie Enthalpiespanne ließe dann auf eine höhere Katalysatoreffizienz schließen.

Die Anwendung des 'energetic span'-Modells in der rationalen Katalysatorentwicklung bringt jedoch Nachteile in seiner praktischen Anwendbarkeit mit sich. Dies ist vor allem der Fall, wenn im Katalysezyklus weitere Spezies mit ähnlichen Energien wie der höchste Übergangszustand oder das niedrigste Intermediat auftreten. Würde beispielsweise bei der Berechnung des höchsten Übergangszustands mit einer anderen Metall/Ligand-Kombinationen die freie Enthalpie unter die eines anderen Übergangszustands fallen, so würde nun ein anderer Übergangszustand der höchste sein, der jeweils wiederum neu berechnet werden müsste. Gleiches trifft für die Intermediate zu. Im Gegensatz zur rationalen Katalysatorentwicklung auf Grundlage der Eyring-Theorie, bei der nur Reaktand und Übergangszustand des geschwindigkeitsbestimmenden Schritts neuberechnet werden müssen, müssten beim 'energetic span'-Modell möglicherweise mehrere Spezies neuberechnet werden, um sicherzustellen, dass sich mit anderen Katalysatoren der höchste Übergangszustand und das niedrigste Intermediat nicht ändern.

Bisher wurden DFT-Rechnungen in zahlreichen Fällen eingesetzt, um erfolgreich Reaktionsmechanismen aufzuklären, oft auch in Kombination mit spektroskopischen oder massenspektrometrischen Experimenten und Katalyseversuchen. Sehr häufig gelang es jedoch nicht, aus diesen Erkenntnissen Leitstrukturen für effizientere Katalysatorsysteme abzuleiten. Beispielsweise konnten Gooßen, Koley und Thiel den kompletten Reaktionsmechanismus der Palladium-katalysierten Suzuki-Kupplung von Carbonsäureanhydriden **1.3-1** mit Arylboronsäuren **1.3-2** zu Arylketonen **1.3-4** mit Hilfe von DFT-Rechnungen aufklären (Schema 2).[42,43] Es zeigte sich, dass ein komplexes Netzwerk mehrerer miteinander verknüpfter Katalysezyklen existiert, die jeweils sehr ähnliche Energieprofile aufweisen. Auch innerhalb der Zyklen sind die Aktivierungsbarrieren einzelner Reaktionsschritte von vergleichbarer Höhe. Somit können geringfügige Änderungen des Katalysatorsystems den

geschwindigkeitsbestimmenden Schritt verschieben. Es ist zum Beispiel bekannt, dass elektronenarme Phosphine wie Triphenylphosphin die Aktivierungsbarriere der reduktiven Eliminierung absenken und die der oxidativen Addition erhöhen, wohingegen elektronenreiche Phosphine wie Trimethylphosphin gegenteilig die Aktivierungsbarriere der reduktiven Eliminierung erhöhen und die der oxidativen Addition absenken.[44,45] Somit war es in diesem Fall nicht möglich, durch rationale Katalysatorentwicklung mit Hilfe von DFT-Rechnungen, welche sich auf die am geschwindigkeitsbestimmenden Schritt beteiligten Spezies beschränken, Voraussagen für effizientere Katalysatorsysteme zu treffen. Vielmehr hätte die überwiegende Mehrzahl der Intermediate und Übergangszustände für jeden potentiellen Katalysator neu berechnet werden müssen, was keinen Vorteil gegenüber dem klassischen Katalysatorscreening gebracht hätte.

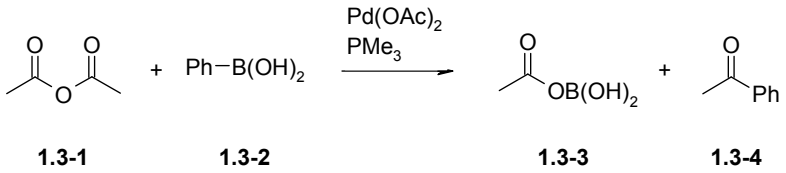

Schema 2. *Suzuki-Kupplung von Carbonsäureanhydriden mit Arylboronsäuren*.

Ein Beispiel für eine erfolgreiche rationale Katalysatorentwicklung wurde von Li und Gevorgyan präsentiert.[46] DFT-Rechnungen waren hierbei in der Lage, die Regioselektivität einer 2- bzw. 3-Silylfuransynthese in Abhängigkeit des verwendeten Goldkatalysators korrekt vorauszusagen. Auch sind Beispiele rationaler Katalysatorentwicklung im Bereich der heterogenen Katalyse bekannt, die von Mpourmpakis und Vlachos in einem Übersichtsartikel zusammengefasst wurden.[47]

2 Ziele der Arbeit

Die Zielsetzung dieser Arbeit bestand im Einsatz von DFT-Rechnungen zum mechanistischen Verständnis und zur rationalen Entwicklung homogenkatalytischer Reaktionen.

In einem ersten Projekt sollte ein Katalysatorsystem entwickelt werden, welches es ermöglicht, die Reaktionstemperatur der decarboxylierenden Kreuzkupplung deutlich abzusenken und die Anwendungsbreite der Reaktionen auszudehnen. Dies sollte die Etablierung der decarboxylierenden Kreuzkupplung als alternatives, nachhaltiges Synthesekonzept zur regioselektiven C–C- und C–Heteroatom-Bindungsknüpfung ausgehend von kostengünstigen, einfach handhabbaren, leicht lagerbaren sowie luft- und wasserunempfindlichen Carbonsäuren als Startmaterialien vorantreiben. Langfristiges Ziel ist es, dadurch klassische Synthesewege mit beispielsweise stöchiometrischem Einsatz teurer Organometallspezies zu ersetzen. Somit hätte die decarboxylierende Kreuzkupplung das Potential, Anwendung im industriellen Maßstab zu finden.

Aufgrund erster Hinweise, dass die Extrusion von Kohlendioxid geschwindigkeits-bestimmend ist, sollten zunächst effizientere Decarboxylierungskatalysatoren entwickelt werden. Hierbei sollten DFT-Rechnungen zur Voraussage von Leitstrukturen eingesetzt werden, um die aufwendige und zeitraubende Synthese maßgeschneiderter Liganden zu vermeiden. Basierend auf den Berechnungen sollten neue Strukturvorschläge für effizientere Decarboxylierungskatalysatoren gemacht werden, deren Anwendbarkeit in der Protodecarboxylierung überprüft werden sollte, mit dem Ziel, die Reaktionstemperatur deutlich absenken zu können.

Die Erkenntnisse aus der Protodecarboxylierungsreaktion sollten anschließend auf die weitaus komplexere decarboxylierende Kreuzkupplung übertragen werden, mit dem Ziel, auch diese bei wesentlich niedrigeren Temperaturen durchführen und das Substratspektrum erweitern zu können. Sollte dies so einfach nicht gelingen, wäre ein detailliertes Verständnis des Reaktionsmechanismus der decarboxylierenden Kreuzkupplung unabdingbar. Hierzu müssten alle Elementarschritte mit Hilfe DFT-Rechnungen untersucht, verschiedene Reaktionspfade miteinander verglichen und der energetisch günstigste Katalysezyklus aufgestellt werden. Dies sollte dann die Identifikation des geschwindigkeitsbestimmenden Schritts mit dem Ziel einer rationalen Katalysatorentwicklung ermöglichen.

In einem zweiten Projekt sollte die mechanistische Untersuchung der Ru-katalysierten Hydroamidierung terminaler Alkine durch Einsatz von DFT-Rechnungen unterstützt werden. Nachdem bereits durch Isotopenmarkierungsexperimente und diverse spektroskopische und spektrometrische Methoden drei von fünf potentiellen Reaktionsmechanismen ausgeschlossen werden konnten, erlaubten die experimentellen Ergebnisse die Eingrenzung auf einen der verbliebenen Katalysezyklen.

Da nur begrenzte Informationen über die Konfigurationen der Intermediate verfügbar waren, war das Ziel, mit Hilfe von DFT-Rechnungen, zu überprüfen, ob es sich bei den Intermediaten um stabile Minima handelt und zu klären, welche räumliche Anordnung der Liganden am günstigsten ist. Ferner sollte der Koordinationsmodus des Alkins während der Reaktion untersucht und geklärt werden, wie die Regio- und Stereochemie kontrolliert wird. Die gewonnenen Erkenntnisse sollten einen Leitfaden für die zukünftige rationale Entwicklung effizienterer Hydroamidierungskatalysatoren darstellen.

In einem dritten Projekt sollten DFT-Rechnungen dazu dienen, Beiträge zum mechanistischen Verständnis der Palladium-katalysierten Isomerisierung von Allylestern zu Enolestern zu liefern. Aufgrund der Vermutung, dass ein Palladiumhydrid-Komplex die katalytisch aktive Spezies darstellt, sollte die Bildung verschiedener Palladiumhydrid-Spezies ausgehend vom homodinuklearen Palladiumkatalysator $[Pd(\mu\text{-}Br)(P^tBu_3)]_2$ untersucht werden, mit dem Ziel, die katalytisch aktive Spezies der Reaktion zu identifizieren.

Dies sollte dazu dienen, Aufschluss über die einzigartige Reaktivität des homodinuklearen Palladiumkatalysators zu erlagen. Die Ergebnisse sollten einen Wegweiser für kommende Entwicklungen Palladium-katalysierter Doppelbindungsisomerisierungsreaktionen darstellen.

3 Ergebnisse und Diskussion

3.1 Kupfer- und Silber-katalysierte Protodecarboxylierung von Carbonsäuren

Die Carbonsäuregruppe zählt zu den am häufigsten vorkommenden funktionellen Gruppen in organischen Verbindungen. Aufgrund ihrer strukturellen Vielfältigkeit und ihrer geringen Kosten stellen Carbonsäuren attraktive Substrate für die organische Synthese dar. In den letzten Jahren wurde eine Vielzahl verschiedener übergangsmetallkatalysierter Transformationen ausgehend von Carbonsäuren entwickelt.[48–50] Hierzu zählen unter anderem decarboxylierende Kupplungsreaktionen, welche regioselektive C–C- und C–Heteroatom-Bindungsknüpfungen erlauben und nachhaltige Alternativen gegenüber bestehenden abfallintensiven Prozessen darstellen, die teure und empfindliche Organometallverbindungen einsetzen.[51–53] In redox-neutralen decarboxylierenden Kreuzkupplungen findet die Kupfer-katalysierte Extrusion von Kohlendioxid aus Carbonsäuren statt, und das Kohlenstoffatom, welches die Carbonsäuregruppe getragen hatte, bildet dann regioselektiv eine Bindung mit einem elektrophilen Kohlenstoff- oder Heteroatom unter Palladium-Katalyse.[54]

Die praktische Anwendbarkeit dieser Transformationen ist jedoch durch die Notwendigkeit sehr hoher Reaktionstemperaturen und durch die Toleranz eines nur kleinen Substratspektrums eingeschränkt. Da aus experimentellen Beobachtungen geschlossen wurde, dass die Extrusion von Kohlendioxid den geschwindigkeitsbestimmenden Schritt darstellt,[55] besteht das Ziel in der Entwicklung effizienterer Decarboxylierungskatalysatoren, um die Reaktionstemperaturen absenken und die Anwendungsbreite der Reaktionen ausdehnen zu können. Die Protodecarboxylierung stellt eine ideale Testreaktion für die Entwicklung effizienterer Cokatalysatoren für decarboxylierende Kreuzkupplungen dar, da sie leicht durchzuführen und mechanistisch relativ gut verstanden ist.

Zu Beginn dieser Arbeiten war der Reaktionsmechanismus der übergangsmetallkatalysierten Protodecarboxylierung von Carbonsäuren **3.1-1** bereits bekannt.[56,57] Der Katalysezyklus, welcher nur aus zwei Schritten, der Decarboxylierung und der Protolyse, besteht, ist in Schema 3 dargestellt. In der Entwicklung der Cu/Pd-katalysierten decarboxylierenden Kreuzkupplung zeigte sich, dass bereits Spuren von Wasser zur Bildung der freien Arene **3.1-2** führen.[55] In späteren Arbeiten stellte sich heraus, dass dies ebenfalls bei der Ag/Pd-

katalysierten decarboxylierenden Kreuzkupplung der Fall ist.[58] Daher kann davon ausgegangen werden, dass im Katalysezyklus der Kupfer- und Silber-katalysierten Protodecarboxylierung (Schema 3) die Protolyse einen sehr schnellen Reaktionsschritt darstellt und somit die Decarboxylierung geschwindigkeitsbestimmend ist.

Bei dem Einsatz von Gold als Katalysatormetall lässt sich die gegenteilige Reaktivität beobachten. Da hier die Protolyse geschwindigkeitsbestimmend ist, gelang es Nolan et al. durch Gold-vermittelte Decarboxylierung von Carbonsäuren Aryl–Gold-Komplexe zu synthetisieren, die in der Gegenwart von Wasser stabil sind.[59] Erst durch die Verwendung von Adamantan-1-carbonsäure als Additiv war die Entwicklung einer Gold-katalysierten Protodecarboxylierung von Carbonsäuren möglich.[60]

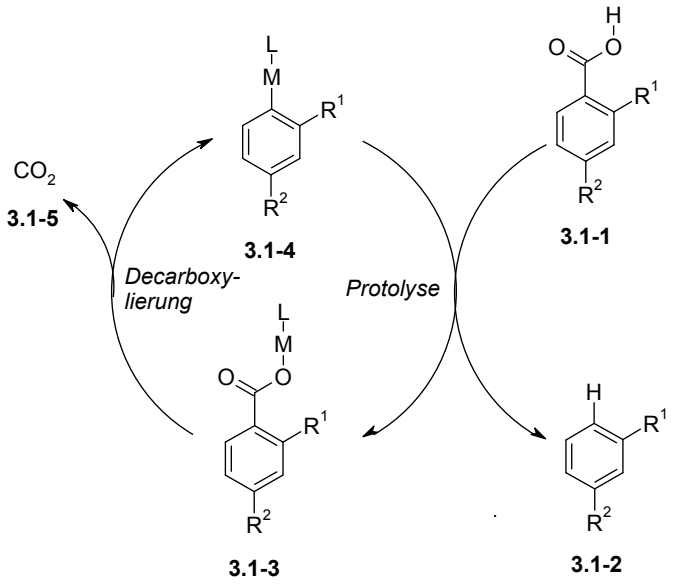

Schema 3. *Reaktionsmechanismus der übergangsmetallkatalysierten Protodecarboxylierung*.

Zunächst wurde damit begonnen, den Decarboxylierungsschritt von 2- und 4-Fluorbenzoesäure, einer reaktiven und einer unreaktiven aromatischen Carbonsäure, mit DFT-Rechnungen zu untersuchen. Da bekannt ist, dass die Extrusion von Kohlendioxid **3.1-5** nur über einen einzigen Übergangszustand verläuft,[56,57] mussten lediglich die Geometrien von Edukt **3.1-3**, Übergangszustand **3.1-6** und den Produkten **3.1-4** sowie **3.1-5** optimiert und deren Energien berechnet werden (Schema 4). Dies wurde zunächst für den derzeit besten Decarboxylierungskatalysator,[55,56,61–66] ein System bestehend aus Kupfer(I) und 1,10-Phenanthrolin, durchgeführt. Die Untersuchung des Reaktionsschritts mit unterschiedlichen Substituenten in 4- und 7-Position des 1,10-Phenanthrolinliganden erlaubte

die Berechnung der freien Reaktionsenthalpien, der freien Aktivierungsenthalpien und der relativen Geschwindigkeitskonstanten für die verschiedenen Katalysatoren. Eine geringere berechnete Barriere und somit höhere Geschwindigkeitskonstante sollte für eine höhere Katalysatoreffizienz sprechen oder eine Absenkung der Temperatur unter Erhalt der Katalysatoreffizienz erlauben.

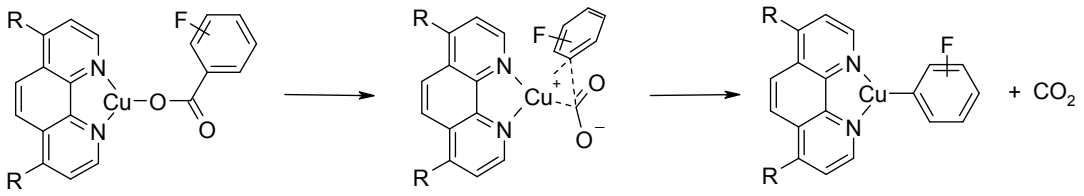

Schema 4. *Decarboxylierung mit 4,7-disubstituierten 1,10-Phenanthrolinliganden*.

Für die Kupfer-basierten Katalysatorsysteme wurden sowohl für 2- als auch für 4-Fluorbenzoesäure die niedrigsten Aktivierungsbarrieren und damit die höchsten relativen Geschwindigkeitskonstante für Phenanthrolinliganden mit elektronenschiebenden Substituenten berechnet (Table 1 und Table 2 in *ChemCatChem*). Die Ergebnisse der DFT-Rechnungen wurden daraufhin mit Katalyseversuchen zur Protodecarboxylierung verglichen, um festzustellen, ob die DFT-Rechnungen geeignet sind, Voraussagen für die Katalysatoreffizienz treffen zu können. Tatsächlich konnte mit 4,7-Dimethoxyphenanthrolin die höchste Ausbeute für die Decarboxylierung von 2-Fluorbenzoesäure verzeichnet werden (81% statt 65% für unsubstituiertes 1,10-Phenanthrolin, Table 3 in *ChemCatChem*). Bei der Reaktion von 4-Fluorbenzoesäure brach die Ausbeute auf 6% ein. Dies lässt sich durch die mangelnde thermische Stabilität von 4,7-Dimethoxy-1,10-phenanthrolin erklären, welches in der Protodecarboxylierung von *para*-substituierten Benzoesäuren den sehr hohen Reaktionstemperaturen von 170 °C über 16 Stunden ausgesetzt ist, statt den 2 Stunden wie bei *ortho*-substituierten Benzoesäuren. Für die Decarboxylierung von 4-Fluorbenzoesäure ist 4,7-Diphenyl-1,10-phenanthrolin der aktivste Ligand, vermutlich da er die größte thermische Stabilität besitzt und sich nicht bereits nach wenigen Stunden bei 170 °C zersetzt.

Durch den Vergleich der DFT-Rechnungen mit den Experimenten konnte gezeigt werden, dass die theoretischen Betrachtungen die Reaktivität der Katalysatoren zumindest für *ortho*-substituierte Benzoesäuren richtig voraussagen. Jedoch war der zu erwartende und beobachtete Reaktivitätsgewinn viel zu klein, um die Reaktionstemperatur deutlich absenken

zu können. Deshalb wurde daraufhin die Berechnung von der Variation des Liganden hin zur Variation des Katalysatormetalls verlagert.

Für einen Decarboxylierungskatalysator mit Silber als Zentralmetall und *N*-Methyl-2-Pyrrolidon (NMP) als Ligand wurden für *ortho*-substituierte Benzoesäuren deutlich niedrigere Aktivierungsbarrieren und wesentlich höhere Reaktionsgeschwindigkeiten berechnet (Table 1 in *ChemComm*, Table 4 in *ChemCatChem*). Diese Voraussagen erwiesen sich als zutreffend und erlaubten die Entwicklung einer Protodecarboxylierung mit einem Katalysatorsystem bestehend aus AgOAc und K_2CO_3 in NMP, welches die Protodecarboxylierung von *ortho*-substituierten Benzoesäuren **3.1-1** bereits bei 120 °C erlaubt, 50 °C niedriger als die des Kupfer-basierten Systems (Schema 5).

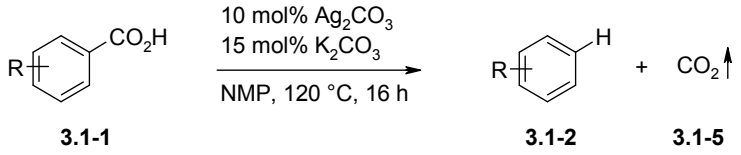

3.1-1 **3.1-2** **3.1-5**

NMP = *N*-Methyl-2-pyrrolidon

Schema 5. *Silber-katalysierte Protodecarboxylierung von Carbonsäuren*.

Die Ergebnisse der Silber-katalysierten Protodecarboxylierung von Carbonsäuren wurden zunächst in einer 'communication' in *Chemical Communications* veröffentlicht, bevor ein Vergleich der Kupfer- und Silber-katalysierten Protodecarboxylierung von Carbonsäuren in einem 'full paper' in *ChemCatChem* publiziert wurde. Sämtliche Ergebnisse können den englischsprachigen Originaltexten beider Veröffentlichungen entnommen werden, die im Folgenden abgedruckt sind.

Beide Publikationen entstanden im Rahmen von Kooperationsprojekten. Dabei wurden alle DFT-Rechnungen allein von mir geplant, durchgeführt und ausgewertet. Die durch meine Ergebnisse getroffenen Vorrausagen bildeten anschließend die Grundlage für experimentelle Arbeiten, welche aus Katalyseversuchen, der Entwicklung des Katalysatorsystems und der Bestimmung der Anwendungsbreite der Reaktion bestanden und von Frau Prof. Dr. Nuria Rodríguez, Herrn Dr. Christophe Linder und Herrn Dr. Paul P. Lange durchgeführt wurden.

„L. J. Gooßen, C. Linder, N. Rodríguez, P. P. Lange, A. Fromm, *Chem. Commun.* **2009**, 7173−7175: *Silver-Catalysed Protodecarboxylation of Carboxylic Acids*. DOI: 10.1039/B912509D. − Reproduced by permission of The Royal Society of Chemistry.“

RSC | Advancing the Chemical Sciences

Royal Society of Chemistry
Thomas Graham House
Science Park
Milton Road
Cambridge
CB4 0WF

Tel: +44 (0)1223 420 066
Fax: +44 (0)1223 423 623
Email: contracts-copyright@rsc.org

www.rsc.org

Acknowledgements to be used by RSC authors

Authors of RSC books and journal articles can reproduce material (for example a figure) from the RSC publication in a non-RSC publication, including theses, without formally requesting permission providing that the correct acknowledgement is given to the RSC publication. This permission extends to reproduction of large portions of text or the whole article or book chapter when being reproduced in a thesis.

The acknowledgement to be used depends on the RSC publication in which the material was published and the form of the acknowledgements is as follows:

- For material being reproduced from an article in *New Journal of Chemistry* the acknowledgement should be in the form:
  - [Original citation] - Reproduced by permission of The Royal Society of Chemistry (RSC) on behalf of the Centre National de la Recherche Scientifique (CNRS) and the RSC
- For material being reproduced from an article *Photochemical & Photobiological Sciences* the acknowledgement should be in the form:
  - [Original citation] - Reproduced by permission of The Royal Society of Chemistry (RSC) on behalf of the European Society for Photobiology, the European Photochemistry Association, and RSC
- For material being reproduced from an article in *Physical Chemistry Chemical Physics* the acknowledgement should be in the form:
  - [Original citation] - Reproduced by permission of the PCCP Owner Societies
- For material reproduced from books and any other journal the acknowledgement should be in the form:
  - [Original citation] - Reproduced by permission of The Royal Society of Chemistry

The acknowledgement should also include a hyperlink to the article on the RSC website.

The form of the acknowledgement is also specified in the RSC agreement/licence signed by the corresponding author.

Except in cases of republication in a thesis, this express permission does not cover the reproduction of large portions of text from the RSC publication or reproduction of the whole article or book chapter.

A publisher of a non-RSC publication can use this document as proof that permission is granted to use the material in the non-RSC publication.

VAT Registration Number: GB 342 1764 71 Registered Charity Number: 207890

COMMUNICATION www.rsc.org/chemcomm | ChemComm

Silver-catalysed protodecarboxylation of carboxylic acids†

Lukas J. Gooßen,* Christophe Linder, Nuria Rodríguez, Paul P. Lange and Andreas Fromm

Received (in Cambridge, UK) 25th June 2009, Accepted 7th October 2009
First published as an Advance Article on the web 28th October 2009
DOI: 10.1039/b912509d

A silver-based catalyst system has been discovered that effectively promotes the protodecarboxylation of various carboxylic acids at temperatures of 80–120 °C—more than 50 °C below those of the best known copper catalysts.

In recent years, numerous catalytic transformations have been developed that have substantially extended the use of carboxylic acids as building blocks in organic synthesis.[1] Decarboxylative coupling reactions in particular are of high preparative utility, as they allow using carboxylate salts as substitutes for costly organometallic reagents in C–C bond forming reactions. In these transformations, the carbon nucleophiles are generated *via* extrusion of CO_2 from carboxylate salts and can subsequently be coupled with a range of carbon electrophiles.[2] The decarboxylation of carboxylic acids is also the initiating step in preparatively valuable oxidative couplings, *e.g.* decarboxylative Heck reactions,[3] C–S couplings,[4] and tandem decarboxylation/C–H activation reactions.[5] To date, the practical applicability of all these transformations is limited by their requirement of rather high temperatures, as well as their tolerance of only a narrow spectrum of functional groups. Considering that the extrusion of CO_2 is believed to be the rate-determining step in all these processes, the development of more effective decarboxylation catalysts is the key towards lowering the reaction temperatures and thereby extending the scope of these transformations to more sensitive derivatives. The protodecarboxylation of aromatic carboxylates is an ideal test reaction for the development of more effective co-catalysts for decarboxylative coupling reactions (Scheme 1), as it is easily performed and mechanistically relatively well-understood.

Moreover, it is itself an important synthetic tool, allowing removal of surplus carboxylate groups left behind as a result of the chosen synthetic route. The decarboxylation of simple arenecarboxylates usually involves extreme reaction temperatures. Moreover, in the early protocols, stoichiometric amounts of copper[6] or silver[7] complexes are required to mediate this process. Mercury-mediated protodecarboxylations readily proceed at temperatures of 100 °C, but their synthetic utility is limited by the toxicity of the organomercury(II) compounds.[8] Recently, we disclosed a protodecarboxylation of arenecarboxylic

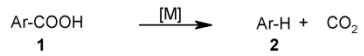

Scheme 1 Metal-mediated decarboxylation of benzoic acids.

FB Chemie – Organische Chemie, TU Kaiserslautern, Erwin-Schroedinger-Strasse, Geb. 54, 67663, Kaiserslautern, Germany. E-mail: goossen@chemie.uni-kl.de; Fax: +49 (631) 205-3921
† Electronic supplementary information (ESI) available: Experimental data, procedures for all compounds and computational details. See DOI: 10.1039/b912509d

acids in which only catalytic amounts of a copper mediator are necessary.[9] The new protocol involves a copper/1,10-phenanthroline-complex as the catalyst for an effective decarboxylation of a wide spectrum of aromatic carboxylic acids within 16 h at 170 °C. Independently, Kozlowski *et al.*[10] disclosed a catalytic protodecarboxylation protocol for particularly electron-rich bis-*ortho*-substituted aromatic carboxylic acids.[11] It proceeds readily at 70 °C, but involves the use of as much as 20 mol% of expensive $Pd(O_2CCF_3)_2$ as the catalyst.

We herein present an effective and economical silver-based low-temperature protodecarboxylation catalyst.[12] In our search for a new catalyst generation, we performed numerous DFT calculations modelling the extrusion of CO_2 from various copper and silver carboxylate complexes. In this context, we calculated the structures and energies for the starting materials, transition states and products for the decarboxylation of both a 1,10-phenanthroline/copper(I)-2-fluorobenzoate complex and the corresponding silver(I) system (Table 1).[13] Under standard conditions at 298 K, the extrusion of CO_2 from the copper carboxylate **3a** is endergonic and has an activation barrier of $\Delta G^{\neq}_{298}$ = 31.1 kcal mol^{-1}. For the silver(I) carboxylate **3′a**, this transformation is exergonic and has a significantly lower activation barrier of only of $\Delta G^{\neq}_{298}$ = 29.6 kcal mol^{-1}.

As phenanthroline is not a common ligand for silver, we suspected at first that this result might be an artefact caused by an unrealistic ligand environment. We thus performed additional calculations on the decarboxylation of a silver(I)-2-fluorobenzoate complex which is ligated solely by two NMP molecules (**5**). The structures and energies obtained are depicted

Table 1 Relative energies for the decarboxylation of 2-fluorobenzoic acid with silver and copper catalysts[a]

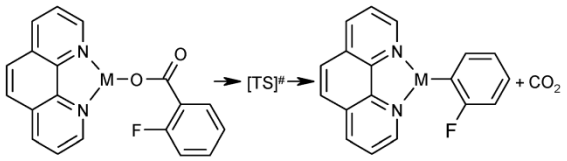

3 4

	M	ΔE^{R}_{tot}	ΔG^{R}_{298}	$\Delta E^{\neq}_{tot}$	$\Delta G^{\neq}_{298}$
3a → **4a**	Cu	13.91	2.10	32.36	31.11
3′a → **4′a**	Ag	11.04	−0.45	31.36	29.56

[a] *Computational conditions*: Gaussian03;[14] B3LYP[15]/6–311+G(2d,p)[16]//B3LYP/6–31G(d)[17] for H, C, N, O, F; Stuttgart RSC 1997 ECP[18] for Cu, Ag, scaling factor for thermal corrections: f = 0.9804.[19] ΔE^{R}_{tot}, ΔG^{R}_{298}, $\Delta E^{\neq}_{tot}$ and $\Delta G^{\neq}_{298}$ are expressed in kcal mol^{-1}.

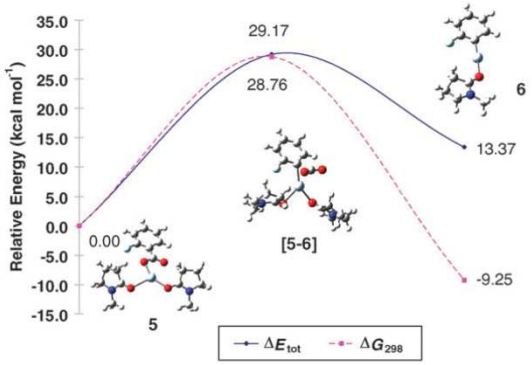

Fig. 1 Calculated reaction path for metal-catalyzed protodecarboxylation.

in Fig. 1. The reaction to the NMP-stabilized 2-fluorophenyl silver complex **6** was found to also be exergonic (-9.3 kcal mol^{-1}), and the activation barrier was as low as 28.8 kcal mol^{-1}. We were positively surprised by these results, as silver complexes had so far been inferior to copper complexes in all our experimental decarboxylation studies. Moreover, silver is an untypical mediator for protodecarboxylations,[20] and is required in overstoichiometric amounts as a co-mediator in decarboxylative couplings.[2,3,5]

Intrigued by the predictions of our DFT studies, we performed a series of test reactions using the decarboxylation of 2-methoxybenzoic acid as a model system. This substrate was chosen due to its similar electronic properties to the 2-fluoro derivative used in the calculations, but leading to a less volatile product that is more easily analyzed and isolated. In order to get a first idea of the relative reaction rates for copper- and silver-based catalysts, we compared the respective conversions for the protodecarboxylation of 2-methoxybenzoic acid obtained at 10 mol% catalyst loading after 15 min at 140 °C. A copper(I) oxide/1,10-phenanthroline complex gave only trace amounts of the product anisole (**2a**), whereas the corresponding silver(I) oxide/1,10-phenanthroline system afforded 20% conversion. This result confirms the improved catalytic activity of silver(I) over copper(I).

We next optimized the catalyst and conditions in a series of screening experiments. Selected results are summarized in Table 2. As previously reported, the protodecarboxylation of the deactivated 2-methoxybenzoic acid with Cu(I) oxide/1,10-phenanthroline in a mixture of NMP and quinoline at 170 °C was low. Under identical conditions, silver(I) oxide initially gave disappointing results, but the reaction became very effective in the absence of the basic co-solvent quinoline (entries 2, 3). The rate acceleration achieved by using silver allowed us to reduce the reaction temperature to 120 °C without obtaining substantially decreased yields (entry 4). The counter-ion on the silver had a marked effect on the reaction outcome, the basic acetate giving best results (entries 5–8). Some of the mono- and bidentate nitrogen ligands, triarylphosphines and -arsines tested including 1,10-phenanthroline were found to have a beneficial effect on the reaction yields (entries 9–14) in comparison to silver acetate alone (entry 15). Suspecting that the principal role of such ligands might be to act as a mild base, we also investigated

Table 2 Optimization of the reaction conditions[a]

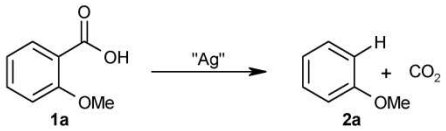

Entry	Catalyst	Ligand	Additive	Solvent	T/°C	**2a**(%)
1	Cu_2O	phen	—	NMP/quin	170	24
2	Ag_2O	phen	—	〃	〃	22
3	〃	〃	—	NMP	〃	85
4	〃	〃	—	〃	120	60
5	AgOTf	〃	—	〃	〃	0
6	AgO	〃	—	〃	〃	20
7	Ag_2CO_3	〃	—	〃	〃	39
8	AgOAc	〃	—	〃	〃	70
9	〃	5-NO_2-phen	—	〃	〃	51
10	〃	4,7-di-Ph-phen	—	〃	〃	47
11	〃	2,2′-bipyridine	—	〃	〃	46
12	〃	quin	—	〃	〃	21
13	〃	$AsPh_3$	—	〃	〃	11
14	〃	PPh_3	—	〃	〃	0
15	〃	—	—	〃	〃	24
16	〃	—	K_2CO_3	〃	〃	98
17	〃	—	〃	DMSO	〃	57
18	〃	—	〃	DMF	〃	77
19[b]	〃	—	〃	NMP	〃	79
20	〃	—	〃	〃	100	17
21[c]	〃	—	〃	〃	80	60

[a] *Reaction conditions*: 1 mmol 2-methoxybenzoic acid, 10 mol% catalyst (5 mol% Cu_2O, Ag_2O and Ag_2CO_3), 10 mol% ligand, 15 mol% additive, 2 mL solvent, 16 h. Conversions were determined by GC analysis using *n*-tetradecane as internal standard. phen = 1,10-phenanthroline, quin = quinoline. [b] After 8 h. [c] Using 2-nitrobenzoic acid.

carbonate bases as additives. Unligated silver in the presence of 15 mol% potassium carbonate, in particular, indeed led to substantially improved yields over all silver/ligand combinations (entry 16). Comparative experiments confirmed that NMP was the best choice of solvent (entries 17–19).

Under thus optimized conditions, 79% of the product was formed already within only 8 h reaction time (entry 19). Any further reduction in temperature considerably affected the yields for this particular substrate (entry 20). However, activated benzoic acids such as 2-nitrobenzoic acid gave satisfactory yields even at a reaction temperature of only 80 °C (entry 21).

We next investigated the generality of the optimized protocol using various aromatic and heteroaromatic carboxylic acids at a temperature of 120 °C. Selected results are summarized in Table 3. The yields are shown in comparison to those obtained with Cu_2O/phenanthroline at 170 °C.[9] We were pleased to find that the protodecarboxylation proceeded in high selectivities with, at most, traces of side products arising from homocoupling or transesterification reactions. The reaction time of 16 h was sufficient to achieve good conversions for most substrates. The examples demonstrate that the scope of the new Ag-catalyst is broader than that of the published Pd-system.[10] Moreover, its performance nicely complements that of the Cu-catalyst, the latter being particularly suited for *meta*- and *para*-substituted benzoic acids, while the Ag-system is highly effective for many *ortho*-substituted or heterocyclic derivatives that gave low or no yields with the Cu-catalyst. Examples include

Table 3 Scope of the transformation[a]

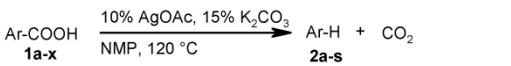

Entry		Ar–COOH	Ar–H	AgOAc: Yield/%	Cu_2O: Yield/%
1	**1a**	2-MeO–C_6H_4–COOH	**2a**	83	24[9]
2	**1b**	2-NO_2–C_6H_4–COOH	**2b**	92	87[9]
3	**1c**	2-NO_2-5-MeO–C_6H_3–COOH	**2c**	88	90[9]
4	**1d**	2,4,5-MeO–C_6H_2–COOH	**2d**	43	—
5	**1e**	2,4-MeO–C_6H_3–COOH	**2e**	89	—
6	**1f**	2,6-MeO–C_6H_3–COOH	**2e**	87	—
7	**1g**	2-Br–C_6H_4–COOH	**2f**	76	0
8	**1h**	2-Br-4,5-MeO–C_6H_2–COOH	**2g**	95	—
9	**1i**	2,6-Cl–C_6H_3–COOH	**2h**	76	0
10	**1j**	2,4-Cl–C_6H_3–COOH	**2h**	74	—
11	**1k**	2-Cl–5-NO_2–C_6H_3–COOH	**2i**	85	—
12	**1l**	2-MeS(*O*)$_2$–C_6H_4–COOH	**2j**	89	60[9]
13	**1m**	2-CF_3–C_6H_4–COOH	**2k**	(91)	(22)[9]
14	**1n**	2-*i*PrOC(*O*)–C_6H_4–COOH	**2l**	71	82[9]
15	**1o**	2-Ac–C_6H_4–COOH	**2m**	58	87[9]
16	**1p**	2-CN C_6H_4 COOH	**2n**	(11)	
17	**1q**	4-HO–C_6H_4–COOH	**2o**	17	—
18	**1r**	1-naphthyl–COOH	**2p**	45	83[9]
19	**1s**	2-thienyl–COOH	**2q**	(80)	(58)[9]
20	**1t**	3-thienyl–COOH	**2q**	(36)	—
21[b,c]	**1u**	cinnamic acid	**2r**	(76)	—
22[c]	**1v**	2-thiopheneglyoxylic acid	**2s**	(41)	—
23[d]	**1w**	3-MeO–C_6H_4–COOH	**2a**	(38)	—
24[d]	**1x**	4-MeO–C_6H_4–COOH	**2a**	(14)	80[9]

[a] *Reaction conditions*: 2 mmol carboxylic acid, 10 mol% AgOAc, 15 mol% K_2CO_3, 4 mL NMP, 120 °C, 16 h, isolated yields. GC yields are given in parentheses and were determined using *n*-tetradecane as the internal standard. [b] Using 4 mL of DMAC. [c] 140 °C. [d] 160 °C.

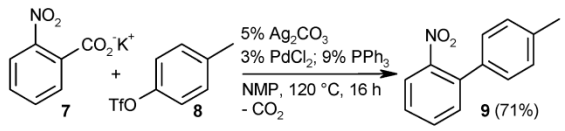

Scheme 2 Ag/Pd-catalysed decarboxylative biaryl synthesis.

2-methoxybenzoic, 2-halobenzoic, and heteroarenecarboxylic acids. At a more elevated temperature of 140 °C, an even wider range of carboxylates can be converted, *e.g.* α-oxocarboxylic acids and cinnamic acid, and above 160 °C, turnover is achieved even for some *meta*- and *para*-substituted benzoic acids.

The new decarboxylation catalyst is likely to open up entirely new opportunities for low-temperature decarboxylative cross-couplings. In a first test reaction at 120 °C, we observed a 71% yield in the reaction of 2-nitrobenzoic acid with 4-tolyl triflate using a non-optimized catalyst system consisting of 5 mol% of silver carbonate, 3 mol% of $PdCl_2$ and 9 mol% of PPh_3 (Scheme 2). Having thus achieved a reduction in the temperature by 50 °C also for decarboxylative cross-couplings, we are optimistic that after careful adjustments in the Pd co-catalyst, an effective, generally applicable, low-temperature decarboxylative cross-coupling is in close reach.

Moreover, now that aryl nucleophiles are accessible from carboxylic acids at such low temperatures, their generation may be combined with other types of more temperature-sensitive functionalizations.

We thank W. R. Thiel and C. van Wüllen for help with the DFT calculations, the Deutsche Forschungsgemeinschaft, Saltigo GmbH, and NanoKat for funding, and the A. v. Humboldt Foundation for a scholarship to N. R.

Notes and references

1 L. J. Gooßen, N. Rodríguez and K. Gooßen, *Angew. Chem., Int. Ed.*, 2008, **47**, 3100; L. J. Gooßen, K. Gooßen, N. Rodríguez, M. Blanchot, C. Linder and B. Zimmermann, *Pure Appl. Chem.*, 2008, **80**, 1725.
2 C. Peschko, C. Winklhofer and W. Steglich, *Chem.–Eur. J.*, 2000, **6**, 1147; L. J. Gooßen, G. Deng and L. M. Levy, *Science*, 2006, **313**, 662; P. Forgione, M. C. Brochu, M. St-Onge, K. H. Thesen, M. D. Bailey and F. Bilodeau, *J. Am. Chem. Soc.*, 2006, **128**, 11350; L. J. Gooßen, N. Rodríguez, B. Melzer, C. Linder, G. Deng and L. M. Levy, *J. Am. Chem. Soc.*, 2007, **129**, 4824; J.-M. Becht, C. Catala, C. Le Drian and A. Wagner, *Org. Lett.*, 2007, **9**, 1781; L. J. Gooßen, F. Rudolphi, C. Oppel and N. Rodríguez, *Angew. Chem., Int. Ed.*, 2008, **47**, 3043; L. J. Gooßen, B. Zimmermann and T. Knauber, *Angew. Chem., Int. Ed.*, 2008, **47**, 7103; L. J. Gooßen, N. Rodríguez and C. Linder, *J. Am. Chem. Soc.*, 2008, **130**, 15248; J. Moon, M. Jeong, H. Nam, J. Ju, J. H. Moon, H. M. Jung and S. Lee, *Org. Lett.*, 2008, **10**, 945.
3 A. G. Myers, D. Tanaka and M. R. Mannion, *J. Am. Chem. Soc.*, 2002, **124**, 11250; A. Maehara, H. Tsurugi, T. Satoh and M. Miura, *Org. Lett.*, 2008, **10**, 1159; P. Hu, J. Kan, W. Su and M. Hong, *Org. Lett.*, 2009, **11**, 2341.
4 Z. Duan, S. Ranjit, P. Zhang and X. Liu, *Chem.–Eur. J.*, 2009, **15**, 3666.
5 A. Voutchkova, A. Coplin, N. E. Leadbeater and R. H. Crabtree, *Chem. Commun.*, 2008, 6312; C. Wang, I. Piel and F. Glorius, *J. Am. Chem. Soc.*, 2009, **131**, 4194.
6 A. F. Shepard, N. R. Winslow and J. R. Johnson, *J. Am. Chem. Soc.*, 1930, **52**, 2083; M. Nilsson, *Acta Chem. Scand.*, 1966, **20**, 423; T. Cohen and R. A. Schambach, *J. Am. Chem. Soc.*, 1970, **92**, 3189; A. Cairncross, J. R. Roland, R. M. Henderson and W. F. Shepard, *J. Am. Chem. Soc.*, 1970, **92**, 3187.
7 J. Chodowska-Palicka and M. Nilsson, *Acta Chem. Scand.*, 1970, **24**, 3353.
8 H. Gilman and G. F. Wright, *J. Am. Chem. Soc.*, 1933, **55**, 3302.
9 L. J. Gooßen, W. R. Thiel, N. Rodríguez, C. Linder and B. Melzer, *Adv. Synth. Catal.*, 2007, **349**, 2241; L. J. Gooßen, F. Manjolinho, B. A. Khan and N. Rodríguez, *J. Org. Chem.*, 2009, **74**, 2620.
10 J. S. Dickstein, C. A. Mulrooney, E. M. O'Brien, B. J. Morgan and M. C. Kozlowski, *Org. Lett.*, 2007, **9**, 2441.
11 For acid mediated decarboxylations of such compounds, see: R. W. Hay and M. J. Taylor, *Chem. Commun.*, 1996, 525b.
12 For an independently developed silver-based protodecarboxylation see: J. Cornella, C. Sanchez, D. Banawa and I. Larrosa, *Chem. Commun.*, 2009, DOI: 10.1039/b916646g.
13 See in comparison: N. R. Gunawardena and T. B. Brill, *J. Phys. Chem. A*, 2001, **105**, 1876; J. Li and T. B. Brill, *J. Phys. Chem. A*, 2003, **107**, 2667; M. Staikova and D. J. Donaldson, *J. Phys. Chem. A*, 2005, **109**, 597.
14 *GAUSSIAN 03, Revision E.01*, Gaussian, Inc., Wallingford CT, 2004; for full citation see the ESI†.
15 C. Lee, W. Yang and R. G. Parr, *Phys. Rev. B: Condens. Matter Mater. Phys.*, 1988, **37**, 785; A. D. Becke, *J. Chem. Phys.*, 1993, **98**, 5648; P. J. Stephens, J. F. Devlin, C. F. Chabalowski and M. J. Frisch, *J. Phys. Chem.*, 1994, **98**, 11623.
16 R. Krishnan, J. S. Binkley, R. Seeger and J. A. Pople, *J. Chem. Phys.*, 1980, **72**, 650.
17 P. C. Hariharan and J. A. Pople, *Theor. Chim. Acta*, 1973, **28**, 213.
18 M. Dolg, U. Wedig, H. Stoll and H. Preuss, *J. Chem. Phys.*, 1987, **86**, 866; D. Andrae, U. Häußermann, M. Dolg, H. Stoll and H. Preuss, *Theor. Chim. Acta*, 1990, **77**, 123.
19 M. W. Wong, *Chem. Phys. Lett.*, 1996, **256**, 391.
20 For related silver-mediated protodecarboxylation see: J. M. Anderson and J. K. Kochi, *J. Am. Chem. Soc.*, 1970, **92**, 1651; J. M. Anderson and J. K. Kochi, *J. Org. Chem.*, 1970, **35**, 986.

„Reprinted with permission from L. J. Gooßen, N. Rodríguez, C. Linder, P. P. Lange, A. Fromm, *ChemCatChem* **2010**, *2*, 430–442: *Comparative Study of Copper- and Silver-Catalyzed Protodecarboxylations of Carboxylic Acids*. DOI: 10.1002/cctc.200900277. Copyright © 2010 WILEY-VCH Verlag GmbH & Co. KGaA, Weinheim."

JOHN WILEY AND SONS LICENSE TERMS AND CONDITIONS

Sep 11, 2014

This is a License Agreement between Andreas Fromm ("You") and John Wiley and Sons ("John Wiley and Sons") provided by Copyright Clearance Center ("CCC"). The license consists of your order details, the terms and conditions provided by John Wiley and Sons, and the payment terms and conditions.

All payments must be made in full to CCC. For payment instructions, please see information listed at the bottom of this form.

License Number	3465931044076
License date	Sep 11, 2014
Licensed content publisher	John Wiley and Sons
Licensed content publication	ChemCatChem
Licensed content title	Comparative Study of Copper- and Silver-Catalyzed Protodecarboxylations of Carboxylic Acids
Licensed copyright line	Copyright © 2010 WILEY-VCH Verlag GmbH & Co. KGaA, Weinheim
Licensed content author	Lukas J. Gooßen,Nuria Rodríguez,Christophe Linder,Paul P. Lange,Andreas Fromm
Licensed content date	Mar 18, 2010
Start page	430
End page	442
Type of use	Dissertation/Thesis
Requestor type	Author of this Wiley article
Format	Print and electronic
Portion	Full article
Will you be translating?	No
Title of your thesis / dissertation	DFT-Studien zum mechanistischen Verständnis und zur rationalen Entwicklung homogenkatalytischer Reaktionen
Expected completion date	Sep 2014
Expected size (number of pages)	150
Total	0.00 EUR

CHEMCATCHEM

DOI: 10.1002/cctc.200900277

Comparative Study of Copper- and Silver-Catalyzed Protodecarboxylations of Carboxylic Acids

Lukas J. Gooßen,* Nuria Rodríguez, Christophe Linder, Paul P. Lange, and Andreas Fromm[a]

The protodecarboxylation of aromatic carboxylic acids by various copper and silver catalysts is investigated with the help of density functional calculations and experimental studies. The computational results reveal that the catalytic activity of copper(I)–1,10-phenanthroline catalysts increases with the introduction of electron-rich substituents at the phenanthroline ligand. They also predicted that for some substrates, silver complexes should possess a substantially higher decarboxylating activity than copper, which is confirmed by experimental studies, leading to the discovery of a silver(I) catalyst that effectively promotes the protodecarboxylation of various carboxylic acids at temperatures in the range of 80–120 °C—more than 50 °C below those of the best known copper(I) catalyst. The scope of the new system complements that of the copper(I)-based method as it includes benzoates for example, with halogen or ether groups in the *ortho* positions.

Introduction

Carboxylic acid groups are among the most common functionalities in organic molecules. Decarboxylative coupling reactions, in which this functional group plays a key role, have recently emerged as powerful tools for C–C bond formation (Scheme 1).[1]

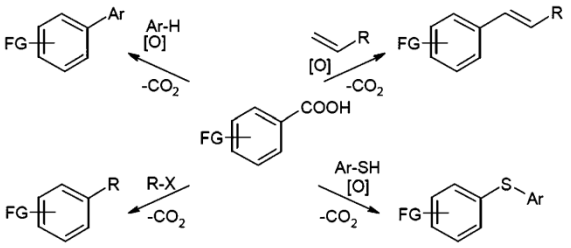

Scheme 1. Decarboxylative coupling reactions.

They proceed by the extrusion of CO_2 from a carboxylate salt, to generate a carbon nucleophile, and its subsequent coupling with a variety of carbon electrophiles.[2] The decarboxylation of carboxylic acids is also the initiating step in preparatively valuable oxidative couplings, such as decarboxylative Heck reactions,[3] C–S couplings,[4] tandem decarboxylation/C–H activation reactions,[5] allylations,[6] and conjugate additions.[7] Unfortunately, these transformations all currently suffer from the rather high reaction temperatures required and/or the narrow range of substrates that are tolerated, limitations that depend on the performance of the decarboxylation catalyst. The protodecarboxylation, in itself an important synthetic tool for the removal of surplus carboxylate groups, is an ideal test reaction for the development of more effective cocatalysts for decarboxylative coupling reactions (Scheme 2).

The decarboxylation of simple arenecarboxylates (Scheme 3) usually involves extreme reaction conditions. This is the case for all early protodecarboxylation procedures, whereby copper

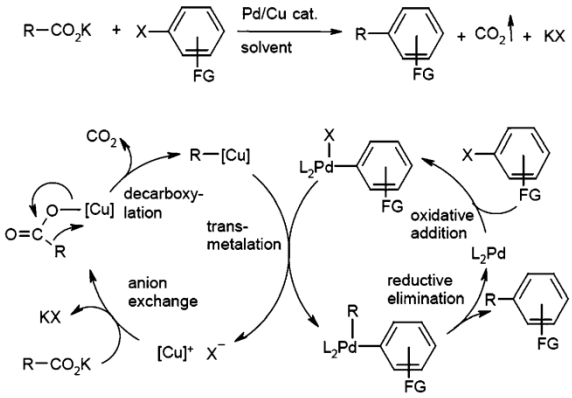

Scheme 2. Catalytic cycle for decarboxylative cross-coupling reactions; R = aryl, heteroaryl, vinyl, acyl; X = I, Br, Cl, OTf.

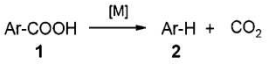

Scheme 3. Protodecarboxylation of benzoic acids.

complexes are used as stoichiometric mediators.[8] Synthetic applications of the milder mercury-mediated process are limited by the necessity for stoichiometric mercury salts and the intermediacy of toxic organomercury(II) species.[9]

In the context of our research on decarboxylative cross-coupling reactions, we recently developed the first protodecar-

[a] Prof. Dr. L. J. Gooßen, Dr. N. Rodríguez, C. Linder, P. P. Lange, A. Fromm
FB Chemie—Organische Chemie, TU Kaiserslautern
Erwin-Schroedinger-Strasse, Geb. 54, 67663 Kaiserslautern (Germany)
Fax: (+49) 631-205-3921
E-mail: goossen@chemie.uni-kl.de

boxylation of arenecarboxylic acids requiring only catalytic amounts of a metal mediator.[10] By using copper(I)–1,10-phenanthroline-type catalysts, a broad range of diversely functionalized aromatic carboxylic acids was effectively decarboxylated within 16 h at 170 °C. In parallel, Kozlowski et al. developed a protocol for the catalytic protodecarboxylation of particularly electron-rich bis-*ortho*-substituted aromatic carboxylic acids that proceeds at temperatures as low as 70 °C, albeit in the presence of 20 mol% of the expensive $Pd(O_2CCF_3)_2$.[11] Interestingly, these substrates also decarboxylate at similarly low temperatures in the presence of strong Brønsted acids in large excess.[12] The latter decarboxylation clearly cannot be combined with any in situ functionalization but only with a protonation step.

An effective and economical low-temperature decarboxylation catalyst that can be used both for protodecarboxylations and decarboxylative couplings thus remains of substantial interest. In previous studies, we had found copper(I)–1,10-phenanthroline complexes to actively promote decarboxylation at temperatures around 170 °C.[2d,f–h,10] The mechanism of copper-mediated decarboxylation was investigated by the groups of Nilsson, Cohen, Shepard, and Liu, as well as our group.[2l,8,10a] In all cases, a radical mechanism could be excluded based on experimental evidence. Instead, the decarboxylation is believed to have proceeded via the insertion of copper into the aryl–COO bond and a subsequent hydrolytic cleavage of the Cu–C bond. We investigated various potential reaction pathways with the help of density functional (DFT) calculations and found only one mechanism to be energetically feasible. This mechanism was recently confirmed by Liu and co-workers, who performed calculations on this Cu-mediated decarboxylation step in the context of decarboxylative cross-couplings.[2l]

An obvious step towards improving the catalytic activity of copper-complexes appeared to be the introduction of suitable substituents on the phenanthroline ring system. However, the synthesis of a diverse set of substituted 1,10-phenanthrolines proved to be far from trivial. In order to guide our synthetic efforts towards the most promising ligand lead structures and to allow a better understanding of the results of our screening experiments, we performed a series of DFT calculations in continuation of earlier mechanistic investigations on the parent structure.[10a,13] These investigations led to the discovery of a silver-based catalyst with much-improved protodecarboxylation activity at low temperatures. Some of the results have been disclosed within preliminary communications.[10,14] Herein, we present a detailed discussion of the DFT studies along with additional theoretical and experimental studies for copper- and silver-based catalyst systems.

Results and Discussion

DFT studies on the decarboxylation of copper(I) carboxylates

In our search for more active decarboxylation catalysts, we employed DFT calculations (Gaussian03;[15] B3LYP[16]/6-311+G(2d,p)[17]//B3LYP/6-31G(d)[18] for H, C, N, O, F, S; Stuttgart RSC 1997 ECP[19] for Cu) to model the structure and energies of starting materials, transition states and products for the decarboxylation of copper(I) 2-fluorobenzoate complexes ligated by various 1,10-phenanthroline derivatives. 2-Fluorobenzoic acid is an example representative of an activated benzoic acid that is known to decarboxylate reasonably fast in the presence of copper catalysts. In addition to the unsubstituted 1,10-phenanthroline, we performed calculations on 4,7-disubstituted 1,10-phenanthroline ligands with increasingly electron-donating substituents ($CN < Ph < Me < SPh < OPh < OMe < NMe_2$) *para* to the nitrogen donor atoms. For all ligands, we determined the total energies of reaction (ΔE^R_{tot}) and activation ($\Delta E^{\neq}_{tot}$), the free enthalpies of reaction (ΔG^R) and activation ($\Delta G^{\neq}$), and the relative reaction rates (k) in comparison to the decarboxylation with the unsubstituted phenanthroline at both room temperature (298 K) and the typical reaction temperature of 170 °C (443 K; Table 1). The additional calculations for the actual reaction temperature of 170 °C should allow a more precise comparison especially of the expected relative reaction rates for different complexes due to their strong temperature dependence.

The extrusion of CO_2 from copper benzoates in forming an aryl–copper bond is believed to be rate-determining for both protodecarboxylations and Pd/Cu-catalyzed decarboxylative couplings. Our computational results indicated that this decarboxylation step is endergonic at room temperature, regardless of the electronic properties of the 1,10-phenanthrolines (ΔG^R_{298}). However, it becomes exergonic at temperatures around 90 °C (363 K). At 170 °C, it is exergonic within a small range for all phenanthroline ligands ($\Delta G^R_{443} = -1.3$ to -3.4 kcal mol^{-1}; 1 kcal = 4.184 kJ). The reactions with phenanthroline complexes carrying electron-donating substituents are the least exergonic. However, the results indicated that modifying the electronic properties of the phenanthroline ligand would only have a very limited effect on the thermodynamics of the decarboxylation step.

To better understand the kinetics of this reaction, we next turned our attention to the calculated transition states, activation barriers, and reaction rates. The structures of all transition states display very similar features. The copper is located in a distorted tetrahedral environment made up of the two phenanthroline nitrogen atoms, the CO_2 carbon, and the 2-fluorophenyl residue. The latter binds through its carbon-centered lone pair both to the CO_2 carbon and the $[(phen)Cu]^+$ fragment. The imaginary frequency resembles the lengthening of the aryl–CO_2 bond with a concomitant shortening of the aryl–copper bond. Follow-up intrinsic reaction coordinate (IRC) calculations confirmed that this transition state indeed connects the reactant with the product. For the unsubstituted phenanthroline, the aryl–CO_2 bond length is 1.90 Å and the aryl–copper bond length 2.03 Å, indicative of an early transition state. The structures are almost identical for the substituted phenanthroline derivatives.

The calculated activation barrier of $\Delta G^{\neq} = 31.4$ kcal mol^{-1} for unsubstituted phenanthroline at a reaction temperature of 170 °C appears to be realistic for a catalyst with a rather low turnover frequency.[21] The transition states for complexes with

Table 1. Selected results from the DFT calculations on the decarboxylation of 4,7-disubstituted 1,10-phenanthroline copper(I) 2-fluorobenzoates.[a]

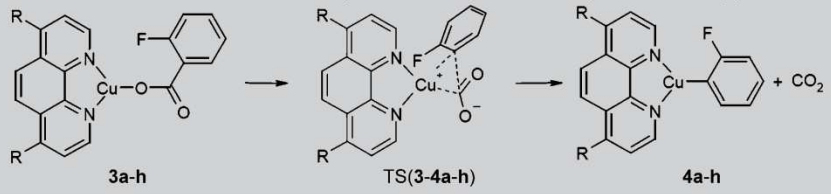

3a-h TS(3-4a-h) 4a-h

	R	ΔE^{R}_{tot}	ΔG^{R}_{298}	ΔG^{R}_{443}	d(Ar–CO_2)	d(Ar–Cu)	$\Delta E^{\neq}_{tot}$	$\Delta G^{\neq}_{298}$	$\Delta G^{\neq}_{443}$	k_{298}	k_{443}
3a→4a	H	13.9	2.1	−2.8	1.90	2.03	32.4	31.1	31.4	1.0	1.0
3b→4b	CN	13.6	1.6	−3.4	1.91	2.03	33.5	31.9	32.0	0.3	0.5
3c→4c	Ph	14.0	2.5	−2.3	1.90	2.03	32.2	30.9	31.1	1.5	1.4
3d→4d	Me	14.1	2.3	−2.6	1.89	2.03	32.1	30.9	31.2	1.5	1.3
3e→4e	SPh	14.2	2.5	−2.3	1.89	2.03	31.9	31.1	31.6	1.0	0.7
3f→4f	OPh	14.2	3.2	−1.3	1.89	2.03	31.9	31.3	31.9	0.8	0.6
3g→4g	OMe	14.2	2.8	−1.9	1.89	2.03	31.8	30.8	31.1	1.9	1.4
3h→4h	NMe_2	14.3	2.8	−2.0	1.89	2.03	31.6	30.3	30.6	3.8	2.5

[a] Computational conditions: Gaussian03;[15] B3LYP[16]/6-311+G(2d,p)[17]//B3LYP/6-31G(d)[18] for H, C, N, O, F, S; Stuttgart RSC 1997 ECP[19] for Cu; scaling factor for thermal corrections $f = 0.9804$.[20] Bond lengths are given in Å; ΔE^{R}_{tot}, ΔG^{R}_{298}, ΔG^{R}_{443}, $\Delta E^{\neq}_{tot}$, $\Delta G^{\neq}_{298}$ and $\Delta G^{\neq}_{443}$ are expressed in kcal mol^{-1}.

substituted phenanthrolines have similar energies to the starting materials, but with clear trends: Phenanthrolines with electron-donating groups led to a lowering of the activation barrier ($\Delta G^{\neq} = 31.2$ kcal mol^{-1} for 4,7-dimethyl-1,10-phenanthroline, 31.1 kcal mol^{-1} for 4,7-dimethoxy-1,10-phenanthroline and 30.6 kcal mol^{-1} for 4,7-bis(dimethylamino)-1,10-phenanthroline), while electron-withdrawing substituents had the opposite effect. The calculated reaction path for the decarboxylation of 4,7-dimethoxy-1,10-phenanthroline-ligated copper 2-fluorobenzoate is depicted in Figure 1.

The reaction rates relative to the unsubstituted copper(I)–1,10-phenanthroline-catalyzed process were calculated using the Eyring equation ($k = \frac{k_B T}{h} e^{\frac{-\Delta G^{\neq}}{RT}}$) from the free activation enthalpies. The rate enhancement achievable by using the most electron-rich ligand, bis(dimethylamino)-1,10-phenanthroline, was found to amount only to a factor of 2.5. This was a setback because such a modest improvement would hardly justify the longwinded multistep synthesis of this ligand (Table 1, **3h→4h**).

Very similar trends were evident for the decarboxylation of 4-fluorobenzoate, which we modeled as a simple example typical of a *para*-substituted and, thus, non-activated benzoic acid. The reaction pathway was again confirmed by IRC calculations. The extrusion of CO_2 was calculated to be endergonic at both room temperature and a reaction temperature of 170 °C for all phenanthroline derivatives ($\Delta G^{R}_{443} = 5$–6 kcal mol^{-1}; Table 2). The experimentally observed slow turnover of 4-substituted benzoic acids in copper(I)-catalyzed protodecarboxylations is driven by the continuous supply of thermal energy to the system as well as the continuous removal of gaseous CO_2.

In contrast to the decarboxylation of the *ortho* derivative, which proceeds via an early transition state with a short aryl–CO_2 bond (1.90 Å) and a long aryl–copper bond (2.03 Å) typical

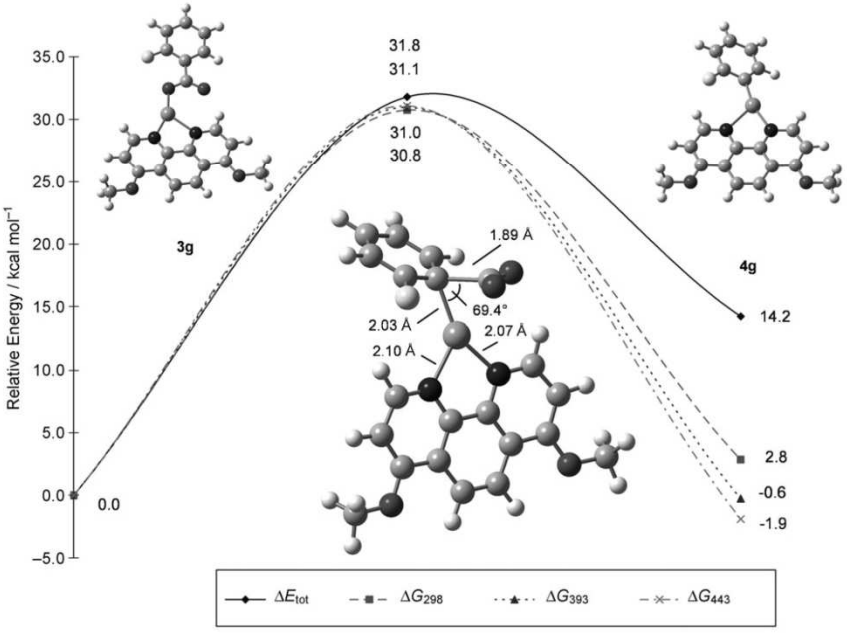

Figure 1. Calculated reaction paths for the copper(I)-catalyzed decarboxylation at several reaction temperatures.

of an exergonic reaction, the *para* derivative is associated with a late transition state with a long aryl–CO_2 bond (2.05 Å) and a short aryl–copper bond (1.98 Å), indicative of an endergonic reaction.[10a] Again, the different substituents did not have a marked effect on the bond lengths in the transition state.

The activation barriers for the protodecarboxylation of 4-fluorobenzoate were predicted to be higher by 3–4 kcal mol^{-1} than for the 2-substituted derivative, which would translate to a decrease in the reaction rate by a factor of around 24.5, which was consistent with experimental studies performed in our group.[10a] The effects of the phenanthroline substituents on the reaction rate at 170 °C were calculated to be even smaller than for the 2-substituted derivatives, all relative rates being in the range of 0.36–1.68. Again, the highest rate of decarboxylation was predicted for the phenanthroline complexes with the most electron-rich substituents.

Table 3. Protodecarboxylation with different ligands.[a]

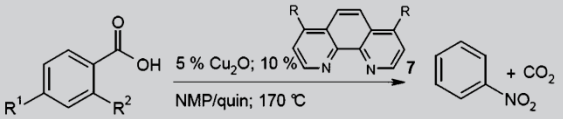

1a-b **2a**

1a R^1= H, R^2= NO_2

1b R^1= NO_2, R^2= H

Entry	R	Ligand	**1a**→**2a** [%][b]	**1b**→**2a** [%][c]
1	H	**7a**	65	43
2	CN	**7b**	64	10
3	Ph	**7c**	55	57
4	Me	**7d**	75	0
5	SPh	**7e**	57	34
6	OPh	**7f**	57	0
7	OMe	**7g**	81	6

[a] Reaction conditions: Carboxylic acid (1 mmol), Cu_2O (5 mol%), ligand (10 mol%), 3:1 NMP/quin (2 mL), 170 °C. Conversions were determined by GC analysis using *n*-tetradecane as internal standard. quin = quinoline; [b] t = 2 h; [c] t = 12 h.

Protodecarboxylation experiments using copper(I) catalysts

Overall, our calculations suggested that the introduction of electron-rich substituents at the phenanthroline ligand should lead to more active catalysts. Unfortunately, they also predicted that the original plan, which was to reach a new level of catalytic activity in decarboxylation reactions by tuning the electronic properties of the phenanthroline copper catalyst, had only limited prospects.

To verify these predictions, we performed a series of copper-catalyzed protodecarboxylation experiments using diversely substituted 1,10-phenanthrolines as ligands (Table 3). Some phenanthrolines were obtained from commercial sources, whereas others were synthesized according to literature procedures. As test substrates for the protodecarboxylation experiments, we chose nitro- rather than fluoro-substituted benzoic acids, as the low boiling point of the fluorobenzene product would have complicated the reaction procedure and determination of yields. In agreement with the DFT calculations, the protodecarboxylation of 2-nitrobenzoic acid proceeded at a much higher rate than that of 4-nitrobenzoic acid in a quinoline/*N*-methylpyrrolidone (NMP) mixture using phenanthroline–copper catalysts, being complete within 5 rather than 24 h. The addition of TEMPO (2,2,6,6-tetramethylpiperidine-*N*-oxyl, 10 mol%) as a radical trap had no influence on the yields (>90% under otherwise identical conditions) confirming that this reaction does not proceed by a radical mechanism, in excellent agreement with experiments by Cohen et al., who ruled out such a mechanism on the basis of kinetic investigations, radical trap experiments, and stereochemical studies.[8c]

Table 2. Selected results from the DFT calculations on the decarboxylation of 4,7-disubstituted 1,10-phenanthroline copper(I) 4-fluorobenzoates.[a]

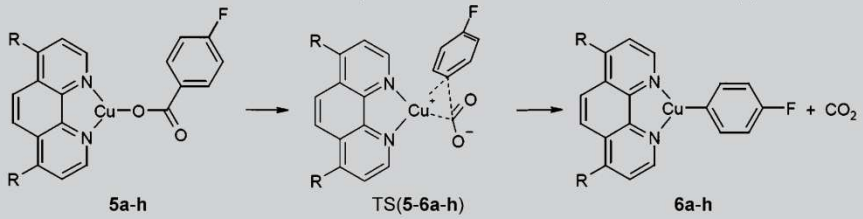

5a-h TS(**5-6a-h**) **6a-h**

	R	ΔE^{R}_{tot}	ΔG^{R}_{298}	ΔG^{R}_{443}	d(Ar–CO_2)	d(Ar–Cu)	$\Delta E^{\pm}_{tot}$	$\Delta G^{\pm}_{298}$	$\Delta G^{\pm}_{443}$	k_{298}	k_{443}
5a→**6a**	H	24.0	10.8	5.3	2.05	1.98	36.2	34.3	34.2	1.0	1.0
5b→**6b**	CN	23.9	10.8	5.2	2.05	1.98	37.4	35.2	35.1	0.2	0.4
5c→**6c**	Ph	24.2	11.2	5.7	2.04	1.98	35.9	34.2	34.3	1.1	0.9
5d→**6d**	Me	24.2	11.1	5.6	2.04	1.98	35.9	34.1	34.1	1.3	1.1
5e→**6e**	SPh	24.3	11.3	5.1	2.04	1.98	35.6	34.4	34.7	0.8	0.6
5f→**6f**	OPh	24.1	11.0	5.4	2.04	1.98	35.5	34.2	34.4	1.2	0.8
5g→**6g**	OMe	24.4	11.1	5.5	2.04	1.98	35.6	33.9	34.0	1.8	1.2
5h→**6h**	NMe_2	24.5	10.9	5.2	2.04	1.98	35.4	33.7	33.7	2.6	1.7

[a] Computational conditions: Gaussian03;[15] B3LYP[16]/6-311+G(2d,p)[17]//B3LYP/6-31G(d)[18] for H, C, N, O, F, S; Stuttgart RSC 1997 ECP[19] for Cu; scaling factor for thermal corrections f = 0.9804.[20] Bond lengths are given in Å; ΔE^{R}_{tot}, ΔG^{R}_{298}, ΔG^{R}_{443}, $\Delta E^{\pm}_{tot}$, $\Delta G^{\pm}_{298}$ and $\Delta G^{\pm}_{443}$ are expressed in kcal mol^{-1}.

The decarboxylation experiments with 2-nitrobenzoic acid were stopped at incomplete conversion after 2 h reaction time, to allow a rough comparison of catalyst turnovers. After this time, a 65% conversion was reached with unsubstituted phenanthroline. As predicted by the DFT calculations, the turnover rates for the other phenanthroline ligands were in the same range (55–81%). The highest conversion was indeed achieved with 4,7-dimethoxy-1,10-phenanthroline, the ligand with the most electron-donating substituents. Unfortunately, the clear trend predicted by the calculations could not fully be reproduced in the experiments. Despite being more electron-rich than the parent compound **7a**, the use of ligands **7d**, **7e**, **7f**, and **7g** gave lower conversions, which we attribute to their decomposition occurring in parallel to the desired reaction.

Possible decomposition reactions include proton abstraction from the methyl groups in **7d**, hydrolysis of thioether and ether groups in **7e** and **7f**, and rearrangement reactions in analogy to the thermal rearrangement of 4-alkoxypyridines to 1-alkyl-4-pyridones in **7g**.[22] These reactions would all lead to structures that are unable to act as ligands to copper. As a result, the conversions were a factor of both catalyst efficiency and ligand stability.

The stability issue became yet more significant in the decarboxylation experiments of 4-nitrobenzoic acid, which was submitted to 12 rather than 2 h of thermal stress. When the reactions were stopped after 12 h at 170 °C, only 43% conversion had occurred with the unsubstituted phenanthroline–copper complex. Most other catalysts partially or fully decomposed, as visible by precipitation of brown solids from the previously clear reaction solutions. Therefore, rather than giving the expected trend, most catalysts led to almost no conversion. In agreement with our earlier results,[10a] 4,7-diphenyl-1,10-phenanthroline was the most effective ligand for the protodecarboxylation of deactivated carboxylic acids (Table 3, entry 3). We rationalize this finding by the high thermal stability of this derivative.

These experimental results explain why it had been so difficult to rationally design new ligand generations based purely on experimental findings. In contrast, the DFT calculations allowed assessment of the catalytic activity independently from other factors such as stability.

DFT studies on the decarboxylation of silver(I) carboxylates

After having investigated the potential of copper catalysts with modified phenanthroline ligands as lead structures for low-temperature decarboxylation catalysts by both theoretical and experimental studies, we next turned our attention to complexes of other metals. Our first choice was silver, since we had observed modest reaction turnover in previous protodecarboxylation experiments using silver(I) salts as catalyst.[2d]

Upon changing the metal center from copper to silver in our calculations of the phenanthroline–metal carboxylates, we were surprised at the magnitude of improvement of the decarboxylation step, both in terms of thermodynamic and kinetic parameters. The extrusion of CO_2 from 1,10-phenanthroline–silver 2-fluorobenzoate (scheme in Table 4) is exergonic even at room temperature ($\Delta G^R_{298} = -0.5$ kcal mol^{-1}). At 120 °C (393 K), the desired operating temperature for our next-generation decarboxylation catalyst, ΔG^R_{393} amounts to −3.6 kcal mol^{-1}. In comparison to the structurally related copper complex, the calculated activation barrier at 120 °C was reduced by as much as 1.8 kcal mol^{-1} to 29.5 kcal mol^{-1}, which would translate to an appreciable rate acceleration by a factor of 9.6 (Table 4).

Considering that phenanthroline is not a common ligand for silver(I), we suspected at first that this result was an artifact caused by an unrealistic ligand environment. However, follow-up calculations in which the silver(I) was stabilized solely by NMP molecules confirmed the observed trend. The structures and energies obtained for the decarboxylation of silver 2-fluorobenzoate are depicted in Figure 2.

In the silver carboxylate complex, two NMP molecules coordinate to the silver center through their oxygen atom. Additional calculations revealed that other structures with only a single NMP ligand or with two NMP ligands coordinating in a different fashion are all higher in energy. The extrusion of CO_2 proceeds via an early transition state, in which once again the aryl residue binds both to the CO_2 carbon (2.04 Å) and the silver center (2.21 Å). Both NMP molecules remain coordinated to the silver. The imaginary frequency resembles a lengthening of the aryl–CO_2 bond with a concomitant shortening of the aryl–silver bond. After release of CO_2, an aryl–silver complex

Table 4. Relative energies for the decarboxylation of 2-fluorobenzoic acid with silver and copper catalysts.[a]

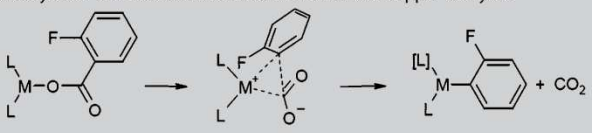

3a,**3'a**, **3'i** TS(**3-4a**,i) **4a**,**4'a**, **4'i**

	L	M	ΔE^R_{tot}	ΔG^R_{298}	ΔG^R_{393}	d(Ar–CO_2)	d(Ar–M)	$\Delta E^{\neq}_{tot}$	$\Delta G^{\neq}_{298}$	$\Delta G^{\neq}_{393}$	k_{298}	k_{393}
3a→**4a**	phen	Cu	13.9	2.1	−1.1	1.90	2.03	32.4	31.1	31.3	1.0	1.0
3'a→**4'a**	phen	Ag	11.0	−0.5	−3.6	1.92	2.22	31.4	29.6	29.5	13.7	9.6
3'i→**4'i**	NMP	Ag	13.4	−9.3	−15.5	2.04	2.21	29.2	28.8	29.2	52.6	14.9

[a] Computational conditions: Gaussian03;[15] B3LYP[16]/6-311+G(2d,p)[17]//B3LYP/6-31G(d)[18] for H, C, N, O, F, S; Stuttgart RSC 1997 ECP[19] for Cu; scaling factor for thermal corrections $f = 0.9804$.[20] Bond lengths are given in Å; ΔE^R_{tot}, ΔG^R_{298}, ΔG^R_{443}, $\Delta E^{\neq}_{tot}$, $\Delta G^{\neq}_{298}$ and $\Delta G^{\neq}_{443}$ are expressed in kcal mol^{-1}; phen = 1,10-phenanthroline.

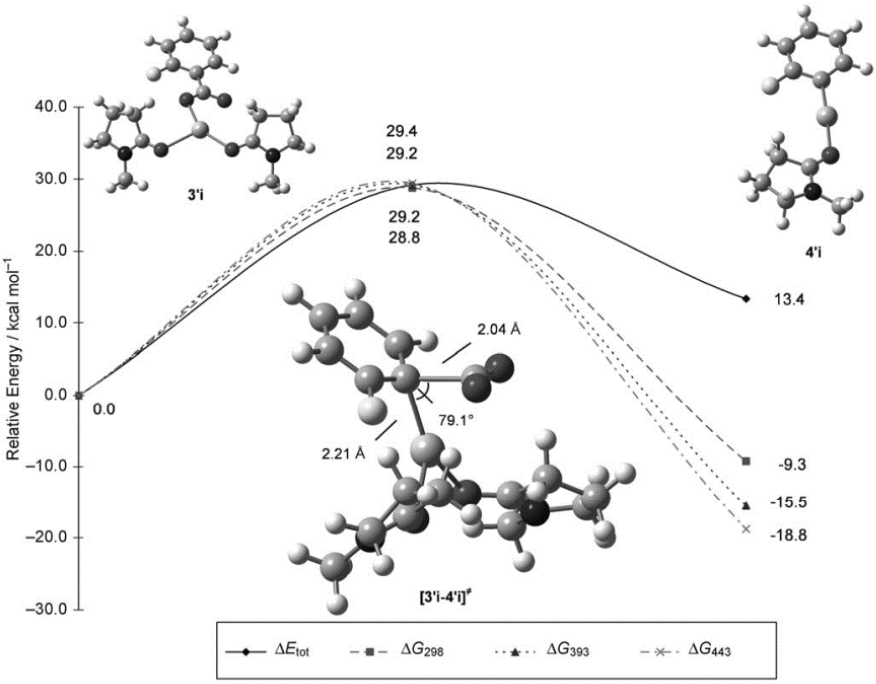

Figure 2. Calculated reaction path for the silver(I)-catalyzed decarboxylation at several reaction temperatures.

forms which is stabilized by only one molecule of NMP. This reaction pathway was confirmed by IRC studies, which revealed that one of the two NMP molecules dissociates from the silver atom in the course of the decarboxylation. The resulting aryl–silver–NMP complex has a linear structure typical for silver(I) complexes. Regardless of the starting geometry, no structure could be identified in which a second molecule of NMP would coordinate to the silver center of the aryl–silver complex.

The decarboxylation of NMP-stabilized silver 2-fluorobenzoate is more exergonic than that of the corresponding phenanthroline complex, both at room temperature ($\Delta G^{R}_{298} = -9.3$ kcal mol^{-1}) and at 120 °C (393 K; $\Delta G^{R}_{393} = -15.5$ kcal mol^{-1}). This may partially be due to the entropy increase resulting from the concomitant release of one of the NMP molecules.

The activation barrier was found to be only 29.2 kcal mol^{-1}, which would translate to a rate acceleration by a factor of 14.9 at 120 °C compared to the copper(I)–1,10-phenanthroline system. When assuming that every 10 °C reduction in temperature would result in roughly a halving of the reaction rate, this rate enhancement might indeed allow the desired reduction of the reaction temperature by at least 40 °C.

We were surprised by this result because we had repeatedly tested silver(I) catalysts in protodecarboxylations and had always found them to possess lower activities than copper catalysts. However, a closer inspection of these experiments revealed that we had mostly used 4-substituted carboxylic acids as test substrates at temperatures of at least 160 °C,[2b] and in all cases had recorded signs of catalyst decomposition. Moreover, silver(I) is an untypical mediator for protodecarboxylations[23] and, in contrast to copper(I), so far needed to be used in overstoichiometric amounts to function as a co-mediator in decarboxylative couplings.[2e,5a] Only oxidative decarboxylations are known to proceed under reasonably mild conditions, but by radical mechanisms.

To find out if complexes of non-*ortho*-substituted carboxylates would decarboxylate equally well, we next modeled the extrusion of CO_2 from silver 4-fluorobenzoate (Table 5). For the 1,10-phenanthroline complexes, the decarboxylation was found to be thermodynamically only slightly more favorable for the silver(I) than for the copper complex. Moreover, for this non-*ortho*-substituted benzoate, the activation barrier for the silver(I) complexes was in the same range as for the copper(I) complexes ($\Delta G^{\neq}_{393} = 33.2$ and $\Delta G^{\neq}_{393} = 34.2$ kcal mol^{-1}, respectively). This would translate to a much smaller rate enhancement ($k_{rel} = 3.9$ at 120 °C) than for the 2-fluorobenzoate.

For the more realistic, NMP-stabilized silver(I) carboxylate, the extrusion of CO_2 is exergonic already at room temperature ($\Delta G^{R}_{298} = -0.7$ kcal mol^{-1}). The structure of the transition state is similar to that calculated for the 2-fluorobenzoate, except that the aryl–CO_2 bond is elongated to 2.15 Å, whereas the aryl-silver bond is shortened to 2.19 Å, indicative of a late transition state. The reaction pathway was confirmed by IRC studies, which revealed that the CO_2 initially remains bound between the two NMP ligands, but as soon as the CO_2 is removed, one molecule of NMP dissociates. The free enthalpy of activation was calculated to be almost identical to that of the corresponding phenanthroline–copper(I) complex. The rate of decarboxylation at 120 °C was predicted to be lower than that of the phenanthroline–copper(I) complex. This result is intriguing because it suggests that we may have previously missed out on finding the higher activity of silver(I) complexes in our experimental studies only because we had used *para*-substituted carboxylic acids as test substrates.

Protodecarboxylation experiments using silver(I) catalysts

Motivated by the concurrence of the predictions resulting from our DFT studies and the experimental results for the copper(I) catalysts, we revived our experimental studies on silver(I)-catalyzed protodecarboxylations. Considering that silver(I) catalysts were predicted to be advantageous mainly for *ortho*-substituted derivatives, we chose the protodecarboxyla-

Table 5. Relative energies for the decarboxylation of 4-fluorobenzoic acid with silver and copper catalysts.[a]

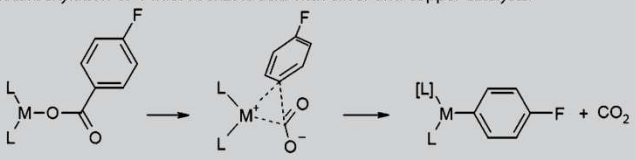

	L	M	ΔE^{R}_{tot}	ΔG^{R}_{298}	ΔG^{R}_{393}	d(Ar–CO_2)	d(Ar–M)	$\Delta E^{\neq}_{tot}$	$\Delta G^{\neq}_{298}$	$\Delta G^{\neq}_{393}$	k_{298}	k_{393}
5a→6a	phen	Cu	24.0	10.8	7.2	2.05	1.98	36.2	34.3	34.2	1.0	1.0
5′a→6′a	phen	Ag	21.1	7.8	4.1	2.10	2.18	34.9	33.2	33.2	6.2	3.9
5′i→6′i	NMP	Ag	21.7	−0.7	−6.9	2.16	2.19	35.0	34.0	34.2	1.5	1.0

[a] Computational conditions: Gaussian03;[15] B3LYP[16]/6-311+G(2d,p)[17]//B3LYP/6-31G(d)[18] for H, C, N, O; Stuttgart RSC 1997 ECP[19] for Cu and Ag; scaling factor for thermal corrections $f = 0.9804$.[20] Bond lengths are given in Å; ΔE^{R}_{tot}, ΔG^{R}_{298}, ΔG^{R}_{393}, $\Delta E^{\neq}_{tot}$, $\Delta G^{\neq}_{298}$ and $\Delta G^{\neq}_{393}$ are expressed in kcal mol^{-1}.

tion of 2-methoxybenzoic acid as a model system, on the grounds that the substrate has similar electronic properties to the 2-fluoro-derivative for which the calculations were performed, but does not decarboxylate quite as easily as the 2-nitrobenzoate. The decarboxylation product, anisole, is less volatile and more easily analyzed and isolated than fluorobenzene.

We began by comparing the rates of protodecarboxylation using either 2.5% Cu_2O–5% 1,10-phenanthroline or 2.5% Ag_2O–5% 1,10-phenanthroline as catalysts at a slightly reduced temperature of 140 °C. After 15 min, the silver(I) catalyst had already afforded 20% conversion, whereas the copper(I) catalyst had solely given trace amounts of anisole. After 2.5 h, anisole was obtained in a yield of 79% using silver(I), compared to 29% for copper(I). The comparative kinetic study is depicted in Figure 3.

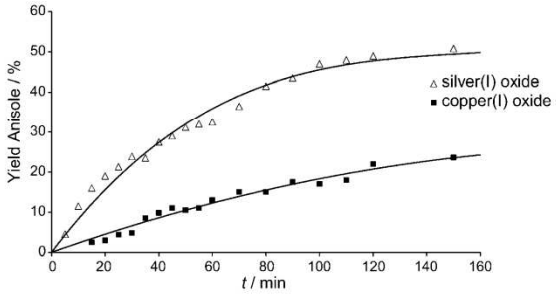

Figure 3. Protodecarboxylation of 2-methoxybenzoic acid at 140 °C using copper(I)- and silver(I)-based catalysts.

To identify the best experimental conditions, we systematically tested various combinations of metal salts, ligands, solvents, and reaction conditions. Selected results are summarized in Table 6. As previously reported,[10a] the protodecarboxylation of the deactivated 2-methoxybenzoic acid with Cu_2O–1,10-phenanthroline in a mixture of NMP and quinoline gave only 24% yield after 16 h at 170 °C in the presence of 10% of a copper(I)–1,10-phenanthroline complex (Table 6, entry 1). However, a slight modification sufficed to give a highly effective silver(I)-based catalyst.[14] The basic cosolvent quinoline, which is beneficial for the copper(I)-based protocols, turned out to have an adverse effect on the silver(I)-catalyzed reaction (Table 6, entries 2, 3).

Table 6. Optimization of the reaction conditions.[a]

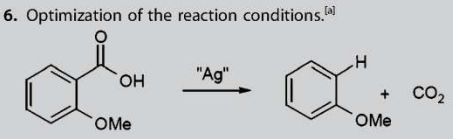

1c **2b**

Entry	Catalyst	Ligand	Additive	Solvent	T [°C]	Yield [%]
1	Cu_2O	phen	–	NMP/quin[b]	170	24
2	Ag_2O	phen	–	"	"	22
3	"	"	–	NMP	"	85
4[c]	"	"	–	"	"	85
5	"	"	–	"	120	60
6	AgO	"	–	"	"	20
7	Ag_2CO_3	"	–	"	"	39
8	AgOAc	"	–	"	"	70
9	"	–	–	"	"	24
10	"	5-NO_2-phen	–	"	"	51
11	"	4,7-Ph_2-phen	–	"	"	47
12	"	bathocuproine	–	"	"	46
13	"	2,2′-biquinoline	–	"	"	36
14	"	2,2′-bipyridine	–	"	"	46
15	"	DMAP	–	"	"	43
16	"	quin	–	"	"	21
17	"	–	K_2CO_3	"	"	98
18	"	–	Na_2CO_3	"	"	66
19	"	–	Cs_2CO_3	"	"	70
20	"	–	K_2CO_3	DMSO	"	57
21	"	–	"	DMF	"	77
22[d]	"	–	"	NMP	"	79
23	"	–	"	"	100	17
24[e]	"	–	"	"	80	60

[a] Reaction conditions: 2-Methoxybenzoic acid (1 mmol), Ag source (10 mol%; 5 mol% Cu_2O, Ag_2O, and Ag_2CO_3), additive (15 mol%), solvent (2 mL), ligand (10 mol%), 16 h. Conversions were determined by GC analysis using *n*-tetradecane as internal standard. phen = 1,10-phenanthroline, DMAP = 4-dimethylaminopyridine, quin = quinoline; [b] 3:1 NMP/quin (2 mL); [c] after 0.5 h; [d] after 8 h; [e] using 2-nitrobenzoic acid.

In pure NMP, when heating **1c** in the presence of 5 mol% of a silver(I) oxide–1,10-phenanthroline catalyst to 170 °C, 85% anisole yield was already detected after 30 min (Table 6, entries 3, 4; see also Figure 2). It turned over at such a high rate that the reaction temperature could further be reduced to 120 °C (Table 6, entry 5). Additional optimization at this temperature revealed that the counterion on the silver had a marked effect on the reaction outcome. Whereas silver acetate proved to be the silver source of choice, other silver(I) or silver(II) salts were less effective (Table 6, entries 6–8).

Having found in the DFT studies that the phenanthroline ligand was unlikely to contribute to the activity of the silver(I) catalyst, we were surprised to find that the reaction initially did not proceed well in the absence of this ligand (Table 6, entry 9). Various other basic ligands were tested, including mono- and bidentate nitrogen ligands, but the best yields were still achieved with 1,10-phenanthroline (Table 6, entries 10–16). Suspecting that the principal role of the phenanthroline was to act as a mild base, promoting the ligand exchange at the silver center rather than acting as a ligand itself, we investigated carbonate bases as additives in place of the nitrogen ligands and observed another increase in the yields (Table 6, entries 17–19). This improvement confirmed that the silver(I) catalyst indeed does not require chelating N,N ligands, but that only one equivalent of base with regard to the silver must be provided to ensure that a silver carboxylate can form, even when the silver was initially ligated to a weakly basic counterion. The best yields were achieved using AgOAc as a precatalyst in the presence of 15 mol% potassium carbonate and without added phenanthroline, in contrast to the copper protocol, whereby phenanthroline was required as a ligand even though the strongly basic copper oxide was used as a precatalyst.

NMP was confirmed to be the best choice of solvent (Table 6, entries 20, 21). After only 8 h, 79% of the product had formed already (Table 6, entry 22). Any further reduction in the temperature considerably slowed the reaction for this substrate (Table 6, entry 23). However, activated benzoic acids such as 2-nitrobenzoic acids were smoothly converted even at 80 °C—a vast improvement over the copper(I)-based methods (Table 6, entry 24).

Table 7. Scope of the transformation.[a]

Ar-COOH (**1a-x**, **8a-c**, **9-12**) —Ag or Cu catalyst system→ Ar-H (**2a-q**, **13a-b**, **14-17**) + CO_2

Ar–CO_2H	Formula	Ar–H	AgOAc: yield [%]	Cu_2O: yield [%]
8a	2-thienyl-CO_2H	**13a**	80[b]	58[b]
8b	3-Me-2-thienyl-CO_2H	**13b**	78[b]	73[b]
8c	3-thienyl-CO_2H	**13a**	36[b]	78[b,c]
9	isoquinolinic-1-acid	**14**	54[b]	85[b]
10	1-Me-pyrrole-2-CO_2H	**15**	77[b]	68[b]
1a	2-$NO_2C_6H_4$-CO_2H	**2a**	92	87
1c	2-$MeOC_6H_4$-CO_2H	**2b**	83	24
1d	2-NO_2-5-$MeOC_6H_3$-CO_2H	**2c**	88	90
1e	2,4,5-$(MeO)_3C_6H_2$-CO_2H	**2d**	43	0
1f	2,4-$(MeO)_2C_6H_3$-CO_2H	**2e**	89	0
1g	2,6-$(MeO)_2C_6H_3$-CO_2H	**2e**	87	0
1h	2-Br-C_6H_4-CO_2H	**2f**	76	0
1i	2-Br-4,5-$(MeO)_2C_6H_2$-CO_2H	**2g**	95	0
1j	2,6-$Cl_2C_6H_3$-CO_2H	**2h**	76	0
1k	2,4-$Cl_2C_6H_3$-CO_2H	**2h**	74	0
1l	2-Cl-5-$NO_2C_6H_3$-CO_2H	**2i**	85	0
1m	2-$MeS(O)_2C_6H_4$-CO_2H	**2j**	90	60
1n	2-$CF_3C_6H_4$-CO_2H	**2k**	91[b]	22[b]
1o	2-*i*PrOC(O)C_6H_4-CO_2H	**2l**	71	82
1p	2-AcC_6H_4-CO_2H	**2m**	58	87
1q	2-FC_6H_4-CO_2H	**2n**	74[b]	79[b]
11	cinnamic acid	**16**	76[b,d,e]	43[b]
12	2-thiopheneglyoxylic acid	**17**	41[b,e]	31[b]
1r	4-HOC_6H_4-CO_2H	**2o**	17	75[c]
1s	3-$MeOC_6H_4$-CO_2H	**2b**	38[b,f]	54[c]
1t	4-$MeOC_6H_4$-CO_2H	**2b**	14[b,f]	80[c]
1u	3-$NO_2C_6H_4$-CO_2H	**2a**	0	89[c]
1b	4-$NO_2C_6H_4$-CO_2H	**2a**	0	68[c]
1v	4-CNC_6H_4-CO_2H	**2p**	0	83[c]
1w	4-AcC_6H_4-CO_2H	**2m**	0	75[c]
1x	4-$AcNHC_6H_4$-CO_2H	**2q**	0	76[c]

[a] Silver-catalyzed protodecarboxylation: Carboxylic acid (2 mmol), AgOAc (10 mol%), K_2CO_3 (15 mol%), NMP (4 mL), 120 °C, 16 h, yields refer to isolated product. Copper-catalyzed protodecarboxylation: Carboxylic acid (1.00 mmol), Cu_2O (5 mol%), 1,10-phenanthroline (10 mmol%), NMP (1.5 mL), quinoline (0.5 mL), 170 °C, yields refer to isolated product; [b] GC yields determined using *n*-tetradecane as the internal standard; [c] 4,7-diphenyl-1,10-phenanthroline (0.10 mmol); [d] DMAc (4 mL) instead of NMP; [e] $T = 140$ °C; [f] $T = 160$ °C.

Scope of the silver(I)- and copper(I)-catalyzed protodecarboxylations

We explored the generality and efficiency of both the silver- and the copper-based procedures in direct comparison to each other using various aromatic and heteroaromatic carboxylic acids. The reactions with the copper catalysts were performed at a temperature of 170 °C using 1,10-phenanthroline for *ortho*-substituted derivatives, and 4,7-diphenyl-1,10-phenanthroline for the non-activated derivatives.[10a] The reactions with the silver catalyst were carried out at a temperature of only 120 °C using potassium carbonate as an additive. Selected results are summarized in Table 7.

The scope of either method is much wider than that of the Pd catalyst reported in the literature.[11] For most heterocyclic carboxylic acids and several *ortho*-substituted benzoic acids, good conversions were achieved with both systems. The selectivity was high throughout, with at most traces of side products arising from homocoupling or transesterification reactions. Lower yields were due only to incomplete conversion. For benzoic acids bearing particularly electron-rich substituents in the 2-position, the silver catalyst was superior to the copper systems. It cleanly catalyzed the decarboxylation even of benzoic acids with several alkoxy substituents, which gave no conversion with the copper systems. 2-Halobenzoic acids are another class of compounds that was converted solely by the silver catalyst. Sensitive substrates, among them cinnamic acid, gave better yields with the silver system, presumably due to the milder reaction conditions.

The main strength of the copper catalyst lies with the decarboxylation of *meta*- and *para*-substituted benzoic acids. Such compounds often gave low or no conversion with the silver-based system at 120 °C and even at 160 °C gave catalytic turnover only for particularly electron-rich *meta*- and *para*-substituted benzoic acids. For this substrate type, the copper catalyst has a much wider applicability.

The examples demonstrate how well the two methods complement each other. Almost every aromatic carboxylic acid can be decarboxylated in good yield with one of the two systems. The experimental findings are in excellent agreement with the predictions made by our DFT calculations that silver(I) catalysts should be more effective than copper systems for *ortho*-substituted benzoates, but less effective for *para*-substituted derivatives.

Conclusion and Outlook

Overall, copper(I)- and silver(I)-based decarboxylation catalysts were developed that allow the protodecarboxylation of various carboxylic acids in good yields. The advantages of the silver-based catalyst are the low reaction temperature of 120 °C, and its applicability to electron-rich benzoic acids with halo- or alkoxy substituents in the 2-position. The copper–phenanthroline system required a higher temperature of 170 °C but gave better results for non *ortho*-substituted benzoic acids.

The development of the silver catalyst was guided by DFT calculations, which predicted that silver salts of *ortho*-substituted benzoates should decarboxylate much more rapidly than the corresponding phenanthroline–copper(I) complexes. The calculations also provided an explanation as to why this higher activity of silver(I) catalysts was not observed in earlier experimental protodecarboxylation studies: We had employed model substrates unsuitable for silver(I) catalysts, and carried out the reactions at too high temperatures.

Moreover, the computational studies revealed that the activity of the copper(I) catalysts might be improved by employing phenanthrolines with electron-rich substituents. This information is very useful, as such a clear trend was not observed in the experimental studies. Under the forcing conditions of catalytic protodecarboxylations, the thermal stability of a ligand is as important for the catalyst turnover as its activating effect. The difficulty in distinguishing between these two effects when interpreting experimental results had previously complicated a rational ligand design. The challenge for future improvements will be to synthesize particularly electron-rich, yet thermally and hydrolytically stable N,N ligands, so that the theoretical findings can translate into the development of a new generation of decarboxylation catalysts.

The new silver(I)-based decarboxylation catalyst not only represents a major advance in the field of protodecarboxylations, but is likely to open up entirely new opportunities for low-temperature decarboxylative cross-couplings, as confirmed in a first test reaction, in which the silver decarboxylation catalyst was employed in combination with a standard palladium cross-coupling catalyst (Scheme 4). Using 5 mol% of silver carbonate, 3 mol% of $PdCl_2$, and 9 mol% of PPh_3, an encouraging

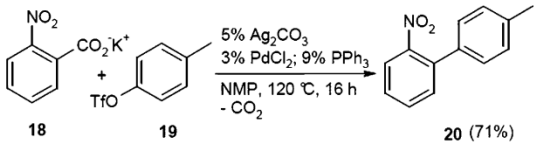

18 **19** **20** (71%)

Scheme 4. Ag/Pd-catalyzed decarboxylative biaryl synthesis.

71% yield was obtained in the cross-coupling of 2-nitrobenzoic acid with 4-tolyl triflate at a reaction temperature of only 120 °C.

With the prospect of achieving a 50 °C reduction in the reaction temperature also for decarboxylative cross-couplings, we are optimistic that after careful adjustments to the Pd cocatalyst and optimization of the reaction conditions, an effective, generally applicable, low-temperature decarboxylative cross-coupling protocol can be developed. Moreover, now that aryl nucleophiles are accessible from carboxylic acids at such low temperatures, their generation may be combined with other types of more temperature-sensitive functionalizations, such as conjugate additions and epoxide-opening reactions.

Experimental Section

General methods

Reactions were performed in oven-dried glassware under a nitrogen atmosphere containing a Teflon-coated stirrer bar and dry septum. For the exclusion of atmospheric oxygen from the reaction media, three freeze–pump–thaw cycles were performed before the reagents were mixed. Solvents were purified by standard procedures prior to use. All reactions were monitored by GC using *n*-tetradecane as an internal standard. Response factors of the products with regard to *n*-tetradecane were obtained experimentally by analyzing known quantities of the substances. GC analyses were carried out using an HP-5 capillary column (phenyl methyl siloxane, 30 m×320×0.25, 100/2.3-30-300/3) and a time program beginning with 2 min at 60 °C, followed by 30 °C min^{-1} ramp to 300 °C, then 3 min at this temp. NMR spectra were obtained on Bruker AMX 400 or on Bruker Avance 600 systems using $CDCl_3$, as solvent, with proton and carbon resonances at 400/600 MHz and 101/151 MHz, respectively. Mass spectral data were acquired on a GC-MS Saturn 2100 T (Varian).

1-Methyl-2-pyrrolidone (NMP) was dried by removing water as a toluene azeotrope. All inorganic bases were dried for 2 h in vacuo at room temperature prior to use. All other compounds are commercially available and were used without further purification. With the exception of brine, washing solutions are half saturated, unless otherwise noted.

Method A: General procedure for the silver-catalyzed protodecarboxylation of carboxylic acids

An oven-dried vessel was charged with the carboxylic acid (**1a–t, 8a–c, 9–12**; 2.00 mmol), AgOAc (33.7 mg, 0.20 mmol) and K_2CO_3 (41.5 mg, 0.30 mmol). After flushing the vessel with alternating vacuum and nitrogen purge cycles, degassed NMP (4 mL) was added by syringe and the resulting mixture was stirred at 120 °C for 16 h. Then, it was allowed to cool to room temperature, diluted

with diethyl ether (2 mL), poured into aqueous HCl (1N, 10 mL) and extracted repeatedly with diethyl ether (2 mL portions). The combined organic layers were washed with aqueous $NaHCO_3$ (4 mL) and brine (4 mL), dried over $MgSO_4$, and filtered. The corresponding arene (**2a–o, 13a–b, 14–17**) was obtained in pure form after removal of the solvent by distillation over a Vigreux column.

Method B: General procedure for the copper-catalyzed protodecarboxylation of carboxylic acids

An oven-dried vessel was charged with the carboxylic acid (**1a–d, 1m–x, 8a–c, 9–12**; 1.00 mmol), Cu_2O (7.2 mg, 0.05 mmol) and the ligand (0.10 mmol). After flushing the vessel with alternating vacuum and nitrogen purge cycles, a solution of NMP (1.5 mL) and quinoline (0.5 mL) was added by syringe. The resulting mixture was stirred at 170 °C and monitored by HPLC until full conversion, poured into aqueous HCl (5N, 2 mL) and extracted repeatedly with diethyl ether (2 mL portions). The combined organic layers were washed with aqueous $NaHCO_3$ (4 mL) and brine (4 mL), dried over $MgSO_4$, and filtered. The corresponding arene (**2a–c, 2j–q, 13a–b, 14–17**) was obtained in pure form after removal of the solvent by distillation over a Vigreux column.

Synthesis

Syntheses were carried out according to Method A unless otherwise stated.

Nitrobenzene (**2a**): Compound **2a** was prepared from 2-nitrobenzoic acid (**1a**; 334 mg, 2.00 mmol), yielding **2a** as a yellow liquid (225 mg, 92%). The spectroscopic data (NMR, GC-MS) matched those reported in the literature for nitrobenzene [CAS: 98-95-3].
Compound **2a** was also prepared according to Method B from 2-nitrobenzoic acid (**1a**; 167 mg, 1.00 mmol) and using 1,10-phenanthroline (18 mg, 0.10 mmol) in 87% yield (107 mg). In analogy, 4-nitrobenzoic acid (**1b**; 167 mg, 1.00 mmol) and 3-nitrobenzoic acid (**1u**; 167 mg, 1.00 mmol) were decarboxylated using 4,7-diphenyl-1,10-phenanthroline (33 mg, 0.10 mmol) as the ligand, to give compound **2a** in 68% (84 mg) and 89% (109 mg) yield respectively.

Anisole (**2b**): Compound **2b** was prepared from 2-methoxybenzoic acid (**1c**; 304 mg, 2.00 mmol), yielding **2b** as a colorless liquid (178 mg, 83%). The spectroscopic data (NMR, GC-MS) matched those reported in the literature for anisole [CAS: 100–66–3]. In analogy, compound **2b** was also prepared from 3-methoxybenzoic acid (**1s**; 152 mg, 1.00 mmol) and 4-methoxybenzoic acid (**1t**; 152 mg, 1.00 mmol), at a reaction temperature of 160 °C and using *n*-tetradecane (50 μL) as an internal gas chromatographic standard. The yields of compound **2b** were determined by quantitative GC to be 38% and 14% respectively, based on a response factor obtained using commercially available anisole [CAS: 100-66-3].
Compound **2b** was also prepared according to Method B from 2-methoxybenzoic acid (**1c**; 152 mg, 1.00 mmol) and 1,10-phenanthroline (18 mg, 0.10 mmol) in 24% yield (26 mg). In analogy, 3-methoxybenzoic acid (**1s**; 167 mg, 1.00 mmol) and 4-methoxybenzoic acid (**1t**; 167 mg, 1.00 mmol) were decarboxylated using 4,7-diphenyl-1,10-phenanthroline (33 mg, 0.10 mmol) as the ligand, to give compound **2b** in 54% (58 mg) and 80% (86 mg) yield, respectively.

4-Nitroanisole (**2c**): Compound **2c** was prepared from 5-methoxy-2-nitrobenzoic acid (**1d**; 394 mg, 2.00 mmol), yielding **2c** as a yellow solid (m.p. 51–53 °C, 270 mg, 88%). The spectroscopic data (NMR, GC-MS) matched those reported in the literature for 4-nitroanisole [CAS: 100-17-4].

Compound **2c** was also prepared according to Method B from 5-methoxy-2-nitrobenzoic acid (**1d**; 197 mg, 1.00 mmol) and 1,10-phenanthroline (18 mg, 0.10 mmol) in 90% yield (151 mg).

1,2,4-Trimethoxybenzene (**2d**): Compound **2d** was prepared from 2,4,5-trimethoxybenzoic acid (**1e**; 424 mg, 2.00 mmol), yielding **2d** as a colorless liquid (145 mg, 43%). The spectroscopic data (NMR, GC-MS) matched those reported in the literature for 1,2,4-trimethoxybenzene [CAS: 135-77-3].

1,3-dimethoxybenzene (**2e**): Compound **2e** was prepared from 2,4-dimethoxybenzoic acid (**1f**; 364 mg, 2.00 mmol), yielding **2e** as a colorless liquid (246 mg, 89%). The spectroscopic data (NMR, GC-MS) matched those reported in the literature for 1,3-dimethoxybenzene [CAS: 151-10-0]. Compound **2e** was also prepared from 2,6-dimethoxybenzoic acid (**1g**; 364 mg, 2.00 mmol) to give compound **2e** in 87% yield (239 mg).

Bromobenzene (**2f**): Compound **2f** was prepared from 2-bromobenzoic acid (**1h**; 402 mg, 2.00 mmol), yielding **2f** as a colorless liquid (237 mg, 76%). The spectroscopic data (NMR, GC-MS) matched those reported in the literature for bromobenzene [CAS: 108-86-1].

4-Bromoveratrole (**2g**): Compound **2g** was prepared from 2-bromo-4,5-dimethoxybenzoic acid (**1i**; 522 mg, 2.00 mmol), yielding **2g** as a colorless liquid (412 mg, 95%). The spectroscopic data (NMR, GC-MS) matched those reported in the literature for 4-bromoveratrole [CAS: 2859-78-1].

1,3-Dichlorobenzene (**2h**): Compound **2h** was prepared from 2,6-dichlorobenzoic acid (**1j**; 382 mg, 2.00 mmol), yielding **2h** as a colorless liquid (223 mg, 76%). The spectroscopic data (NMR, GC-MS) matched those reported in the literature for 1,3-dichlorobenzene [CAS: 541-73-1]. Compound **2h** was also prepared from 2,4-dichlorobenzoic acid (**1k**; 328 mg, 2.00 mmol) to give compound **2h** in 74% yield (218 mg).

1-Chloro-4-nitrobenzene (**2i**): Compound **2i** was prepared from 2-chloro-5-nitrobenzoic acid (**1l**; 403 mg, 2.00 mmol), yielding **2i** as a colorless liquid (268 mg, 85%). The spectroscopic data (NMR, GC-MS) matched those reported in the literature for 1-chloro-4-nitrobenzene [CAS: 100-00-5].

Methyl phenyl sulfone (**2j**): Compound **2j** was prepared from 2-(methylsulfonyl)benzoic acid (**1m**; 400 mg, 2.00 mmol), yielding **2j** as a white solid (m.p. 87–88 °C, 280 mg, 90%). The spectroscopic data (NMR, GC-MS) matched those reported in the literature for methyl phenyl sulfone [CAS: 3112-85-4].

Compound **2j** was also prepared according to Method B from 2-(methylsulfonyl)benzoic acid (**1m**; 200 mg, 1.00 mmol) and 1,10-phenanthroline (18 mg, 0.10 mmol) in 60% yield (94 mg).

Trifluoromethylbenzene (**2k**): Compound **2k** was prepared from 2-(trifluoromethyl)benzoic acid (**1n**; 190 mg, 1.00 mmol) and using *n*-tetradecane (50 μL) as an internal gas chromatographic standard. The yield of compound **2k** was determined by quantitative GC to be 91%, based on a response factor obtained using commercial trifluoromethylbenzene [CAS: 98-08-8].

Compound **2k** was also prepared according to Method B from 2-(trifluoromethyl)benzoic acid (**1n**; 190 mg, 1.00 mmol), 1,10-phenanthroline (18 mg, 0.10 mmol) and using *n*-tetradecane (50 μL) as an internal gas chromatographic standard. The yield of compound **2k** was determined by quantitative GC to be 22%.

Isopropyl benzoate (**2l**): Compound **2l** was prepared from 2-(isopropyloxycarbonyl)benzoic acid (**1o**; 416 mg, 2.00 mmol), yielding **2l** as a yellow liquid (234 mg, 71%). The spectroscopic data (NMR, GC-MS) matched those reported in the literature for isopropyl benzoate [CAS: 939-48-0].
Compound **2l** was also prepared according to Method B from 2-(isopropyloxycarbonyl)benzoic acid (**1o**; 208 mg, 1.00 mmol) and 1,10-phenanthroline (18 mg, 0.10 mmol) in 82% yield (134 mg).

Acetophenone (**2m**): Compound **2m** was prepared from 2-acetylbenzoic acid (**1p**; 328 mg, 2.00 mmol), yielding **2m** as a yellow liquid (139 mg, 58%). The spectroscopic data (NMR, GC-MS) matched those reported in the literature for acetophenone [CAS: 98-86-2].
Compound **2m** was also prepared according to Method B from 2-acetylbenzoic acid (**1p**; 164 mg, 1.00 mmol) and 1,10-phenanthroline (18 mg, 0.10 mmol) in 87% yield (104 mg). In analogy, 4-acetylbenzoic acid (**1w**; 164 mg, 1.00 mmol) was decarboxylated using 4,7-diphenyl-1,10-phenanthroline (33 mg, 0.10 mmol) to give compound **2m** in 75% yield (90 mg).

Fluorobenzene (**2n**): Compound **2n** was prepared from 2-fluorobenzoic acid (**1q**; 140 mg, 1.00 mmol) and using *n*-tetradecane (50 μL) as an internal gas chromatographic standard. The yield of compound **2n** was determined by quantitative GC to be 74%, based on a response factor obtained using commercial fluorobenzene [CAS: 462-06-6].
Compound **2n** was also prepared according to Method B from 2-fluorobenzoic acid (**1q**; 140 mg, 1.00 mmol), 1,10-phenanthroline (18 mg, 0.10 mmol) and using *n*-tetradecane (50 μL) as an internal gas chromatographic standard. The yield of compound **2n** was determined by quantitative GC to be 79%.

Phenol (**2o**): Compound **2o** was prepared from 4-hydroxybenzoic acid (**1r**; 276 mg, 2.00 mmol), yielding **2o** as a yellow liquid (32 mg, 17%). The spectroscopic data (NMR, GC-MS) matched those reported in the literature for phenol [CAS: 108-95-2].
Compound **2o** was also prepared according to Method B from 4-hydroxybenzoic acid (**1u**; 138 mg, 1.00 mmol) and 4,7-diphenyl-1,10-phenanthroline (33 mg, 0.10 mmol) in 75% yield (70 mg).

Thiophene (**13a**): Compound **13a** was prepared from thiophene-2-carboxylic acid (**8a**; 128 mg, 1.00 mmol) and using *n*-tetradecane (50 μL) as an internal gas chromatographic standard. The yield of compound **13a** was determined by quantitative GC to be 80%, based on a response factor obtained using commercial thiophene [CAS: 110-02-1]. Compound **13a** was also prepared from thiophene-3-carboxylic acid (**8c**; 128 mg, 1.00 mmol) to give compound **13a** in 36% yield.
Compound **13a** was also prepared according to Method B from thiophene-2-carboxylic acid (**8a**; 128 mg, 1.00 mmol), 1,10-phenanthroline (18 mg, 0.10 mmol) and using *n*-tetradecane (50 μL) as an internal gas chromatographic standard. The yield of compound **13a** was determined by quantitative GC to be 58%. In analogy, thiophene-3-carboxylic acid (**8c**; 128 mg, 1.00 mmol) was decarboxylated using 4,7-diphenyl-1,10-phenanthroline (33 mg, 0.10 mmol) in 78% yield.

3-Methylthiophene (**13b**): Compound **13b** was prepared from 3-methylthiophene-2-carboxylic acid (**8b**; 142 mg, 1.00 mmol) and using *n*-tetradecane (50 μL) as an internal gas chromatographic standard. The yield of compound **13b** was determined by quantitative GC to be 78%, based on a response factor obtained using commercial 3-methylthiophene [CAS: 616-44-4].
Compound **13b** was also prepared according to Method B from 3-methylthiophene-2-carboxylic acid (**8b**; 142 mg, 1.00 mmol), 1,10-phenanthroline (18 mg, 0.10 mmol) and using *n*-tetradecane (50 μL) as an internal gas chromatographic standard. The yield of compound **13b** was determined by quantitative GC to be 73%.

Isoquinoline (**14**): Compound **14** was prepared from isoquinoline-1-carboxylic acid (**9**; 173 mg, 1.00 mmol) and using *n*-tetradecane (50 μL) as an internal gas chromatographic standard. The yield of compound **14** was determined by quantitative GC to be 54%, based on a response factor obtained using commercial isoquinoline [CAS: 119-65-3].

Compound **14** was also prepared according to Method B from isoquinoline-1-carboxylic acid (**9**; 173 mg, 1.00 mmol), 1,10-phenanthroline (18 mg, 0.10 mmol) and using *n*-tetradecane (50 μL) as an internal gas chromatographic standard. The yield of compound **14** was determined by quantitative GC to be 85%.

1-Methyl-1*H*-pyrrole (**15**): Compound **15** was prepared from 1-methyl-1H-pyrrole-2-carboxylic acid (**10**; 125 mg, 1.00 mmol) and using *n*-tetradecane (50 μL) as an internal gas chromatographic standard. The yield of compound **15** was determined by quantitative GC to be 77%, based on a response factor obtained using commercial 1-methyl-1H-pyrrole [CAS: 96-54-8].

Compound **15** was also prepared according to Method B from 1-methyl-1H-pyrrole-2-carboxylic acid (**10**; 173 mg, 1.00 mmol), 1,10-phenanthroline (18 mg, 0.10 mmol) and using *n*-tetradecane (50 μL) as an internal gas chromatographic standard. The yield of compound **15** was determined by quantitative GC to be 68%.

Styrene (**16**): Compound **16** was prepared from cinnamic acid (**11**; 148 mg, 1.00 mmol) in DMAc (4 mL) at 140 °C, and using *n*-tetradecane (50 μL) as an internal gas chromatographic standard. The yield of compound **16** was determined by quantitative GC to be 76%, based on a response factor obtained using commercial styrene [CAS: 100-42-5].

Compound **16** was also prepared according to Method B from cinnamic acid (**11**; 148 mg, 1.00 mmol), 1,10-phenanthroline (18 mg, 0.10 mmol) and using *n*-tetradecane (50 μL) as an internal gas chromatographic standard. The yield of compound **16** was determined by quantitative GC to be 43%.

2-Thiophenecarboxaldehyde (**17**): Compound **17** was prepared from 2-thiopheneglyoxylic acid (**12**; 156 mg, 1.00 mmol) and using *n*-tetradecane (50 μL) as an internal gas chromatographic standard. The yield of compound **17** was determined by quantitative GC to be 41%, based on a response factor obtained using commercial 2-thiophenecarboxaldehyde [CAS: 98-03-3].

Compound **17** was also prepared according to Method B from 2-thiopheneglyoxylic acid (**12**; 156 mg, 1.00 mmol), 1,10-phenanthroline (18 mg, 0.10 mmol) and using *n*-tetradecane (50 μL) as an internal gas chromatographic standard. The yield of compound **17** was determined by quantitative GC to be 31%.

Benzonitrile (**2p**): Compound **2p** was prepared according to Method B from 4-cyanobenzoic acid (**1v**; 147 mg, 1.00 mmol) and 4,7-diphenyl-1,10-phenanthroline (33 mg, 0.10 mmol), yielding **2p** as a colorless liquid (86 mg, 83%). The spectroscopic data (NMR, GC-MS) matched those reported in the literature for benzonitrile [CAS: 100-47-0].

Acetanilide (**2q**): Compound **2q** was prepared from 4-acetamidobenzoic acid (**1x**; 179 mg, 1.00 mmol) and 4,7-diphenyl-1,10-phenanthroline (3c; 33 mg, 0.10 mmol) following the general procedure, yielding **2q** as a white solid (103 mg, 76%). The spectroscopic data (NMR, GC-MS) matched those reported in the literature for acetanilide [CAS: 103-84-4].

Synthesis of ligands

4,7-Dichloro-1,10-phenanthroline [CAS: 5394-23-0] was synthesized using the literature procedure.[24]

4,7-Dicyano-1,10-phenanthroline (**7b**): To 4,7-dichloro-1,10-phenanthroline (250 mg, 1.00 mmol) was added a solution of sodium sulfite (630 mg, 5.00 mmol) in water (10 mL) and the mixture was heated at 100 °C until a clear solution was observed. The resulting solution was acidified to pH 4 by addition of 1 N HCl and stored in the refrigerator. The white solid that formed was removed by filtration and dried. After reducing the filtrate to 5 mL, another crop of white solid was obtained to afford 4,7-disulfonato-1,10-phenanthroline (339 mg, 99%). ^{1}H NMR (400 MHz, [D$_6$]DMSO): δ = 9.06 (d, J = 4.3 Hz, 2H), 8.80 (s, 2H), 8.05 (d, J = 4.3 Hz, 2H), ^{13}C NMR (151 MHz, [D$_6$]DMSO): δ = 150.4, 147.4, 142.3, 126.3, 123.8, 123.3 ppm. IR: $\tilde{\nu}$ = 1230, 1205, 1045 cm^{-1} (s, SO_3).

4,7-Disulfonato-1,10-phenathroline (340 mg, 1.00 mmol) and potassium cyanide (650 mg, 10.0 mmol) were dried at 100 °C for 2 h under vacuum. Both solids were ground to a fine powder and thoroughly mixed in the process. The mixture of solids was heated with a Bunsen burner until melting took place. The resultant tarry mixture was extracted with aqueous K_2CO_3-solution (50%, 20 mL) and chloroform (20 mL). The organic layer was dried ($MgSO_4$), filtered, and the solvent evaporated in vacuo to afford **7b** as a yellow solid (30 mg, 13%). ^{1}H NMR (200 MHz, $CDCl_3$): δ = 9.37 (d, J = 4.4 Hz, 2H), 8.39 (s, 2H), 8.03 (d, J = 4.4 Hz, 2H), ^{13}C NMR (50 MHz, $CDCl_3$): δ = 150.7, 146.0, 127.3, 126.9, 125.8, 119.4, 114.9 ppm. IR: $\tilde{\nu}$ = 2233 cm^{-1} (s, CN).

4,7-dimethyl-1,10-phenanthroline (**7d**): Compound **7d** was synthesized using a modified procedure by Butt and Topsom[25] starting from freshly sublimed *o*-phenylenediamine (3.25 g, 30.0 mmol) and methyl vinylketone (12.2 mL, 150 mmol) to afford **7d** as an orange solid (m.p. 198 °C, 312 mg, 5%). The spectroscopic data (NMR) matched those reported in the literature for 4,7-dimethyl-1,10-phenanthroline [CAS: 3248-05-3].

4,7-Bis(phenylthio)-1,10-phenanthroline (**7e**): Under an atmosphere of nitrogen, thiophenol (3 mL, 29.2 mmol) was added slowly to 4,7-dichloro-1,10-phenanthroline (250 mg, 1.00 mmol) and finely powdered potassium hydroxide (280 mg, 5.00 mmol), the resulting mixture was heated at 100 °C for 16 h. After cooling to room temperature, aqueous KOH (30% w/w, 10 mL) was added and the precipitated product was filtered and washed with aqueous KOH (30%, 20 mL) and water (25 mL). Recrystallization from methanol/diethyl ether afforded **7e** as a pale yellow solid (m.p. 211 °C (decomp.), 330 mg, 83%). 1H NMR (400 MHz, [D$_6$]DMSO): δ = 8.83 (d, J = 4.8 Hz, 2H), 8.30 (s, 2H), 7.66 (d, J = 2.4 Hz, 4H), 7.58 (d, J = 2.4 Hz, 6H), 7.05 ppm (d, J = 4.8 Hz, 2H).

4,7-Diphenoxy-1,10-phenanthroline (**7f**): 4,7-Dichloro-1,10-phenanthroline (250 mg, 1.00 mmol), finely powdered potassium hydroxide (280 mg, 5.00 mmol) and phenol (4.71 g, 50.0 mmol) were heated at 100 °C for 16 h. After cooling to room temperature, aqueous KOH (30%, 10 mL) was added and the precipitated product was filtered, washed with aqueous KOH (30%, 20 mL) and water (25 mL). Recrystallization from chloroform/hexane afforded **7f** as a light tan solid (m.p. 181 °C, 316 mg, 87%). The spectroscopic data (NMR) matched those reported in the literature for 4,7-diphenoxy-1,10-phenanthroline [CAS: 95943-00-3].

4,7-Dimethoxy-1,10-phenanthroline (**7g**): 4,7-Dichloro-1,10-phenanthroline (250 mg, 1.00 mmol) and potassium methoxide (600 mg, 8.50 mmol) were heated in methanol (5 mL) at 80 °C for 24 h. After cooling to room temperature, crystallization with diethyl ether afforded **7g** as a white solid (m.p. 208 °C, 225 mg, 93%). The spectroscopic data (NMR) matched those reported in the literature for 4,7-dimethoxy-1,10-phenanthroline [CAS: 92149-07-0].

Acknowledgements

We thank W. R. Thiel and C. van Wüllen for help with the DFT calculations, the Deutsche Forschungsgemeinschaft, Saltigo GmbH, and NanoKat for funding, and the A. v. Humboldt Foundation for a scholarship to N. R.

Keywords: arenes · carboxylic acids · catalysis · copper · decarboxylation · silver

[1] a) L. J. Gooßen, N. Rodríguez, K. Gooßen, *Angew. Chem.* **2008**, *120*, 3144–3164; *Angew. Chem. Int. Ed.* **2008**, *47*, 3100–3120; b) L. J. Gooßen, K. Gooßen, N. Rodríguez, M. Blanchot, C. Linder, B. Zimmermann, *Pure Appl. Chem.* **2008**, *80*, 1725–1731.

[2] a) C. Peschko, C. Winklhofer, W. Steglich, *Chem. Eur. J.* **2000**, *6*, 1147–1152; b) L. J. Gooßen, G. Deng, L. M. Levy, *Science* **2006**, *313*, 662–664; c) P. Forgione, M. C. Brochu, M. St-Onge, K. H. Thesen, M. D. Bailey, F. Bilodeau, *J. Am. Chem. Soc.* **2006**, *128*, 11350–11351; d) L. J. Gooßen, N. Rodríguez, B. Melzer, C. Linder, G. Deng, L. M. Levy, *J. Am. Chem. Soc.* **2007**, *129*, 4824–4833; e) J.-M. Becht, C. Catala, C. Le Drian, A. Wagner, *Org. Lett.* **2007**, *9*, 1781–1783; f) L. J. Gooßen, F. Rudolphi, C. Oppel, N. Rodríguez, *Angew. Chem.* **2008**, *120*, 3085–3088; *Angew. Chem. Int. Ed.* **2008**, *47*, 3043–3045; g) L. J. Gooßen, B. Zimmermann, T. Knauber, *Angew. Chem.* **2008**, *120*, 7211–7214; *Angew. Chem. Int. Ed.* **2008**, *47*, 7103–7106; h) L. J. Gooßen, N. Rodríguez, C. Linder, *J. Am. Chem. Soc.* **2008**, *130*, 15248–15249; i) J. Moon, M. Jeong, H. Nam, J. Ju, J. H. Moon, H. M. Jung, S. Lee, *Org. Lett.* **2008**, *10*, 945–948; j) L. J. Gooßen, C. Linder, N. Rodríguez, P. P. Lange, *Chem. Eur. J.* **2009**, *15*, 9336–9349; k) R. Shang, Y. Fu, J. B. Li, S. L. Zhang, Q. X. Guo, L. Liu, *J. Am. Chem. Soc.* **2009**, *131*, 5738–5739; l) R. Shang, Y. Fu, Y. Wang, Q. Xu, H.-Z. L. Liu, *Angew. Chem.* **2009**, *121*, 9514–9518; *Angew. Chem. Int. Ed.* **2009**, *48*, 9350–9354.

[3] a) A. G. Myers, D. Tanaka, M. R. Mannion, *J. Am. Chem. Soc.* **2002**, *124*, 11250–11251; b) A. Maehara, H. Tsurugi, T. Satoh, M. Miura, *Org. Lett.* **2008**, *10*, 1159–1162; c) P. Hu, J. Kan, W. Su, M. Hong, *Org. Lett.* **2009**, *11*, 2341–2344.

[4] Z. Duan, S. Ranjit, P. Zhang, X. Liu, *Chem. Eur. J.* **2009**, *15*, 3666–3669.

[5] a) A. Voutchkova, A. Coplin, N. E. Leadbeater, R. H. Crabtree, *Chem. Commun.* **2008**, 6312–6314; b) C. Wang, I. Piel, F. Glorius, *J. Am. Chem. Soc.* **2009**, *131*, 4194–4195.

[6] D. K. Rayabarapu, J. A. Tunge, *J. Am. Chem. Soc.* **2005**, *127*, 13510–13511.

[7] Z.-M. Sun, P. Zhao, *Angew. Chem.* **2009**, *121*, 6854–6858; *Angew. Chem. Int. Ed.* **2009**, *48*, 6726–6730.

[8] a) A. F. Shepard, N. R. Winslow, J. R. Johnson, *J. Am. Chem. Soc.* **1930**, *52*, 2083–2090; b) M. Nilsson, *Acta Chem. Scand.* **1966**, *20*, 423–426; c) T. Cohen, R. A. Schambach, *J. Am. Chem. Soc.* **1970**, *92*, 3189–3190; d) A. Cairncross, J. R. Roland, R. M. Henderson, W. F. Shepard, *J. Am. Chem. Soc.* **1970**, *92*, 3187–3189.

[9] H. Gilman, G. F. Wright, *J. Am. Chem. Soc.* **1933**, *55*, 3302–3314.

[10] a) L. J. Gooßen, W. R. Thiel, N. Rodríguez, C. Linder, B. Melzer, *Adv. Synth. Catal.* **2007**, *349*, 2241–2246; b) L. J. Gooßen, F. Manjolinho, B. A. Khan, N. Rodríguez, *J. Org. Chem.* **2009**, *74*, 2620–2623.

[11] J. S. Dickstein, C. A. Mulrooney, E. M. O'Brien, B. J. Morgan, M. C. Kozlowski, *Org. Lett.* **2007**, *9*, 2441–2444.

[12] R. W. Hay, M. J. Taylor, *Chem. Commun.* **1966**, 525b.

[13] K. Chuchev, J. J. BelBruno, *THEOCHEM* **2007**, *807*, 1.

[14] L. J. Gooßen, C. Linder, N. Rodriguez, P. P. Lange, A. Fromm, *ChemComm* **2009**, 7173–7175.

[15] *Gaussian 03*, Revision E.01, Gaussian, Inc., Wallingford CT, **2004**; for full citation see the Supporting Information.

[16] a) C. Lee, W. Yang, R. G. Parr, *Phys. Rev. B* **1988**, *37*, 785–789; b) A. D. Becke, *J. Chem. Phys.* **1993**, *98*, 5648–5652; c) P. J. Stephens, J. F. Devlin, C. F. Chabalowski, M. J. Frisch, *J. Phys. Chem.* **1994**, *98*, 11623–11627.
[17] R. Krishnan, J. S. Binkley, R. Seeger, J. A. Pople, *J. Chem. Phys.* **1980**, *72*, 650–654.
[18] P. C. Hariharan, J. A. Pople, *Theor. Chim. Acta* **1973**, *28*, 213–222.
[19] a) M. Dolg, U. Wedig, H. Stoll, H. Preuss, *J. Chem. Phys.* **1987**, *86*, 866–872; b) D. Andrae, U. Häußermann, M. Dolg, H. Stoll, H. Preuss, *Theor. Chim. Acta* **1990**, *77*, 123–141.
[20] M. W. Wong, *Chem. Phys. Lett.* **1996**, *256*, 391–399.
[21] a) N. R. Gunawardena, T. B. Brill, *J. Phys. Chem. A* **2001**, *105*, 1876–1881; b) J. Li, T. B. Brill, *J. Phys. Chem. A* **2003**, *107*, 2667–2673; c) M. Staikova, M. Oh, D. J. Donaldson, *J. Phys. Chem. A* **2005**, *109*, 597–602.
[22] a) L. Haitinger, A. Lieben, *Chem. Ber.* **1885**, *18*, 929–931; b) F. You, R. J. Tweig, *Tetrahedron Lett.* **1999**, *40*, 8759–8762.
[23] For related silver(I)-mediated protodecarboxylations see: a) J. Chodowska-Palicka and M. Nilsson, *Acta Chem. Scand.* **1970**, *24*, 3353–3361; b) J. M. Anderson, J. K. Kochi, *J. Am. Chem. Soc.* **1970**, *92*, 1651–1659; c) J. M. Anderson, J. K. Kochi, *J. Org. Chem.* **1970**, *35*, 986–989.
[24] G. I. Graf, D. Hastreiter, L. E. da Silva; R. A. Rebelo; A. G. Montalban, A. McKillop, *Tetrahedron* **2002**, *58*, 9095–9100; R. A. Rebelo; A. G. Montalban, A. McKillop, *Tetrahedron* **2002**, *58*, 9095–9100.
[25] G. Butt, R. D. Topsom, *J. Heterocyclic Chem.* **1981**, *18*, 641.

Received: October 30, 2009
Revised: December 6, 2009
Published online on March 18, 2010

Nach Erreichen des Ziels, Katalysatoren für Protodecarboxylierungsreaktionen zu entwickeln, die eine Absenkung der Reaktionstemperatur auf 120 °C ermöglichen, gelang es anschließend Gooßen et al., diese neuen Silber-basierten Decarboxylierungskatalysatoren in der decarboxylierenden Kreuzkupplung für die Biarylsynthese anzuwenden.[58] Aufgrund der sehr hohen Affinität von Silberverbindungen zu Halogenidionen müssten bei der decarboxylierenden Kreuzkupplung von Arylhalogeniden stöchiometrische Mengen an Silber eingesetzt werden. Da Triflatanionen kaum an Silber koordinieren, bildeten vorhergehende Arbeiten zur Kupplung von Aryltriflaten[1,66] den Ausgangspunkt für den Einsatz von Silber-basierten Decarboxylierungsmediatoren in katalytischen Mengen. Basierend auf den Ergebnissen zur Silber-katalysierten Protodecarboxylierung war es nun möglich, eine Ag/Pd-katalysierte decarboxylierende Kreuzkupplung von Aryltriflaten **3.1-8** mit aromatischen Carboxylaten **3.1-7** zu entwickeln, die bei einer Reaktionstemperatur von lediglich 130 °C abläuft (Schema 6). Die große Anwendungsbreite dieser Reaktion wurde an 26 Beispielen verdeutlicht.

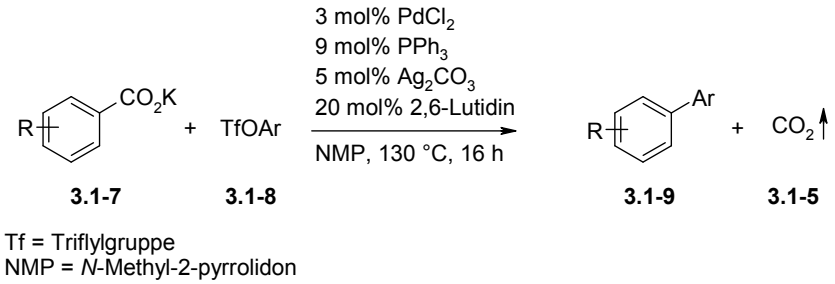

Schema 6. *Ag/Pd-katalysierte decarboxylierende Kreuzkupplung bei 130 °C.*

3.2 Der Mechanismus der Cu/Pd-katalysierten decarboxylierenden Kreuzkupplung

Nachdem es gelungen war, die Reaktionstemperatur der decarboxylierenden Kreuzkupplungen mit Hilfe eines Ag/Pd-basierten Katalysatorsystemen deutlich abzusenken, bestand das nächste Ziel in der Entwicklung eines Cu/Pd-basierten Katalysatorsystems, welches die Reaktion bei ähnlich niedrigen Temperaturen ermöglicht.

Durch experimentelle Beobachtungen ist bekannt, dass bei den ersten Cu/Pd-katalysierten decarboxylierenden Kreuzkupplungen von aromatischen Carboxylaten mit Arylhalogeniden, die bei 160 °C abliefen, der Decarboxylierungsschritt geschwindigkeitsbestimmend war.[55] In Protodecarboxylierungsreaktionen ermöglichten weiterentwickelte Decarboxylierungs-

katalysatoren bereits Temperaturen von lediglich 100–120 °C.[67,68] In der Kreuzkupplung mit Aryltriflaten und Arylmesylaten sind jedoch weiterhin Temperaturen von 150 °C erforderlich.[1,66,69,70] Daraus lässt sich folgern, dass der Decarboxylierungsschritt nicht notwendigerweise geschwindigkeitsbestimmend ist.

Um nun durch rationale Katalysatorentwicklung Leitstrukturen für effizientere Katalysatorsysteme zu ermitteln, war zunächst ein detailliertes Verständnis des komplexen Reaktionsmechanismus von zentraler Bedeutung. Daher wurde der in Schema 7 dargestellte Katalysezyklus der Cu/Pd-katalysierten decarboxylierenden Kreuzkupplungen eingehend mit Hilfe von DFT-Rechnungen untersucht. Dies wurde für 2- und 4-Fluorbenzoat durchgeführt.

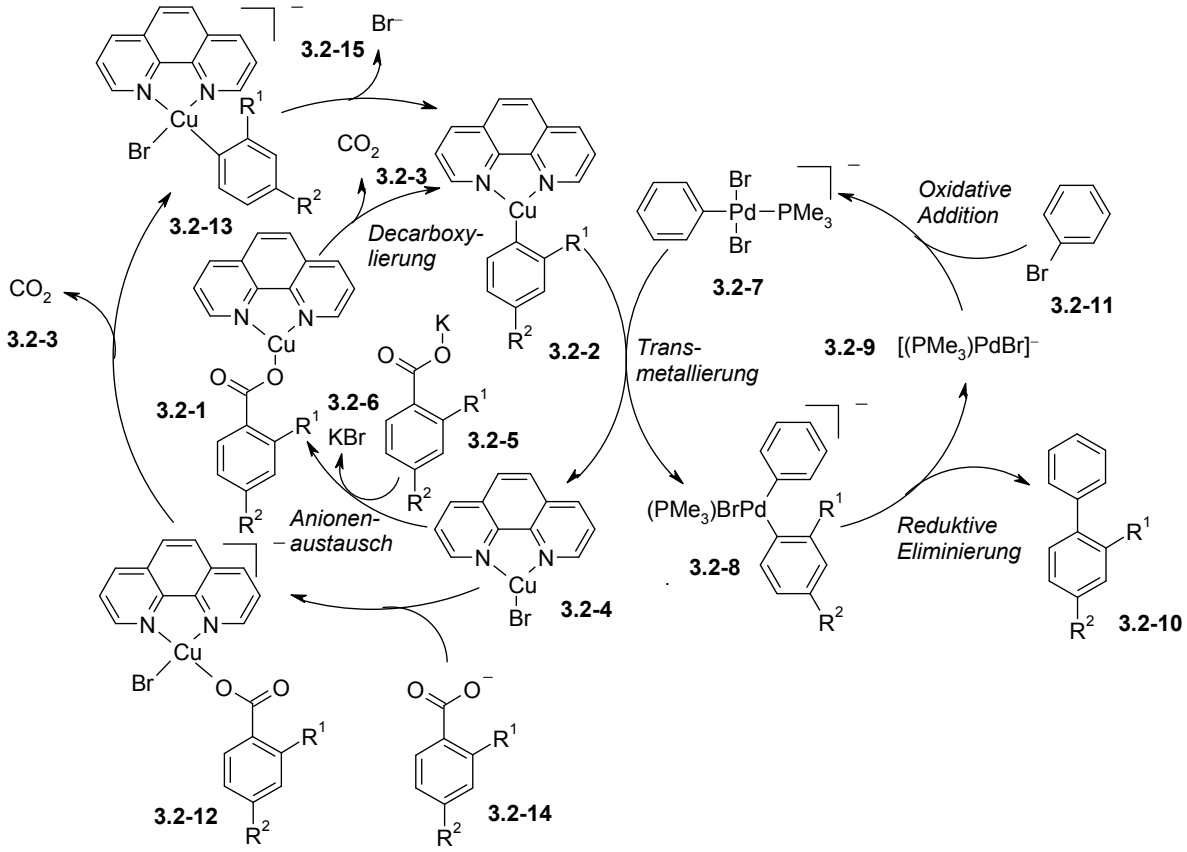

Schema 7. *Berechnete Katalysezyklen der decarboxylierenden Kreuzkupplung*.

Die Ergebnisse der DFT-Rechnungen ergaben, dass in Abhängigkeit des aromatischen Carboxylats die Decarboxylierung oder die Transmetallierung geschwindigkeitsbestimmend sein kann. Bemerkenswert ist, dass in der Transmetallierung zunächst die Bildung eines bimetallischen Cu−Pd-Addukts erforderlich ist. Dieser Teilschritt ist zwar leicht exotherm, jedoch stark endergonisch, so dass er einen Großteil zur Gesamtaktivierungsbarriere beiträgt.

Aus diesen Ergebnissen ließ sich schlussfolgern, dass der Einsatz von verbrückenden, bidentaten Liganden, welche dazu fähig sind, die beiden Katalysatormetalle in räumliche Nähe zueinander zu bringen, die Reaktion begünstigen sollte. Tatsächlich war es möglich, durch Verwendung eines *P*,*N*-Liganden eine Cu/Pd-katalysierte decarboxylierende Kreuzkupplung von aromatischen Carboxylaten **3.2-5** mit Aryltriflaten **3.2-16** bei nur 100 °C zu entwickeln (Schema 8), was einer Absenkung der Reaktionstemperatur um 50 °C entspricht.

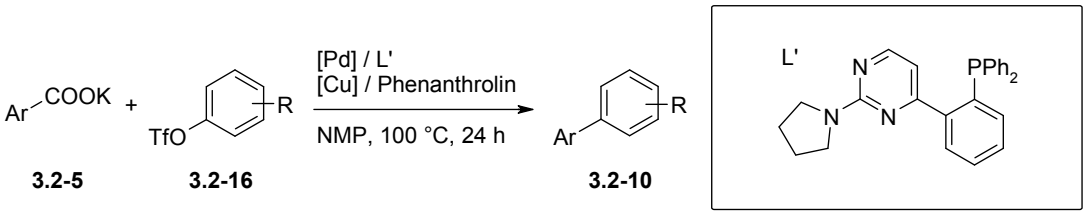

3.2-5 **3.2-16** **3.2-10**

Tf = Triflylgruppe
NMP = *N*-Methyl-2-pyrrolidon

Schema 8. *Decarboxylierende Kreuzkupplung mit P,N-Liganden bei tiefen Temperaturen*.

Die Ergebnisse zur Untersuchung des Mechanismus der Cu/Pd-katalysierten decarboxylierenden Kreuzkupplung wurden im *Journal of the American Chemical Society* veröffentlicht. Sämtliche Ergebnisse können dem englischsprachigen Originaltext der Veröffentlichung entnommen werden, die im Folgenden abgedruckt ist.

Die Veröffentlichung entstand im Rahmen eines Kooperationsprojekts. Hierbei wurde der Reaktionsmechanismus der Cu/Pd-katalysierten decarboxylierenden Kreuzkupplung von mir aufgeklärt, indem die Geometrien aller Edukte, Produkte, Katalysatoren, Intermediate und Übergangszustände optimiert wurden. Durch IRC-Rechnungen wurden die Übergangzustände verifiziert und anschließend die Reaktionspfade aufgestellt. Alle Frequenzrechnungen und 'single point energy'-Rechnungen sowie die Identifizierung des geschwindigkeits-bestimmenden Schritts unter Anwendung des 'energetic span'-Konzepts auf einen vereinfachten Katalysezyklus wurden in enger Kooperation mit Herrn Prof. Dr. Christoph van Wüllen durchgeführt. Die durch die DFT-Rechnungen getroffenen Vorrausagen erlaubten die Entwicklung einer Cu/Pd-katalysierten decarboxylierenden Kreuzkupplung mit *P*,*N*-Liganden bei nur 100 °C, die von Frau Dipl.-Chem. Dagmar Hackenberger durchgeführt wurde. Daher wird die Veröffentlichung *JACS* 2014 auch einen Teil ihrer Dissertation bilden.

„Reprinted with permission from A. Fromm, C. van Wüllen, D. Hackenberger, L. J. Gooßen, *J. Am. Chem. Soc.* **2014**, *136*, 10007−10023: *Mechanism of Cu/Pd-Catalyzed Decarboxylative Cross-Couplings: A DFT Investigation*. DOI: 10.1021/ja503295x. Copyright 2014 American Chemical Society."

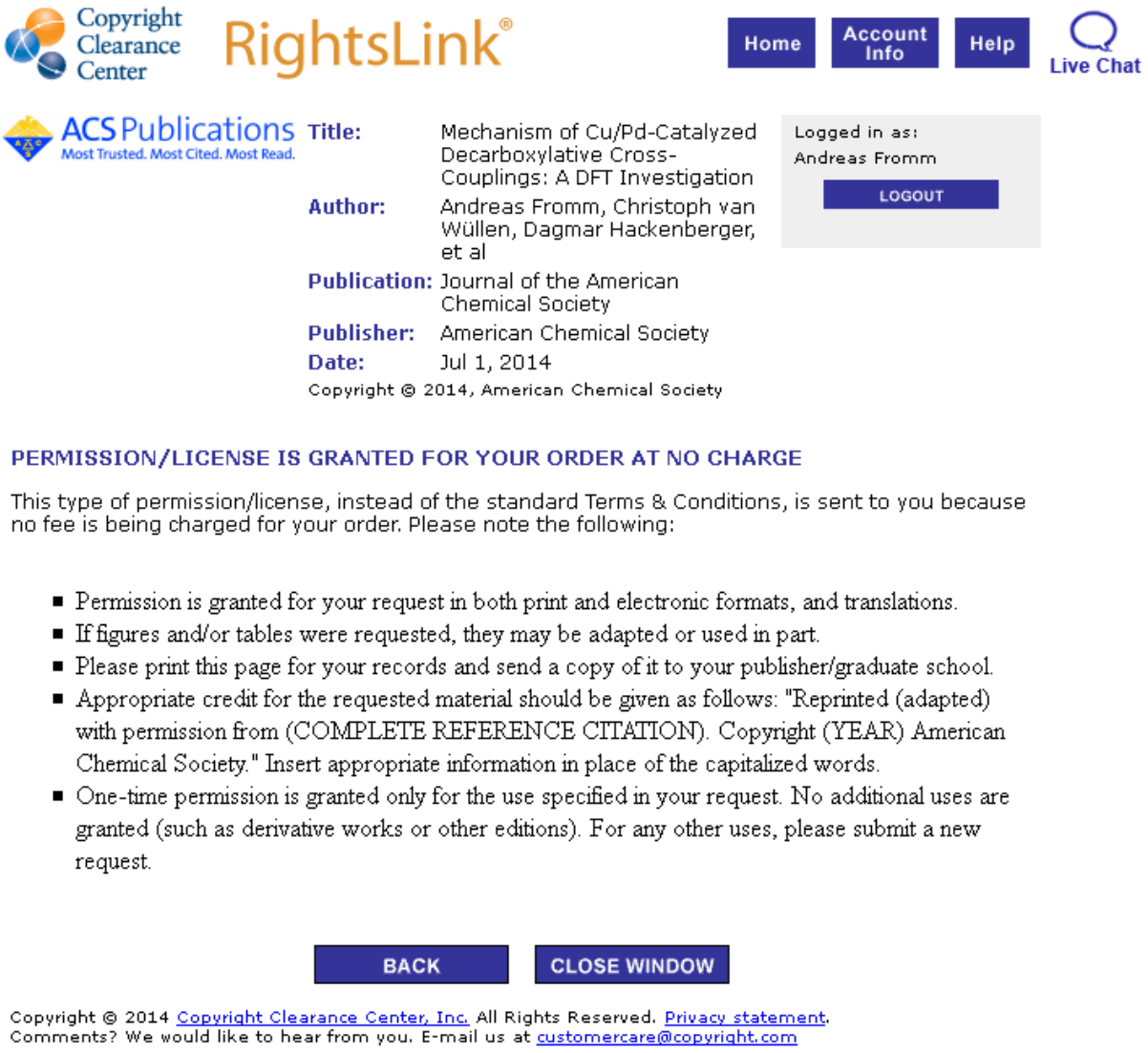

Copyright Clearance Center RightsLink®

Home | Account Info | Help | Live Chat

ACS Publications
Most Trusted. Most Cited. Most Read.

Title:	Mechanism of Cu/Pd-Catalyzed Decarboxylative Cross-Couplings: A DFT Investigation
Author:	Andreas Fromm, Christoph van Wüllen, Dagmar Hackenberger, et al
Publication:	Journal of the American Chemical Society
Publisher:	American Chemical Society
Date:	Jul 1, 2014

Copyright © 2014, American Chemical Society

Logged in as: Andreas Fromm
LOGOUT

PERMISSION/LICENSE IS GRANTED FOR YOUR ORDER AT NO CHARGE

This type of permission/license, instead of the standard Terms & Conditions, is sent to you because no fee is being charged for your order. Please note the following:

- Permission is granted for your request in both print and electronic formats, and translations.
- If figures and/or tables were requested, they may be adapted or used in part.
- Please print this page for your records and send a copy of it to your publisher/graduate school.
- Appropriate credit for the requested material should be given as follows: "Reprinted (adapted) with permission from (COMPLETE REFERENCE CITATION). Copyright (YEAR) American Chemical Society." Insert appropriate information in place of the capitalized words.
- One-time permission is granted only for the use specified in your request. No additional uses are granted (such as derivative works or other editions). For any other uses, please submit a new request.

BACK | CLOSE WINDOW

Copyright © 2014 Copyright Clearance Center, Inc. All Rights Reserved. Privacy statement.
Comments? We would like to hear from you. E-mail us at customercare@copyright.com

JACS
JOURNAL OF THE AMERICAN CHEMICAL SOCIETY
Article
pubs.acs.org/JACS

Mechanism of Cu/Pd-Catalyzed Decarboxylative Cross-Couplings: A DFT Investigation

Andreas Fromm, Christoph van Wüllen, Dagmar Hackenberger, and Lukas J. Gooßen*

Fachbereich Chemie and Forschungszentrum OPTIMAS, TU Kaiserslautern, Erwin-Schrödinger-Straße, 67663 Kaiserslautern, Germany

Supporting Information

ABSTRACT: The reaction mechanism of decarboxylative cross-couplings of benzoates with aryl halides to give biaryls, which is cooperatively catalyzed by copper/palladium systems, was investigated with DFT methods. The geometries and energies of all starting materials, products, intermediates, and transition states of the catalytic cycle were calculated for the two model reactions of potassium 2- and 4-fluorobenzoate with bromobenzene in the presence of a catalyst system consisting of copper(I)/1,10-phenanthroline and the anionic monophosphine palladium complex $[Pd(PMe_3)Br]^-$. Several neutral and anionic pathways were compared, and a reasonable catalytic cycle was identified. The key finding is that the transmetalation has a comparably high barrier as the decarboxylation, which was previously believed to be solely rate-determining. The electronic activation energy of the transmetalation is rather reasonable, but the free energy loss in the initial Cu/Pd adduct formation is high. These results suggested that research aimed at further improving the catalyst should target potentially bridging bidentate ligands likely to assist in the formation of bimetallic intermediates. Experimental studies confirm this somewhat counterintuitive prediction. With a bidentate, potentially bridging ligand, designed to support the formation of bimetallic adducts, the reaction temperature for decarboxylative couplings was reduced by 70 °C to only 100 °C.

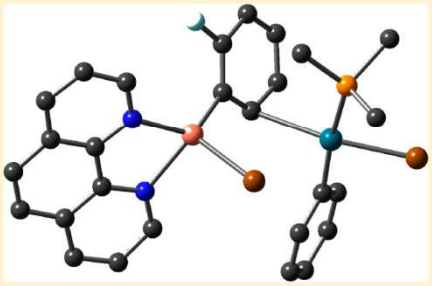

INTRODUCTION

Decarboxylative couplings have become a powerful tool for the selective formation of carbon−carbon and carbon−heteroatom bonds. In these transformations, CO_2 is extruded from a carboxylic acid precursor, and the carbon atom that has carried the carboxylic group then forms a bond with an electrophilic carbon or heteroatom. Following pioneering contributions by Nilsson, Tsuji, and Myers,[1] a redox-neutral decarboxylative biaryl synthesis was discovered in 2006 in which aromatic carboxylic acids are coupled with various aryl bromides in the presence of a copper/palladium bimetallic catalyst system (Scheme 1).[2]

Scheme 1. Decarboxylative Coupling Reactions

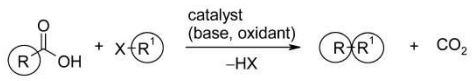

Since then, bimetallic systems have been used for decarboxylative couplings of benzoates and α-imino-[3] and α-oxocarboxylates[4] with aryl iodides, bromides,[5] chlorides,[6] triflates,[7] tosylates,[8] and mesylates.[9] Decarboxylative couplings with monometallic catalysts include Cu-mediated arylations of perfluorinated arenecarboxylic acids,[10] Rh-catalyzed decarboxylative 1,2-additions,[11] Pd-catalyzed decarboxylative allylations[12] and arylations of five-ring heteroarene carboxylates,[13] of alkynylcarboxylates,[14] and of oxalic acid monoesters,[15] and Mannich-type reactions.[16] Oxidative decarboxylative cross-couplings have been used for Heck-type vinylations,[1f−h,17] C−H arylations,[18] couplings of amino acids,[19] and various C−heteroatom bond formations.[20]

The concept of decarboxylative couplings has distinct advantages over traditional cross-coupling reactions in the regiospecific formation of C−C bonds, because it relies on inexpensive and broadly available carboxylate salts instead of expensive and sensitive preformed organometallic reagents as the source of carbon nucleophiles.

Typical catalyst systems and the reaction scope are shown in Scheme 2.

Especially in redox-neutral couplings of aromatic carboxylate salts, bimetallic copper/palladium systems have proven to be the most generally applicable catalysts. For these systems, a mechanistic outline consisting of two interlinked catalytic cycles has been proposed (Scheme 3).[2,5] The ligand environment at the copper center is designed to promote the extrusion of CO_2 with the highest possible efficiency, while the palladium catalyst is independently optimized for the cross-coupling step. The proposed catalytic cycle starts with an anion exchange at the copper center, in the course of which the aromatic carboxylate is transferred to the copper complex **a** to give the metal carboxylate **b**. In the decarboxylation step, an organocopper

Received: April 2, 2014
Published: June 26, 2014

dx.doi.org/10.1021/ja503295x | J. Am. Chem. Soc. 2014, 136, 10007−10023

Scheme 2. Representative Decarboxylative Cross-Couplings with Bimetallic Cu/Pd Catalyst Systems[a]

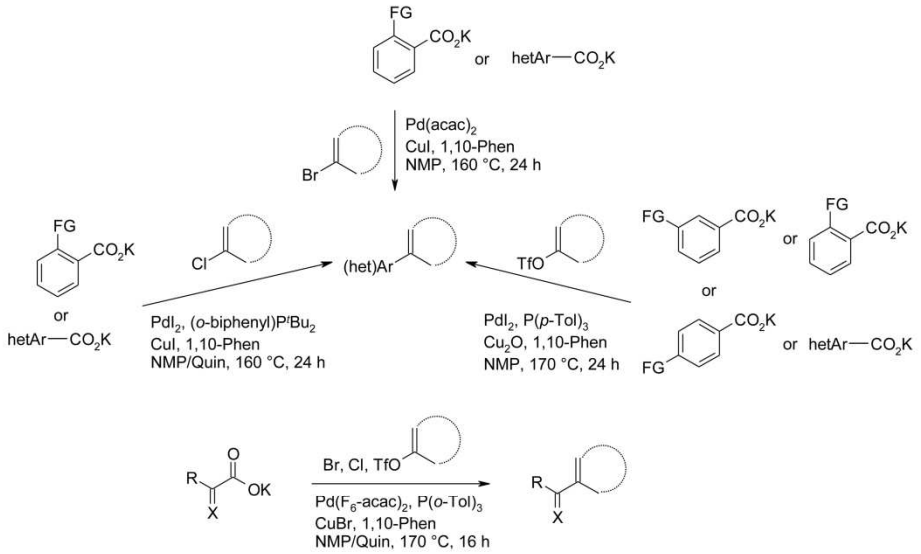

[a]Ar = aryl, FG = functional group, hetAr = heteroaryl, Phen = phenanthroline, Quin = quinoline, X = O, NR.

Scheme 3. Mechanism Proposed for Decarboxylative Cross-Couplings

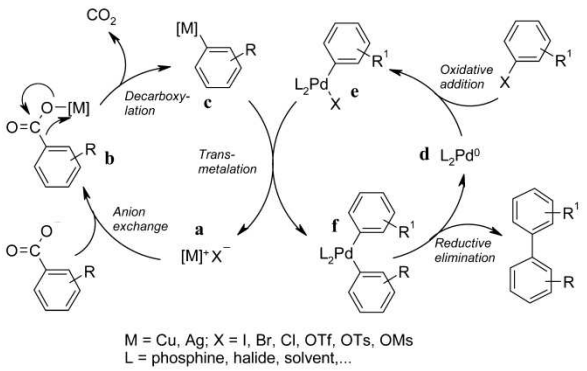

species **c** is generated by extrusion of CO_2. A subsequent transmetalation links the two catalytic cycles. In this step, an aryl residue is transferred from the copper species **c** onto a palladium species **e** that has been generated by oxidative addition of the aryl electrophile to a low-valent palladium(0) cocatalyst **d**, and the original copper species **a** is regenerated. The resulting diaryl palladium species **f** undergoes reductive elimination, in which the new carbon–carbon bond is formed, the biaryl product is released, and the palladium(0) species **d** is regenerated.

At present, most decarboxylative couplings still require temperatures in excess of 160 °C, which, in practice, represents the main limitation of this elegant reaction type. The rational development of catalysts that promote decarboxylative couplings at lower temperatures is, thus, in the focus of current research activities. In this context, mechanistic investigations and theoretical studies are of vital importance.[21]

However, DFT modeling of the mechanistically complex decarboxylative couplings catalyzed by bimetallic systems poses a considerable challenge, which has so far precluded the calculation even of simplified models. Computational studies of this reaction have to date been limited to the decarboxylation step (**b** → **c** in Scheme 3).[22] That this step was rate-determining in the early reaction protocols became evident from the observation that Cu-catalyzed protodecarboxylations required temperatures that were at least as high as those of decarboxylative cross-couplings (170 °C). In contrast, Pd-mediated cross-couplings of aryl–copper species are known to proceed at much lower temperatures.

These DFT calculations confirmed[22] that the extrusion of CO_2 from phenanthroline copper benzoates is endothermic by 9.9–28.8 kcal mol^{-1} and endergonic (0.8–17.5 kcal mol^{-1}) and has a considerable activation barrier of 27.2–36.1 kcal mol^{-1}.[21c] Another correct prediction derived from these calculations was that for a narrow range of substitution patterns, e.g. *o*-methoxybenzoates, the energy barrier for the decarboxylation is substantially lower when copper is replaced by silver, whereas the majority of carboxylates lose CO_2 more easily when coordinated to copper rather than silver complexes.[7c]

Pd-catalyzed cross-couplings of organometallic reagents have been intensively studied by DFT calculations.[23] For Suzuki-type couplings of carboxylic anhydrides with arylboronic acids, various catalytic cycles were computed starting from neutral $(PMe_3)_2Pd(0)$ (**4**), anionic tricoordinate Amatore–Jutand-type $[(PMe_3)_2Pd(0)OAc]^-$ (**5**), and anionic dicoordinate $[(PMe_3)$-$PdOAc]^-$ (**6**) (Figure 1).[24] With the anionic dicoordinate palladium complex **6**, the energy profile obtained was most favorable overall so that this species appears to be the optimal candidate for calculations of related Pd-catalyzed couplings.

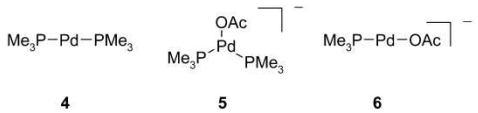

Figure 1. Pd-species investigated in Suzuki-type cross-couplings.

Scheme 4. DFT Investigations of Decarboxylative Cross-Couplings with Monometallic Catalysts

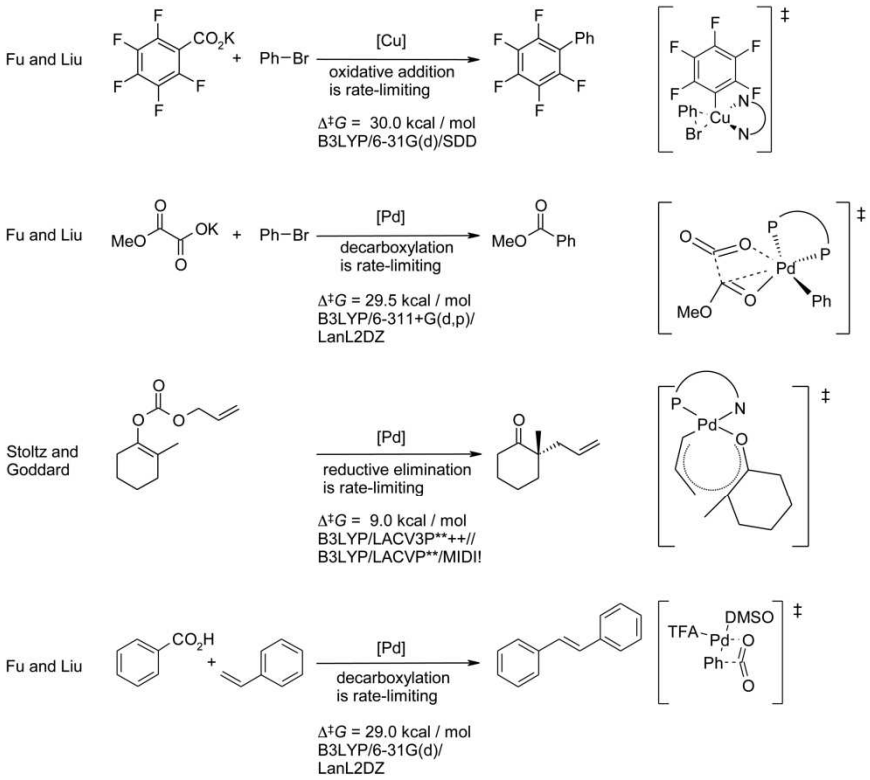

Scheme 5. Model Reactions of Potassium 2- and 4-Fluorobenzoate with Bromobenzene

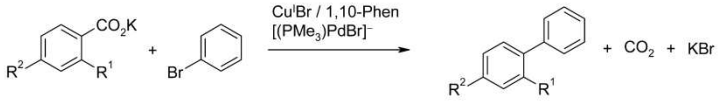

7a: R^1 = F, R^2 = H **8** **9a**: R^1 = F, R^2 = H **3** **10**
7b: R^1 = H, R^2 = F **9b**: R^1 = H, R^2 = F

As mentioned above, some particularly activated substrates can be decarboxylatively coupled with aryl electrophiles by using monometallic catalysts. The reduced complexity of such monometallic systems has permitted in-depth mechanistic investigations (see Scheme 4). DFT studies were reported for Pd-catalyzed decarboxylative cross-couplings of oxalic acid monoesters,[15] decarboxylative allylations of enol carbonates,[12,25] decarboxylative cross-couplings of polyfluorobenzoates with aryl electrophiles,[26] Myers' Pd-catalyzed decarboxylative Heck vinylation,[17a] and certain intramolecular decarboxylative couplings.[27]

For the mechanistically more complex decarboxylative couplings mediated by bimetallic catalyst systems, a similarly detailed computational study would be of substantial value. With state-of-the-art catalysts, the protodecarboxylation of *o*-nitrobenzoic acids with a copper/phenanthroline system can meanwhile be performed at 100 °C,[28] while decarboxylative cross-couplings with aryl triflates, in which copper/phenanthroline systems are employed as the decarboxylation cocatalysts, still do not proceed below 150 °C.[7a,b] Thus, the decarboxylation is not necessarily rate-determining, and it is no longer sufficient to single out the decarboxylation step in computational studies to obtain a lead for further catalyst optimization. Instead, computational modeling should cover the entire catalytic cycle. A particular challenge lies in modeling the transmetalation step, in which an organic residue is transferred from a fully ligated copper complex to a phosphine-stabilized arylpalladium species.[29]

■ MODEL SYSTEM

We herein investigate the decarboxylative coupling of bromobenzene (**8**) with (a) potassium 2-fluorobenzoate (**7a**) as an example of a highly reactive arenecarboxylate and (b) potassium 4-fluorobenzoate (**7b**) as an example of an arenecarboxylate with low reactivity (Scheme 5).

The catalyst system employed in the calculations of these representative model reactions is composed of 1,10-phenanthroline copper(I) bromide, which is known to display a substantially greater decarboxylation activity than simple copper(I) salts,[2] and an anionic Pd(0) bromide catalyst with the simplified but still reasonably realistic ligand PMe_3.

Comparative studies performed upfront, in combination with related literature studies, confirmed that the catalytic cycle

dx.doi.org/10.1021/ja503295x | J. Am. Chem. Soc. 2014, 136, 10007−10023

Scheme 6. Catalytic Cycles Calculated for Decarboxylative Cross-Couplings

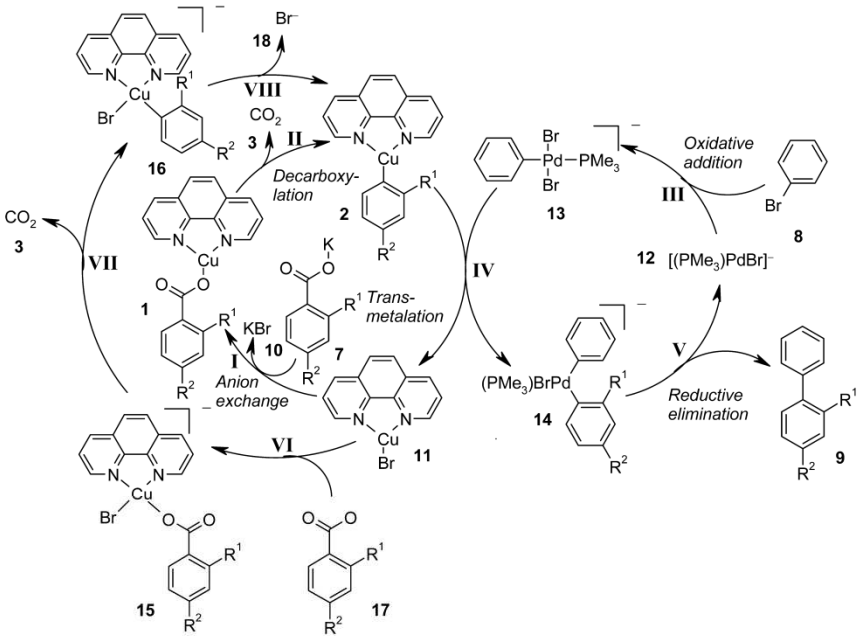

shown in Scheme 6 is a realistic mechanistic model. For example, computational studies of Suzuki-type couplings led to the conclusion that catalytic cycles starting from various Pd(0) species, each of which may be present in solution, will have comparable energy profiles also in couplings with other carbon nucleophiles.[24] Among them, a pathway starting from $[(PMe_3)PdOAc]^-$ (**6**) (Figure 1) had proven to be the most advantageous overall. It thus appeared to be reasonable to use an analogous cycle based on similar structural units as a starting point for computing the cycle of the Pd-catalyst in the decarboxylative cross-coupling. For the Cu-catalyst, two different catalytic cycles were computed, both starting from 1,10-phenanthroline copper(I) bromide. The first solely involves neutral species, whereas in the second, an additional bromide is bound to copper during the decarboxylation step. This was calculated to find a possible explanation for the profound influence of bromide ions on the decarboxylation of non-*ortho*-substituted benzoates.

Both variants of the catalyst cycle were successfully calculated. Minima with reasonable structures and energies could be found for all intermediates, and transition states connecting these intermediates could be located. The computational studies led us to conclude that decarboxylative cross-couplings follow a neutral pathway consisting of the anion exchange (step I) and the decarboxylation step (step II) at the copper catalyst, the oxidative addition (step III) of the bromobenzene to the Pd catalyst, the transmetalation process (step IV) between the resulting palladium and copper species, and the reductive elimination (step V) of the biaryl product with regeneration of the Pd catalyst. Subsequently, the computational study of an anionic variant of the Cu-cycle is presented, which starts with the coordination (step VI) of the carboxylate to the copper catalyst, followed by decarboxylation (step VII) and bromide decoordination (step VIII). This alternative cycle was found to be less favorable.

■ COMPUTATIONAL METHOD

All calculations were performed with use of the Gaussian 03 or Gaussian 09 software packages.[30] The B3LYP exchange-correlation functional[31] was used in all cases. For the geometry optimizations, the polarized split-valence 6-31+G(d) basis set[32] was employed for all atoms except Cu and Pd, where a scalar-relativistic effective core potential[33] replaced 10 (Cu) or 28 (Pd) core electrons, together with the valence basis sets[33] in double-ζ quality. Spherical basis functions (5D, 7F) were used in all cases. In contrast to our previous studies,[21c,22] some of the species investigated are anionic, so that diffuse basis functions were included in the basis set. Note that the valence basis sets for Cu and Pd already contain diffuse functions from the outset.

All geometries of minima (intermediates) and transition states were fully optimized for isolated (gas-phase) molecules. To locate the transition states, we first performed a relaxed potential energy surface scan in which the reaction coordinate was kept fixed at several defined distances, while all other degrees of freedom were optimized. In these scans, a series of structures were optimized in which the reaction coordinate was increased stepwise. The structure with the highest energy was then used as a starting point for the synchronous transit-guided quasi-Newton method[34] to locate the transition state with a molecular Hessian of exactly one negative eigenvalue. To identify the minima connected to the transition states thus identified, the intrinsic reaction coordinate (IRC)[35] was followed downhill for 10 points in both directions and the two resulting molecular geometries were used as starting points for subsequent geometry optimizations. Sometimes, additional intermediates were discovered this way. In these cases, the process described above was repeated until the reaction pathway was complete. For each molecular structure (intermediate or transition state), the calculated electronic energy (but not the molecular structure and harmonic vibrational frequencies) was improved by a single-point calculation in which the 6-31+G(d) basis (for all atoms except Cu and Pd) was replaced by the better polarized valence triple-ζ type 6-311+G(2d,p).[36] For Cu and Pd, the *d* functions of the original basis sets were decontracted slightly from [411] to [3111], and a single set of *f* functions (taken from the def2-TZVP basis sets,[37] η_f(Cu) = 2.233, η_f(Pd) = 1.24629) was added for both elements.

The above calculations provided electronic energies under vacuum (E_{tot}). To model the reaction energies more closely resembling

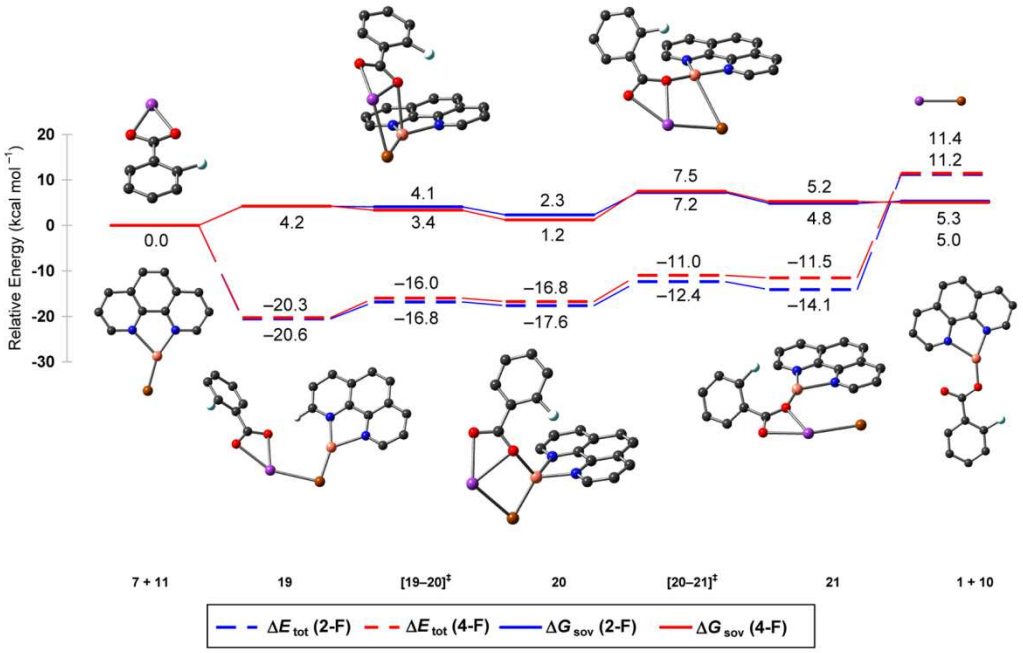

Figure 2. B3LYP/6-31+G(d) optimized structures for the anion exchange of potassium 2-fluorobenzoate and phenanthroline copper(I) bromide; hydrogens are omitted for clarity. Energy and solution Gibbs energy profiles overlaid for 2- and 4-fluorobenzoate. Color code: C, black; H, white; Br, brown; Cu, orange; F, turquoise; K, purple; N, blue; O, red.

experimental conditions, further terms were added, namely zero-point vibrational energy, thermal corrections to the energy, solvation and entropic effects, as well as empirical dispersion corrections. This way, an approximation to the Gibbs energy in solution (G_{sov}) was obtained.

Solvent effects were included by estimating the Gibbs energy of solvation for all intermediates and transition states using the conductor-like polarizable continuum model[38] (CPCM) of Gaussian 09, which is an implementation of the conductor-like screening solvation model[39] (COSMO). This model is particularly well-suited for polar solvents such as *N*-methyl-2-pyrrolidone (NMP, ε = 32.55), which is the most effective solvent for decarboxylative cross-couplings.

To calculate the zero-point vibrational energies, the harmonic frequencies calculated (with the small basis) were scaled by a factor of 0.9613 as suggested by Wong.[40] The thermal correction to the Gibbs energy of each component depends on its concentration in the solution. Note that in the Gaussian program one has to specify the concentration as a pressure value, using the ideal gas law $p_i = RTn_i/V$, where p_i is the pressure, R the gas constant, T the absolute temperature, n_i the molar quantity, and V the reaction volume. Typical experiments, as modeled in our calculations, involve approximately 1 mmol of starting material and product in a reaction volume of 2 mL, which corresponds to a pressure of 1,844,115 Pa (18.2 atm) at a reaction temperature of 443 K. The amount of catalyst is lower by a factor of 20, so that we used a pressure of 101,325 Pa (1 atm) for all species involving Cu and/or Pd. The experimental solubility data of CO_2 in NMP[41] show that under the experimental conditions, the molar fraction of CO_2/NMP is clearly less than 0.01, most likely about 0.001 when extrapolating temperature and pressure, which implies that most of the CO_2 leaves the NMP solution. The resulting CO_2 concentration in the reaction mixture corresponds to a partial pressure of 101,325 Pa (1 atm) for an ideal gas. Because of the ideal gas approximation, the molar Gibbs energy for a given temperature T and pressure p was computed from the results for p_0 = 1 atm as $G(T,p) = G(T,p_0) + RT \ln(p/p_0)$.

For any sequence of elementary steps that involve a single species, the reaction profile does not depend on the concentration. This changes if association and dissociation steps are involved. These considerations are relevant in this context because we have two coupled catalytic cycles. Reducing the catalyst load (both Cu and Pd) reduces the reaction rate of the steps involving only Cu or only Pd linearly, while the transmetalation step is affected quadratically. Therefore, the relative rates of the transmetalation compared to the other elementary steps depend on the catalyst load, with lower loads disfavoring the transmetalation. This is taken into account in our Gibbs energy profiles.

It is known that standard DFT methods neglect or severely underestimate London dispersion interactions.[42] A robust and numerically inexpensive way to cure this deficiency is to add an empirical dispersion correction that sums up the contribution of all atom pairs. We used Grimme's D3 parametrization[43] and calculated the dispersion correction for all minima and transition states. These values are included in our final solution Gibbs energies G_{sov}. This correction significantly lowers the Gibbs energy of an encounter complex with respect to the two fragments, but also lowers the Gibbs energy of a tight transition state with respect to a loose intermediate.

Note that the solvation model as used in our calculations does not include nonelectrostatic solute−solvent interactions: in a numerical experiment, we found zero contributions when we set the dielectric constant to zero. This means that the loss of solute−solvent dispersion interaction upon formation of an adduct, which is a consequence of reducing the surface of the solute(s), is not taken into account. Therefore, we think that the dispersion interaction in solution is somewhat overestimated in our calcualtions, although the combination of empirical dispersion and solvent corrections has been reported to work well.[44]

In the Supporting Information, the electronic energies (with and without solvation), the calculated Gibbs energies at 298 and 443 K (at 1 and 18.2 atm), the empirical dispersion corrections, and the final solution Gibbs energy including empirical dispersion corrections G_{sov} are documented. The diagrams in this paper contain the electronic energy E_{tot} (since molecular geometries and vibrational frequencies are obtained at this level) and solution Gibbs energy G_{sov} profiles including empirical dispersion corrections (which govern the reactivity). Throughout the text, all bond lengths are given in Å and

relative energies are expressed in kcal mol^{-1}. All ball-and-stick models are rendered with GaussView 5.[45]

MODELING THE CATALYTIC CYCLE BY DFT

Anion Exchange. In the anion exchange step, the potassium benzoate (**7a**/**b**) reacts with the phenanthroline copper bromide catalyst **11** to afford the corresponding phenanthroline copper benzoate (**1a**/**b**) along with potassium bromide (**10**). The energy and solution Gibbs energy profiles for the model substrates, 2- and 4-fluorobenzoate are depicted in Figure 2, along with the optimized structures for the *o*-fluoro derivates.

The anion exchange starts with the formation of an encounter complex **19** between the substrates **7** and **11**. This process is exothermic in the gas phase (Δ_rE_{tot} = −20.6 kcal mol^{-1}) but endergonic by Δ_rG_{sov} = 4.2 kcal mol^{-1}. This difference has two origins. First, entropy is lost when forming the adduct, even more so because the copper catalyst **11** is present only in low concentration compared to the substrate **7**. This entropy loss strongly contributes to the increase in Gibbs energy at the elevated reaction temperature (170 °C). Second, solvation disfavors adduct formation, since the combined solvation energies for **7** and **11** are larger than that for the adduct **19**. In the adduct, the C(2)−H bond of the 1,10-phenanthroline points toward one of the carboxylate oxygens, resulting in a short C−H···O (2.03 Å) and a long K−Br distance (3.26 Å). A Cu−O bond has not formed at this stage. The K−O bond is slightly elongated to 2.64 Å compared to 2.55 Å in **7**. Also, the Cu−Br bond is slightly increased to 2.30 Å compared to 2.26 Å in **11**.

Bringing a carboxylic oxygen closer to the copper center leads to the transition state [**19**−**20**]‡. This process has a very small barrier ($\Delta^{‡}E_{tot}$ = 3.8 kcal mol^{-1}). The coordination sphere of the copper is distorted trigonal planar, with the bromine atom only slightly out of the plane formed by the phenanthroline backbone. The atoms Cu, Br, K, and O form an almost planar 4-membered ring. The K−Br (3.16 Å) and Cu−O (*ortho*: 2.77 Å) bonds are long, and the K−O (2.64 Å) and Cu−Br bonds (2.33 Å) are short. The forward motion along the reaction coordinate derived from the normal mode of the imaginary frequency (21 i cm^{-1}) is dominated by the shortening of the Cu−O distance. At the same time, the bromine atom moves out of the plane of the phenanthroline ligand.

In intermediate **20**, the copper atom is now in an almost tetrahedral environment. The K−Br (3.11 Å) and Cu−O (2.15 Å) bonds are further shortened and the K−O (2.66 Å) and Cu−Br bonds (2.41 Å) are elongated.

In the second phase of the anion exchange, a bromide leaves the copper center and eventually forms KBr. Stretching the Cu−Br bond leads to the transition state [**20**−**21**]‡. The activation barrier is rather low ($\Delta^{‡}E_{tot}$ = 5.2 kcal mol^{-1}, $\Delta^{‡}G_{sov}$ = 4.9 kcal mol^{-1}). The copper is in a distorted trigonal planar environment with the oxygen atom only slightly out of the plane of the phenanthroline backbone. The K−Br (3.04 Å) and Cu−O (1.91 Å) bonds are rather short, whereas the K−O (2.71 Å) and Cu−Br bonds are long (3.50 Å). The forward motion along the reaction coordinate derived from the normal mode of the imaginary frequency (21 i cm^{-1}) is dominated by the elongation of the Cu−Br bond and the motion of the oxygen atom into the plane of the phenanthroline ligand.

In the subsequent intermediate **21**, the Cu−Br bond is now fully broken while the K−Br (3.04 Å) and Cu−O (1.91 Å) bond lengths remain almost unchanged and the K−O bond is slightly elongated (2.74 Å).

For the *o*-fluoro model system, intermediate **21** finally dissociates into KBr (**10**) and the product of the anion exchange, the phenanthroline copper 2-fluorobenzoate (**1a**) that decarboxylates subsequently. Cleaving the K−O bond requires some energy (Δ_rE_{tot} = 25.3 kcal mol^{-1}), but the entropically favorable dissociation into two solvated molecules makes this step only slightly endergonic (Δ_rG_{sov} = 0.5 kcal mol^{-1}). The copper atom in **1a** is coordinated to only one of the carboxylate oxygens by a short bond (Cu−O: 1.89 Å) in a distorted trigonal planar environment. The nitrogen donor atoms of the phenanthroline ligand transfer sufficient electron density to the copper(I) cation so that this coordination mode is preferred, while for the electron-poor potassium cation, a coordination to both oxygen atoms is favorable (structure **7**).

The calculations further revealed that for 4-fluorobenzoate, the energy profile of the anion exchange is almost identical with that of the 2-fluorobenzoate (Figure 2, see also the Supporting Information). This result came as a surprise since decarboxylative cross-couplings of aryl halides with 2-fluorobenzoates are well-documented, while the analogous reactions of 4-fluorobenzoates have not yet been achieved. Only aryl electrophiles with noncoordinating groups such as triflates can be coupled with non-*ortho*-substituted benzoates. To rationalize these experimental findings, the salt metathesis of copper(I) halides with potassium benzoates had been postulated to be favorable for *ortho*-substituted derivatives, but unfavorable for non-*ortho*-substituted benzoates. This hypothesis was supported by protodecarboxylation experiments in which benzoic acids (**22**) were converted to the corresponding arenes (**23**) in the presence of a phenanthroline copper system according to Scheme 7. In the absence of halides, this reaction proceeded well both for *ortho*- and non-*ortho*-substituted benzoic acids. Upon the addition of a halide salt, the decarboxylation of non-*ortho*-substituted benzoic acids was fully suppressed, whereas the reactivity of the *ortho*-substituted benzoic acids remained high.[5]

Scheme 7. Influence of Halides on Protodecarboxylations

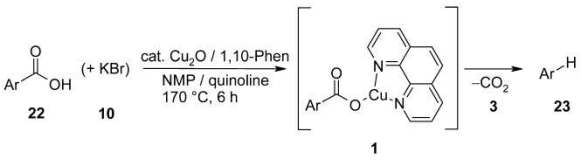

22 10 1 3 23

Ar = 2-F-C_6H_4: 91 % without KBr, 72 % with KBr
Ar = 4-F-C_6H_4: 27 % withoutKBr, 0 % with KBr

In a series of control experiments, similar observations were made also for the decarboxylation of the two fluorobenzoic acid isomers. The addition of 1 equiv of potassium bromide only slightly reduced the yield of the protodecarboxylation of 2-fluorobenzoic acid (**22a**) from 91% to 72% yield in the presence of potassium bromide. 4-Fluorobenzoic acid (**22b**) gave only 27% even in the absence of bromide ions, and when potassium bromide was added, the decarboxylation was completely suppressed.[46]

According to our present DFT studies, the salt exchange between the copper bromide species **11** and the fluorobenzoate isomers (**7a** and **7b**) is energetically very similar. It is slightly endergonic (*ortho*: Δ_rG_{sov} = 5.3 kcal mol^{-1}; *para*: Δ_rG_{sov} = 5.0

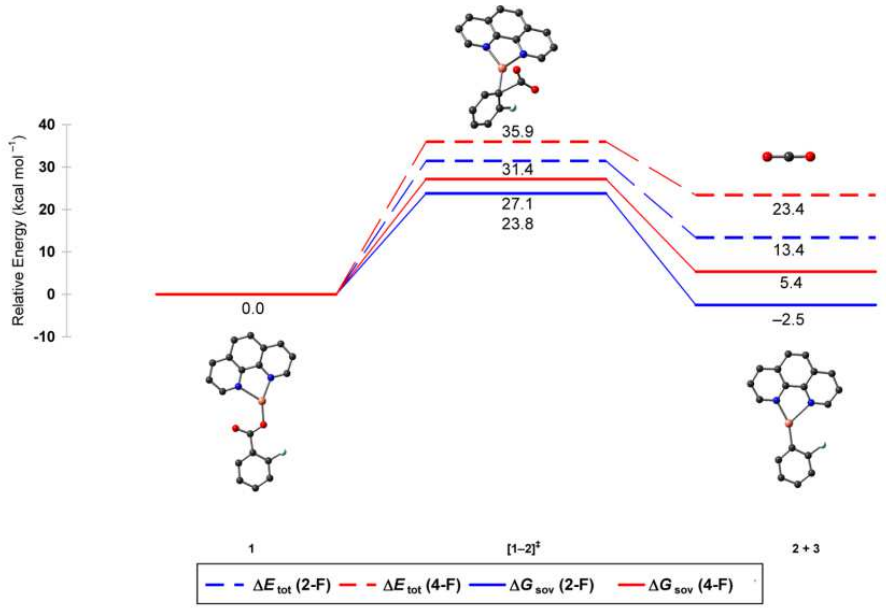

Figure 3. B3LYP/6-31+G(d) optimized structures for the decarboxylation of phenanthroline copper 2-fluorobenzoate; hydrogens are omitted for clarity. Energy and solution Gibbs energy profiles overlaid for 2- and 4-fluorobenzoate. Color code: C, black; Cu, orange; F, turquoise; N, blue; O, red.

kcal mol^{-1}) with low activation barriers. These calculations do not provide any rationale for the hypothesis that the presence of bromide ions suppresses the formation specifically of copper 4-fluorobenzoate complexes, so that the unique reactivity of *ortho*-substituted benzoates must have another reason. A precipitation of KBr, which would not be taken into account by the DFT calculations, is not observed in the experiment.

We therefore carefully explored alternative geometries for the salt exchange product phenanthroline copper 2-fluorobenzoate (**1a**), in which the carboxylate oxygen and the *o*-fluorine would both coordinate to the copper, potentially resulting in a more stable structure. This might be expected to lead to a substantially less endergonic anion exchange step for potassium 2-fluorobenzoate compared to 4-fluorobenzoate. However, no minima for complexes with chelating coordination were found.

We also investigated whether the energy profile is affected by leaving out the potassium counterion in the calculations. The resulting energy barriers are twice as high, and again, no differences of any potential consequence were found between 2- and 4-fluorobenzoates. The energy profiles along with the optimized structures can be found in Figure S1 in the Supporting Information.

Overall, the calculations do not support the previously postulated explanation for the effect of halide ions on the decarboxylation of non-*ortho*-substituted carboxylates. A possible explanation is that the additional bromide ions do not have an effect on the difference in reactivity of the *ortho*- and *para*-substituted benzoates in the anion exchange step but in the decarboxylation step that will be discussed in the next section. The presence of excess bromide salt shifts the equilibrium of the anion exchange step to the side of the copper bromide so that less copper carboxylate is available. This reduces the efficiency of the entire protodecarboxylation process. Since the decarboxylation of *ortho*-substituted benzoates requires less energy than that of non-*ortho*-substituted benzoates, high conversions of *ortho*-substituted benzoic acids can be achieved at temperatures where non-*ortho*-substituted derivatives do not decarboxylate.

Decarboxylation. The decarboxylation step has already been the subject of previous DFT investigations,[21c,22] because it was initially believed to be the only rate-determining step. We have now reinvestigated it using the high-quality basis set with diffuse functions detailed above, included solvent effects, dispersion interactions, and taken into account the concentrations and reaction temperatures.

The extrusion of carbon dioxide from phenanthroline copper 2-fluorobenzoate (**1**) was found to proceed via a concerted mechanism involving only one transition state ([**1**−**2**]‡, Figure 3). An extensive search did not reveal any further intermediates, such as π- or η^2-bound arene−copper complexes.

In the copper 2-fluorobenzoate **1a**, all atoms are coplanar. The two nitrogen−copper bond lengths of the phenanthroline ligand are slightly different (2.0 and 2.2 Å), which indicates that this ligand geometry is not ideal for Cu^{I}. The decarboxylation step can be viewed as a substitution of the carboxylate group by the copper center in a concerted fashion. The activation barrier for the extrusion of CO_2 from 2-fluorobenzoate is relatively high ($\Delta^{‡}E_{tot}$ = 31.4 kcal mol^{-1}, $\Delta^{‡}G_{sov}$ = 23.8 kcal mol^{-1}), but within a realistic range for a reaction that requires a temperature of 160 °C. In the transition state [**1a**−**2a**]‡, the copper atom is in a distorted tetrahedral environment formed by the two phenanthroline nitrogens, the 2-fluorophenyl and the CO_2 carbons. The Cu−N bonds have similar lengths (ca. 2.1 Å). The fluorophenyl moiety binds to both the copper and the CO_2 carbon via its C(1) carbon. The aryl−CO_2 bond is short (1.94 Å) while the aryl−copper bond is relatively long (2.02 Å), which is indicative for a relatively early transition state. The forward motion along the reaction coordinate derived from the normal mode of the imaginary frequency (229

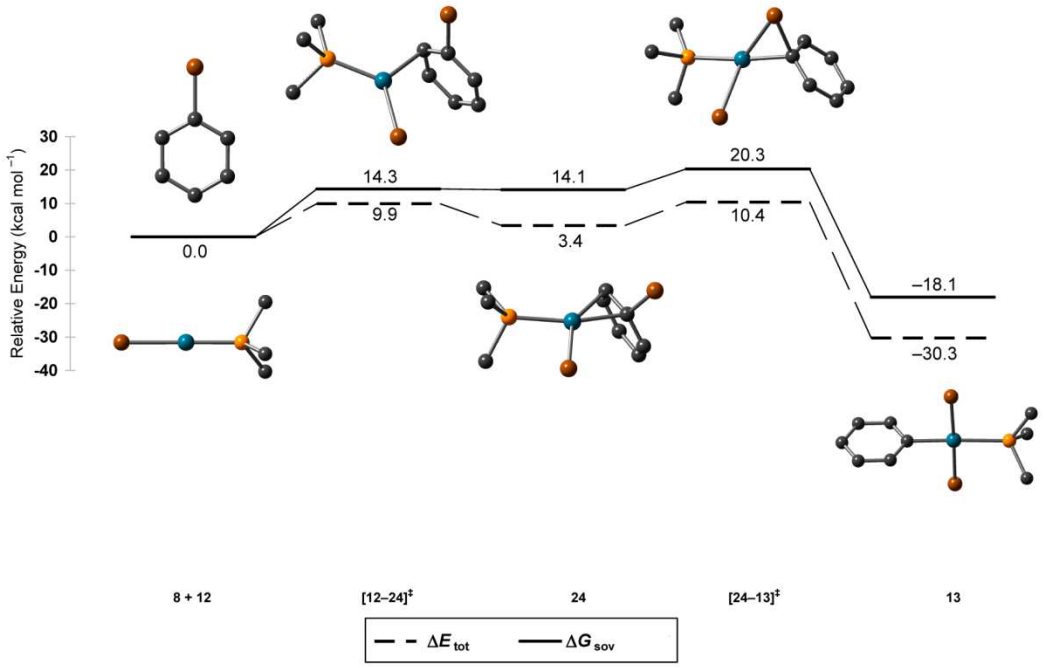

Figure 4. B3LYP/6-31+G(d) optimized structures for the oxidative addition of bromobenzene to $[Pd(PMe_3)Br]^-$; hydrogens are omitted for clarity. Color code: C, black; Br, brown; P, yellow; Pd, green.

i cm^{-1}) is dominated by the elongation of the aryl−CO_2 bond with a concomitant contraction of the aryl−copper bond.

The IRC calculation reveals that the transition state directly leads to the decarboxylation product **2a**. The 2-fluorophenyl ring remains in the plane of the phenanthroline backbone. A weak interaction between a fluorine lone pair and the hydrogen at C(2) of the phenanthroline scaffold, which are separated by a distance of only 2.30 Å, additionally stabilizes this geometry. The phenanthroline coordination is even more asymmetrical than prior to decarboxylation, with Cu−N bonds of 2.0 and 2.4 Å, respectively.

Overall, the decarboxylation of 2-fluorobenzoate is moderately endothermic (Δ_rE_{tot} = 13.4 kcal mol^{-1}). Whereas in the previous, simplified calculations, the decarboxylation had come out endergonic, the present, more refined calculations predict it to be exergonic (Δ_rG_{sov} = −2.5 kcal mol^{-1}) at the calculated reaction temperature of T = 443.15 K. Among other effects, the entropy gained by releasing CO_2 contributes more strongly to the Gibbs energy because we take into account the higher reaction temperature.

The pathway for the decarboxylation of 4-fluorobenzoate is slightly different. The activation barrier for the extrusion of CO_2 is considerably higher ($\Delta^‡E_{tot}$ = 35.9 kcal mol^{-1}, $\Delta^‡G_{sov}$ = 27.1 kcal mol^{-1}), which is in good agreement with the experimental findings that the protodecarboxylation of non-*ortho*-substituted benzoic acids requires higher temperatures and longer reaction times than that of *ortho*-substituted derivatives.[21c] In contrast to the decarboxylation of 2-fluorobenzoate, the transition state originating from 4-fluorobenzoate [**1b**−**2b**]‡ has a long aryl−CO_2 bond (2.06 Å) and a short aryl−copper bond (1.98 Å). This is indicative of a later transition state, which suggests that the decarboxylation is more endergonic for this isomer. The formation of **2b** is indeed strongly endothermic (Δ_rE_{tot} = 23.4 kcal mol^{-1}), but due to the entropically favorable liberation of CO_2, it is only slightly endergonic (Δ_rG_{sov} = 5.4 kcal mol^{-1}). The structure of the decarboxylation product **2b** differs from that for the *ortho*-derivative **2a** in that the 4-fluorophenyl ring is rotated out of the plane of the phenanthroline backbone at an angle of 55.7°, which may be caused by the absence of a hydrogen−fluorine interaction. Overall, the decarboxylation of non-*ortho*-substituted benzoates is both kinetically and thermodynamically significantly less favorable than the analogous reaction of *ortho*-substituted benzoates, a result that is in perfect agreement with experimental observations of protodecarboxylations.[21c]

Oxidative Addition. The catalytic cycle of palladium starts with the oxidative addition of the aryl halide to a Pd^0 species. When starting from the anionic palladium monophosphine complex $[Pd(PMe_3)Br]^-$ (**12**), this reaction step proceeds with particular ease (Figure 4). Upon bringing the bromobenzene (**8**) closer to the palladium center, an η^2-π-complex (**24**) forms via the transition state [**12**−**24**]‡. The activation barrier for this step is rather low for a process in which a bond forms between two separately solubilized molecules ($\Delta^‡E_{tot}$ = 9.9 kcal mol^{-1}, $\Delta^‡G_{sov}$ = 14.3 kcal mol^{-1}). This difference stems from entropy and solvation as discussed above. In the transition state, a bond between the palladium and the C(2) atom of bromobenzene has already formed (Pd−C(2): 2.31 Å), and the previously linear Br−Pd−P bond is bent at an angle of 125.4°. The forward motion along the reaction coordinate derived from the normal mode of the imaginary frequency (62 i cm^{-1}) is dominated by the shortening of the Pd−C(1) and Pd−C(2) distances with simultaneous decrease of the Br−Pd−P angle.

The IRC calculation leads to intermediate **24**, in which the palladium atom is coordinated almost symmetrically to the π-bond between C(1) and C(2) (Pd−C(1): 2.11 Å; Pd−C(2): 2.18 Å). The C−Br bond is slightly elongated from 1.92 to 2.00 Å, and the Br−Pd−P angle has decreased to 90.8°.

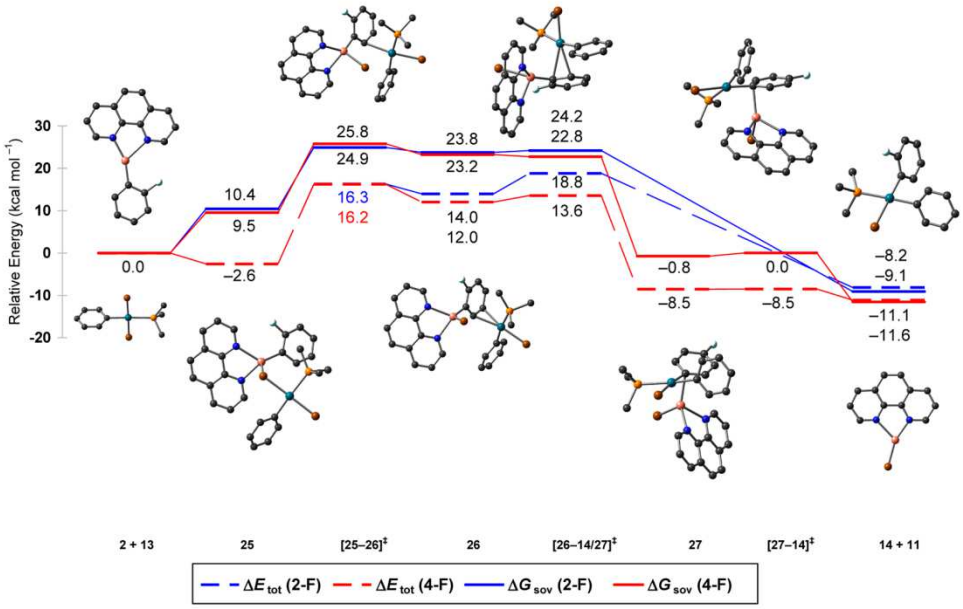

Figure 5. B3LYP/6-31+G(d) optimized structures for the transmetalation of the phenanthroline copper 2-fluorophenyl complex (**2**) with $[Pd(PMe_3)(Ph)Br_2]^-$ (**13**); hydrogens are omitted for clarity. Energy and solution Gibbs energy profiles overlaid for the 2- and 4-fluorophenyl derivative. Color code: C, black; Br, brown; Cu, orange; F, turquoise; N, blue; P, yellow; Pd, green.

Further shortening of the Pd−C(1) bond leads to another transition state [**24**−**13**]‡, that has a Pd−C(1) bond length of 2.03 Å, and in which a Pd−Br bond is starting to form (2.89 Å). The C−Br bond is elongated to 2.22 Å. The forward motion along the reaction coordinate derived from the normal mode of the imaginary frequency (126 i cm^{-1}) is dominated by the movement of the palladium atom into the plane of the aromatic ring, resulting in a shortening of the Pd−C(1) bond, while the bromine moves out of this plane with concomitant elongation of the C−Br bond. The activation barrier for this step is rather low ($\Delta^{‡}E_{tot}$ = 7.0 kcal mol^{-1}, $\Delta^{‡}G_{sov}$ = 6.2 kcal mol^{-1}).

In the final oxidative addition product, the trimethylphosphino(phenyl)dibromopalladate **13**, the palladium is in a slightly distorted square-planar environment with the two bromine ligands *trans* to each other. The Pd−Br(1) and Pd−Br(2) bonds have almost the same lengths (2.54 and 2.52 Å), and the Pd−C distance amounts to 2.03 Å.

The overall oxidative addition process is strongly exothermic (Δ_rE_{tot} = −30.3 kcal mol^{-1}), and although two molecules are converted to one product, it remains exergonic (Δ_rG_{sov} = −18.1 kcal mol^{-1}). Under the reaction conditions of the decarboxylative coupling, the oxidative addition can be expected to proceed very smoothly.

Transmetalation. In the transmetalation step, the phenanthroline copper 2- or 4-fluorophenyl complex **2**, obtained by decarboxylation of copper 2- or 4-fluorophenyl benzoate, has to approach the palladium complex **13**, formed by the oxidative addition, in order to transfer the fluorophenyl group to the palladium center. One would expect to find that the actual transmetalation step would be preceded by the formation of an energetically favorable adduct between **2** and **13**, which would explain that this entropically unfavorable step takes place even at the low experimental concentrations of the two species.

We first sought for attractive interactions between **2a** and **13** by positioning the two fragments close to each other at various angles and orientations. Whereas no energetically favorable interaction was found, e.g., when approaching the palladium and the π-system of the fluorophenyl ring, bringing palladium complex **13** into close proximity to the copper atom in **2a** via its bromine ligand results in the formation of a stable adduct (**25a**, Figure 5). The formation of a long Cu−Br(1) bond (2.82 Å) makes this step energetically favorable (Δ_rE_{tot} = −2.6 kcal mol^{-1}), which makes up for some of the high entropic hurdle and loss of solvation energy associated with forming an adduct at high reaction temperatures. In the present case, the amount of entropy lost is 33.4 cal K^{-1} mol^{-1}, which at 443 K increases Δ_rG_{sov} by 14.8 kcal mol^{-1}. The dispersion interaction additionally stabilizes the adduct by 13.1 kcal mol^{-1}, whereas 9.1 kcal mol^{-1} solvation energy is lost. Together, these factors turn a slightly exothermic step into a moderately endergonic one (Δ_rG_{sov} = 10.4 kcal mol^{-1}). The additional Cu−Br(1) bond changes the coordination environment at the copper center from a coordinatively unsaturated distorted trigonal planar arrangement to a distorted tetrahedral geometry (∠Cu−Br−Pd = 108.8°). The formation of the loose Cu−Br(1) contact (2.82 Å) does not lead to a significant elongation of the Pd−Br(1) bond (2.53 Å), and the geometry of the palladium fragment remains almost unchanged. The fluorophenyl group is bent outward slightly, but is not twisted. A transit scan from **25** with a stepwise elongation of the Cu−Br(1) bond revealed that in the gas phase, the encounter complex **25** is formed without a barrier.

Adduct **25** was found to be the entry point to a transmetalation pathway in which the bromine ligand is transferred from palladium to copper prior to transfer of the fluorophenyl group in the opposite direction. A search for alternative transmetalation pathways in which, for example, the transfer of the fluorophenyl group from Cu to Pd precedes that of the bromine ligand from Pd to Cu, did not yield any results.

This was to be expected in the absence of attractive interactions between the fluorophenyl group and the copper.

Shortening the Cu−Br(1) bond of **25a** to 2.54 Å leads to an energetically reasonable transition state [**25a**−**26a**]‡ ($\Delta^{‡}E_{tot}$ = 18.9 kcal mol^{-1}, $\Delta^{‡}G_{sov}$ = 14.5 kcal mol^{-1}). In [**25a**−**26a**]‡, the palladium is coordinated to the C(2) carbon of the fluorophenyl group over a rather long bond (2.59 Å), while the Pd−Br(1) bond is almost broken (3.65 Å). The tetrahedral environment at the copper is now more symmetrical than in adduct **25a**. The forward motion along the reaction coordinate derived from the normal mode of the imaginary frequency (30 i cm^{-1}) is dominated by the elongation of the Pd−Br(1) bond with a simultaneous shortening of the Pd−C(2) and Pd−C(3) distances. The IRC calculation confirms that this transition state leads to intermediate **26a**, in which the palladium atom is coordinated to the C(2)−C(3) π-bond in an almost symmetrical fashion (Pd−C(2): 2.48 Å; Pd−C(3): 2.52 Å). The Cu−Br(1) bond is slightly shortened to 2.51 Å. Intermediate **26a** is almost as high in energy as the transition state.

Starting from **25a**, no trajectory could be found along which the palladium would directly attack the C(1) carbon of the fluorophenyl group, so that the transfer of the bromine and of the fluorophenyl group would occur in a single step. This finding corresponds well with those for several oxidative addition and transmetalation pathways of other aromatic substrates, which also have been found to involve the intermediate formation of π-complexes to the C(2)−C(3) bond of the arene rings.[24b,47]

Shortening the Pd−C(1) distance leads to a transition state [**26a**−**14a**]‡ across a rather low activation barrier ($\Delta^{‡}E_{tot}$ = 4.8 kcal mol^{-1}, $\Delta^{‡}G_{sov}$ = 0.4 kcal mol^{-1}). In [**26a**−**14a**]‡, the palladium atom has shifted to the C(1)−C(2) π-bond of the fluorophenyl group. The Pd−C(1) bond is slightly longer than the Pd−C(2) bond (Pd−C(1): 2.82 Å; Pd−C(2): 2.60 Å). The copper atom remains in the plane of the fluorophenyl ring, and the Cu−C(1) bond has the same length as in **26a** (1.96 Å). The distance between the copper and palladium atoms is reduced to only 3.30 Å. The forward motion along the reaction coordinate derived from the normal mode of the imaginary frequency (59 i cm^{-1}) is dominated by a lengthening of the Pd−C(2) bond with concomitant shortening of the Pd−C(1) and Cu−Pd bonds, resulting in the transfer of the fluorophenyl group from copper to palladium.

At first sight, it seemed counterintuitive that the copper atom would remain in the plane of the arene ring in transition state [**26a**−**14a**]‡, and that the Cu−C(1) bond length would not significantly contribute to the normal mode corresponding to the imaginary frequency. We would have expected a transition state structure in which the copper would already have moved out of the plane of the fluorophenyl ring and the Cu−C(1) bond would already have been elongated. We therefore investigated the pathway from [**26a**−**14a**]‡ to the transmetalation products **14a** + **11** in some detail by IRC calculations, followed by geometry optimizations. On the way downhill, we came across regions of the potential energy surface with molecular geometries meeting our above expectations, but found no stationary points. Instead, this process confirmed that the transition state [**26a**−**14a**]‡ indeed connects intermediate **26a** with the transmetalation products **14a** + **11**. The somewhat surprising structural features of the transition state are a consequence of its being very early, which conforms to the Hammond postulate.[48] Aryl transfer and separation into two fragments occur simultaneously in this final phase of the transmetalation, which is therefore quite exothermic ($\Delta_r E_{tot}$ = −22.2 kcal mol^{-1}) and even more exergonic ($\Delta_r G_{sov}$ = −32.9 kcal mol^{-1}), because of the substantial gain in entropy and solvation energy.

The products of the transmetalation are the regenerated phenanthroline copper bromide catalyst **11**, which was already described in the anion exchange chapter, and the square-planar *cis*-diaryl palladium complex **14a**. Its Pd−C(1) bond length is further shortened to 2.04 Å, which is almost the same as that of the Pd−C(1′) bond of 2.05 Å. Overall, the entire transmetalation starting from **2a** and **13** and leading to **11** and **14a** is moderately exothermic ($\Delta_r E_{tot}$ = −8.2 kcal mol^{-1}) and exergonic ($\Delta_r G_{sov}$ = −9.1 kcal mol^{-1}).

The reaction pathway for the transfer of the 4-fluorophenyl group from the aryl copper complex **2b** to the palladium complex **13** is different from that of the 2-fluorophenyl complex **2a**. Both the geometries and the energies of several structures involved are markedly different. Moreover, an additional intermediate is involved in the transmetalation for the 4-fluorophenyl derivative.

Adduct **25b** and the first transition state [**25b**−**26b**]‡ have closely related structural features and relative energies to their *ortho*-regioisomers. Compared to **26a**, intermediate **26b** is lower in energy by −2.0 kcal mol^{-1} and the Gibbs energy is lower by −0.6 kcal mol^{-1}. According to our calculations, this can be attributed to the energy of solvation and explained with greater structural differences between these intermediates. After elongation of the Pd−Br contact in [**25**−**26**]‡, the 4-fluorophenyl group rotates around the Cu−C bond, which does not occur with the 2-fluorophenyl group. The structures of **26a** and **26b** provided in the Supporting Information are displayed with the fluorophenyl groups and coordinated palladium fragments in the same orientation. In **26a**, the phenanthroline points to the left and the bromine to the right of the copper. In **26b**, the phenanthroline points downward and the bromine upward. The Cu−Br bond in **26b** is somewhat longer (2.60 Å) than in [**25b**−**26b**]‡ (2.52 Å). The Pd−C(2) bond in **26b** is shorter by ca. 0.2 Å compared to the Pd−C(3) bond (Pd−C(2): 2.41 Å; Pd−C(3): 2.60 Å).

The energetic hurdle between **26b** and the transition state [**26b**−**27**]‡ amounts to $\Delta^{‡}E_{tot}$ = 1.6 kcal mol^{-1}. This barrier is only one-third as high as that for the *ortho*-substituted derivative and can again be attributed to structural differences. The Pd−C(2) bond is slightly shorter (2.46 Å) than in [**26a**−**14a**]‡ (2.60 Å), and the distance between copper and palladium of 3.55 Å in [**26b**−**27**]‡ is longer compared to 3.30 Å in [**26a**−**14a**]‡.

In contrast to the *ortho*-intermediate, **26b** does not lead to the transmetalation products **14b** + **11** in a single step. It involves an additional intermediate **27** in which the palladium fragment is in a nearly square-planar environment. The palladium atom has almost moved into the plane of the fluorophenyl ring, and the Pd−C(1) bond has shortened to 2.10 Å. The copper atom has moved below the plane of the fluorophenyl ring but is still connected to its *ipso* carbon over a very long Cu−C(1) bond (2.32 Å). The Pd−C(1)−Cu angle of 77.8° is very small, so that the two transition metals are in close proximity to each other. The Pd−Cu distance is as short as 2.77 Å, which is smaller than the sum of their van der Waals radii (3.03 Å).[49] Completing the transmetalation from intermediate **27** requires only little activation energy (transition state [**27**−**14b**]‡: $\Delta^{‡}E_{tot}$ = 0.0 kcal mol^{-1}, $\Delta^{‡}G_{sov}$ = 0.8 kcal mol^{-1}), so that the existence or nonexistence of the intermediate virtually has

dx.doi.org/10.1021/ja503295x | J. Am. Chem. Soc. 2014, 136, 10007−10023

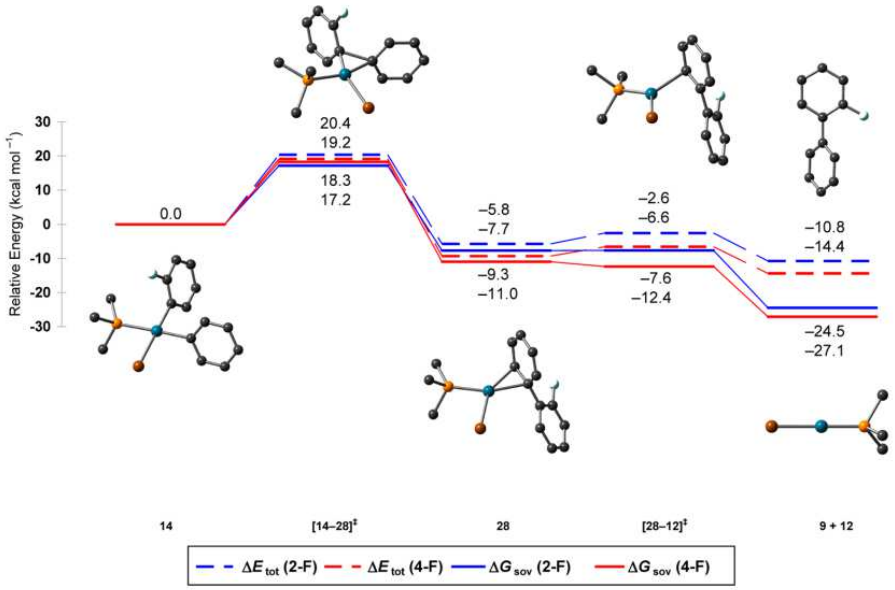

Figure 6. B3LYP/6-31+G(d) optimized structures for the reductive elimination of $[Pd(PMe_3)(2\text{-F-Ph})(Ph)Br]^-$; hydrogens are omitted for clarity. Energy and solution Gibbs energy profiles overlaid for the 2- and 4-fluorophenyl derivative. Color code: C, black; Br, brown; F, turquoise; P, yellow; Pd, green.

no effect on the reactivity. Still, we invested some effort in finding a corresponding intermediate for the *ortho*-case. Thus, the optimized structure **27** was transformed into its *ortho*-derivative by replacing F by H and either of the two *o*-hydrogens by fluorine. However, for either of these structures, new geometry optimizations directly led to the transmetalation products. The existence of the intermediate **27** for the *para*- but not the *ortho*-case may be explained with electronic effects due to the fluorine substituent. The mesomeric effects of the fluorine substituent are comparable for the *ortho*- and *para*-positions, but the inductive effect on the *ipso* carbon of the fluorine in the *ortho*-position is certainly higher due to the smaller number of interjacent σ-bonds. In the 4-fluorophenyl ring, the electron-donating mesomeric effect of the fluorine predominates over the inductive effect and pushes sufficient electron density into the *ipso*-carbon to bind both transition metals simultaneously and lending stability to intermediate **27**. Contrarily, in the 2-fluorophenyl ring, the short-range electron-withdrawing inductive effect outweighs the mesomeric effect. The *ipso*-carbon thus lacks the electron density required to coordinate to palladium and copper at the same time.

Intermediate **27** features the shortest Pd–Cu distance (2.77 Å) observed in all these calculations. This begs the question whether there is an interaction or even a bond between copper and palladium. This is very difficult to answer with DFT calculations. Methods such as the analysis of the natural bond order (NBO), the bond critical point (BCP), or the shared electron number (SEN) with DFT are often regarded as inconclusive. Therefore, we looked for literature on bimetallic complexes with similarly short copper–palladium distances in which metal–metal interactions and bonds are discussed.

Kawamura et al. crystallized $[Pd_3(S_2CN^nPr_2)_6Cu_2][PF_6]_2$ and found slightly longer Pd–Cu distances of 2.864(4) and 2.896(4) Å.[50] Their XPS binding studies suggest weak Pd–Cu bonding interactions. However, the authors were unable to prove the existence of direct Pd–Cu bonding. Peng and Rohmer crystallized $[Cu_2Pd(dpa)_4Cl_2]$ (dpa = dipyridylamine) with somewhat shorter Pd–Cu distances of 2.4971(3) and 2.5022(3) Å.[51] For this complex, magnetic susceptibility measurements revealed an antiferromagnetic coupling between the two Cu^{II} metal centers connected to the Pd atom, which could be confirmed by powder EPR experiments, DFT calculations, and wave function theory calculations.[52] Osakada et al. observed Pd–Cu distances of 2.462(1) and 2.632(1) Å in crystallized $[Pd(\mu\text{-CuI})(Pd(dmpe))_3(\mu_3\text{-GePh}_2)_3]$.[53] ^1H and $^{13}C\{^1H\}$ NMR experiments of the complex at various temperatures revealed that Cu forms a stable Pd–Cu bond to the core palladium and a labile Pd–Cu bond to one edge palladium. Because interactions or even bonds between copper and palladium could be proven for these complexes, which all possess short Pd–Cu distances in the same range as our intermediate **27**, we believe that attractive interactions between the copper and palladium atoms are at play also in the transmetalation step of decarboxylative cross-couplings.

Overall, our DFT results show that the transmetalation process is exothermic (*ortho*: $\Delta_rE_{tot} = -8.2$ kcal mol^{-1}; *para*: $\Delta_rE_{tot} = -11.1$ kcal mol^{-1}) as well as exergonic (*ortho*: $\Delta_rG_{sov} = -9.1$ kcal mol^{-1}; *para*: $\Delta_rG_{sov} = -11.6$ kcal mol^{-1}). However, the process starts with the formation of a bimetallic adduct that is endergonic (*ortho*: $\Delta_rG_{sov} = 10.4$ kcal mol^{-1}; *para*: $\Delta_rG_{sov} = 9.5$ kcal mol^{-1}). Furthermore, the transmetalation faces high activation barriers for its transition states that we will compare with those for the other elementary steps at the end of this section.

Reductive Elimination. In the reductive elimination step, the biaryl product **9** is liberated from the square-planar *cis*-diarylpalladium complex **14**, regenerating the initial palladium catalyst **12** (Figure 6). Both for the *ortho*- and the *para*-substituted model compounds, the overall process is moderately exothermic (*ortho*: $\Delta_rE_{tot} = -10.8$ kcal mol^{-1}; *para*: $\Delta_rE_{tot} = -14.4$ kcal mol^{-1}) and strongly exergonic (*ortho*: $\Delta_rG_{sov} =$

dx.doi.org/10.1021/ja503295x | J. Am. Chem. Soc. 2014, 136, 10007–10023

Scheme 8. Anionic Reaction Pathways Investigated for the Anion Exchange, Decarboxylation, and Adduct Formation

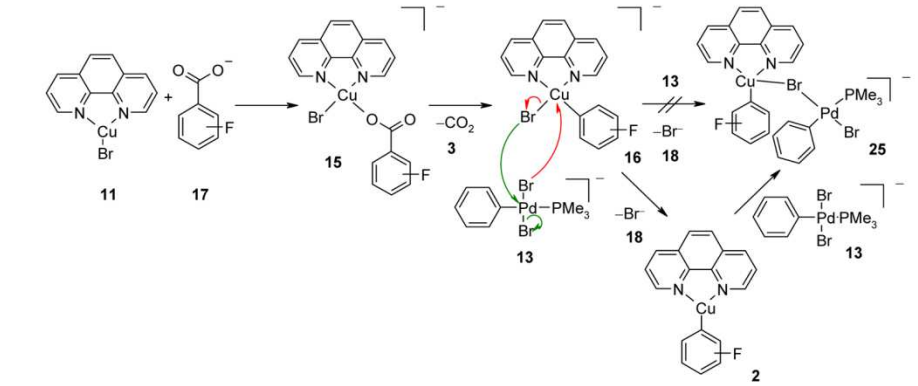

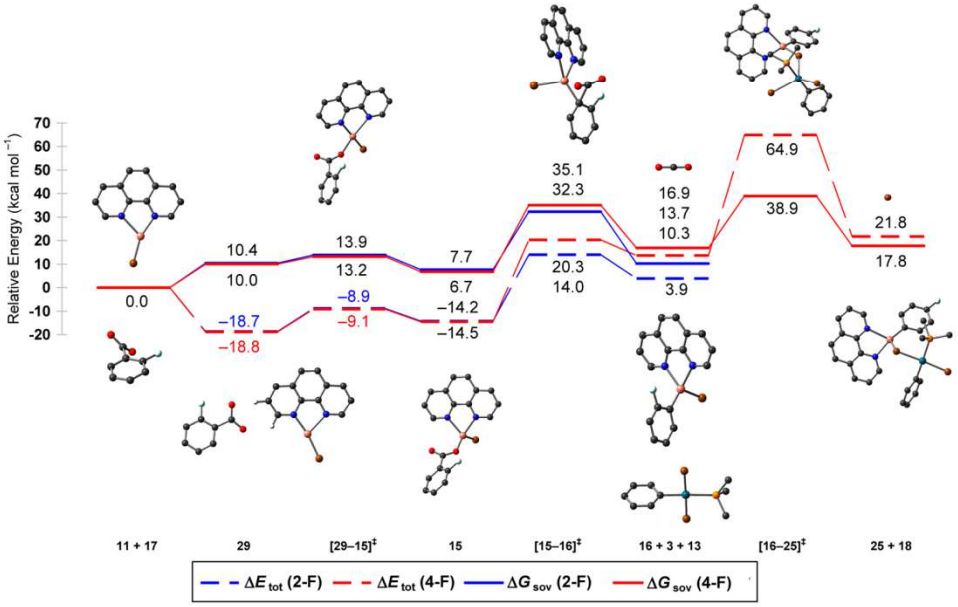

Figure 7. B3LYP/6-31+G(d) optimized structures for the anionic reaction pathway for anion exchange, decarboxylation, and adduct formation; hydrogens are omitted for clarity. Energy and solution Gibbs energy profiles overlaid for 2- and 4-fluorobenzoate. Color code: C, black; Br, brown; Cu, orange; F, turquoise; N, blue; O, red; P, yellow; Pd, green.

−24.5 kcal mol^{-1}; *para*: $\Delta_r G_{sov}$ = −27.1 kcal mol^{-1}), since two molecules form from one.

Starting from **14a**, a first transition state [**14a**–**28a**]‡ was found by reducing the C(1) and C(1′) distance between the two aromatic rings in the square-planar complex to 1.88 Å. The barrier for its formation is comparatively low ($\Delta^{‡}E_{tot}$ = 20.4 kcal mol^{-1}, $\Delta^{‡}G_{sov}$ = 17.2 kcal mol^{-1}). The Pd–C bond lengths and the P–Pd–Br angle remain almost unchanged (Pd–C(1): 2.07 Å; Pd–C(1′): 2.11 Å; P–Pd–Br: 88.6°). The forward motion along the reaction coordinate derived from the normal mode of the imaginary frequency (306 i cm^{-1}) is dominated by a shortening of the aryl–aryl bond, while the angle between the planes of the aromatic rings is reduced.

An IRC calculation revealed that transition state [**14a**–**28a**]‡ connects structure **14a** with intermediate **28a**. In **28a**, the aryl–aryl bond is fully formed with a final length of 1.49 Å, but the palladium remains η^2-coordinated to the C(1′)–C(2′) bond of the biaryl product (Pd–C(1′): 2.25 Å; Pd–C(2′): 2.17 Å; P–Pd–Br: 94.7°).

The energy barrier for the release of the Pd(0) catalyst **12** is very low ($\Delta^{‡}E_{tot}$ = 3.2 kcal mol^{-1}, $\Delta^{‡}G_{sov}$ = 0.03 kcal mol^{-1}). In the transition state [**28a**–**12a**]‡, which was found by increasing the distance between palladium and the phenyl ring, the palladium atom remains coordinated to C(2′) over a distance of 2.35 Å, and the P–Pd–Br angle has increased to 126.1°. The forward motion along the reaction coordinate derived from the normal mode of the imaginary frequency (54 i cm^{-1}) is dominated by a lengthening of the Pd–C bond with simultaneous opening of the P–Pd–Br angle (Pd–C(2′): 2.35 Å; P–Pd–Br: 126.1).

A further IRC calculation showed that this transition state connects directly to the linear anionic monophosphine palladium complex **12** and the biaryl **9a**. In **9a**, the angle between the planes of the two aromatic rings amounts to 44.3°.

dx.doi.org/10.1021/ja503295x | J. Am. Chem. Soc. 2014, 136, 10007–10023

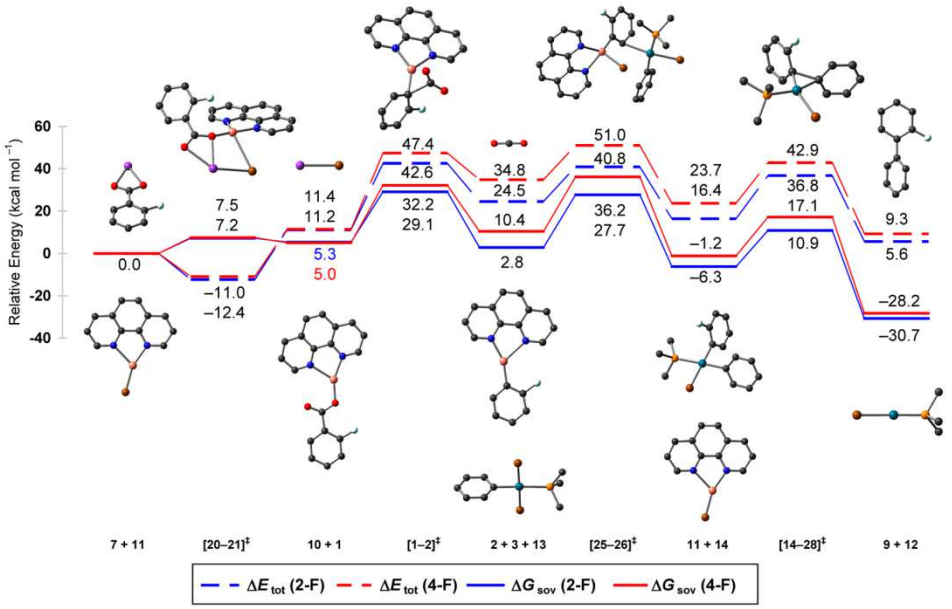

Figure 8. B3LYP/6-31+G(d) optimized structures for the simplified reaction profile; hydrogens are omitted for clarity. Energy and solution Gibbs energy profiles overlaid for the 2- and 4-fluorophenyl derivative. Color code: C, black; Br, brown; Cu, orange; F, turquoise; K, purple; N, blue; O, red; P: yellow; Pd, green.

As can be seen in Figure 6, the reaction pathway for the 4-fluorophenyl derivative is almost identical with that for the 2-derivative. The main activation barrier ($\Delta^{\ddagger}E_{tot}$ = 19.2 kcal mol^{-1}, $\Delta^{\ddagger}G_{sov}$ = 18.3 kcal mol^{-1}) and the imaginary frequency of the transition state [**14b**–**28b**]‡ (316 i cm^{-1}) are almost identical with those for the 2-derivative. In biaryl **9b**, the dihedral angle is slightly smaller than in **9a** (41.4° versus 44.3°), since the *o*-hydrogen requires less space than the fluorine atom.

Anionic Copper Cycle. In the transformations discussed above, all Cu^{I} intermediates were neutral and tricoordinated. An alternative pathway can be envisaged in which the carboxylate anion adds to copper complex **11** leading to a tetracoordinate anionic copper species, which after extrusion of CO_2 undergoes the transmetalation (Scheme 8). In this alternative pathway, the equivalent to the anion exchange step would be the coordination of the carboxylate **17** to the copper complex **11**. The resulting anionic copper complex **15** would decarboxylate to the anionic copper complex **16**. Complex **16** would then react with the palladium catalyst **13** in an associative substitution reaction to give adduct **25**, which would be the starting point for the transmetalation process. Alternatively to this associative pathway, one could also imagine that the bromide would decoordinate from **16** to give the fluorophenyl copper phenanthroline complex **2**, which would associate with **13** to give the adduct **25**. The energy and solution Gibbs energy profiles for the anionic pathway (**11** → **15** → **16** → **25**) are shown in Figure 7.

The formation of adduct **15a** from 2-fluorobenzoate **17a** and the copper complex **11** is exothermic ($\Delta_r E_{tot}$ = −14.2 kcal mol^{-1}) in the gas phase and proceeds via an encounter complex **29a** and a transition state [**29a**–**15a**]‡. Due to the loss of entropy and solvation energy, this step is endergonic ($\Delta_r G_{sov}$ = 7.7 kcal mol^{-1}), with a barrier ($\Delta^{\ddagger}G_{sov}$ = 13.9 kcal mol^{-1}) that is higher than in the neutral anion exchange pathway (see Figure 2).

The anionic copper complex **15a** can then directly decarboxylate via transition state [**15a**–**16a**]‡, instead of first releasing the bromine ligand. The Gibbs activation energy of $\Delta^{\ddagger}G_{sov}$ = 24.6 kcal mol^{-1} is higher than that for the decarboxylation of the neutral phenanthroline copper 2-fluorobenzoate **1a** ($\Delta^{\ddagger}G_{sov}$ = 23.8 kcal mol^{-1}).

Two pathways are imaginable for the associative substitution reaction of the anionic copper complex **16** with the palladium catalyst **13** each leading to formation of a bromine bridge between the two metals. One of the Pd-bound bromide ligands may attack the copper center and replace its bromide (red arrows, Scheme 8), or conversely the Cu-bound bromide may attack the palladium center with loss of a Pd-bound bromide (green arrows). For the first pathway, we were unable to find any feasible pathway in our DFT calculations. For the second, a transition state [**16b**–**25b**]‡ could be located only for the *p*-fluoro-substituted derivative. The activation barrier is very high ($\Delta^{\ddagger}E_{tot}$ = 51.2 kcal mol^{-1}, $\Delta^{\ddagger}G_{sov}$ = 22.0 kcal mol^{-1}). For the *ortho*-derivative **16a**, the only pathway we found required dissociation of the bromide. This dissociation of bromide is thermodynamically downhill for both the *ortho*- and the *para*-derivative (**16a**/**16b**), and leads to the phenanthroline copper fluorophenyl complex **2a**/**2b**, so that the neutral pathway is re-entered. When similar calculations were performed with potassium ions, we found direct elimination of KBr and a direct re-entry into the neutral pathway. Overall, the anionic complexes **15a**/**b** do not open up a pathway with a low energy profile that is more favorable for *ortho*- than for non-*ortho*-substituted benzoates and could explain why the former substrates react more readily in decarboxylative couplings.

Summary Assessment of the Catalytic Cycle. Improving a catalyst based on theoretical modeling requires a recipe for extracting the catalyst efficiency from the plethora of energetic data obtained in the calculations. The energetic span concept by Amatore and Jutand[54] says that the largest possible

rate and, correspondingly, the highest turnover number of the catalytic cycle is obtained for the lowest Gibbs energy span, which is the Gibbs energy difference between the highest transition state and lowest intermediate of the entire cycle. This concept has been refined by Kozuch and Shaik[55] by taking into account overall exergonicity. In our case, the situation is more complicated because of the two intertwined catalytic cycles, which join and separate at the transmetalation. The approximation behind the energy span concept is that the concentration c_i of a catalyst intermediate i is given by $c_i = c_0 \exp(-\Delta G_i/RT)$, where c_0 is the overall catalyst concentration and ΔG_i the Gibbs energy of i with respect to the most stable intermediate, where most of the catalyst is trapped. Both our calculated energy profile and our experience with related catalytic reactions tell us that the palladium catalyst is capable of providing the oxidative addition product **13** at a much faster rate than the cross-coupling proceeds, and according to our calculations, the oxidative addition is exergonic ($\Delta_r G = -18.1$ kcal mol^{-1}). Therefore, we can simplify the kinetic model by assuming that the stationary concentration of **13** is given by the overall amount of palladium catalyst. In other words, we consider a reaction with a single catalytic cycle in which one of the educts is **13** at its catalytic concentration, instead of the aryl bromide **8** at a stoichiometric concentration. We then apply the energetic span concept to the energy profile derived from this single cycle, which involves four steps (anion exchange, CO_2 extrusion, transmetalation, reductive elimination). Since none of these steps feature an intermediate lower in Gibbs energy than either their educts or their products, we need only consider a single effective activation energy given by the highest transition state of each step. This resulting simplified energy diagram is shown in Figure 8.

The energy barriers of this simplified reaction profile with the highest barrier at $\Delta^{\ddagger}G_{sov} = 36.2$ kcal mol^{-1} are consistent with a reaction that takes place at temperatures around 160 °C.

For the *ortho*-case, the largest Gibbs energy span, which represents the apparent activation energy of the overall cycle, is between the starting materials (**7a** + **11**) and the decarboxylation transition state [**1a**−**2a**]‡ (29.1 kcal mol^{-1}). For the *para*-case, the largest Gibbs energy span is between the starting materials (**7b** + **11**) and the transmetalation transition state [**25b**−**26b**]‡ (36.2 kcal mol^{-1}). This implies that for the *ortho*-case, the decarboxylation transition state and for the *para*-case, the transmetalation transition state is the rate-limiting transition state. Considering each step individually, one would come to a different conclusion since for the *ortho*-case, the barrier is lower in the decarboxylation (23.8 kcal mol^{-1}) compared to the transmetalation (24.9 kcal mol^{-1}), whereas for the *para*-case the barrier is higher in the decarboxylation (27.1 kcal mol^{-1}) than in the transmetalation (25.8 kcal mol^{-1}). This contrast stems from the exergonicity/endergonicity of the decarboxylation step as its products are the starting point for the subsequent transmetalation. For the *ortho*-case the decarboxylation is exergonic by −2.5 kcal mol^{-1} which decreases the starting point and the highest transition state of the transmetalation, while for the *para*-case the decarboxylation is endergonic by 5.4 kcal mol^{-1}, which increases the starting point and the highest transition state of the transmetalation, which explains the outcome of the overall reaction profile. For the *ortho*-case the difference between the heights of the decarboxylation (29.1 kcal mol^{-1}) and transmetalation transition state (27.7 kcal mol^{-1}) lies within the inaccuracy of the computational method. It is safe to say that the decarboxylation and the transmetalation are so similar in energy that it probably depends on the individual substrate which of these two steps will be rate-determining.

As discussed above, the reason for the high overall barrier of the transmetalation is the entropic penalty associated with forming an adduct of two species present only in catalytic amounts, together with a loss in solvation energy. The accuracy of some contributions to the activation energy such as solvent effects is difficult to assess. However, such systematic errors are likely to cancel out when calculating the *para*/*ortho* difference in the Gibbs energy span. This difference is considerable (7.1 kcal mol^{-1}), and agrees with the experimental observation that 4-fluorobenzoate is substantially less reactive than its *ortho*-isomer. Interestingly, the largest contribution to this difference stems from the exer-/endergonicity of the decarboxylation step, where the difference between *para* and *ortho* is $\Delta\Delta_r G_{sov} = 7.6$ kcal mol^{-1}.

Based on this profile, it can also be understood why the presence of halide anions can affect the reaction rate. The presence of excess bromide shifts the equilibrium of the anion exchange step to the side of the copper bromide so that less copper carboxylate is available. If for a given substrate the decarboxylation is the rate-determining step in a decarboxylative cross-coupling, the presence of excess bromide should have a similar effect, because it increases the energy span between **7** + **11** and [**1**−**2**]‡ + **10** by about 3 kcal mol^{-1}.

Experimental Studies. The above DFT studies suggest that the transmetalation is rate-limiting for substrates that decarboxylate comparatively easily. Bidentate ligands designed to bridge the two metals and bring them into close spatial proximity can be expected to facilitate this step. To test this hypothesis, we first searched for a benzoic acid that decarboxylates with particular ease. We performed a series of protodecarboxylation experiments in which various benzoic acids **22** were heated to 100 °C in the presence of 5 mol % Cu_2O and 10 mol % 1,10-phenanthroline (Table 1). No conversion was observed at this low temperature for most carboxylic acids tested, including 2- and 4-fluorobenzoic acid (**22a** or **22b**) (entries 1 and 2). However, 2-nitrobenzoic acid (**22c**) was smoothly converted into nitrobenzene (**30**) in near-quantitative yield (entry 5).

Table 1. Protodecarboxylation of Benzoic Acids[a]

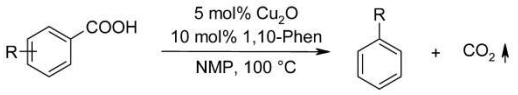

22 **23** or **30** **3**

entry	carboxylic acid	R	*t*/h	product	yield/%
1	**22a**	2-F	6	**23**	3
2	**22b**	4-F	6	**23**	0
3	**22c**	2-NO_2	6	**30**	64
4	**22d**	4-NO_2	6	**30**	0
5	**22c**	2-NO_2	24	**30**	99

[a]Reaction conditions: 0.5 mmol of carboxylic acid, 5 mol % Cu_2O, 10 mol % 1,10-Phen, 2.0 mL of NMP, 100 °C, GC yield after calibration.

It could thus be expected that the decarboxylation is not the rate-limiting step in a decarboxylative cross-coupling of 2-nitrobenzoic acid (**22c**) at 100 °C. We next performed various decarboxylative couplings at this temperature. Among all aryl electrophiles tested, triflates were the sole substrates to provide

Table 2. Decarboxylative Cross-Couplings with Monodentate and Bridging Ligands[a]

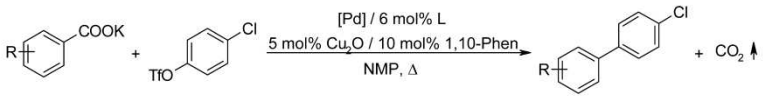

7 31 32 3

entry	carboxylate	R	temp/°C	L	product	yield/%
1	**7c**	2-NO_2	100	P(*p*-Tol)$_3$	**32c**	9
2	**7d**	4-NO_2	100	P(*p*-Tol)$_3$	**32d**	0
3[b]	**7c**	2-NO_2	170	P(*p*-Tol)$_3$	**32c**	84 (91)[7a]
4	**7c**	2-NO_2	100	L1	**32c**	0
5	**7c**	2-NO_2	100	L2	**32c**	0
6	**7c**	2-NO_2	100	L3	**32c**	0
7	**7c**	2-NO_2	100	L4	**32c**	40
8[c]	**7c**	2-NO_2	100	L4	**32c**	88

[a]Reaction conditions: 0.5 mmol of potassium carboxylate, 1 mmol of triflate, 5 mol % Cu_2O, 10 mol % 1,10-Phen, 2 mol % PdI_2, 6 mol % L, 2.0 mL of NMP, 100 °C, 24 h, GC yield after calibration. [b]1 mmol of potassium carboxylate, 2 mmol of triflate, 5 mol % Cu_2O, 10 mol % 1,10-Phen, 2 mol % PdI_2, 6 mol % P(*p*-Tol)$_3$, 4.0 mL of NMP, 170 °C, 1 h, GC yield after calibration, isolated yield in parentheses. [c]0.75 mmol of potassium carboxylate, 0.5 mmol of triflate, 5 mol % Cu_2O, 10 mol % 1,10-Phen, 3 mol % Pd(acac)$_2$, 6 mol % L4, 4.0 mL of NMP, 100 °C, 24 h, GC yield after calibration.

the coupling products in small amounts. For this reason, we investigated the coupling of 4-chlorophenyl triflate (**31**) with several potassium nitrobenzoates **7** as the model systems. With the best known catalyst system (Table 2), no conversion was observed in the coupling of potassium 4-nitrobenzoate (**7d**) with 4-chlorophenyl triflate (**31**) (entry 2), and potassium 2-nitrobenzoate (**7c**) gave less than 10% of 4-chloro-2′-nitrobiphenyl (**32c**) (entry 1). According to the literature, cross-couplings of aryl triflates with potassium benzoates with Cu/Pd systems and monodentate *p*-tolylphosphine have to be performed at 170 °C to give high yields.[7a,b]

We then replaced the *p*-tolylphosphine ligand by various bidentate P,N-ligands (Figure 9).[9,56] Among these, the

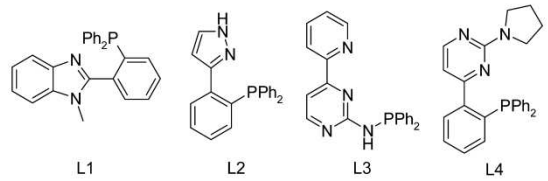

Figure 9. Bidentate P,N-ligands.

aminopyrimidinyl phosphines, especially ligand L4, developed by Thiel et al. in the context of other coupling reactions were most effective (entry 7).[56c] After slight modifications to the reaction conditions, the coupling product **32c** was detected in high yield (88%) already at 100 °C (entry 8).

Lowering the reaction temperature by as much as 70 °C is a decisive improvement over the state of the art, which we attribute to the ability of this ligand to bring copper and palladium into close proximity and thus assist the transmetalation step. The presence of bimetallic Cu−Pd complexes was confirmed by ESI-MS investigations of the reaction mixture, suggesting that their formation is no longer rate-determining.[28] Further experimental studies with the bidentate ligands, including the structural investigation of Cu/Pd adducts detected by ESI-MS, are underway. We are convinced that the concept of bringing the two metals together by bridging ligands will allow reaching new levels of efficiency in decarboxylative couplings of activated benzoates.

Conclusions and Outlook. The geometries and energies of all starting materials, products, intermediates, and transition states of the catalytic cycle were calculated for the decarboxylative cross-coupling of potassium 2- and 4-fluorobenzoate with bromobenzene in the presence of a catalyst system consisting of copper(I)/1,10-phenanthroline and the anionic monophosphine palladium complex [Pd(PMe$_3$)Br]$^-$. Among all pathways investigated, a catalytic cycle via neutral copper complexes was found to be most favorable. It consists of a carboxylate−bromide exchange at the copper center to give an uncharged copper carboxylate, followed by a decarboxylation step in which an organocopper species is generated. A palladium species that has been formed by oxidative addition of the aryl electrophile to a low-valent palladium(0) species accepts the aryl group from the copper in the subsequent transmetalation step, which links the catalytic cycles of the copper and palladium catalysts. The resulting diarylpalladium species undergoes reductive elimination, releasing the biaryl product and regenerating the palladium(0) species (Scheme 6).

Based on realistic assumptions on the inherent accuracy of these calculations, the energetic span model cannot unambiguously decide whether the decarboxylation or the transmetalation is rate-determining. This implies that depending on the substrate, either step can pose the main limitation in the catalyst performance. This is in sharp contrast to the current opinion that it is only the decarboxylation step that needs to be addressed in the catalyst improvement. The calculations also do not support the hypothesis that the difference in reactivity between *ortho*- and non-*ortho*-substituted carboxylates in the reaction with aryl halides is caused by the anion exchange step. The low reactivity of the latter is probably caused by the higher barrier of the decarboxylation process, which is further increased in relation to the starting material if excess halide salt is present.

In the transmetalation, the electronic activation energy is not overly high. It is the free energy loss in the initial adduct formation that makes it difficult. This result suggests that future research aimed at further improving the catalyst should also target the transmetalation and not only the decarboxylation step. This was confirmed by an experimental study, in which

the reaction temperature of a decarboxylative coupling was lowered by 70 °C by a P,N-ligand designed to facilitate adduct formation between copper and palladium. In combination with these experimental findings, the mechanistic studies presented herein are likely to induce a paradigm shift in the development of more active catalyst generations for decarboxylative cross-coupling reactions.

■ ASSOCIATED CONTENT

Supporting Information

Energies, graphical representations, geometrical parameters and Cartesian coordinates of all DFT-optimized structures. This material is available free of charge via the Internet at http://pubs.acs.org.

■ AUTHOR INFORMATION

Corresponding Author

goossen@chemie.uni-kl.de; vanwullen@chemie.uni-kl.de

Notes

The authors declare no competing financial interest.

■ ACKNOWLEDGMENTS

We thank W. R. Thiel for help with the DFT calculations and for providing P,N-ligands, K. Gooßen for help proofreading the manuscript, and M. F. Grünberg for technical assistance. We also thank the DFG (GO 853/5-2 and SFB-TRR 88 "3Met") and Landesgraduiertenförderung Rheinland-Pfalz (fellowship to A.F.) for funding.

■ REFERENCES

(1) (a) Nilsson, M. *Acta Chem. Scan.* **1966**, *20*, 423−426. (b) Nilsson, M.; Ullenius, C. *Acta Chem. Scand.* **1968**, *22*, 1998−2002. (c) Chodowska-Palicka, J.; Nilsson, M. *Acta Chem. Scand.* **1970**, *24*, 3353−3361. (d) Shimizu, I.; Yamada, T.; Tsuji, J. *Tetrahedron Lett.* **1980**, *21*, 3199−3202. (e) Tsuji, J.; Yamada, T.; Minami, I.; Yuhara, M.; Nisar, M.; Shimizu, I. *J. Org. Chem.* **1987**, *52*, 2988−2995. (f) Myers, A. G.; Tanaka, D.; Mannion, M. R. *J. Am. Chem. Soc.* **2002**, *124*, 11250−11251. (g) Tanaka, D.; Myers, A. G. *Org. Lett.* **2004**, *6*, 433−436. (h) Tanaka, D.; Romeril, S. P.; Myers, A. G. *J. Am. Chem. Soc.* **2005**, *127*, 10323−10333.

(2) Goossen, L. J.; Deng, G.; Levy, L. M. *Science* **2006**, *313*, 662−664.

(3) (a) Rudolphi, F.; Song, B.; Goossen, L. J. *Adv. Synth. Catal.* **2011**, *353*, 337−342. (b) Collet, F.; Song, B.; Rudolphi, F.; Goossen, L. J. *Eur. J. Org. Chem.* **2011**, 6486−6501.

(4) (a) Goossen, L. J.; Rudolphi, F.; Oppel, C.; Rodríguez, N. *Angew. Chem.* **2008**, *120*, 3085−3088; *Angew. Chem., Int. Ed.* **2008**, *47*, 3043−3045. (b) Grünberg, M. F.; Gooßen, L. J. *J. Organomet. Chem.* **2013**, *744*, 140−143.

(5) Goossen, L. J.; Rodríguez, N.; Melzer, B.; Linder, C.; Deng, G.; Levy, L. M. *J. Am. Chem. Soc.* **2007**, *129*, 4824−4833.

(6) Goossen, L. J.; Zimmermann, B.; Knauber, T. *Angew. Chem.* **2008**, *120*, 7211−7214; *Angew. Chem., Int. Ed.* **2008**, *47*, 7103−7106.

(7) (a) Goossen, L. J.; Rodriguez, N.; Linder, C. *J. Am. Chem. Soc.* **2008**, *130*, 15248−15249. (b) Goossen, L. J.; Linder, C.; Rodríguez, N.; Lange, P. P. *Chem.—Eur. J.* **2009**, *15*, 9336−9349. (c) Goossen, L. J.; Lange, P. P.; Rodríguez, N.; Linder, C. *Chem.—Eur. J.* **2010**, *16*, 3906−3909.

(8) Goossen, L. J.; Rodríguez, N.; Lange, P. P.; Linder, C. *Angew. Chem.* **2010**, *122*, 1129−1132; *Angew. Chem., Int. Ed.* **2010**, *49*, 1111−1114.

(9) Song, B.; Knauber, T.; Goossen, L. J. *Angew. Chem.* **2013**, *125*, 3026−3030; *Angew. Chem., Int. Ed.* **2013**, *52*, 2954−2958.

(10) Shang, R.; Fu, Y.; Wang, Y.; Xu, Q.; Yu, H. Z.; Liu, L. *Angew. Chem.* **2009**, *121*, 9514−9518; *Angew. Chem., Int. Ed.* **2009**, *48*, 9350−9354.

(11) Sun, Z. M.; Zhao, P. *Angew. Chem.* **2009**, *121*, 6854−6858; *Angew. Chem., Int. Ed.* **2009**, *48*, 6726−6730.

(12) Weaver, J. D.; Recio, A., III; Grenning, A. J.; Tunge, J. A. *Chem. Rev.* **2010**, *111*, 1846−1913.

(13) (a) Peschko, C.; Winklhofer, C.; Steglich, W. *Chem.—Eur. J.* **2000**, *6*, 1147−1152. (b) Forgione, P.; Brochu, M. C.; St-Onge, M.; Thesen, K. H.; Bailey, M. D.; Bilodeau, F. *J. Am. Chem. Soc.* **2006**, *128*, 11350−11351. (c) Bilodeau, F.; Brochu, M. C.; Guimond, N.; Thesen, K. H.; Forgione, P. *J. Org. Chem.* **2010**, *75*, 1550−1560. (d) Miyasaka, M.; Fukushima, A.; Satoh, T.; Hirano, K.; Miura, M. *Chem.—Eur. J.* **2009**, *15*, 3674−3677. (e) Miyasaka, M.; Hirano, K.; Satoh, T.; Miura, M. *Adv. Synth. Catal.* **2009**, *351*, 2683−2688. (f) Arroyave, F. A.; Reynolds, J. R. *Org. Lett.* **2010**, *12*, 1328−1331.

(14) (a) Moon, J.; Jeong, M.; Nam, H.; Ju, J.; Moon, J. H.; Jung, H. M.; Lee, S. *Org. Lett.* **2008**, *10*, 945−948. (b) Moon, J.; Jang, M.; Lee, S. *J. Org. Chem.* **2009**, *74*, 1403−1406. (c) Kima, H.; Lee, P. H. *Adv. Synth. Catal.* **2009**, *351*, 2827−2832. (d) Park, K.; Bae, G.; Moon, J.; Choe, J.; Song, K. H.; Lee, S. *J. Org. Chem.* **2010**, *75*, 6244−6251. (e) Zhang, W.-W.; Zhang, X.-G.; Li, J.-H. *J. Org. Chem.* **2010**, *75*, 5259−5264. (f) Zhao, D.; Gao, C.; Su, X.; He, Y.; You, J.; Xue, Y. *Chem. Commun.* **2010**, *46*, 9049−9051. (g) Park, K.; Bae, G.; Park, A.; Kim, Y.; Choe, J.; Song, K. H.; Lee, S. *Tetrahedron Lett.* **2011**, *52*, 576−580. (h) Park, A.; Park, K.; Kim, Y.; Lee, S. *Org. Lett.* **2011**, *5*, 944−947.

(15) Shang, R.; Fu, Y.; Li, J. B.; Zhang, S. L.; Guo, Q. X.; Liu, L. *J. Am. Chem. Soc.* **2009**, *131*, 5738−5739.

(16) Yin, L.; Kanai, M.; Shibasaki, M. *J. Am. Chem. Soc.* **2009**, *131*, 9610−9611.

(17) (a) Zhang, S. L.; Fu, Y.; Shang, R.; Guo, Q. X.; Liu, L. *J. Am. Chem. Soc.* **2010**, *132*, 638−646. (b) Hu, P.; Kan, J.; Su, W. P.; Hong, M. C. *Org. Lett.* **2009**, *11*, 2341−2344. (c) Fu, Z.; Huang, S.; Su, W.; Hong, M. *Org. Lett.* **2010**, *12*, 4992−4995. (d) Sun, Z.-M.; Zhang, J.; Zhao, P. *Org. Lett.* **2010**, *12*, 992−995. (e) Goossen, L. J.; Zimmermann, B.; Knauber, T. *Beilstein J. Org. Chem.* **2010**, *6*, 43−51.

(18) (a) Voutchkova, A.; Coplin, A.; Leadbeater, N. E.; Crabtree, R. H. *Chem. Commun.* **2008**, 6312−6314. (b) Wang, C. Y.; Piel, L.; Glorius, F. *J. Am. Chem. Soc.* **2009**, *131*, 4194−4195. (c) Cornella, J.; Lu, P.; Larrosa, I. *Org. Lett.* **2009**, *11*, 5506−5509. (d) Zhang, F.; Greaney, M. F. *Angew. Chem.* **2010**, *122*, 2828−2831; *Angew. Chem., Int. Ed.* **2010**, *49*, 2768−2771.

(19) (a) Gledhill, A. P.; McCall, C. J.; Threadgill, M. D. *J. Org. Chem.* **1986**, *51*, 3196−3201. (b) Huang, W. H.; Wang, M. L.; Yue, H. *Synthesis* **2008**, 1342−1344. (c) Bi, H.-P.; Zhao, L.; Liang, Y.-M.; Li, C.-J. *Angew. Chem.* **2009**, *121*, 806−809; *Angew. Chem., Int. Ed.* **2009**, *48*, 792−795. (d) Bi, H.-P.; Chen, W.-W.; Liang, Y.-M.; Li, C.-J. *Org. Lett.* **2009**, *11*, 3246−3249.

(20) (a) Duan, Z. Y.; Ranjit, S.; Zhang, P. F.; Liu, X. G. *Chem.—Eur. J.* **2009**, *15*, 3666−3669. (b) Jia, W.; Jiao, N. *Org. Lett.* **2010**, *12*, 2000−2003. (c) Ranjit, S.; Duan, Z.; Zhang, P.; Liu, X. *Org. Lett.* **2010**, *12*, 4134−4136.

(21) (a) President's Information Technology Advisory Committee. *Computational Science: Ensuring America's Competitiveness*; Arlington, VA, 2005. (b) Mpourmpakis, G.; Vlachos, D. G. *MRS Bull.* **2011**, *36*, 211−215. and references therein (c) Goossen, L. J.; Rodríguez, N.; Linder, C.; Lange, P. P.; Fromm, A. *ChemCatChem.* **2010**, *2*, 430−442. (d) Dudník, A. S.; Xia, Y.; Li, Y.; Gevorgyan, V. *J. Am. Chem. Soc.* **2010**, *132*, 7645−7655.

(22) Goossen, L. J.; Thiel, W. R.; Rodríguez, N.; Linder, C.; Melzer, B. *Adv. Synth. Catal.* **2007**, *349*, 2241−2246.

(23) (a) Braga, A. A. C.; Ujaque, G.; Maseras, F. *Organometallics* **2006**, *25*, 3647−3658. and references therein (b) Kozuch, S.; Shaik, S.; Jutand, A.; Amatore, C. *Chem.—Eur. J.* **2004**, *10*, 3072−3080. (c) Kozuch, S.; Amatore, C.; Jutand, A.; Shaik, S. *Organometallics* **2005**, *24*, 2319−2330.

(24) (a) Goossen, L. J.; Koley, D.; Hermann, H.; Thiel, W. *J. Am. Chem. Soc.* **2005**, *127*, 11102−11114. (b) Goossen, L. J.; Koley, D.; Hermann, H.; Thiel, W. *Organometallics* **2006**, *25*, 54−67.

(25) Keith, J. A.; Behenna, D. C.; Mohr, J. T.; Ma, S.; Marinescu, S. C.; Oxgaard, J.; Stoltz, B. M.; Goddard, W. A., III *J. Am. Chem. Soc.* **2007**, *129*, 11876−11877.
(26) Shang, R.; Xu, Q.; Jiang, Y.-Y.; Wang, Y.; Liu, L. *Org. Lett.* **2010**, *12*, 1000−1003.
(27) Xie, H.; Lin, F.; Lei, Q.; Fang, W. *Organometallics* **2013**, *32*, 6957−6968.
(28) Hackenberger, D.; Song, B.; Grünberg, M. F.; Farsadpour, S.; Taghizadeh Ghoochany, L.; Menges, F.; Burkhardt, L.; Niedner-Schatteburg, G.; Thiel, W. R.; Goossen, L. J., *unpublished results.*
(29) Recently, related studies have investigated the transfer of an aryl group from palladium to gold: Perez-Temprano, M. H.; Casares, J. A.; de Lera, A. R.; Alvarez, R.; Espinet, P. *Angew. Chem., Int. Ed.* **2012**, *51*, 4917−4920.
(30) (a) *Gaussian 03*, Revision E.01; Gaussian, Inc.: Wallingford, CT, 2004. (b) *Gaussian 09*, Revision D.01; Gaussian, Inc.: Wallingford, CT, 2013; for full citations see the Supporting Information.
(31) (a) Stephens, P. J.; Devlin, F. J.; Chabalowski, C. F.; Frisch, M. J. *J. Phys. Chem.* **1994**, *98*, 11623−11627. (b) Becke, A. D. *J. Chem. Phys.* **1993**, *98*, 5648−5652. (c) Becke, A. D. *Phys. Rev. A* **1988**, *38*, 3098−3100. (d) Lee, C.; Yang, W.; Parr, R. G. *Phys. Rev. B* **1988**, *37*, 785−789.
(32) (a) Ditchfield, R.; Hehre, W. J.; Pople, J. A. *J. Chem. Phys.* **1971**, *54*, 724−728. (b) Hehre, W. J.; Ditchfield, R.; Pople, J. A. *J. Chem. Phys.* **1972**, *56*, 2257−2261. (c) Hariharan, P. C.; Pople, J. A. *Theor. Chim. Acta* **1973**, *28*, 213−222. (d) Clark, T.; Chandrasekhar, J.; Spitznagel, G. W.; Schleyer, P. v. R. *J. Comput. Chem.* **1983**, *4*, 294−301. (e) Rassolov, V. A.; Pople, J. A.; Ratner, M. A.; Windus, T. L. *J. Chem. Phys.* **1998**, *109*, 1223−1229. (f) Binning, R. C., Jr.; Curtiss, L. A. *J. Comput. Chem.* **1990**, *11*, 1206−1216. (g) Dunning, T. H. *J. Chem. Phys.* **1977**, *66*, 1382−1383.
(33) (a) Dolg, M.; Wedig, U.; Stoll, H.; Preuss, H. *J. Chem. Phys.* **1987**, *86*, 866−872. (b) Andrae, D.; Häußermann, U.; Dolg, M.; Stoll, H.; Preuss, H. *Theor. Chim. Acta* **1990**, *77*, 123−141.
(34) (a) Peng, C.; Schlegel, H. B. *Isr. J. Chem.* **1994**, *33*, 449−454. (b) Peng, C.; Ayala, P. Y.; Schlegel, H. B.; Frisch, M. J. *J. Comput. Chem.* **1996**, *17*, 49−56.
(35) (a) Fukui, K. *Acc. Chem. Res.* **1981**, *14*, 363−368. (b) Hratchian, H. P.; Schlegel, H. B. In *Theory and Applications of Computational Chemistry: The First 40 Years*; Dykstra, C. E., Frenking, G., Kim, K. S., Scuseria, G., Eds.; Elsevier: Amsterdam, The Netherlands, 2005; pp 195−249. (c) Hratchian, H. P.; Schlegel, H. B. *J. Chem. Phys.* **2004**, *120*, 9918−9924. (d) Hratchian, H. P.; Schlegel, H. B. *J. Chem. Theory Comput.* **2005**, *1*, 61−69.
(36) (a) Krishnan, R.; Binkley, J. S.; Seeger, R.; Pople, J. A. *J. Chem. Phys.* **1980**, *72*, 650−654. (b) Curtiss, L. A.; McGrath, M. P.; Blaudeau, J.-P.; Davis, N. E.; Binning, R. C.; Radom, L. *J. Chem. Phys.* **1995**, *103*, 6104−6113. (c) Blaudeau, J.-P.; McGrath, M. P.; Curtiss, L. A.; Radom, L. *J. Chem. Phys.* **1997**, *107*, 5016−5021.
(37) Weigend, F.; Ahlrichs, R. *Phys. Chem. Chem. Phys.* **2005**, *7*, 3297−3305.
(38) (a) Barone, V.; Cossi, M. *J. Phys. Chem. A* **1998**, *102*, 1995−2001. (b) Cossi, M.; Rega, N.; Scalmani, G.; Barone, V. *J. Comput. Chem.* **2003**, *24*, 669−681.
(39) (a) Klamt, A.; Schüürmann, G. *J. Chem. Soc., Perkin Trans. 2* **1993**, 799−805. (b) Schäfer, A.; Klamt, A.; Sattel, D.; Lohrenz, J. C. W.; Eckert, F. *Phys. Chem. Chem. Phys.* **2000**, *2*, 2187−2193.
(40) Wong, M. W. *Chem. Phys. Lett.* **1996**, *256*, 391−399.
(41) Murrieta-Guevara, F.; Romero-Martínez, A.; Trejo, A. *Fluid Phase Equilib.* **1988**, *44*, 105−115.
(42) Johnson, E. R.; Mackie, I. D.; DiLabio, G. A. *J. Phys. Org. Chem.* **2009**, *22*, 1127−1135.
(43) Grimme, S.; Antony, J.; Ehrlich, S.; Krieg, H. *J. Chem. Phys.* **2010**, *132*, 154104.
(44) Riley, K. E.; Vondrasek, J.; Hobza, P. *Phys. Chem. Chem. Phys.* **2007**, *9*, 5555−5560.
(45) *GaussView 5.0.8*; Gaussian, Inc.: Wallingford, CT, 2008.
(46) See the Supporting Information for details.
(47) (a) Goossen, L. J.; Koley, D.; Hermann, H.; Thiel, W. *Chem. Commun.* **2004**, 2141−2143. (b) Goossen, L. J.; Koley, D.; Hermann, H.; Thiel, W. *Organometallics* **2005**, *24*, 2398−2410.
(48) Hammond, G. S. *J. Am. Chem. Soc.* **1955**, *77*, 334−338.
(49) Bondi, A. *J. Phys. Chem.* **1964**, *68*, 441−451.
(50) Ebihara, M.; Tokoro, K.; Maeda, M.; Ogami, M.; Imaeda, K.; Sakurai, K.; Masuda, H.; Kawamura, T. *J. Chem. Soc., Dalton Trans.* **1994**, 3621−3635.
(51) Liu, I. P.-C.; Lee, G.-H.; Peng, S.-M.; Bénard, M.; Rohmer, M.-M. *Inorg. Chem.* **2007**, *46*, 9602−9608.
(52) Maynau, D.; Bolvin, H.; Van den Heuvel, W.; Bénard, M.; Rohmer, M.-M.; Ben Amor, N. *C. R. Chim.* **2012**, *15*, 170−175.
(53) Tanabe, M.; Ishikawa, N.; Chiba, M.; Ide, T.; Osakada, K.; Tanase, T. *J. Am. Chem. Soc.* **2011**, *133*, 18598−18601.
(54) Amatore, C.; Jutand, A. *J. Organomet. Chem.* **1999**, *576*, 254−278.
(55) Kozuch, S.; Shaik, S. *Acc. Chem. Res.* **2011**, *44*, 101−110.
(56) (a) Sun, Y.; Hienzsch, A.; Grasser, J.; Herdtweck, E.; Thiel, W. R. *J. Organomet. Chem.* **2006**, *691*, 291−298. (b) Sarcher, C.; Farsadpour, S.; Taghizadeh Ghoochany, L.; Sun, Y.; Thiel, W. R.; Roesky, P. W. *Dalton Trans.* **2014**, *43*, 2397−2405. (c) Farsadpour, S.; Taghizadeh Ghoochany, L.; Sun, Y.; Thiel, W. R. *Eur. J. Inorg. Chem.* **2011**, *29*, 4603−4609.

Nach der Veröffentlichung der optimierten Reaktionsbedingungen der Cu/Pd-katalysierten decarboxylierenden Kreuzkupplung mit *P*,*N*-Liganden bei 100 °C in *JACS* 2014 wurde die Anwendungsbreite der Reaktion von Gooßen, Thiel und Niedner-Schatteburg et al. untersucht. Weiterhin lieferten ESI-MS-Studien Hinweise auf die Fähigkeit des verwendeten *P*,*N*-Liganden, Kupfer und Palladium gleichzeitig zu koordinieren. Eine Publikation dieser Ergebnisse ist gerade in Vorbereitung.[71]

Zwischenzeitlich gelang es Gooßen et al., die Cu/Pd-katalysierte decarboxylierende Kreuzkupplung auch auf den Einsatz von Alkenylhalogeniden auszuweiten.[72] Dies erlaubt die Synthese von Arylalkenen, verbreiteten Strukturmotiven von Naturstoffen, biologisch aktiven Substanzen und funktionellen Wirkstoffen, ausgehend von aromatischen Carbonsäuren bei nur 130 °C.

3.3 Mechanistische Untersuchung der Ru-katalysierten Hydroamidierung terminaler Alkine

Das Strukturelement der Enamide kommt in Naturstoffen mit interessanten biologischen Eigenschaften sowie in pharmazeutischen Wirkstoffen,[73] die antibiotische,[74] anthelmintische,[75] antimykotische und zytotoxische[76–78] sowie Antitumor-Aktivität[79,80] zeigen, vor. Weiterhin können Enamide als vielseitige synthetische Intermediate, besonders in perizyklischen und photochemischen Reaktionen für die Darstellung von Heterozyklen,[81] sowie in [4+2]-Zykloadditionen,[82,83] Kreuzkupplungsreaktionen,[84] Heck-Olefinierungen,[85] enantioselektiven Additionen[86,87] oder asymmetrischen Hydrierungen,[88,89] eingesetzt werden.

Da traditionelle Enamidsynthesen oft harsche Reaktionsbedingungen verlangen, zur Bildung von *E*/*Z*-Produktgemischen führen oder teure und schlecht verfügbare Ausgangsstoffe erfordern, hat sich in den letzten Jahren die Addition von Amiden **3.3-1** an terminale Alkine **3.3-2**, die sogenannte Hydroamidierung, als besonders zweckdienliche Synthese für Enamide **3.3-3** entwickelt (Schema 9). Da bei dieser Transformation alle Atome aus den Edukten im Produktmolekül enthalten sind und somit keine Koppelprodukte als Abfall entstehen, zeichnet sich die Hydroamidierung als besonders nachhaltig aus.

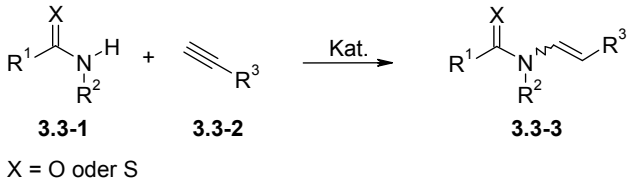

Schema 9. *Addition von Amiden an terminale Alkine*.

Innerhalb der letzten Jahre wurde eine Reihe an Ruthenium-katalysierten Reaktionen zur Addition verschiedener *N*-Nukleophile wie Amide, Thioamide und Imide an interne Alkine entwickelt, die alle eine hohe Chemo-, Regio- und Stereoselektivität aufweisen. Bemerkenswert ist, dass alle Varianten mit *anti*-Markovnikov-Selektivität ablaufen. Obwohl die Hydroamidierung mittlerweile einen hohen Entwicklungsstand besitzt und in der organischen Chemie breite Anwendung, unter anderem in der Synthese zahlreicher Naturstoffe, gefunden hat, ist ihr Reaktionsmechanismus immer noch Gegenstand von Spekulationen. Daher war es das Ziel dieser Arbeit, den Koordinationsmodus des Alkins während der Reaktion zu untersuchen und zu klären, wie die Regio- und Stereochemie kontrolliert wird. Dies soll am Beispiel der *E*-selektiven Addition sekundärer Amide an terminale Alkine erfolgen.

Insgesamt fünf potentielle Katalysezyklen wurden mit verschiedenen mechanistischen Studien und Kontrollexperimenten untersucht. Dabei kamen Isotopenmarkierungs-experimente, bei denen das Amid oder das Alkin mit Deuterium markiert waren, Bestimmungen von kinetischen Isotopeneffekten mittels *in situ* IR-Spektroskopie, *in situ* ^{1}H-, ^{2}H-, ^{13}C- ^{31}P-, H,P-HMQC- und P,P-COSY-NMR- sowie *in situ* ESI-MS- und ESI-MS-CID-MS-Experimente zum Einsatz. Basierend auf diesen Untersuchungen konnten drei potentielle Reaktionsmechanismen ausgeschlossen werden. Die Gesamtheit der Ergebnisse erlaubte die Schlussfolgerung, dass die Hydroamidierung nach dem in Schema 10 vorgeschlagenen Katalysezyklus abläuft.

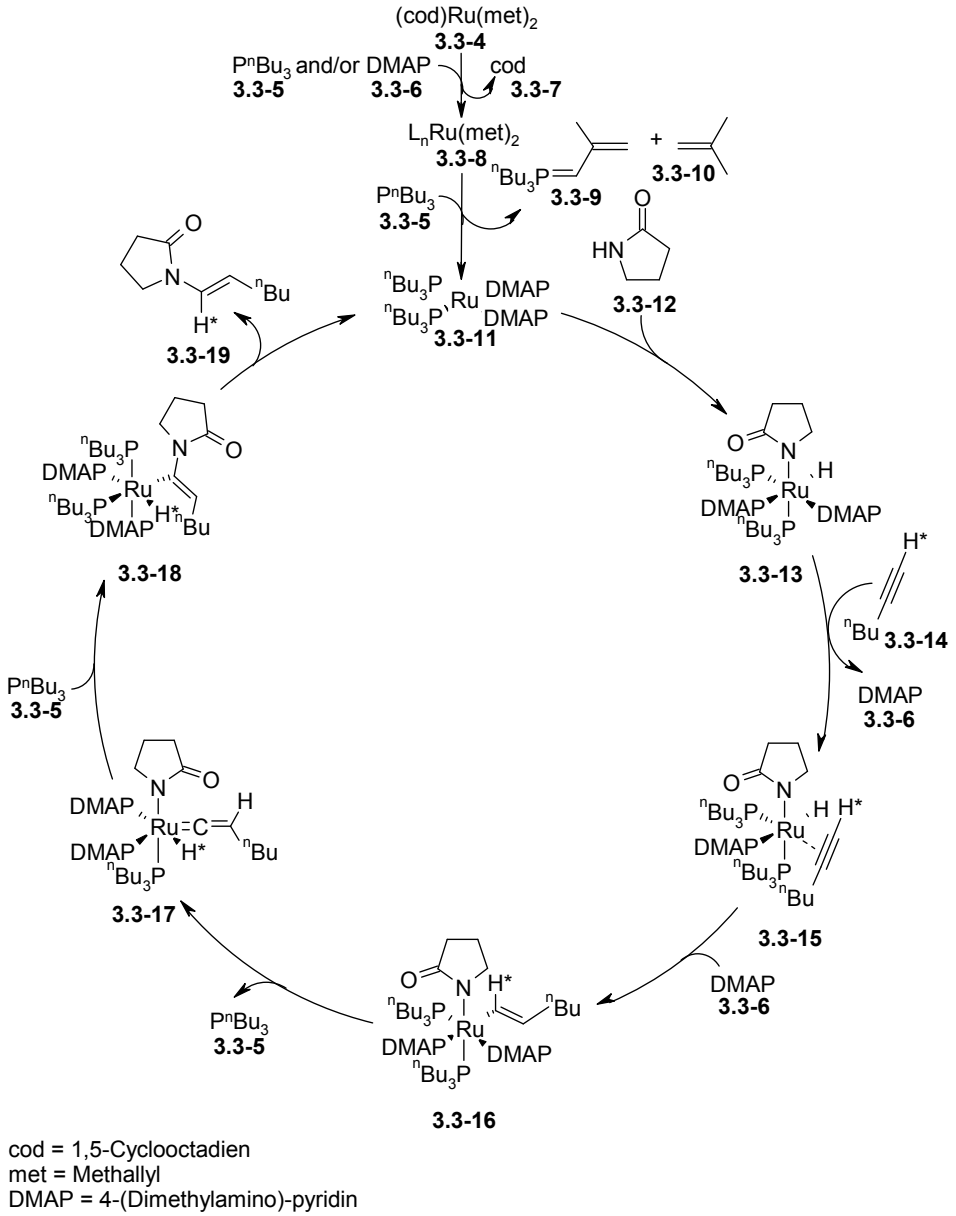

Schema 10. *Katalysezyklus der E-selektiven Hydroamidierung von 1-Hexen und 2-Pyrrolidon*.

Die Intermediate im vorgeschlagenen Katalysezyklus wurden größtenteils durch ESI-MS- und teilweise durch NMR-Experimente identifiziert. Da nur eingeschränkte Erkenntnisse über die Konfigurationen der Intermediate vorlagen, war das Ziel meines Beitrags zu diesem Forschungsprojekt, mit Hilfe von DFT-Rechnungen, zu überprüfen, ob es sich bei den in Schema 10 dargestellten Strukturen um stabile Minima handelt und zu klären, welche räumliche Anordnung der Liganden am günstigsten ist.

Tatsächlich konnte für jedes durch ESI-MS-Experimente postuliertes Intermediat ein stabiles Minimum gefunden werden. Die Geometrien der berechneten Strukturen sind in Schema 10

abgebildet. Zunächst wird am Präkatalysator **3.3-4** ein neutraler 1,5-Cyclooctadienligand (cod, **3.3-7**) durch einen ebenfalls neutralen Tri-*n*-butylphosphinliganden (**3.3-5**) oder 4-(Dimethylamino)-pyridinliganden (DMAP, **3.3-6**) ersetzt. Der Ru^{II}-Komplex **3.3-8** reagiert mit weiterem P^nBu_3 in einer reduktiven Allylierung zum Ru^0-Katalysator **3.3-11** unter Bildung des Phosphorylids **3.3-9** und Isobuten (**3.3-10**). Der Katalysezyklus beginnt mit der oxidativen Addition von 2-Pyrrolidon (**3.3-12**) unter Bildung des pseudo-oktaedrischen Ru^{II}–Hydridkomplexes **3.3-13**. Austausch eines DMAP-Liganden gegen 1-Hexen (**3.3-14**) führt zur Ru^{II}-Spezies **3.3-15**. Nun insertiert das Alkin in die Ru–H-Bindung, während der DMAP-Ligand wieder gebunden wird. Unter Abspaltung von P^nBu_3 lagert der Ru^{II}–Vinylkomplex **3.3-16** in einer 1,2-Hydridwanderung zum Ru^{IV}–Hydrid–Vinylidenkomplex **3.3-17** um. Der nukleophile Angriff des Amidliganden an das Vinylidenkohlenstoffatom führt unter Koordination von P^nBu_3 zur Ru^{II}–Hydridspezies **3.3-18**. Eine reduktive Eliminierung setzt das Enamid **3.3-19** frei und regeneriert den Katalysator.

Insgesamt konnten die Ergebnisse der DFT-Rechnungen die Schlussfolgerungen der experimentellen mechanistischen Studien unterstützen. Die DFT-Rechnungen bestätigen, dass alle postulierten Intermediate stabile Minima sind und keines davon eine unrealistische hohe Energie besitzt. Die Umlagerung zum Ru^{IV}–Hydrid–Vinylidenkomplex **3.3-17** unter 1,2-Hydridverschiebung erklärt die Beschränkung der Hydroamidierung auf terminale Alkine und der Angriff des Stickstoffnukleophils an das Vinylidenkohlenstoffatom ihre *anti*-Markovnikov-Selektivität.

Die Ergebnisse der mechanistischen Untersuchung der Ru-katalysierten Hydroamidierung terminaler Alkine wurden im *Journal of the American Chemical Society* veröffentlicht. Sämtliche Ergebnisse können dem englischsprachigen Originaltext der Veröffentlichung entnommen werden, die im Folgenden abgedruckt ist.

Die Veröffentlichung entstand im Rahmen eines Kooperationsprojekts mit der Arbeitsgruppe von Herrn Professor Dr. Dr. G. Niedner-Schatteburg. Die Deuteriummarkierungsexperimente und die Experimente zur Bestimmung kinetischer Isotopeneffekte wurden von Herrn Dr. Kifah S. M. Salih durchgeführt. Alle ESI-MS-Experimente wurden gemeinsam von Herrn Dr. Matthias Arndt und Herrn Dr. Fabian Menges durchgeführt. Die DFT-Rechnungen zum mechanistischen Verständnis der Hydroamidierung wurden von mir durchgeführt. Alle

restlichen Versuche inklusive der NMR-Experimente wurden von Dr. Matthias Arndt durchgeführt.

„Reprinted with permission from M. Arndt, K. S. M. Salih, A. Fromm, L. J. Goossen, F. Menges, G. Niedner-Schatteburg, *J. Am. Chem. Soc.* **2011**, *133*, 7428−7449: *Mechanistic Investigation of the Ru-Catalyzed Hydroamidation of Terminal Alkynes*. DOI: 10.1021/ja111389r. Copyright 2011 American Chemical Society."

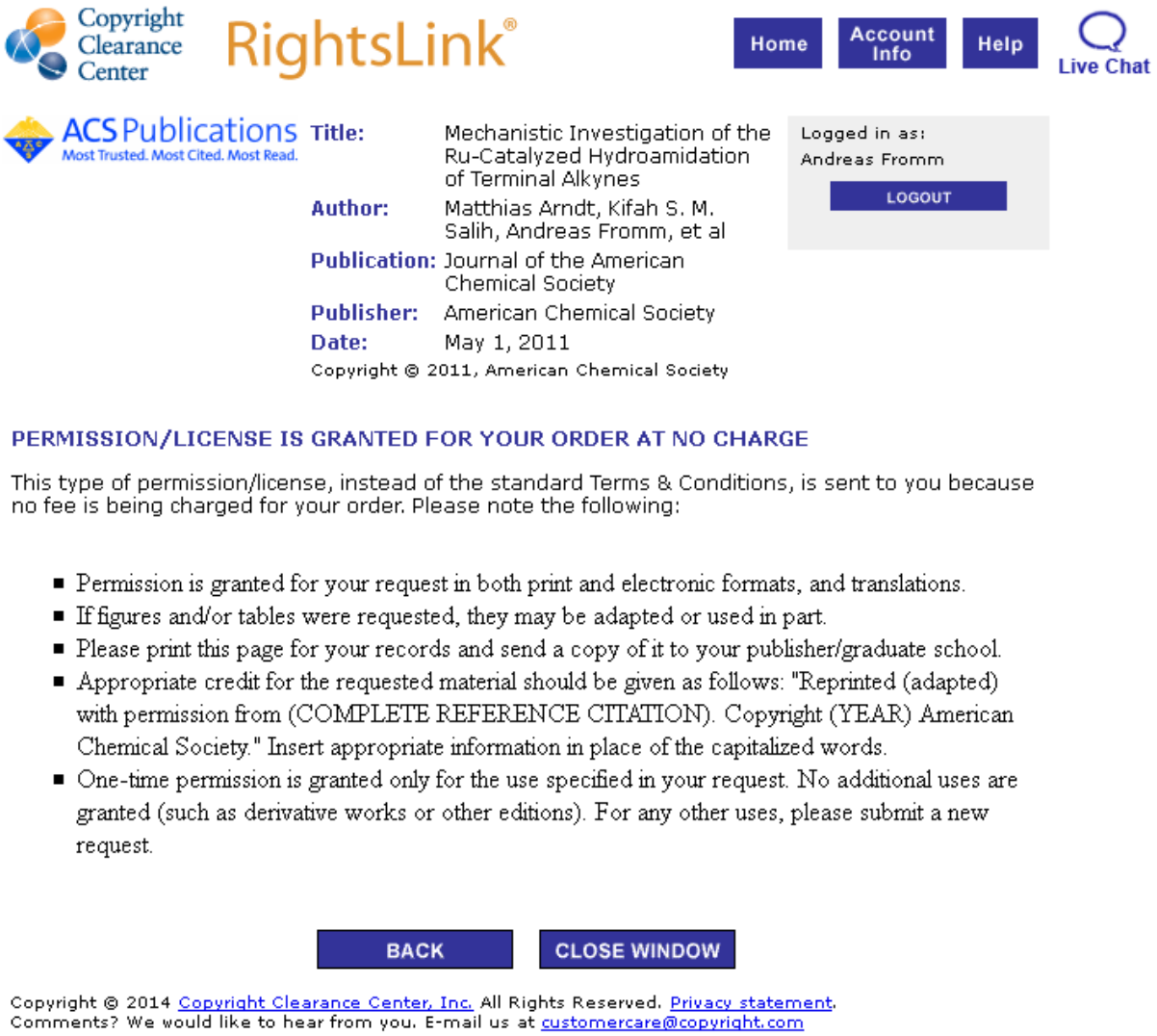

JACS
JOURNAL OF THE AMERICAN CHEMICAL SOCIETY
ARTICLE
pubs.acs.org/JACS

Mechanistic Investigation of the Ru-Catalyzed Hydroamidation of Terminal Alkynes

Matthias Arndt, Kifah S. M. Salih, Andreas Fromm, Lukas J. Goossen,* Fabian Menges, and Gereon Niedner-Schatteburg*

Fachbereich Chemie and State Reaserch Center OPTIMAS, TU Kaiserslautern, Erwin-Schrödinger-Strasse 52−54, 67663 Kaiserslautern, Germany

Supporting Information

ABSTRACT: The ruthenium-catalyzed hydroamidation of terminal alkynes has evolved to become a broadly applicable tool for the synthesis of enamides and enimides. Depending on the catalyst system employed, the reaction leads chemo-, regio-, and stereoselectively to a single diastereoisomer. Herein, we present a comprehensive mechanistic study of the ruthenium-catalyzed hydroamidation of terminal alkynes, which includes deuterium-labeling, in situ IR, in situ NMR, and in situ ESI−MS experiments complemented by computational studies. The results support the involvement of ruthenium−hydride and ruthenium−vinylidene species as the key intermediates. They are best explained by a reaction pathway that consists of an oxidative addition of the amide, followed by insertion of a π-coordinated alkyne into a ruthenium−hydride bond, rearrangement to a vinylidene species, nucleophilic attack of the amide, and finally reductive elimination of the product.

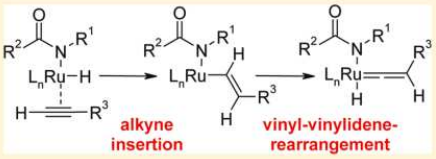

INTRODUCTION

Enamides are valuable structural elements in natural products with interesting biological activities and in pharmaceutical drug lead compounds[1] showing antibiotic,[2] antitumor,[3] anthelmintic,[4] antifungal, and cytotoxic activities (Figure 1).[5]

In addition, enamides can serve as versatile synthetic intermediates, particularly in pericyclic and photochemical reactions for the formation of heterocycles,[6] [4 + 2]-cycloadditions,[7] cross-coupling reactions,[8] Heck olefinations,[9] enantioselective additions,[10] or asymmetric hydrogenations.[11]

Traditional syntheses include the condensation of aldehydes and ketones with amides or dehydration of hemiaminals,[12] the Curtius rearrangement of α,β-unsaturated acyl azides,[13] and the elimination of β-hydroxy-α-silylamides (Peterson reaction).[14] Several metal-catalyzed approaches have also been investigated, such as the isomerization of *N*-allylamides[15] and catalytic cross-coupling reactions of amides and vinyl halides, pseudohalides or enol ethers.[16] Problems often encountered using these methods are the harsh reaction conditions, the formation of (*E*)- and (*Z*)-product mixtures, or the use of expensive or poorly available starting materials.

Over the last years, a particularly convenient synthetic entry to this important substrate class has emerged, namely, the addition of amides to terminal alkynes (Scheme 1).

This reaction mode is the most atom-economic transformation of all the catalytic reactions based on carboxylic acid derivatives that we have investigated over the last years.[17] On the basis of pioneering studies by Heider et al.[18] and Watanabe et al.,[19] who were the first to observe that ruthenium complexes mediate the addition of certain amides to terminal alkynes, we have developed efficient Ru catalysts and established the addition of amide-type nucleophiles to terminal alkynes as a general method for the synthesis of enamide derivatives. The same reaction principle is the basis for a number of preparatively useful Ru-catalyzed addition reactions to alkynes, for example, their hydration with formation of aldehydes,[20] the addition of carboxylic acids to give enol esters,[21] their hydroamination with formation of imines or enamines,[22] their hydrothiolation to vinyl sulfides,[23] and the addition of alcohols to form vinyl ethers.[24]

Over the last years, a range of customized protocols were disclosed for the *anti*-Markovnikov addition of various *N*-nucleophilic amides, thioamides, and imides across terminal C−C triple bonds. They provide an expedient and chemo-, regio-, and stereoselective synthetic entry to enamides, thioenamides, and enimides (Scheme 2).

With a catalyst system generated in situ from bis(2-methallyl)(cycloocta-1,5-diene)ruthenium(II) [(cod)Ru(met)$_2$], tri-*n*-butylphosphine (P(*n*-Bu)$_3$), and 4-dimethylaminopyridine (DMAP), tertiary (*E*)-enamides can be synthesized in high yields and selectivities from terminal alkynes and secondary amides.[25] The stereoselectivity can be reversed in favor of the corresponding (*Z*)-enamides when employing bis-(dicyclohexylphosphino)methane (dcypm) and water instead of P(*n*-Bu)$_3$ and DMAP. The reaction proceeds smoothly even in the presence of sensitive functional groups such as esters, ethers, ketones, halides, or silanes. Various amides, anilides, ureas, bislactams, carbamates, and even amide-type chiral auxiliaries can be

Received: January 3, 2011
Published: April 26, 2011

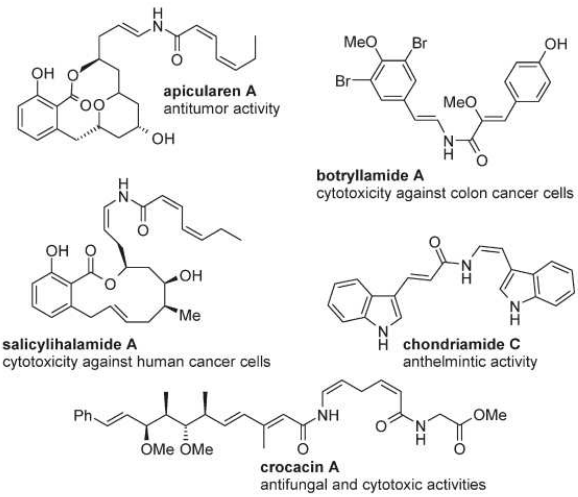

Figure 1. Enamide substructure in bioactive or functional molecules.

Scheme 1. Addition of Amides to Terminal Alkynes

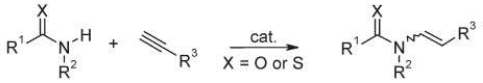

used as N−H nucleophiles. Recently, we have shown that for many substrates, a similar level of activity can be achieved when the catalytically active species is generated in situ from inexpensive ruthenium trichloride hydrate ($RuCl_3 \cdot 3H_2O$), P(*n*-Bu)$_3$, DMAP, K_2CO_3, and water.[26]

Subsequently, modified catalyst systems were developed that allowed extending the substrate scope to thioamides[27] and imides.[28] In this context, we made the discovery that for imides, which are acidic N−H nucleophiles, the addition of a Lewis acid rather than an auxiliary base is essential for achieving turnover of the catalyst.

The conversion of primary amides into secondary enamides is challenging due to the higher nucleophilicity of secondary over primary amides, leading to double vinylation products. However, a catalyst system consisting of the Lewis acid ytterbium(III) triflate in combination with (cod)Ru(met)$_2$ and an electron-rich, sterically demanding bidentate ligand (dcypb, 1,4-bis(dicyclohexylphosphino)butane) allowed the selective conversion of primary amides to secondary enamides.[29] This protocol gives access to (*Z*)-enamides in high yields and selectivities, whereas the (*E*)-enamides can be prepared by subsequent in situ double-bond isomerization with triethylamine at higher reaction temperatures in the same pot. Furthermore, after minor modifications, the same bimetallic system can be used for the *Z*-selective addition of secondary amides and imides to terminal alkynes in the absence of the primary amide functionality, yielding the corresponding enamides and enimides with *Z*/*E*-selectivities greater than 20:1.[30]

The applicability of Ru-catalyzed hydroamidation reactions is illustrated in Figure 2. The examples include the natural products alatamide, lansiumamides A and B, lansamide I, and botryllamides C and E.[29,31] They demonstrate that the hydroamidation of alkynes has meanwhile reached a high level of maturity and can be widely applied in organic synthesis. However, the reaction mechanism has so far remained speculative.

The aims of the present study were to investigate the coordination type of the alkyne during the reaction, to clarify how the regio- and stereochemistry is controlled, and to identify the rate-determining step of the catalytic cycle.

MECHANISTIC CONSIDERATIONS

Numerous potential reaction mechanisms have to be evaluated with appropriately designed mechanistic studies and control experiments.

Several catalytic cycles have previously been proposed for the Ru-catalyzed addition of nucleophiles such as amides, amines, carboxylic acids, and water to C−C triple bonds. The first mechanism for *anti*-Markovnikov-selective hydroamidations was postulated by Watanabe but was not supported by experimental data (Scheme 3).[19]

This mechanism will further be referred to as *Mechanism A*. It involves the oxidative addition of an amide, insertion of a π-coordinated alkyne into the Ru−N or Ru−H bond, and reductive elimination of the enamide product. Stabilizing interactions between the oxygen atom of the carbonyl group and the Ru center in a four- or six-membered intermediate (**17** and **18**) that forms following alkyne insertion were used to explain the regioselectivity, in both cases leading to the formation of the *anti*-Markovnikov product. Uchimaru proposed a similar mechanism for the Markovnikov-selective Ru-catalyzed hydroamination of terminal alkynes,[22a] in which a π-coordinated alkyne inserts into the Ru−N bond of a Ru-amine species. The Markovnikov selectivity is explained by the formation of a sterically less hindered Ru-enamine intermediate.

Indications for *Mechanism A* would be provided by a dependence of the rate-determining step on the acidity of the amide and the electronic and steric properties of the Ru-complex. Moreover, Ru-hydride species may be detectable via ^{1}H NMR or electrospray ionization mass spectroscopy (ESI−MS) investigations if concentrations are high enough, and the reaction of 1-deuterioalkynes should give rise to a product deuterated exclusively in the 1-position.

Dixneuf proposed a different mechanism to explain the selective formation of *anti*-Markovnikov addition products in the addition of carboxylic acids to alkynes. His pathway can directly be translated to hydroamidation reactions (Scheme 4).[32]

This mechanism will further be referred to as *Mechanism B*. Its key step is the formation of a Ru−vinylidene complex **20** via a 1,2-proton shift at the alkyne moiety, followed by an attack of a nucleophile in the α-position to the ruthenium center. After protonolysis of the ruthenium intermediate **25** and regeneration of the active ruthenium species **19**, an *anti*-Markovnikov enol ester **26** or enamide **6**−**13** is formed. In contrast, the alternative direct addition of a nucleophile to a coordinated alkyne should result in the formation of the Markovnikov product. This mechanism provides a sound explanation for the *anti*-Markovnikov selectivity of the reaction and its limitation to terminal alkynes. Experiments with isolated Ru−vinylidene complexes confirmed that their reaction with nucleophiles will indeed lead to the addition product. As an alternative to vinylidene formation via a 1,2-proton shift, a sequence consisting of an oxidative addition of the alkyne C(sp)−H bond to ruthenium followed by a 1,3-proton shift was also proposed as an entry to this mechanism.

Mechanism B would again predict a dependence of the reaction rate on the electronic and steric properties of the Ru-complex,

Journal of the American Chemical Society ARTICLE

Scheme 2. Ru-catalyzed Addition of *N*-Nucleophiles to Terminal Alkynes

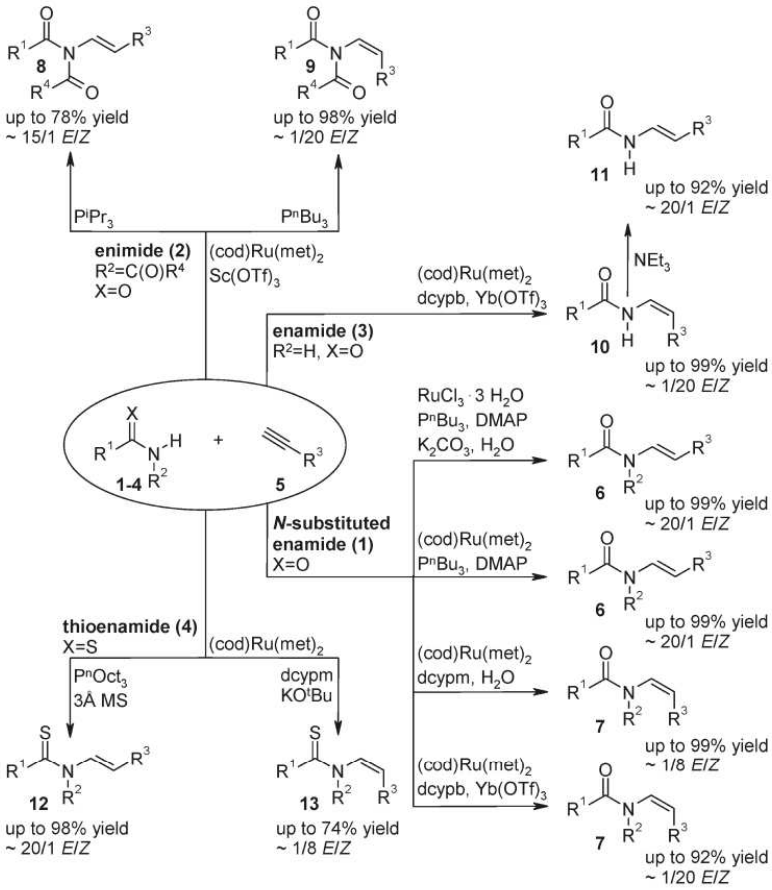

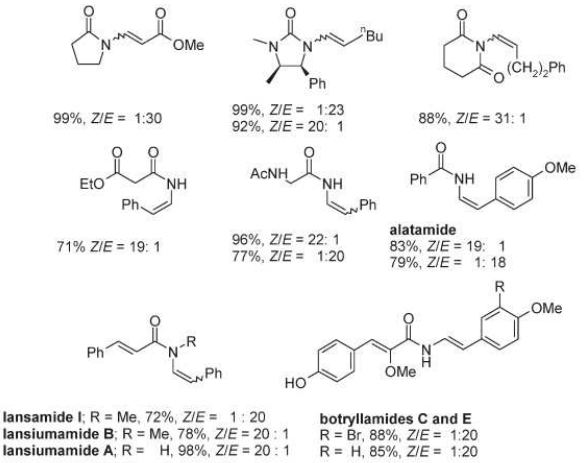

Figure 2. Representative example for the addition of terminal alkynes.

Scheme 3. *Mechanism A*: Hydroamidation Pathway Postulated by Watanabe

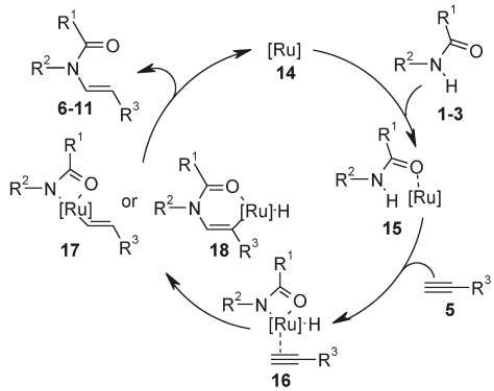

and the reaction would benefit from the stabilizing effect of electron-donating ligands on the high oxidation state of the ruthenium center. We assume the vinylidene formation to be a relatively slow reaction step. Therefore, in contrast to *Mechanism A*, the acidity of the alkyne C(sp)−H bond rather than that of the amide N−H bond should have an additional influence on the C−H bond cleaving vinylidene formation step. Therefore,

Journal of the American Chemical Society ARTICLE

Scheme 4. *Mechanism B:* **Hydroamidation in Analogy to Dixneuf's Carboxylation of Terminal Alkynes**

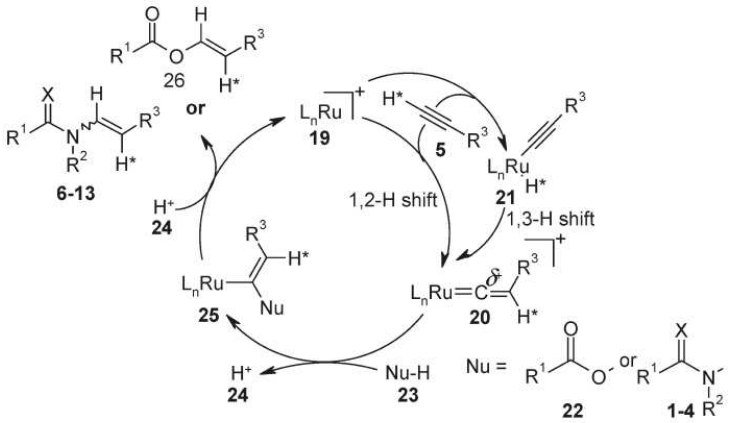

Scheme 5. *Mechanism C*: **Hydroamidation in Analogy to Wakatsuki's Hydration of Terminal Alkynes**

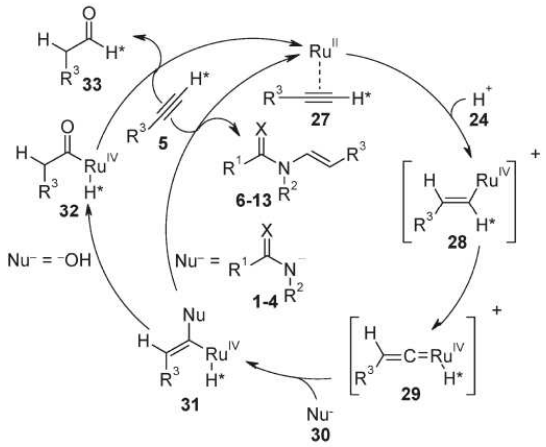

Scheme 6. *Mechanism D*: **Hydroamidation via Oxidative Addition of the Amide, Insertion of the Alkyne, and Ru−Vinyl/−Vinylidene Rearrangement**

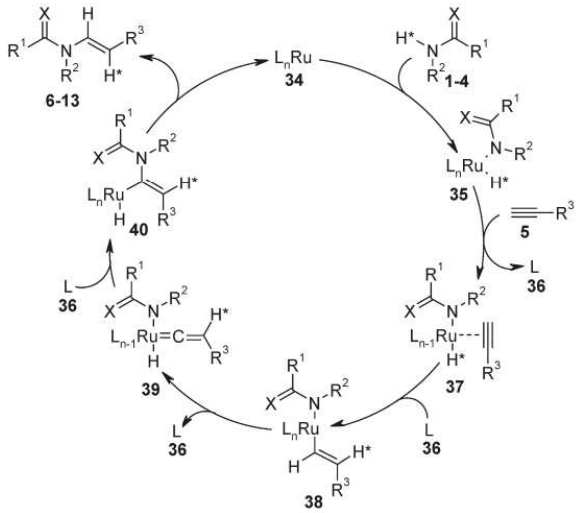

kinetic isotope effects should be measurable in experiments with 1-deuterioalkynes, and the resulting product should exclusively be deuterated in the 2-position, because proton shifts to the internal alkyne C-atom are postulated. ESI−MS and in situ IR experiments could help to verify reactive intermediates.

Vinylidene intermediates have been confirmed for other ruthenium-catalyzed addition reactions.[32] One example is the addition of alcohols to alkynes, where a 1,2-proton shift was observed in isotopic labeling experiments.[24b] However, the intermediacy of vinylidene intermediates does not necessarily call for proton shifts, and alternative mechanisms for Ru−vinylidene formation have been proposed for the hydration of terminal alkynes[20b] and for stoichiometric reactions of terminal alkynes with ruthenium−hydride complexes.[33] On the basis of computational studies, Wakatsuki and Caulton concluded that vinylidene intermediates are formed via rearrangement of Ru-vinyl species for these reactions, whereas pathways via 1,2- or 1,3-proton shifts are energetically unfavorable (see Schemes 5 and 6).

For the hydration of terminal alkynes, the absence of proton shifts was corroborated by deuterium-labeling experiments. Wakatsuki et al. thus derived a different mechanism involving Ru−vinylidene intermediates.[20b] Again, this may be translated to hydroamidation reactions (Scheme 5).

The key step in this mechanism, which will further be referred to as *Mechanism C*, is the protonation of a π-coordinated alkyne resulting in the formation of a cationic Ru^{IV}−vinyl intermediate **28**. Its rearrangement to the Ru−H−vinylidene species **29** was proposed to be the rate-determining step. Addition of a nucleophile and reductive elimination gives the aldehyde **33** or the enamide **6**−**13**, respectively. In this mechanism, the alkyne C(sp)-proton is transferred to the metal center and subsequently reattached to its original carbon atom. For the hydration of alkynes, 1,2-proton shifts were indeed not observed in deuteration studies. This mechanism offers an explanation for the *anti*-Markovnikov selectivity and the limitation to terminal alkynes. However, it involves cationic intermediates in the high oxidation states of +4 or even +6, depending on whether the Ru=C bond in species **29** is

viewed as a covalent bond or a as the coordination of a neutral carbene ligand to the metal center. This may be reasonable for hydration reactions in aqueous solvents, but is less likely for hydroamidations under almost neutral conditions in toluene.

If the hydroamidation proceeded via *Mechanism C*, the use of protic and more polar solvents should result in a higher reaction rate. Again, electron-donating ligands should enhance the catalyst activity due to their stabilizing effect on higher oxidation states of the ruthenium center, and sterically demanding ligands should facilitate the reductive elimination of the product. During the slow vinylidene formation step, the C(sp) proton is transferred to the ruthenium center. This proton may be detectable via ^{1}H NMR. When comparing the reactions of alkynes and 1-deuterioalkynes, a primary kinetic isotope effect is expected, as a C−D rather than a C−H bond has to be cleaved. The resulting product should be deuterated exclusively in the 1-position.

Caulton and co-workers investigated pathways leading to the formation of Ru−vinylidene intermediates.[33] They found that π-coordinated alkynes readily insert into Ru−H bonds to form Ru−vinyl complexes. The Ru−vinyl species then rearrange to Ru−H−vinylidene complexes. They isolated all postulated Ru intermediates and confirmed the pathways by DFT calculations. These showed reasonable energy barriers for the proposed pathway, and substantially higher barriers for an oxidative addition of the alkyne followed by a 1,3-proton shift. It is possible to incorporate this alternative route to vinylidene species into a new catalytic cycle for hydroamidations, which will further be referred to as *Mechanism D* (Scheme 6).

This catalytic cycle starts with the oxidative addition of an amide to an active Ru^0 species (**34**). After insertion of the alkyne into the Ru−hydride bond and rearrangement to the vinylidene species **39**, the amide attacks the carbon atom α to the ruthenium center, leading to the *anti*-Markovnikov enamide product (**6**−**13**) via reductive elimination. The oxidation state of the Ru center changes from 0 via +2 to +4 during the catalytic cycle, or only from 0 to +2 if the vinylidene ligand is interpreted as neutral carbene. The vinylidene formation proceeds without proton shifts, and at the end of the reaction, the alkyne proton is linked to the original C-atom.

For *Mechanism D*, a dependence of the reaction rate on the acidity of the N−H group of the amide as well as the C(sp)−H function of the alkyne should be detectable, resulting in measurable kinetic isotope effects both when *N*-deuterated amides or 1-[*D*]-alkynes are used as starting materials. Electron-rich ligands will stabilize the high oxidation state of the ruthenium center, and the use of sterically demanding ligands should facilitate the reductive elimination step. Reaction intermediates might be identifiable via ESI−MS and in situ IR experiments. It might also be interesting to investigate by in situ NMR whether the Ru-complexes are capable of activating N−H bonds.

In our previous work, we had excluded reaction mechanisms starting from Ru^0 species because no coupling product of the methylallyl ligands from the (cod)Ru(met)$_2$ precursor could be detected, and instead, free isobutene was observed via GC−MS and ^{1}H NMR spectroscopy, which appeared to support a redox-neutral ligand-exchange reaction.[29] A control experiment with 1-[*D*]-hex-1-yne showed no 1,2-proton shift during the reaction.[28] In situ NMR and ESI−MS experiments of the catalyst preformation step confirmed that all ligands of (cod)Ru(met)$_2$ are exchanged, and that cationic Ru-amide-phosphine and Ru-amide-phosphine-DMAP species are formed in the addition of secondary amides to terminal alkynes.[26] On the basis of these

Scheme 7. Redox-Neutral *Mechanism E* for the Hydroamidation of Terminal Alkynes

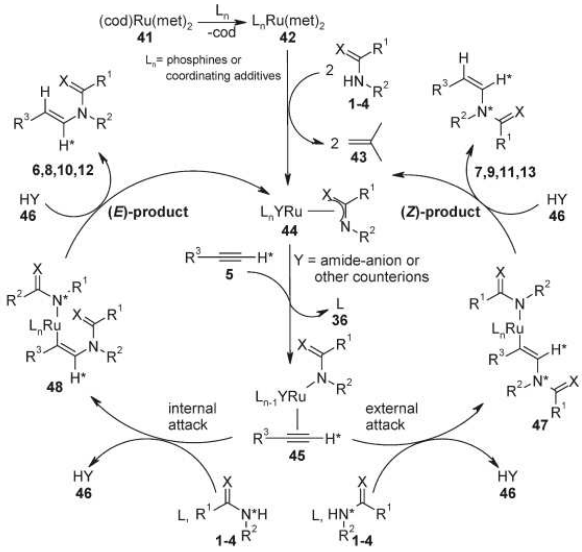

experiments, we postulated a redox-neutral ligand exchange mechanism, which will further be referred to as *Mechanism E* (Scheme 7).

In the catalyst preformation step, all ligands initially bound to the Ru-precursor are exchanged, with formation of ruthenium^{II}−amide complexes **44**. In the first step of the catalytic cycle, the alkyne coordinates to the ruthenium center (**45**). Depending on the steric bulk of the phosphines, the amide attacks from either the inner or the outer coordination resulting in the formation of *E*- or *Z*-configured enamides (**6**−**13**). Bulky ligands are likely to favor an external attack resulting in the formation of an (*E*)-Ru−enamide complex **47**, which releases the corresponding (*Z*)-enamide (**7**, **9**, **11**, or **13**) after protonolysis, along with a regenerated active Ru^{II}-species **44**. In contrast, an insertion of the alkyne into the Ru−N-bond of a coordinated amide is favorable in the presence of smaller ligands, giving rise to (*E*)-enamides (**6**, **8**, **10**, or **12**). Over the entire cycle, the Ru center remains in the oxidation state +2. A likely driving force behind the reaction is the continuous exchange of basic for more acidic ligands at the metal center.[34] *Mechanism E* offers an explanation for the stereochemistry of the hydroamidation, but cannot adequately address the limitation to terminal alkynes and selectivity for the *anti*-Markovnikov products.

If *Mechanism E* holds true, an inverse secondary kinetic isotope effect should be detectable for 1-deuterioalkynes, because it involves a rehybridization from sp to sp^2, which is more favorable for the stronger C−D bond.[35] Furthermore, no ruthenium−hydride species should be detectable via ^{1}H NMR. The nucleophilicity of the amide should have a strong influence on the reaction rate, and additives that increase the nucleophilic character of the amide should enhance the reaction rate. The ruthenium center remains in the oxidation state of +2 and merely activates the alkyne for nucleophilic attack by removing electron-density from the π-system. Therefore, less electron-rich phosphines should lead to a higher catalyst activity, whereas sterically demanding phosphines should lead to a reduced activity because the

Table 1. Overview of Experimental Findings for a Set of Control Experiments

Experimental finding	Expected outcome for *Mechanism*				
	A	*B*	*C*	*D*	*E*
1,2-proton shift in experiments with 1-[*D*]-alkynes	No	Yes	No	No	No
Primary kinetic isotope effect in hydroamidation competition experiments with 1-[*H/D*]-alkynes	No	Yes	Yes	Yes	No
Primary kinetic isotope effect in hydroamidation competition experiments with *N*-[*H/D*]-amides	Yes	Yes	Yes	Yes	Yes
Inverse secondary kinetic isotope effect in hydroamidation competition experiments with 1-[*H/D*]-alkynes	Yes	No	No	No	Yes
Detection of Ru-hydride species in ^{1}H-NMR hydroamidation experiments in absence of the alkyne	Yes	No	No	Yes	No
Detection of Ru-hydride species in ^{1}H-NMR hydroamidation experiments in absence of the amide	No	Yes	Yes	No	No
Detection of Ru-amide species in ESI-MS hydroamidation experiments in absence of the alkyne	Yes	No	No	Yes	Yes
Intermediacy of cationic species in the catalytic cycle	No	Yes	Yes	No	No

ligand-exchange reactions and the formation of the ruthenium—enamide intermediate are disfavored.

An overview of all predictions we made in this paragraph for *Mechanisms A*—*E* in a set of control experiments is presented in Table 1. These predictions are made under the assumption that the concentrations of all characteristic intermediates are high enough for detection and that the reaction steps leading to possible kinetic isotope effects (KIE) are slow.

All mechanisms presented above are in principle feasible, but give contradictory predictions for the outcome of simple control experiments and spectroscopic studies. The combined experimental findings presented herein provide strong evidence that the reaction proceeds via *Mechanism D*.

■ DEUTERATION STUDIES OF HYDROAMIDATIONS

We started our mechanistic investigation with hydroamidation experiments using 1-deuterioalkynes. *Mechanisms A*, *C*, *D*, and *E* predict that the deuterium should end up in the geminal position to the amide nitrogen, whereas *Mechanism B* predicts that the deuterium should be transferred to the vicinal carbon. In the inverse experiment, with *N*-deuterioamides and nondeuterated alkynes, the deuterium should be incorporated to the geminal position to the amide nitrogen for *Mechanism B* and bind to the vicinal atom for *Mechanisms A*, *C*, *D*, and *E*.

Deuteration studies were carried out for the additions of primary and secondary amides as well as imides, using both the *E*- and the *Z*-selective methods. The results are summarized in Table 2.

The addition of 2-pyrrolidone (**1a**) to 1-[*D*]-hex-1-yne (**5a**, Deuteration grade, DG = 92%) using the *E*-selective protocol (2 mol % (cod)Ru(met)$_2$, 6 mol % P(*n*-Bu)$_3$, 4 mol % DMAP) led to incorporation of the deuterium almost exclusively in the 1′-position of the corresponding enamide (**6aa**), that is, in geminal position to the amide (entry 1). The 2′-deuterated product (**6ab**) was detected in traces only. In the analogous reaction of 1-[*D*]-2-pyrrolidone (**1b**, DG = 85%) and 1-hexyne (**5b**), the deuterium was transferred to the 2′-position of **6ab** in very high selectivity (entry 2). These results indicate that the predominant mechanism does not involve proton shifts. The trace formation of 2′-deuterated product can be accounted for by H—D exchange reactions at a relatively acidic site of the hydroamidation product, possible competing mechanisms, or unproductive vinylidene rearrangements.

The reaction of 2-pyrrolidone (**1a**) and 1-[*D*]-hex-1-yne (**5a**) under *Z*-selective conditions (2 mol % (cod)Ru(met)$_2$, 3 mol % $Cy_2PCH_2PCy_2$, 2 equiv H_2O) also proceeded mostly without proton shift (entry 3). The ratio between 2′-deuterated (**7ab**) versus 1′-deuterated product (**7aa**) dropped to a moderate value of 4:1 for the inversely deuterated starting materials (entry 4). In both reactions, the deuteration grades in the products were only moderate, which we attribute to the presence of water in the reaction mixture responsible for background H—D exchange reactions. Indeed, when we replaced the water, which is essential for an effective hydroamidation protocol, by deuterium oxide, the deuteration rates in the products (**7aa** and **7ab**) were high (entries 5 and 6). However, the regioselectivity of the deuteration was only moderate, and in the reaction of 1-[*D*]-hex-1-yne (**5a**), a doubly deuterated product was observed. All these findings suggest that background H—D exchange overlays regioselective deuterium incorporation in the presence of water.

The catalytic addition of succinimide (**2a**) to 1-[*D*]-hex-1-yne (**5a**) under *E*-selective conditions (5 mol % (cod)Ru(met)$_2$, 15 mol % P(*i*-Pr)$_3$, 4 mol % Sc(OTf)$_3$) proceeds without proton shift and leads exclusively to the incorporation of the deuterium in the 1′-position of the corresponding enimide product (**8aa**, entry 7). When using the inversely deuterated starting materials, the deuterium is mainly incorporated in the 2′-position of the enimide product (**8ab**, entry 8). In addition to the expected products, traces of the product deuterated in the α-position to the imide carbonyl group were detected, which can be rationalized by H/D exchange at this acidic position.[36]

Journal of the American Chemical Society ARTICLE

Table 2. Hydroamidation with Deuterated Starting Materials[a]

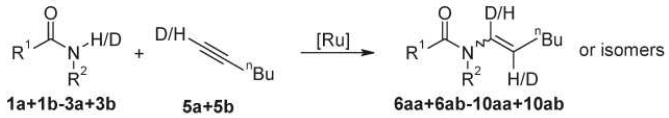

1a+1b-3a+3b 5a+5b 6aa+6ab-10aa+10ab

Entry	Amide	Alkyne	Products	Yield / Ratio **6aa**:**6ab**
1	 **1a**	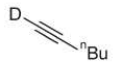 **5a**, DG = 92%	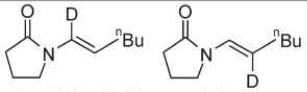 **6aa**, DG = 85% **6ab**	92% >30:1
2	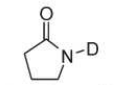 **1b**, DG = 85%	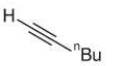 **5b**	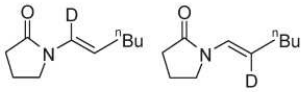 **6aa** **6ab**, DG = 80%	91% <1:30
3[b]	 **1a**	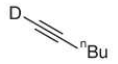 **5a**, DG = 92%	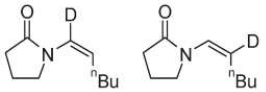 **7aa**, DG = 55% **7ab**	89% 12:1
4[b]	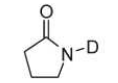 **1b**, DG = 85%	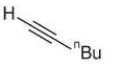 **5b**	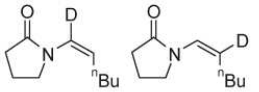 **7aa** **7ab**, DG = 13%	90% 1:4
5[c]	 **1a**	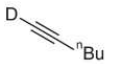 **5a**, DG = 92%	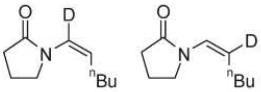 **7aa**, DG = 4% **7ab**, DG = 4%	80% 1:1[d]
6[c]	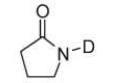 **1b**, DG = 85%	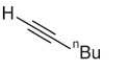 **5b**	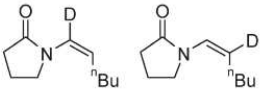 **7aa**, DG = 30% **7ab**, DG = 69%	91% 1:2
7[e]	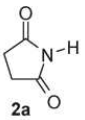 **2a**	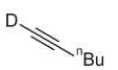 **5a**, DG = 92%	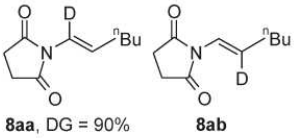 **8aa**, DG = 90% **8ab**	75% >30:1
8[e,f]	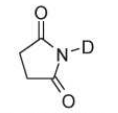 **2b**, DG = 81%	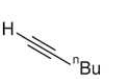 **5b**	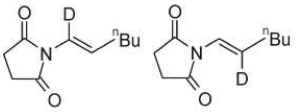 **8aa** **8ab**, DG = 56%	92% <1:30[g]
9[h]	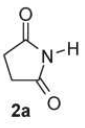 **2a**	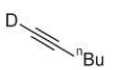 **5a**, DG = 92%	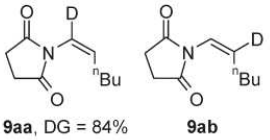 **9aa**, DG = 84% **9ab**	92% >30:1

dx.doi.org/10.1021/ja111389r |J. Am. Chem. Soc. 2011, 133, 7428–7449

Table 2. Continued

Entry	Amide	Alkyne	Products	Yield Ratio **6aa**:**6ab**
10[h]	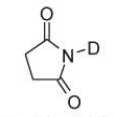 **2b**, DG = 81%	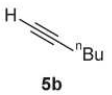 **5b**	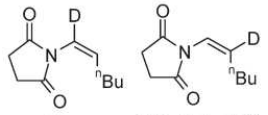 **9aa** **9ab**, DG = 83%	91% <1:30[g]
11[i]	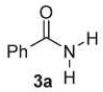 **3a**	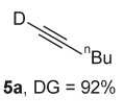 **5a**, DG = 92%	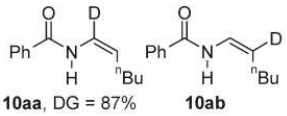 **10aa**, DG = 87% **10ab**	89% >30:1
12[i]	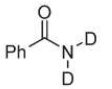 **3b**, DG = 75%	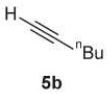 **5b**	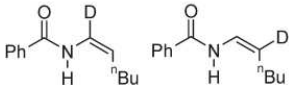 **10aa** **10ab**, DG = 62%	87% <1:30

[a] *Reaction conditions*: Amide or imide (1.00 mmol), alkyne (2.00 mmol), (cod)Ru(met)$_2$ (2 mol %), P(*n*-Bu)$_3$ (6 mol %), DMAP (4 mol %), toluene (3 mL), 100 °C, 15 h, selectivity determined by ^{1}H NMR; DG = deuteration grade. [b] $Cy_2PCH_2PCy_2$ (3 mol %) instead of P(*n*-Bu)$_3$, H_2O (2.00 equiv) instead of DMAP. [c] $Cy_2PCH_2PCy_2$ (3 mol %) instead of P(*n*-Bu)$_3$, D_2O (2.00 equiv) instead of DMAP. [d] The doubly deuterated product was mainly formed with a DG of 91%. [e] (cod)Ru(met)$_2$ (5 mol %), P(*i*-Pr)$_3$ (15 mol %), Sc(OTf)$_3$ (4 mol %), DMF-d_7 (3 mL), 60 °C, 15 h, isolated yields, selectivities determined by ^{1}H NMR. [f] DMF (3 mL) instead of DMF-d_7. [g] A product deuterated in the 3-position of the imide was detected in traces. [h] (cod)Ru(met)$_2$ (2 mol %), P(*n*-Bu)$_3$ (6 mol %), Sc(OTf)$_3$ (4 mol %), DMF (3 mL), 60 °C, 15 h, isolated yields, selectivities determined by ^{1}H NMR. [i] (cod)Ru(met)$_2$ (5 mol %), dcypb (6 mol %), Yb(OTf)$_3$ (4 mol %), DMF (3 mL), 60 °C, 6 h, isolated yields, selectivity determined by ^{1}H NMR.

Similar results were observed also for the *Z*-selective protocol (2 mol % (cod)Ru(met)$_2$, 6 mol % P(*n*-Bu)$_3$, 4 mol % Sc(OTf)$_3$). Thus, the reaction of succinimide (**2a**) with 1-[*D*]-hex-1-yne (**5a**) yielded the enimide mainly deuterated in the 1′-position (**9aa**, entry 9), whereas the addition of *N*-[*D*]-succinimide (**2b**, DG = 81%) to 1-hexyne (**5b**) led to the formation of the product with near-quantitative deuterium incorporation in the 2′-position (**9ab**, entry 10). The hydroamidation therefore also proceeded without proton shift, as did the reaction of the secondary amides **1a** and **1b**.

The reaction of benzamide (**3a**) with 1-[*D*]-hex-1-yne (**5a**) under *Z*-selective conditions (5 mol % (cod)Ru(met)$_2$, 6 mol % dcypb, 4 mol % Yb(OTf)$_3$) furnished the corresponding enamide **10aa** deuterated exclusively in the 1′-position (entry 11). Analogously, the deuterium was selectively incorporated in the reaction of *N*,*N*-[D_2]-benzamide (**3b**, DG = 75%) and 1-hexyne (**5b**) under otherwise identical conditions (**10ab**, entry 12). It is worth mentioning that, in contrast to the previously reported hydroamidation protocol for the addition of primary amides,[29] we had to perform these two deuteration experiments without water, because in the presence of water H−D exchange reactions overlaid regioselective deuterium incorporation.

On the basis of these results, the formation of vinylidene intermediates via a 1,2-proton shift or via oxidative addition of the alkyne followed by a 1,3-proton shift as postulated in *Mechanism B* can be ruled out for both *E*- and *Z*-selective hydroamidation reactions. *Mechanisms A*, *C*, *D*, and *E* are all in agreement with the results of the present deuteration studies.

KINETIC INVESTIGATIONS OF HYDROAMIDATIONS

We next investigated the kinetics of hydroamidations by means of in situ IR spectroscopy. Using a ReactIR 45 m FT-IR spectrometer (3.2 scans/s, 8 cm^{-1} resolution), we monitored the hydroamidation of 2-pyrrolidinone (**1a**) and 1-hexyne (**5b**) by the disappearance of the C−C triple bond valence oscillation of 1-hexyne (**5b**) at 2122 cm^{-1} and the appearance of a C=O valence oscillation of the enamide product (**6a**) at 1725 cm^{-1}. Figure 3 illustrates the starting material consumption as well as the product formation and the temperature inside the reaction vessel over a period of 30 min. The reaction starts almost immediately after the reaction vessel is placed in an aluminum block preheated to 100 °C and is complete within several minutes.

Evaluation of the spectroscopic data with the iC IR software using the ConcIRT algorithm also allowed to detect the appearance of short-lived reaction intermediates by their C=C vibration stretches at 1607 cm^{-1} (see Supporting Information). This frequency is in an area typical for ruthenium−vinylidene species.[37] However, in-depth studies under carefully optimized conditions would be required to unambiguously confirm these species.

Attempts to slow down the reaction by lowering the temperature were unsuccessful. Below 100 °C, the hydroamidation was sluggish, and undesired alkyne dimerization became the predominant process. Even at the optimum reaction temperature, the catalyst preformation did not always proceed at the same speed, so that the variability of overall reaction rates was rather high.

It was therefore unfeasible to perform comparative kinetic studies with deuterated and nondeuterated substrates in separate vessels to determine kinetic isotope effects. Instead, we performed

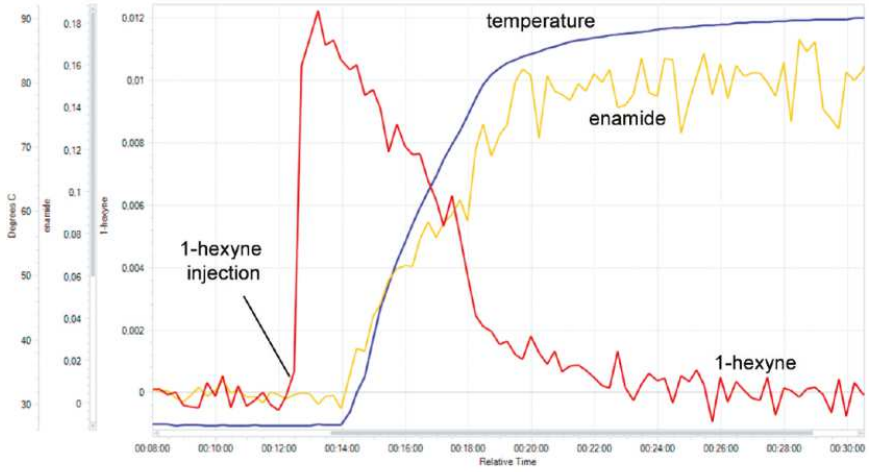

Figure 3. In situ IR-experiment: Concentration trends for the hydroamidation of 1-hexyne (**5b**) with 2-pyrrolidinone (**1a**).

competition experiments in which one of the starting materials was added in large excess as a 1:1 mixture of its deuterated and nondeuterated form (Table 3). From the ratio of hydrogen versus deuterium incorporation in the enamide product, we calculated the relative reaction rates.

In the reaction of 2-pyrrolidinone (**1a**) with 1-hexyne (4 equiv, DG adjusted to 50%), the enamide (**6a**/**6aa**) was obtained with a DG of 39% (entry 1). This translates to a kinetic isotope effect (KIE) of 1.6. Similarly, the reaction of succinimide (**2a**) with 1-hexyne (4 equiv, DG adjusted to 50%) gave a product (**9a**/**9aa**) with 30% DG, translating to a KIE of 2.3 (entry 2). In the analogous reaction of benzamide (**3a**), the product DG was 40% (**10a**/**10aa**), corresponding to a KIE of 1.5 (entry 3).

In all cases, normal kinetic isotope effects (KIE = $k_H/k_D = n_H/n_D$) greater than 1 were observed. During the reaction, the hybridization of the C(1) carbon changes from sp to sp^2 and any intermediate should thus have a higher or the same p-character as the starting material. However, a reaction step during which the p-character of a C−H bond increases is known to lead to an inverse secondary KIE. Thus, the KIE should always have a value smaller than 1, unless the sp C−H bond is cleaved in a slow reaction step, and a sp^2 C−H bond is reinstated at the same carbon atom in a later, non rate-determining step.[35] This implies that, despite their relatively small magnitudes, the values must result from a primary KIE. *Mechanism A*, which does not involve a bond cleavage but rather an insertion of the alkyne into a Ru−H or Ru−N bond with sp to sp^2 rehybridization, can thus be excluded as the main reaction pathway. *Mechanism E* is also incompatible with the observed KIE > 1, as in this process, the C−H bond is also not cleaved.

In *Mechanisms C* and *D*, a rearrangement step from a ruthenium−vinyl to a ruthenium−hydride−vinylidene species takes place, during which the C(sp)−H/D bond is cleaved. The KIE values greater than 1 are in good agreement with these pathways. Although primary KIEs for deprotonation processes usually have values of 4−7, the relatively low values of 1.5−2.3 observed here are easily rationalized when considering that the overall catalytic process consists of several steps. For example, if one reaction step is slower by a factor of 5 because of an isotope effect, but this individual reaction step requires only one-forth of the catalyst turnover time, the overall KIE would be 2 rather than 5.

Table 3. Determination of KIE Values by Competition Experiments[a]

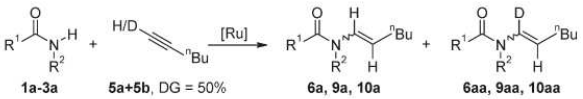

Entry	Amide	Main Product	Ratio **a**/**aa**	KIE
1	 **1a**	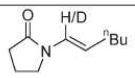 DG = 39%, **6a/6aa**	1.6:1	1.6
2[c]	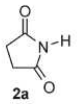 **2a**	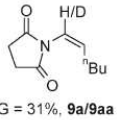 DG = 31%, **9a/9aa**	2.3:1	2.3
3[d]	 **3a**	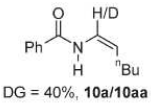 DG = 40%, **10a/10aa**	1.5:1	1.5

[a] *Reaction conditions*: Amide (1.00 mmol), 1-hexyne (2.00 mmol), 1-[*D*]-hex-1-yne (2.00 mmol), (cod)Ru(met)$_2$ (2 mol %), P(*n*-Bu)$_3$ (6 mol %), DMAP (4 mol %), toluene (3 mL), 100 °C, 15 h, product ratio determined by ^{1}H NMR. [b] Determined by the ratio of nondeuterated to deuterated product yields. [c] Sc(OTf)$_3$ (4 mol %) instead of DMAP, DMF (3 mL) instead of toluene, 60 °C, 15 h. [d] (cod)Ru(met)$_2$ (5 mol %), dcypb (6 mol %), Yb(OTf)$_3$ (4 mol %), DMF (3 mL), 60 °C, 6 h.

Indeed, in the reaction of 2-pyrolidinone (4 equiv, DG adjusted to 50%) and hex-1-yne (**5b**) (Scheme 8), the enamide (**6a**/**6ab**) was obtained with a DG of 30%, translating to a KIE of 2.3. The fact that a noticeable KIE is again observed reveals that this step is also relatively slow. The KIE value for each individual step is thus probably larger than 4, resulting in a smaller observed KIE for the overall reaction because the catalytic cycle involves at least two slow steps.

Journal of the American Chemical Society ARTICLE

Scheme 8. Competition Hydroamidation Experiment with 1-[*D*]-2-Pyrrolidinone (1b)

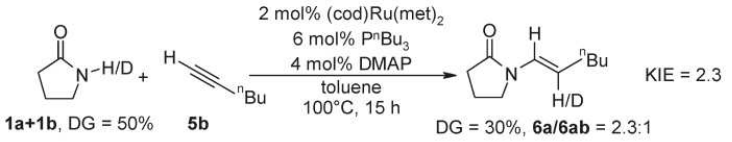

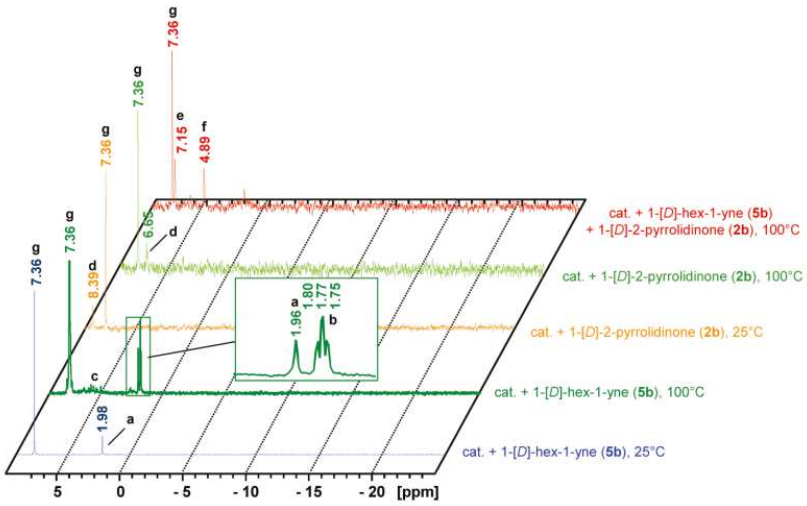

Figure 4. In situ ^{2}H NMR experiments with 1-[*D*]-hex-1-yne (**5b**) and 1-[*D*]-2-pyrrolidinone (**1b**). (a) Free 1-[*D*]-hex-1-yne; (b) triplet signal; (c) oligomerization products; (d) free 1-[*D*]-2-pyrrolidinone; (e) 1′-deuterium of the enamide; (f) 2′-deuterium of the enamide; (g) benzene-d_6.

Another possible explanation for the relatively small values is that the transition state is a nonlinear one.[38]

Overall, only *Mechanisms C* and *D*, both involving Ru−vinylidene intermediates formed without proton shifts, are in agreement with the outcome of both the deuteration studies and the kinetic investigations.

NMR STUDIES OF HYDROAMIDATIONS

We next performed in situ NMR studies with the goal of identifying potential Ru-bound organic fragments. However, the reaction proceeds very rapidly when using increased amounts of Ru catalyst, and the spectra contained numerous signals pertaining to ligands, additives, and byproducts that often obscured relevant species. To specifically monitor species derived from the alkyne and amide starting materials, we used deuterated derivatives and followed the reaction by ^{2}H NMR. This greatly simplified the NMR spectra obtained (Figure 4). Unfortunately, the sensitivity of this spectroscopic method was determined to be rather low.

^{2}H NMR spectra of a mixture containing the catalyst (20 mol % (cod)Ru(met)$_2$, 60 mol % P(*n*-Bu)$_3$, 40 mol % DMAP) and 1-[*D*]-hex-1-yne (**5a**) only were recorded in toluene, using benzene-d_6 as an internal standard (Figure 4 and Supporting Information).

At room temperature, only the signal pertaining to the starting material was visible (a), confirming that the catalyst activation requires elevated temperatures. Indeed, at 100 °C, a new broad triplet (b) was detected at δ = 1.77 ppm (J = 2.2 Hz). Moreover, a series of signals in the range of 4.89−6.20 ppm (c) rapidly appeared and increased in intensity with concomitant consumption of the alkyne, which can be attributed to alkyne oligomerization products. Some of them might also originate from Ru−vinyl species, but an unambiguous assignment of signals to such intermediates was not possible. When both 1-[*D*]-hex-1-yne (**5b**) and 2-pyrrolidinone (**1a**) were present, the same triplet (b) was detected along with a strong signal for the C(1)-deuterated enamide product (e). Alkyne oligomerization products (c) and C(2)-deuterated enamide (f) were detected only in traces.

This triplet (b) was not in good agreement with literature NMR data for ruthenium alkyne and vinyl complexes (Figure 5). Terminal protons of coordinated alkynes should appear around 5 ppm and have a large H−P coupling.[39] Ru−H and Ru−vinyl species should also appear at chemical shifts different than 1.77 ppm.[33] Considering the small value of D−H couplings in ^{2}H NMR spectra[40] and the broad shape of triplet b, this signal might be assigned to the vinylic proton of a Ru−vinylidene−phosphine species. For a known *trans*-[(dppm)$_2$(Cl)Ru=C=CH^{n}Bu]PF$_6$ complex (dppe = bisdiphenylphosphino methane) with the identical 1-hexyne-derived vinylidene ligand, Dixneuf et al. reported a triplet of quintets at 2.5 ppm in the ^{1}H NMR spectrum (Figure 5).[41] Coupling constants of 7.9 and 2.8 Hz for the vinylic proton at the vinylidene entity could be determined, resulting from a coupling to two neighboring protons and a long-range coupling to four phosphine atoms. The chemical shift of triplet b is in good range for such a vinylic proton, considering that the Ru center should be more electron-rich because of the stronger donor capacity of alkyl phosphine compared with the aryl phosphine ligands. That should lead to an upfield shift of the proton signal. The observed coupling constant of 2.2 Hz is in agreement with a long-range

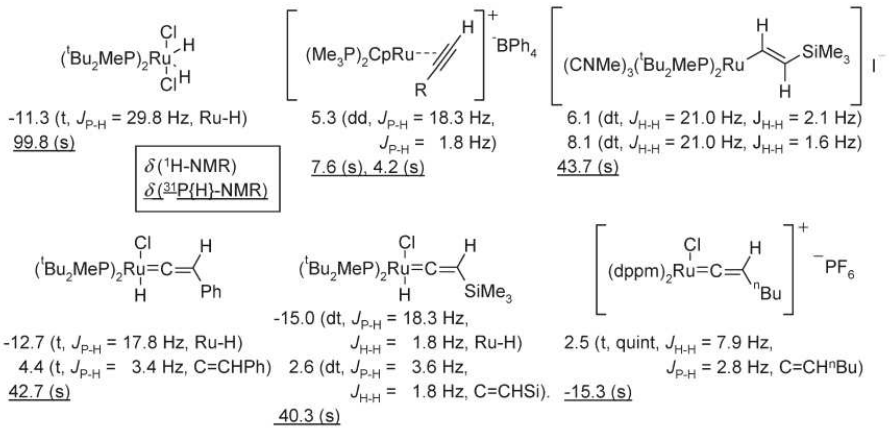

Figure 5. ^{1}H- and ^{31}P NMR chemical shifts for selected ruthenium−phosphine complexes.

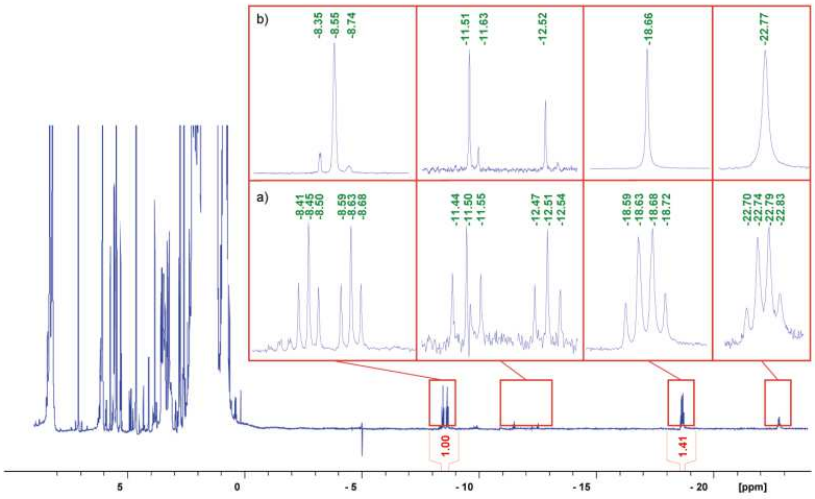

Figure 6. In situ ^{1}H NMR experiments with 2-pyrrolidinone (**1a**) at ambient temperature after heating to 100 °C for 5 min. (a) ^{1}H NMR experiment; (b) ^{1}H{^{31}P}-NMR experiment.

coupling to two phosphine atoms. The broad shape might indicate that the coupling to the neighboring protons, which is expected to be arround 1 Hz for such a D−H coupling,[40] could not be resolved in this in situ ^{2}H NMR experiment. These results suggest that, in the absence of the amide, a Ru−vinylidene species is formed, possibly via 1,2-proton shift. This is in agreement with the observation by Dixneuf that alkyne oligomerization reactions proceed via vinylidene species.[32,42]

In an attempt to find evidence for Ru−H species resulting from the oxidative addition of amides, we recorded the ^{2}H NMR spectrum for a mixture of 1-[*D*]-2-pyrrolidinone (**1b**) with the catalyst system (40 mol % (cod)Ru(met)$_2$, 120 mol % P(*n*-Bu)$_3$, 80 mol % DMAP) in toluene using benzene-d_6 as an internal standard (Figure 4). However, it contained only the signal for the free amide (d). Subsequent addition of 1-[*D*]-hex-1-yne (**5a**) led to a rapid disappearance of this signal with concomitant appearance of the signals for vinylic deuterium atoms of the enamide product (e and f). The reaction simply proceeded too rapidly to allow a detection of any intermediates by ^{2}H NMR.

We next investigated the reaction mixtures with the help of ^{1}H NMR, as this is more sensitive than ^{2}H NMR. In the ^{1}H NMR spectrum of a mixture containing the catalyst (20 mol % (cod)Ru(met)$_2$, 60 mol % P(*n*-Bu)$_3$, 40 mol % DMAP) and 1-hexyne (**5b**) but no amide (see Supporting Information), multiple signals in the range of 4.66−6.12 ppm were observed, but none were detected below 0 ppm in the region characteristic for Ru−H species. Such signals would have been expected for *Mechanisms B* and *C*. A corresponding signal for triplet b observed in the ^{2}H NMR experiment at 1.77 ppm could not be found in the ^{1}H NMR spectrum since the area from 0 to 3 ppm was overlaid with multiple broad proton signals of alkyl groups, for example, from the phosphine ligands.

In contrast, after briefly heating a mixture of the catalyst and 2-pyrrolidinone (**1a**) to 100 °C, the ^{1}H NMR spectrum showed several new signals below 0 ppm (Figure 6): A group of peaks consisting of a duplet of triplets, two triplets and two quartets appeared between −8 and −23 ppm with coupling constants between 22 and 33 Hz for the triplets and quartets and 108 Hz for

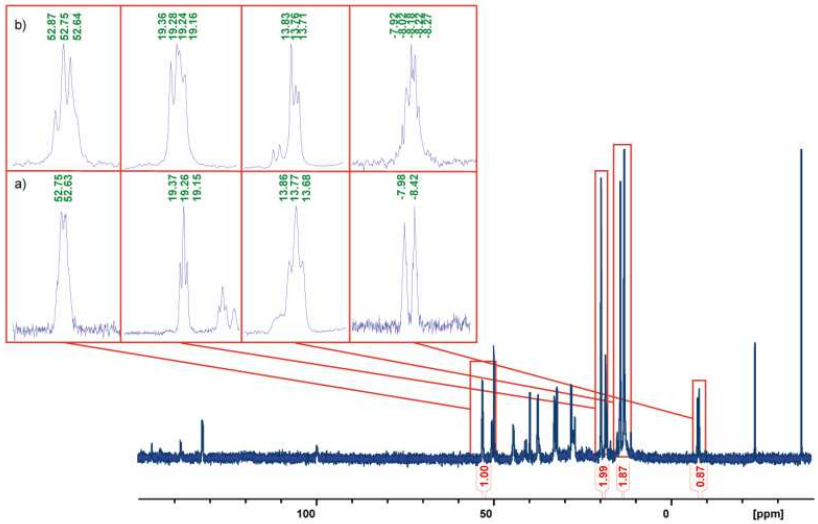

Figure 7. In situ ^{31}P NMR experiments with 2-pyrrolidinone (**1a**) measured at 22 °C after heating to 100 °C for 5 min. (a) ^{31}P NMR experiment; (b) $^{31}P\{^{1}H\}$-NMR experiment.

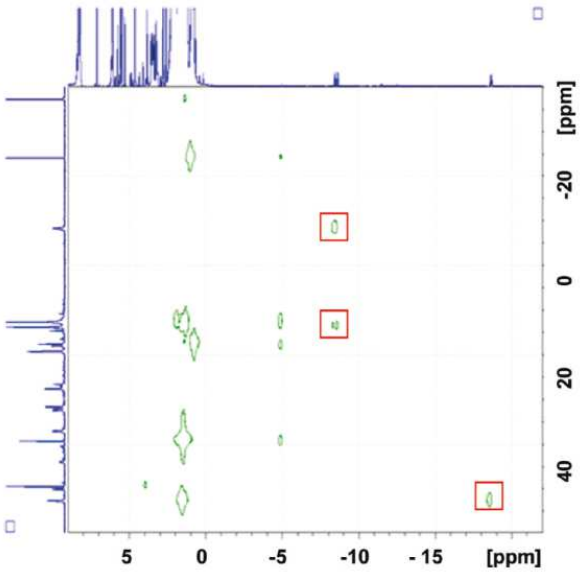

Figure 8. In situ H,P-HMQC experiments with 2-pyrrolidinone (**1a**) at ambient temperature after heating to 100 °C for five minutes.

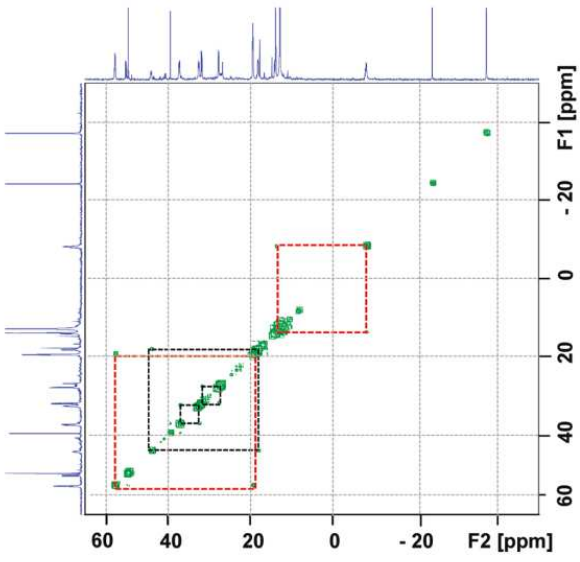

Figure 9. In situ P,P-COSY experiments with 2-pyrrolidinone (**1a**) at ambient temperature after heating to 100 °C for 5 min.

the duplet. Because of the extreme upfield shift of these signals, they are likely to originate from Ru—H species.[33] Coupling constants of 20—30 Hz are typical for *cis* H—Ru—P couplings in ruthenium hydride species stabilized by phosphines. The observed coupling constants of 108 Hz are in the expected range for *trans* H—Ru—P coupling in such complexes.[43] That the observed couplings indeed resulted from H—Ru—P interactions could be verified by phosphorus-decoupled ^{1}H NMR experiments with the same sample. Here, all signals changed to singlets.

The ^{31}P-spectrum revealed that many different phosphine species are present in the reaction mixture (Figure 7). Only the signal at −37.26 ppm could unambiguously be assigned to free tri-*n*-butylphosphine.

H,P-HMQC (Heteronuclear Multiple Quantum Coherence) and P,P-COSY (Correlation spectroscopy) experiments were used to elucidate which of these phosphine signals correspond to the Ru—H species (Figures 8 and 9).

The intensity of the proton signals at −8.55 and −18.66 ppm species was sufficient to detect them in the 2D NMR experiments. The H,P-HMQC (Figure 8) showed cross-peaks between the Ru—H-signal at −8.55 and phosphorus signals at −8.20 ppm and 13.77 ppm, which are in a reasonable range for Ru-coordinated phosphines. The signal at −8.20 ppm integrates as

Scheme 9. In Situ Formation of Ru—H-Phosphine Complexes Starting from (Cod)Ru(met)$_2$ and the Resulting ^{1}H-NMR Coupling Patterns

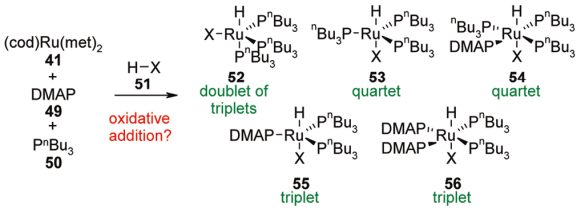

one, the signal at 13.77 ppm as two P-atoms in the ^{31}P- spectrum. In the P,P-COSY spectrum (Figure 9), a cross-peak between the two phosphorus signals is observed, confirming that all signals belong to a single Ru-species likely to contain one hydride and three phosphine ligands. The best interpretation for the H—P coupling constants for the proton signal at −8.55 ppm (J_{H-P} = 27 and 108 Hz) is that two of the phosphines are in *cis*- and one is in *trans*-position to the Ru—H bond (Scheme 9, **52**).

The H,P-HMQC (Figure 8) also showed a cross-peak for the proton signal at −18.66 ppm and the phosphorus signal at 52.69 ppm. A quartet was observed for this proton in the ^{1}H NMR which merged to a singlet in the P-decoupled ^{1}H NMR spectrum. In addition, the P,P-COSY (Figure 9) showed a clear cross-peak between the phosphorus signals at 52.69 and 19.26 ppm. The signal at 52.69 ppm integrates as one P-atom, and the signal at 19.26 ppm as two P-atoms in the ^{31}P- spectrum. These combined findings indicate an octahedral Ru-species with three phosphine ligands and one DMAP ligand in plane (Scheme 9, **54**). Two phosphorus signals are expected for species **54**, one for the two P-atoms next to, and one for the P-atom in *trans* position to the DMAP ligand. Therefore, the observed quartet in the ^{1}H NMR spectrum must actually be a duplet of triplets with nearly identical *cis* H—P couplings, which leads to an overlay of two triplets to one quartet.

The remaining upfield signals in the ^{1}H NMR showed very similar splitting patterns that disappear in the P-decoupled proton spectrum and are also likely to originate from Ru—H phosphine complexes. Beside the duplet of triplets at −8.55 ppm and the pseudo quartet at −18.66 ppm, two triplets at −11.50 and −12.51 ppm and one quartet at −22.77 ppm were detected in the ^{1}H NMR. Their coupling patterns and coupling constants in the range of 24—36 Hz also suggest Ru—H—phosphine complexes with, respectively, two and three phosphines coordinated in *cis*-position to the hydride. Scheme 9 provides for an overview of possible Ru—H species that would be in agreement with the spectroscopic data obtained.

We next added phenylacetylene-2-^{13}C (**5c**) to the NMR sample containing 2-pyrrolidinone (**1a**), 40 mol % (cod)Ru(met)$_2$, 120 mol % P(*n*-Bu)$_3$, 80 mol % DMAP and toluene-d_8 which had shown the signals for Ru—H species, and performed further ^{13}C- and ^{1}H NMR experiments (see Supporting Information).

The proton-decoupled ^{13}C NMR spectrum showed multiple signals below 200 ppm. A triplet detected at 214 ppm and a duplet of duplets of duplets at 216 ppm seemed to originate from Ru—alkyne intermediates, since no signals of an organic fragment should appear at chemical shifts higher than 200 ppm.

It is not straightforward to assign these signals. The coupling constants between 8 and 28 Hz seem to result from carbon—Ru—phosphorus couplings. However, Ru—vinylidene species should appear at chemical shifts higher than 300 ppm, Ru—vinyl species between 120 and 170 ppm, and Ru—alkyne π-complexes around 75 ppm.[44]

The corresponding ^{1}H NMR spectrum showed a duplet of triplets at around −7.4 ppm and a duplet of triplets of duplets at around −8.7 ppm. Before the addition of phenylacetylene-2-^{13}C (**5c**), the signal at −8.7 ppm appeared as a duplet of triplets with H—P couplings of 108 and 27 Hz, whereas after the addition of phenylacetylene-2-^{13}C (**5c**), the H—P couplings changed in part to 87 and 27 Hz and an additional coupling of 7 Hz appeared which must result from a proton-carbon coupling. The H—C coupling might originate from a π-coordination of phenylacetylene-2-^{13}C (**5c**) to species **52** (Scheme 9), the formation of a Ru—vinylidene—hydride such as **29** and **39**, or a Ru—hydride—enamide species such as **31** and **40**.

After heating the reaction mixture briefly to 100 °C, the spectra revealed that the reaction was already complete, as expected for this highly reactive alkyne.

We continued our in situ NMR studies with the investigation of the *Z*-selective hydroamidation of secondary amides (see Supporting Information). The first generation catalyst system for the *Z*-selective hydroamidation of secondary amides proved to be unsuitable for NMR investigations because of the high amount of water (8 equiv) required for this catalyst system,[25] causing massive solubility problems and preventing an effective shimming during the measurements. Therefore, we used a modified protocol of the second generation catalyst system.[30] The experiments were performed in DMF-d_7 instead of chlorobenzene and the paramagnetic Yb(OTf)$_3$ was substituted by diamagnetic Sc(OTf)$_3$. Because of the high catalyst loading (40 mol % (cod)Ru(met)$_2$, 45 mol % dcypb, 80 mol % Sc(OTf)$_3$, 2-pyrrolidinone (**1a**), DMF-d_7) only broad signals were detected in the ^{1}H NMR spectrum. After centrifugation of the suspension in the NMR tube and briefly heating to 100 °C, the ^{1}H NMR spectrum showed several signals between −15 and −25 ppm. These signals below 0 ppm confirm the formation of Ru—hydride species under *Z*-selective reaction conditions, indicating a similar reaction mode for this protocol. Unfortunately, no characteristic H—P couplings could be determined. The corresponding ^{31}P NMR spectrum showed several low intensity phosphorus signals between −20 and 70 ppm.

The results from these NMR studies strongly suggest that Ru—H—phosphine complexes are present in the reaction mixtures of hydroamidation reactions. The experiments also show how readily Ru—H species are formed when an amide is added to a Ru—phosphine catalyst, presumably via oxidative insertion into the N—H bond.[19,22,45] These observations, in combination with the findings of Caulton et al., who reported that Ru—H-complexes rapidly react with alkynes under formation first of Ru—vinyl and then of Ru—vinylidene complexes,[33] all point in the direction of *Mechanism D*. After all, *Mechanisms A* and *D* are the only ones that involve Ru—H species formed via an oxidative addition of N—H nucleophiles. In *Mechanisms E*, Ru—H species are not involved at all and can be ruled out. In *Mechanisms B* and *C*, Ru—H species are formed in the reaction of a Ru-precursor with an alkyne without participation of the amide. However, in the NMR experiments, the fact that Ru—H species were observed in the presence of amide but not in the presence of alkyne contributes to the evidence against *Mechanisms B* and *C*. Considering that the results of the labeling experiments and the kinetic studies are incompatible with

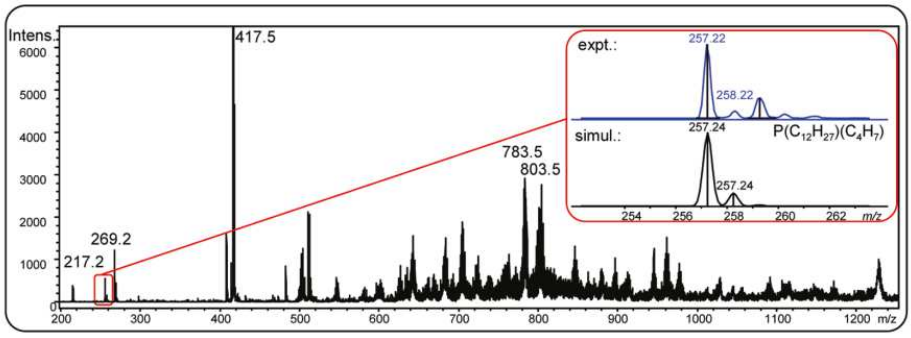

Figure 10. Assignment of $[(n\text{-Bu})_3P{-}C_4H_7]^+$ (m/z = 257.2) as the product of an allylic substitution reaction of methylallyl ligands with tri-*n*-butylphosphine.

Mechanisms A, B, and *E, Mechanism D* at this stage appears to be most likely.

■ IN SITU ESI–MS EXPERIMENTS

The electronspray ionization mass spectroscopy (ESI–MS) has evolved as a key technology in the investigation of reaction mechanism. In pioneering work, Chen et al., for example, used ESI–MS to identify key intermediates for the Ru-catalyzed olefin metathesis,[46] and Pfaltz et al. and di Lena et al. used ESI–MS technology to develop more efficient and more selective catalyst systems.[47] Intrigued by the predictive power of these investigations, we performed a series of in situ ESI–MS experiments with the goals of investigating the catalyst preformation step and identifying reaction intermediates that further support any of the proposed catalytic cycles.

There is ample literature evidence that the cod ligand is immediately replaced by more strongly coordinating phosphine and/or DMAP ligands, giving rise to a $L_nRu(met)_2$ species (L = phosphine, DMAP).[26,29] To differentiate between the proposed mechanisms, the decisive question to be addressed is whether the methylallyl ligands remain bound to Ru^{II} (consistent with *Mechanisms B* and *C*), become protonated and replaced by another ligand (consistent with *Mechanisms B, C* and *E*), or are cleaved via a reductive elimination step leading to Ru^0 species (consistent with *Mechanisms A* and *D*).

In this context, we investigated several combinations of $(cod)Ru(met)_2$, $P(n\text{-Bu})_3$ and DMAP by ESI–MS, both at room temperature and after briefly heating to 100 °C. The spectra obtained at room temperature from all possible solutions showed low overall intensities and no clear assignment to Ru-species was possible (see Supporting Information). This is not surprising, as the expected neutral Ru(II) complexes with strongly coordinating counterions would be hard to detect. However, after briefly heating the solutions to 100 °C, the overall intensities increased and clear signals for Ru^{II} species could be detected in all cases, except for the toluene solution of $(cod)Ru(met)_2$ alone.

The solution of $(cod)Ru(met)_2$ and DMAP showed three signals at m/z = 371.1, 625.2, and 716.3 which could only be matched with the calculated pattern for $[Ru(met)(DMAP)(tol)]^+$ (met = $C_4H_7^-$, DMAP = $C_7H_{10}N_2$, tol = toluene, C_7H_8), $[Ru(met)_2(cod\text{-}H_2)(DMAP)(tol)_2] + H^+$ (cod-H_2 = C_8H_{10}) and $[Ru(met)_2(cod\text{-}H_2)(DMAP)(tol)_3]^+$, illustrating that DMAP indeed coordinates to the Ru center and is able to replace the cod ligand. The dehydrogenation of the cod ligand leading to cyclooctatriene (C_8H_{10}) or anionic cyclooctadienyl fragments ($C_8H_{10}^{2-}$) provides a simple explanation for the observed signal patterns. During the electrospray process, several toluene molecules seemed to condense to the detected cationic Ru-fragments. Such species are highly unstable and unlikely to exist in the reaction solution in significant abundances.

For the toluene solution of $P(n\text{-Bu})_3$ and $(cod)Ru(met)_2$, three signals of Ru species at m/z = 505.3, 761.5, and 779.5 were detected matching the calculated patterns of $[Ru(cod)(P(n\text{-Bu})_3)(tol)(H)]^+$ ($P(n\text{-Bu})_3 = PC_{12}H_{27}$), $[Ru(met)(cod)(P(n\text{-Bu})_3)_2(tol)]^+$ and $[Ru(cod)(P(n\text{-Bu})_3)(tol)_4)] + H^+$.

For the toluene solution of $(cod)Ru(met)_2$, $P(n\text{-Bu})_3$ and DMAP, two strong signals at m/z = 783.5 and 803.5 were detected, that matched the calculated patterns for $[Ru(P(n\text{-Bu})_3)_2(tol)_3(H)]^+$ and $[Ru(P(n\text{-Bu})_3)_3(tol)(H)_2] + H^+$.

Whenever $P(n\text{-Bu})_3$ was present the reaction solution, a series of three signals at m/z = 217.2, 257.2, and 417.5 was detected matching the calculated patterns of $[OPC_{12}H_{26}]^+$, $[(n\text{-Bu})_3P{-}C_4H_7]^+$ and $[O(PC_{12}H_{26})_2]^+$ fragments (Figure 10). The signals for $[OPC_{12}H_{26}]^+$ and $[O(PC_{12}H_{26})_2]^+$ fragments might have been caused by partial oxidation of $P(n\text{-Bu})_3$, but $[(n\text{-Bu})_3P{-}C_4H_7]^+$ fragment must be seen as evidence for a reduction process at the Ru center, in which a phosphine reacts with a methylallyl ligand with formation of a phosphonium salt that can be further deprotonated to the corresponding phosphorus ylide species ($(n\text{-Bu})_3P{=}CH(C_3H_5)$). This coupling is known to occur in the reaction of bis(2-methylallyl)palladium chloride dimer with phosphines giving rise to Pd^0–phosphine complexes such as $Pd(P(n\text{-Bu})_3)_4$.[48]

This suggests that during catalyst preformation, the nucleophilic $P(n\text{-Bu})_3$ attacks one of the methylallyl ligands with formation of a phosphonium salt. In this process, Ru^{II} is reduced to Ru^0 while the second methylallyl ligand is protonated, for example, by the acidic proton of the phosphonium salt, with formation of isobutene. The resulting phosphorus ylide species are known to decompose to the corresponding phosphine oxide and the alkene. Indeed, upon heating the reaction mixture to 100 °C, the intensity of the signal at m/z = 257.2 decreased and a signal at m/z = 217.2 was detected, which is characteristic for tri*n*-butylphosphine oxide ($(n\text{-Bu})_3P{=}O$). The formation of isobutene as well as $(n\text{-Bu})_3P{=}O$ in hydroamidation reactions was previously confirmed via GC- and NMR-spectroscopy.[29a]

We had previously dismissed mechanisms starting from Ru^0 intermediates (*Mechanisms A* and *D*), because we had never detected byproducts resulting from the reductive elimination of

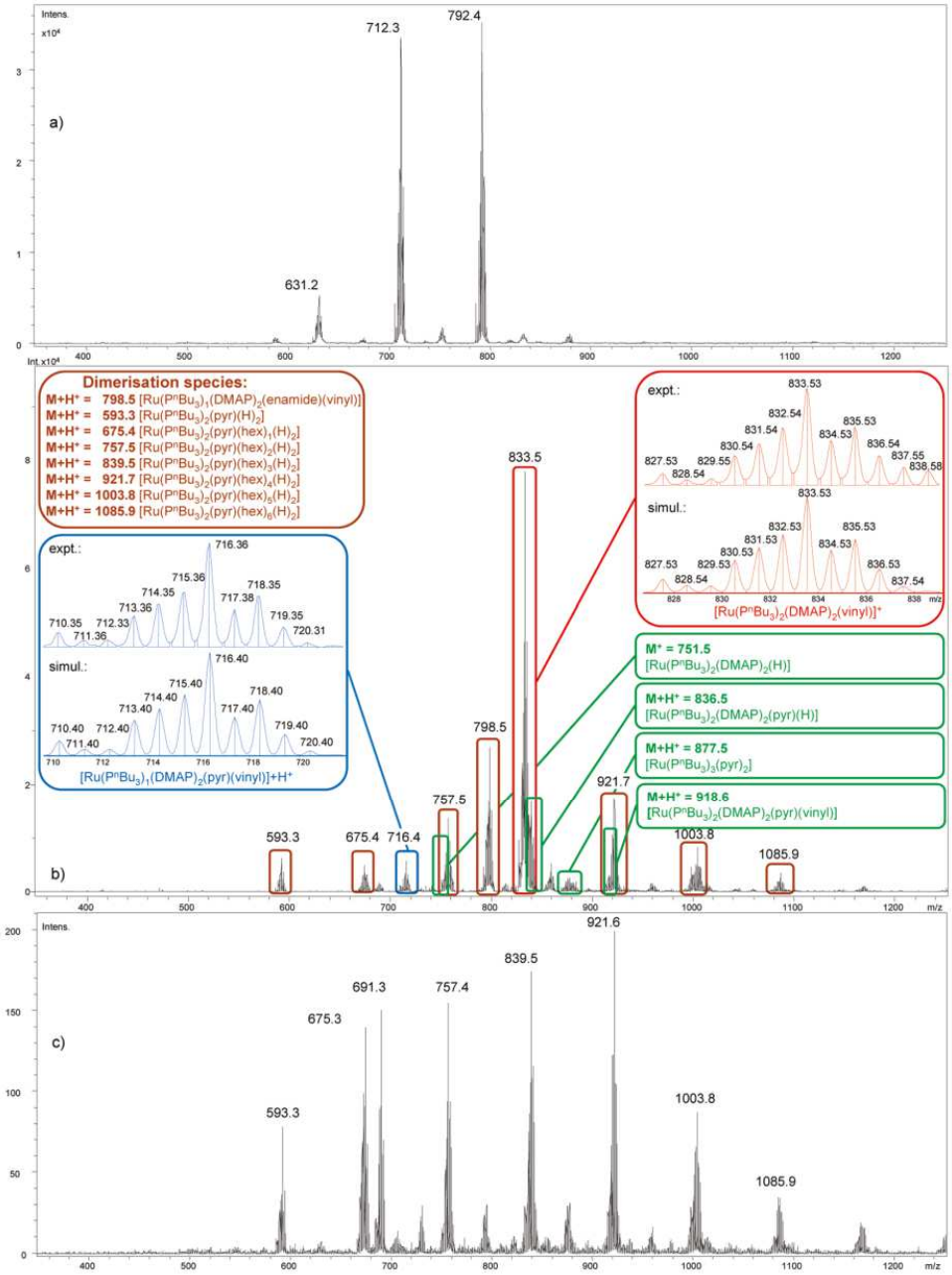

Figure 11. ESI–MS spectra for the *E*-selective hydroamidation of 2-pyrrolidinone (**1a**) and 1-hexyne (**5b**). (a) Heating to 100 °C for 5 min without 1-hexyne; (b) 40 min reaction time; (c) 150 min reaction time.

allyl fragments and had thus favored *Mechanism E*. However, this new experimental data gives at least indirect evidence for the formation of L_nRu^0 species, which unfortunately are particularly hard to detect by ESI–MS, because such species cannot be ionized by ligand dissociation.

We attempted to overcome this hurdle by using charged phosphine ligands. Unfortunately, the spectra obtained using [2-(dicyclohexylphosphino)ethyl] trimethylammonium chloride $[(C_6H_{11})_2P(C_2H_4)N(CH_3)_3Cl]$ instead of P(*n*-Bu)$_3$ were inconclusive. Only few signals of ruthenium intermediates were detected, and they resulted mostly from ruthenium chloride species. In fact, we observed a strong signal at $m/z = 225.2$, which could unambiguously be assigned to a $[(cy)_2P(C_2H_4)]^+$ fragment (cy = cyclohexyl = C_6H_{11}), indicating that the trimethylamine entity is cleaved under the reaction conditions. The exchange of chloride by other counterions, for example, hexafluorophosphate, did not have any beneficial effect on the complexity of the resulting spectra. We also tried to induce a ligand

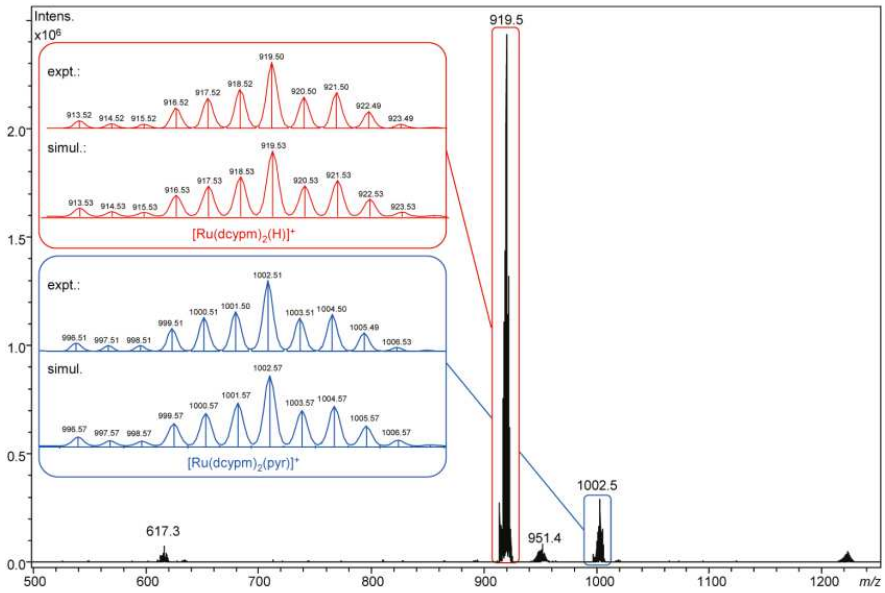

Figure 12. ESI–MS spectrum of a mixture of the catalyst and 2-pyrrolidinone (**1a**) under *Z*-selective hydroamidation conditions and after 5 min at 100 °C.

exchange of P(*n*-Bu)$_3$ by $[(C_6H_{11})_2P(C_2H_4)N(CH_3)_3]^+$ in a preformed catalyst solution (2 mol % (cod)Ru(met)$_2$, 6 mol % P(*n*-Bu)$_3$, 4 mol % DMAP) by adding the charged phosphine ligand afterward. Unfortunately, we could not observe any new Ru species in the corresponding ESI–MS spectra. The charged amonium phosphine ligand was simply not stable enough for in situ ESI–MS experiments. The syntheses of other non-amonium-based charged phosphine ligands, which are also suitable for hydroamidation reactions, are underway.

Next, we added 2-pyrrolidinone (**1a**) to the catalyst system consisting of 2 mol % of (cod)Ru(met)$_2$, 6 mol % of P(*n*-Bu)$_3$ and 4 mol % of DMAP at 100 °C. At this stage, signals at m/z = 712.3 and 792.4 appeared, which, based on their location and exact isotope pattern, could be assigned to $[Ru(P(n\text{-}Bu)_3)_2(DMAP)(pyr)]^+$ (pyr =2-pyrrolidinyl anion, $C_4H_6NO^-$) and $[Ru(P(n\text{-}Bu)_3)_3(pyr)]^+$ (Figure 11, Spectrum a).[26]

These species can result from the dissociation of a 2-pyrrolidinyl anion ($[M\text{-}(pyr)]^+$) of $[Ru(P(n\text{-}Bu)_3)_2(DMAP)(pyr)_2]$ and $[Ru(P(n\text{-}Bu)_3)_3(pyr)_2]$ (*Mechanisms B, C* and *E*) but also from $[Ru(P(n\text{-}Bu)_3)_2(DMAP)(pyr)(H)]$ and $[Ru(P(n\text{-}Bu)_3)_3(pyr)(H)]$ by protonation and H_2 release ($[M + H]^+\text{-}H_2$)[49] during the ionization process (*Mechanisms A* and *D*).

1-Hexyne (**5b**) was then injected to the mixture and further samples were taken after 5, 15, 30, 40, 150, and 470 min at 100 °C (Figure 11, Spectra b and c, and Supporting Information).

Already after 5 min, the signals at m/z = 712.3 and 792.4 disappeared. Strong signals appeared at m/z = 798.4 and 833.5 and weaker signals at m/z = 593.3, 675.4, 716.4, 757.5, 880.5, 921.7, 1003.8, and 1085.9.

The signals at m/z = 833.5 and 918.6 matched the calculated patterns for Ru–vinyl species $[Ru(P(n\text{-}Bu)_3)_2(DMAP)_2(vinyl)]^+$ (vinyl = $C_6H_{11}^-$) and $[Ru(P(n\text{-}Bu)_3)_2(DMAP)_2(pyr)(vinyl)] + H^+$ (Figure 11, Spectrum b). They are both likely to result from the ionization of the $[Ru(P(n\text{-}Bu)_3)_2(DMAP)_2(pyr)(vinyl)]$ complex. Further fragmentation of this species via ESI–MS–CID–MS (CID = collision-induced dissociation) was in agreement with the assignment and showed mainly the cleavage or the gradual decay of DMAP and P(*n*-Bu)$_3$ ligands. This intermediate is in agreement with all postulated mechanisms.

The signal at m/z = 716.4 matched the calculated pattern for $[Ru(P(n\text{-}Bu)_3)(DMAP)_2(pyr)(hex)(H)] + H^+$ (hex = C_6H_{10}) and the weak signal at m/z = 631.3 that of $[Ru(P(n\text{-}Bu)_3)(DMAP)_2(hex)(H)]^+$. Both species are likely to result from the ionization of a $[Ru(P(n\text{-}Bu)_3)(DMAP)_2(pyr)(hex)(H)]$ complex. This might result from a Ru–vinyl complex such as **28** or **38** with a suitable ligand sphere (m/z = 833.5), via vinyl/vinylidene rearrangement with concomitant dissociation of a P(*n*-Bu)$_3$ ligand (consistent with *Mechanisms C* and *D*). The weak signals at m/z = 751.5, 836.5, and 918.6 might be explained by $[Ru(P(n\text{-}Bu)_3)_2(DMAP)_2(H)]^+$, $[Ru(P(n\text{-}Bu)_3)_2(DMAP)_2(pyr)(H)] + H^+$ and $[Ru(P(n\text{-}Bu)_3)_2(DMAP)_2(enamide)(H)] + H^+$ fragments (enamide = $C_{10}H_{16}NO^-$) resulting from the ionization of $[Ru(P(n\text{-}Bu)_3)_2(DMAP)_2(pyr)(H)]$ (*Mechanisms A* and *D*) and $[Ru(P(n\text{-}Bu)_3)_2(DMAP)_2(enamide)(H)]$ (*Mechanisms A* to *E*).

The species at m/z = 798.4 matched the pattern calculated for $[Ru(P(n\text{-}Bu)_3)(DMAP)_2(enamide)(vinyl)] + H^+$ and might result from ionization of $[Ru(P(n\text{-}Bu)_3)(DMAP)_2(enamide)(vinyl)]$. The CID-fragmentation of this species showed the dissociation of a P(*n*-Bu)$_3$ ligand and of a fragment with the mass of the enamide product (**6a**). As it contains two 1-hexyne (**5b**) molecules, this species is likely to be an intermediate in the formation of double alkyne insertion enamide products, which are observed as minor side products in hydroamidations. Its intensity decreases sharply after the first minutes of the reaction, while all other signals discussed above increased and the signal at m/z = 833.5 remained at a high level.

After the hydroamidation reaction was complete (150 min) the intensity of the signals pertaining to hydroamidation intermediates decreased, and a set of signals that had been detected at

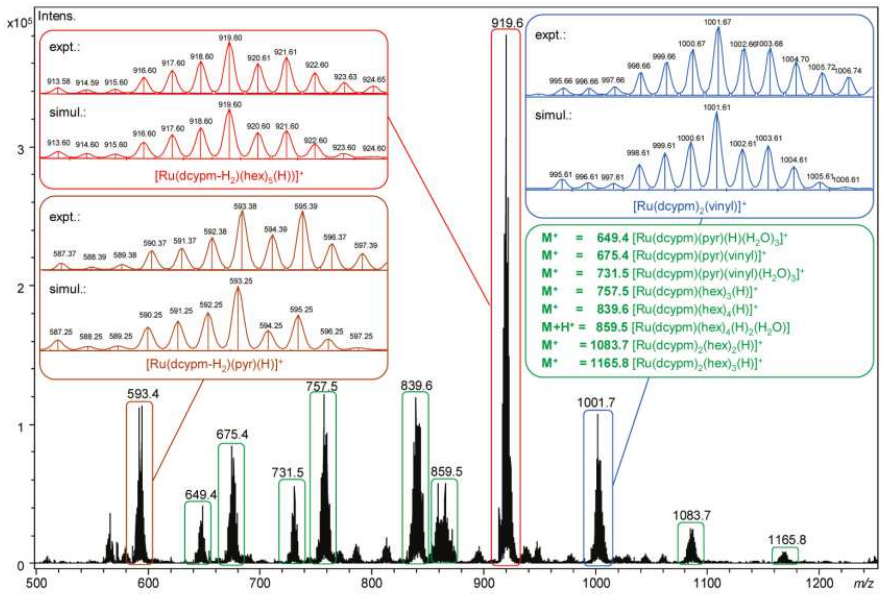

Figure 13. ESI—MS spectrum of a mixture of the catalyst, 2-pyrrolidinone (**1a**) and 1-hexyne (**5b**) under *Z*-selective hydroamidation conditions and after 5 min at 100 °C.

very low intensities earlier on, now became predominant. The signals at m/z = 593.4, 675.4, 757.4, 839.5, 921.6, 1003.7, and 1085.5 (Figure 11, Spectrum c) matched the calculated pattern for a series of Ru^{III} complexes with the chemical composition of $[Ru(P(n\text{-}Bu)_3)_2(pyr)(hex)_x(H)_2] + H^+$ bearing up to six 1-hexyne molecules (**5b**, x = 0—6). These species seem to be intermediates of alkyne oligomerization, which becomes the main reaction once most of the amide is consumed.

Next, we investigated the *Z*-selective hydroamidation of 2-pyrrolidinone (**1a**) and 1-hexyne (**5b**) in an analogous set of ESI—MS experiments.

A reaction mixture of the catalyst (2 mol % (cod)Ru(met)$_2$, 3 mol % dcypm, 8 equiv water) and 2-pyrrolidinone (**1a**) in toluene was heated to 100 °C for 5 min. The spectrum obtained at this stage showed two major signals at m/z = 919.5 and 1002.5, which, based on their location and exact isotope pattern, could be assigned to $[Ru(dcypm)_2(H)]^+$ (dcypm = bis-(dicyclohexylphosphino)methane, $P_2C_{25}H_{46}$) and $[Ru(dcypm)_2(pyr)]^+$ fragments (Figure 12).

Both cationic species seem to result from the same Ru-intermediate $[Ru(dcypm)_2(pyr)(H)]$. The formation of a Ru-intermediate such as **16** and **35** with a suitable ligand sphere can be explained best via oxidative addition of an amide to a neutral Ru^0-phosphine species (consistent with *Mechanisms A* and *D*). It is most likely that the cationic species are formed via dissociation of a 2-pyrrolidinyl anion ($[M\text{-}(pyr)]^+$) or protonation and H_2 release ($[M + H]^+\text{-}H_2$)[49] of $[Ru(dcypm)_2(pyr)(H)]$ during the ionization process. Further fragmentation of both species via ESI—MS—CID—MS (see Supporting Information) was in good agreement with this assignment and showed the same fragmentation species formed via gradual decay of dcypm and additionally via the cleavage of one 2-pyrrolidinyl anion from $[Ru(dcypm)_2(pyr)]^+$ in the case of the species at m/z = 1002.5.

We next injected 1-hexyne (**5b**) to the mixture and further samples were taken after 5, 25, 130, and 360 min at 100 °C (Figure 13 and Supporting Information).

After 5 min of heating in the presence of 1-hexyne (**5b**), the signals at m/z = 919.5 and 1002.5 disappeared and strong signals at m/z = 593.4, 757.5, 839.6, 919.6, and 1001.7 as well as weaker signals at m/z = 649.4, 675.4, 731.5, 859.5, 1083.7, and 1165.8 appeared. The masses often deviated by 2, 4, 6, or 8 mass units from expected molecular formulas. This can be explained with experiments by Leitner et al. who found that dcypb and bis-(dicyclohexylphosphino)propane (dcypp) ligands at Ru-centers easily dehydrogenate.[50] This thermal activation of sp^3 C—H bonds of bisphosphine Ru—bisallyl complexes leads to η^3-cyclooctenyl bridged Ru-complexes and extrusion of up to three protons from one cyclohexyl ring. We believe that similar dehydrogenation reactions took place under our hydroamidation reaction conditions. This would explain why signals that match $[M]^+ - 2, 4, 6,$ or 8 were detected.

The signal at m/z = 916.6 matched the calculated pattern of a $[Ru(dcypm\text{-}H_2)(hex)_5(H)]^+$ fragment (dcypm-H_2 = $Cy_2P(CH_2)P(Cy)(C_6H_9)$, formed via extrusion of H_2) and was confirmed to be nonidentical with the species at m/z = 915.5, observed in the absence of 1-hexyne (**5b**, Figure 12). The ESI—MS—CID—MS (see Supporting Information) of both signals were completely different. Whereas for the peak at m/z = 915.6, inter alia, the stepwise dissociation of four 1-hexyne (**5b**) molecules was observed, and for the peak at m/z = 915.5, stepwise decay of two phosphine ligands was observed. We believe that the species corresponding to the dominating signal at m/z = 915.6 is formed via dissociation of a 2-pyrrolidinyl anion ($[M\text{-}(pyr)]^+$) of $[Ru(dcypm\text{-}H_2)(hex)_5(pyr)(H)]$ or via protonation and H_2 release ($[M + H]^+\text{-}H_2$)[49] of $[Ru(dcypm)(hex)_5(H)_2]$, both presumably intermediates in alkyne oligomerization side reactions.

The smaller signal at m/z = 1001.7 could be assigned to a $[Ru(dcypm)_2(vinyl)]^+$ fragment likely to originate from a

Scheme 10. Catalytic Cycle for the *E*-Selective Hydroamidation of 1-Hexyne (5b) and 2-Pyrrolidinone (1a), L = ligand ($P(n\text{-}Bu)_3$ or DMAP)

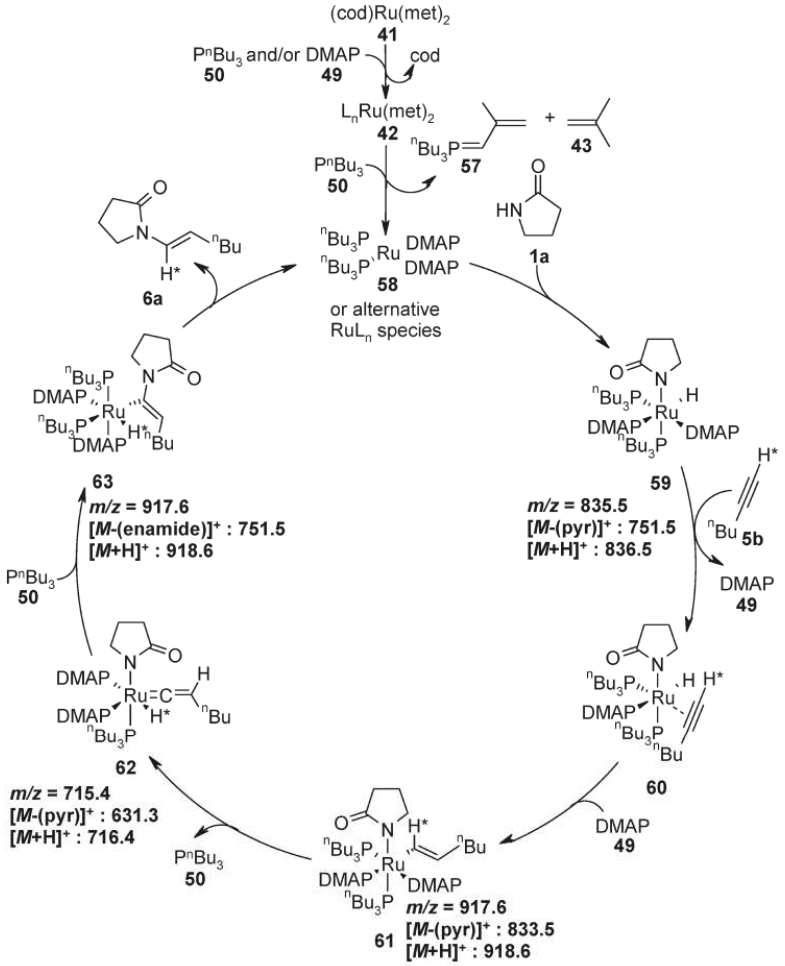

$[Ru(dcypm)_2(vinyl)(pyr)]$ species with the general formula **17**, **18** or **38**, formed by insertion of one 1-hexyne molecule (**5b**) into a Ru−H bond of **16** or **35** (consistent with *Mechanisms A* and *D*). The corresponding Ru−hydride−vinylidene species **39** would show the identical mass and isotope pattern. This is so, since both bidentate phosphine ligands would remain attached to the Ru center even if one of the Ru−P bonds is cleaved during the vinyl/vinylidene rearrangement step (consistent with *Mechanism D*).

Four Ru^{III} species could be assigned to the signals at m/z = 593.4, 649.4, 675.4, and 731.5 matching the calculated patterns of $[Ru(dcypm\text{-}H_2)(pyr)(H)]^+$, $[Ru(dcypm)(pyr)(H)(H_2O)_3]^+$, $[Ru(dcypm)(pyr)(vinyl)]^+$ and $[Ru(dcypm)(pyr)(vinyl)\text{-}(H_2O)_3]^+$ fragments. These species occur with only low intensities. They are most likely formed by oxidation side reaction during the sample extraction and injection into the ESI−MS instrument. Nevertheless, these Ru^{III} complexes—bearing 2-pyrrolidinyl-, hydrido-, and/or 1-hexenyl ligands—suggest that an oxidative addition step of the amide and an insertion step of the alkyne into a Ru−H bond is involved in the catalytic cycle of the *Z*-selective hydroamidation (consistent with *Mechanisms A* and *D*).

The five signals at m/z = 757.5, 839.6, 859.5, 1083.7, and 1165.8 match the calculated patterns of $[Ru(dcypm)_x(hex)_y(H)]^+$ species bearing one or two dcypm ligands (x = 1 or 2) and up to four 1-hexyne molecules (**5b**, y = 1−4). These species are also likely formed via dissociation of a 2-pyrrolidinyl anion ($[M\text{-}(pyr)]^+$) of $[Ru(dcypm)_x(hex)_y(pyr)(H)]$ or via protonation and H_2 release ($[M + H]^+\text{-}H_2$)[49] of $[Ru(dcypm)_x(hex)_y(H)_2]$. They constitute intermediates of the alkyne oligomerization side reaction.

After 25 min of heating, the intensities of all Ru-species remained at a high level and two new Ru-species at m/z = 865.5 and 947.6 could be detected (see Supporting Information). These new signals matched the calculated pattern of $[Ru(dcypm)(hex)_3(OH)(tol)]^+$ and $[Ru(dcypm)(hex)_4(OH)(tol)]^+$ fragments and are most likely formed via protonation and H_2 release ($[M + H]^+\text{-}H_2$)[49] of $[Ru\text{-}(dcypm)(hex)_3(H)(OH)(tol)]$.

The intensities of these two signals increased strongly in the spectra obtained after 130 and 360 min of heating, while the intensities of other signals decreased, indicating that the former correspond to oligomerization intermediates which predominate once most of the amide has been consumed.

■ CONCLUSIONS FROM THE EXPERIMENTAL STUDIES

Overall, most of the mechanisms under consideration were in disagreement with one or more experimental findings. *Mechanism A*, which involves an oxidative addition of the amide followed by an insertion of the alkyne into either the Ru—H or the Ru—N bond, correctly predicted the findings of the deuterium labeling experiments. It is also consistent with the detection of Ru—H species following addition of the amide to the Ru-catalyst and with most species detected by ESI—MS. However, it must be dismissed on the basis that a normal kinetic isotope effect was observed, while *Mechanism A* would have predicted an inverse secondary kinetic isotope effect caused by a change in hybridization of the alkyne-C(1) carbon atom bond from sp to sp^2.

The same experimental findings also rule out the redox-neutral *Mechanism E*, which does not involve Ru—vinylidene intermediates, but instead proceeds via an attack of the amide nucleophile to a π-coordinated alkyne. This pathway is in good agreement with the isotope labeling and the ESI—MS studies, but offers no explanation for the observation of Ru—H-species after the addition of the amide to the catalyst system.

Mechanism B involves the formation of Ru—vinylidene species via 1,2-proton shift followed by an attack of the amide nucleophile. It must be excluded based on the results of the deuterium labeling studies, which unambiguously showed that in contrast to Ru-catalyzed additions of other nucleophiles, hydroamidations do not involve a shift of the terminal alkyne proton to the internal sp-carbon.

Mechanism C, which involves the formation of Ru—vinyl species and their rearrangement to Ru—hydride—vinylidene intermediates, is in agreement with most of the experimental findings. It correctly predicts the results of the deuterium labeling experiments and the observed normal kinetic isotope effect, and is in good agreement with most of the species observed in the ESI—MS studies. However, some of the cationic Ru^{IV} intermediates (**28**, **29** or **31**) should have been easily detectable by ESI—MS. One might also have expected the detection of Ru—H-species in the ^{1}H NMR in the presence of 1-hexyne (**5b**), rather than after the addition of 2-pyrrolidinone (**1a**) to the catalyst system. Moreover, it is unlikely that a protonation step with formation of cationic Ru—vinyl species is a favorable pathway in a nonpolar solvent under almost neutral conditions. The catalytic cycle involves only Ru-species in high oxidation states and offers no

Scheme 11. Selectivity-Determining Step of the Hydroamidation Reaction

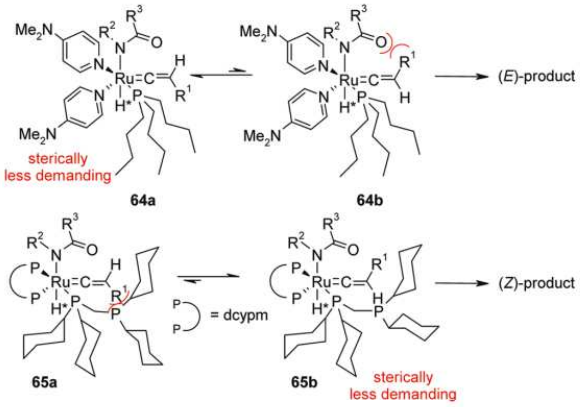

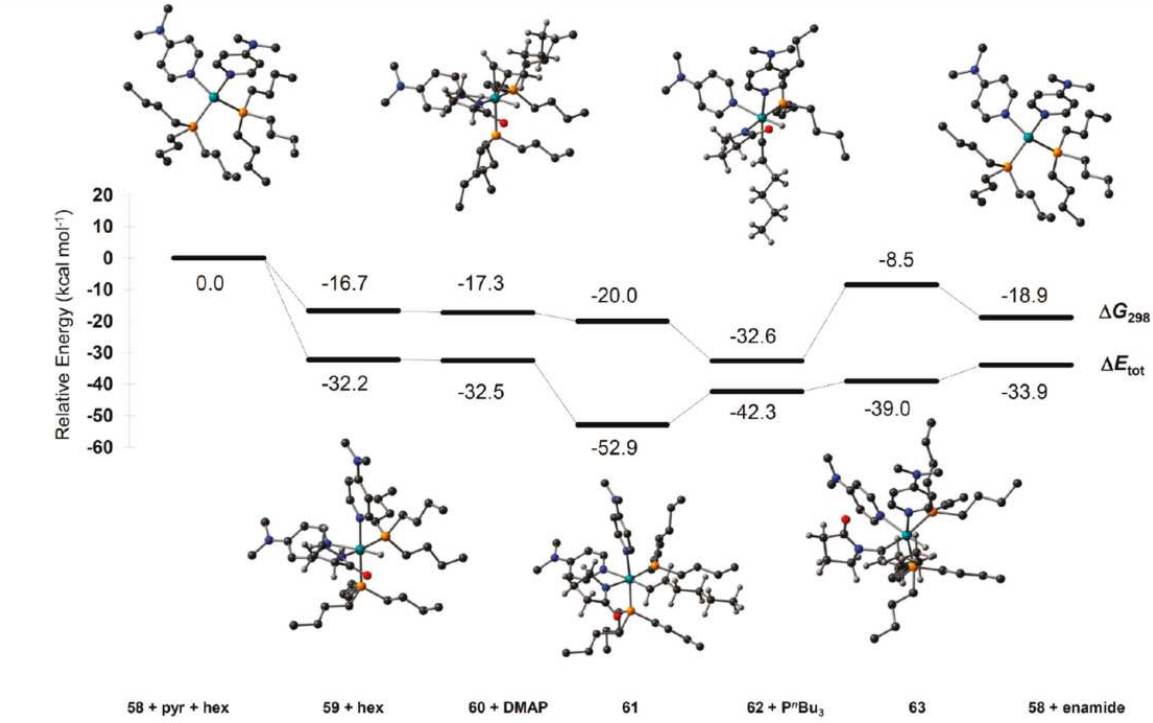

Figure 14. Relative energies and optimized structures of potential hydroamidation intermediates.

explanation for the detection of phosphonium salts known to arise from reductive deallylation processes.

Mechanism D is similar to *Mechanism C* in that it also involves Ru−vinyl intermediates that rearrange to Ru−hydride−vinylidene complexes. It is thus also in full agreement with the deuteration studies and correctly predicts the observed normal kinetic isotope effect. In contrast to *Mechanism C*, it starts from a Ru^0 species and thus offers a good explanation for the detection of phosphonium salts and of many Ru-species in the ESI−MS experiments. Moreover, the findings of the NMR studies are best explained by this mechanism, which starts with the oxidative addition of amides to the Ru-center with formation of Ru−H species. This would explain why after the addition of amides to the catalyst system, ^{1}H NMR signals below 0 ppm were detected, whereas these were not observed when only the alkyne was added to the catalyst.

For these combined reasons, the possible catalytic pathways can be narrowed down to a mechanism closely related to the proposed *Mechansim D*. On the basis of the experimental evidence, we believe that our model reaction, the *E*-selective hydroamidation of 1-hexyne (**5b**) with 2-pyrrolidinone (**1a**), proceeds via the mechanism depicted in Scheme 10.

The catalyst preformation proceeds via a reductive allylation process with release of a phosphorus ylide (**57**) and isobutene (**43**) and formation of a coordinatively unsaturated Ru^0 species bearing several neutral ligands. As the starting point for the depicted catalytic cycle we choose complex **58** with two phosphine and two DMAP ligands on the basis that intermediates with this combination of neutral ligands showed particularly strong signals in the in situ ESI−MS experiments. However, similar catalytic cycles with any combination of DMAP, phosphines, and solvent molecules would also be viable (MS signals at m/z = 751.5 $[M + H]^+$). Oxidative addition of the amide (**1a**) gives rise to an octahedral Ru−hydride complex **59**. This must be a slow step to be in accordance with the KIE of 2.3 found during the kinetic studies. The detection of signals at m/z = 751.5 and 836.5, which would match the $[M\text{-(pyr)}]^+$ and $[M + H]^+$ fragments of complex **59**, is in agreement with this pathway. In the next step, an alkyne (**5b**) coordinates to this species with dissociation of one neutral ligand (**60**). The alkyne then inserts into the Ru−H bond and the open coordination site created in the process is filled with a neutral ligand, leading to Ru^{II}-vinyl intermediate **61**. Signals at m/z = 833.5 and 918.6 can be explained by the presence of $[M\text{-(pyr)}]^+$ and $[M + H]^+$ fragments of species **61**. The high intensity of the signal at m/z = 833.5 along with the observed KIE when using deuterated alkynes, indicates that this step is comparatively slow. 1,2-Hydride shift in Ru^{II}−vinyl complex **61** then gives Ru^{IV}−H−vinylidene species **62**. Only weak ESI−MS signals could be assigned to **62** (m/z = 631.3 $[M\text{-(pyr)}]^+$ and 716.4 $[M + H]^+$). Because of the δ^+ polarization at C(1) of the vinylidene moiety, **62** is susceptible to attack of the amide ligand to afford species **63**. A neutral ligand is likely to coordinate and to refill the empty coordination site. The signals detected at m/z = 751.5 ($[M\text{-(enamide)}]^+$) and 918.6 ($[M + H]^+$) could be assigned to intermediate **63**. Finally, reductive elimination releases the enamide **6a**, regenerating the original catalytic species **58** and closing the catalytic cycle of the hydroamidation.

On the basis of the findings of the deuteration studies and the kinetic investigations, we assume that this pathway is also valid for related hydroamidations with other N−H nucleophiles. The studies presented above did not reveal any fundamental mechanistic differences between the *E*- and *Z*-selective protocols. On the basis of the NMR and ESI−MS studies with reaction mixtures of *Z*-selective hydroamidations, we believe that analogous species as those presented in Scheme 10 (**58**−**63**) are also present. The ligands are dcypm instead of P(*n*-Bu)$_3$ and DMAP before. However, in each step in which a vacant coordination site is required in the catalytic cycle (Scheme 10), one Ru−P bond of the bidentate ligand is cleaved, and therefore, the ligand remains coordinated to the Ru center leading to sterically more demanding Ru complexes. Hence, we conclude that the steric bulk of the ligand sphere is the decisive factor in directing the orientation of the substituent at the vinylidene moiety. As stretched in Scheme 11, the attack of the amide would then lead to enamides with different stereoselectivities depending on the preferred orientation of the vinylidene moiety relative to the amide. More in-depth studies are required to fully understand how the choice of ligands affects the stereoselectivity.

COMPUTATIONAL STUDIES

The Ru intermediates of the proposed catalytic cycle (Scheme 10, *Mechanism D*) have been identified based on ESI−MS and to some extent on NMR data. Since the information on the likely configuration of these intermediates is still limited, we used DFT calculations to look at the stability of each individual structure and possible spatial arrangements of the ligands. All calculations were performed using the Gaussian 03 or Gaussian 09 software package,[S1] with B3LYP[S2]/6-311+G(2d,p)[S3]//B3LYP/6-31G-(d)[S4] for H, C, N, O, P and Stuttgart RSC 1997 ECP[S5] for Ru. A scaling factor for anharmonic corrections of vibrational frequencies of f = 0.9804 was used.[S6]

A stable minimum was found for every postulated intermediate within the catalytic cycle. The calculated structures along with total energies and Gibbs free energies are depicted in Figure 14. The hydrogen atoms of the phosphine and DMAP ligands are omitted for clarity. Larger pictures of the optimized structures are included in the Supporting Information. The oxidative addition of 2-pyrrolidinone (**1a**) to the Ru species **58** with formation of the Ru−hydride complex **59** was calculated to be exothermic by Δ_rE_{tot} = −32.2 kcal mol^{-1} and exergonic by Δ_rG_{298} = −16.7 kcal mol^{-1}. The exchange reaction of DMAP by 1-hexyne (**5b**) to give a π-coordinated complex is almost thermoneutral (Δ_rE_{tot} = −0.3 kcal mol^{-1}, Δ_rG_{298} = −0.6 kcal mol^{-1}). The insertion of the alkyne in the Ru−H bond and refilling of the empty coordination site with one additional DMAP is exothermic and exergonic (Δ_rE_{tot} = −20.4 kcal mol^{-1}, Δ_rG_{298} = −2.7 kcal mol^{-1}). The following formation of vinylidene species **62** with the concomitant release of one phosphine ligand is endothermic (Δ_rE_{tot} = 10.6 kcal mol^{-1}) but exergonic (Δ_rG_{298} = −12.6 kcal mol^{-1}). The subsequent addition of the amide to the vinylidene moiety and the concomitant coordination of a neutral ligand is slightly endothermic (Δ_rE_{tot} = 3.3 kcal mol^{-1}) and highly endergonic (Δ_rG_{298} = 24.2 kcal mol^{-1}). The last reaction step, the reductive elimination of the enamide product requires only a small amount of total energy but releases a large amount of Gibbs free energy (Δ_rE_{tot} = 5.1 kcal mol^{-1}, Δ_rG_{298} = −10.4 kcal mol^{-1}). Overall, the computational studies support the conclusions drawn from the mechanistic studies. They confirm that the proposed catalytic cycle involves stable intermediates with comparable energies. Extensive computational studies using strongly simplified model systems are underway with the goal of calculating the transition states and obtaining reliably predicted kinetic isotope effects.

In summary, the results of our in-depth mechanistic studies of the hydroamidation support a catalytic cycle with ruthenium hydride and vinylidene species as the key intermediates. We thus propose that the reaction proceeds via an oxidative addition of the amide, followed by insertion of a π-coordinated alkyne into a ruthenium−hydride bond, rearrangement to a vinylidene species, nucleophilic attack of the amide, and finally reductive elimination of the product. This catalytic cycle is in agreement with all experimental results and is supported by DFT calculations that confirm the stability of all reaction intermediates.

■ ASSOCIATED CONTENT

Supporting Information. Experimental procedures and full spectroscopic data of the deuterium-labeling, the in situ IR, the in situ NMR, the in situ ESI−MS and the competition experiments. This material is available free of charge via the Internet at http://pubs.acs.org.

■ AUTHOR INFORMATION

Corresponding Author
goossen@chemie.uni-kl.de; gns@chemie.uni-kl.de

■ ACKNOWLEDGMENT

We thank the DFG and NanoKat and OPTIMAS for financial support, Umicore for donating chemicals, Mettler Toledo for giving us access to a ReactIR spectrometer, and the DAAD (K.S. M.S) and Landesgraduiertenförderung Rheinland-Pfalz (M.A. and A.F.) and Hans-Böckler-Stiftung (F.M.) for scholarships, and Dr. M. Blanchot for technical assistance. Part of this work was performed in preparation of the new transregional collaborative research center SFB/TRR 88 3MET.

■ REFERENCES

(1) Yet, L. *Chem. Rev.* **2003**, *103*, 4283–4306.

(2) Sugie, Y.; Dekker, K. A.; Hirai, H.; Ichiba, T.; Ishiguro, M.; Shiomi, Y.; Sugiura, A.; Brennan, L.; Duignan, J.; Huang, L. H.; Sutcliffe, J.; Kojima, Y. *J. Antibiot.* **2001**, *54*, 1060–1065.

(3) (a) McDonald, L. A.; Swersey, J. C.; Ireland, C. M.; Carroll, A. R.; Coll, J. C.; Bowden, B. F.; Fairchild, C. R.; Cornell, L. *Tetrahedron* **1995**, *51*, 5237–5244. (b) Boyd, M. R.; Farina, C.; Belfiore, P.; Gagliardi, S.; Kim, J. W.; Hahakawa, Y.; Beutler, J. A.; Mckee, T. C.; Bowman, B. J.; Bowman, E. J. *J. Pharmacol. Exp. Ther.* **2001**, *297*, 114–120.

(4) Davyt, D.; Entz, W.; Fernandez, R.; Mariezcurrena, R.; Mombrú, A. W.; Saldaña, J.; Domínguez, L.; Coll, J.; Manta, E. *J. Nat. Prod.* **1998**, *61*, 1560–1563.

(5) (a) Vidal, J.-P.; Escale, R.; Girard, J.-P.; Rossi, J.-C. *J. Org. Chem.* **1992**, *57*, 5857–5860. (b) Erickson, K. L.; Beutler, J. A.; Cardellina, J. H.; Boyd, M. R. *J. Org. Chem.* **1997**, *62*, 8188–8192. (c) Jansen, R.; Washausen, P.; Kunze, B.; Reichenbach, H.; Höfle, G. *Eur. J. Org. Chem.* **1999**, 1085–1089.

(6) Carbery, D. R. *Org. Biomol. Chem.* **2008**, *6*, 3455–3460.

(7) (a) Stevenson, P. J.; Graham, L *ARKIVOC* **2003**, *7*, 139–144. (b) Gaulon, C.; Dhal, R.; Chapin, T.; Maisonneuve, V.; Dujardin, G. *J. Org. Chem.* **2004**, *69*, 4192–4202.

(8) Roff, G. J.; Lloyd, R. C.; Turner, N. J. *J. Am. Chem. Soc.* **2008**, *126*, 4098–4099.

(9) Willans, C. E.; Mulders, J. M. C. A.; de Vries, J. G.; de Vries, A. H. M. *J. Organomet. Chem.* **2003**, *687*, 494–497.

(10) Matsubara, R.; Nakamura, Y.; Kobayashi, S. *Angew. Chem.* **2004**, *116*, 1711–1713; *Angew. Chem. Int. Ed.* **2004**, *43*, 1679–1681.

(11) (a) van den Berg, M.; Minnaard, A. J.; Haak, R. M.; Leeman, M.; Schudde, E. P.; Meetsma, A.; Feringa, B. L.; de Vries, H. M.; Maljaars, E. P.; Wilians, C. E.; Hyett, D.; Boogers, A. F.; Hendricks, J. W.; de Vries, J. G. *Adv. Synth. Catal.* **2003**, *345*, 308–323. (b) Blaser, H.-U.; Malan, C.; Pugin, B.; Spindler, F.; Steiner, H.; Studer, M. *Adv. Synth. Catal.* **2003**, *345*, 103–151.

(12) (a) Dupau, P.; Le Gendre, P.; Bruneau, C.; Dixneuf, P. H. *Synlett* **1999**, 1832–1834. (b) Wang, X.; Porco, J. A., Jr. *J. Org. Chem.* **2001**, *66*, 8215–8221. (c) Bayer, A.; Maier, M. E. *Tetrahedron* **2004**, *60*, 6665–6677. (d) Adam, W.; Bosio, S. G.; Turro, N. J. *J. Org. Chem.* **2004**, *69*, 1704–1715. (e) Burk, M. J.; Casy, G.; Johnson, N. B. *J. Org. Chem.* **1998**, *63*, 6084–6098.

(13) (a) Brettle, R.; Mosedale, A. J. *J. Chem. Soc., Perkin Trans. 1* **1988**, 2185–2195. (b) Kuramochi, K.; Watanabe, H.; Kitahara, T. *Synlett* **2000**, 397–399. (c) Sato, M. *J. Org. Chem.* **1961**, *26*, 770–779.

(14) (a) Ager, D. J. *Synthesis* **1984**, 384–398. (b) Fürstner, A.; Brehm, C.; Cancho-Grande, Y. *Org. Lett.* **2001**, *3*, 3955–3957.

(15) Krompiec, S.; Pigulla, M.; Kuźnik, N.; Krompiec, M.; Marciniec, B.; Chadyniak, D.; Kasperczyk, J. *J. Mol. Catal. A: Chem.* **2005**, *225*, 91–101.

(16) (a) Wallace, D. J.; Klauber, D. J.; Chen, C.-Y.; Volante, R. P. *Org. Lett.* **2003**, *5*, 4749–4752; (b) Jiang, L.; Job, G. E.; Klapars, A.; Buchwald, S. L. *Org. Lett.* **2003**, *5*, 3667–3669; (c) Pan, X.; Cai, Q.; Ma, D. *Org. Lett.* **2004**, *6*, 1809–1812; (d) Brice, J. L.; Meerdink, J. E.; Stahl, S. S. *Org. Lett.* **2004**, *6*, 1845–1848; (e) Han, C.; Shen, R.; Su, S.; Porco, J. A., Jr. *Org. Lett.* **2004**, *6*, 27–30; (f) Tracey, M. R.; Hsung, R. P.; Antoline, J.; Kurtz, K. C. M.; Shen, L.; Slafer, B. W.; Zhang, Y. *Sci. Synth.* **2005**, *21*, 387–475; (g) Klapars, A.; Campos, K. R.; Chen, C.; Volante, R. P. *Org. Lett.* **2005**, *7*, 1185–1188; (h) Bolshan, Y.; Batey, R. A. *Angew. Chem.* **2008**, *120*, 2139–2142; *Angew. Chem. Int. Ed.* **2008**, *47*, 2109–2112.

(17) (a) Goossen, L. J.; Döhring, A. *Adv. Synth. Catal.* **2003**, *345*, 943–947. (b) Goossen, L. J.; Paetzold, J.; Winkel, L. *Synlett* **2002**, *10*, 1721–1723. (c) Goossen, L. J.; Ghosh, K. *Chem. Commun* **2001**, *20*, 2084–2085. (d) Goossen, L. J.; Goossen, K.; Rodríguez, N.; Blanchot, M.; Linder, C.; Zimmermann, B. *Pure Appl. Chem.* **2008**, *80*, 1725–1731.

(18) Heider, M.; Henkelmann, J.; Ruehl, T. EP 646571 **1995** [*Chem. Abstr.* **1995**, *123*, 229254].

(19) Kondo, T.; Tanaka, A.; Kotachi, S.; Watanabe, Y. *J. Chem. Soc. Chem. Commun* **1995**, 413–414.

(20) (a) Tokunaga, M.; Wakatsuki, Y. *Angew. Chem.* **1998**, *110*, 3024–3027; *Angew. Chem. Int. Ed.* **1998**, *37*, 2867–2869; (b) Tokunaga, M.; Suzuki, T.; Koga, N.; Fukushima, T.; Horiuchi, A.; Wakatsuki, Y. *J. Am. Chem. Soc.* **2001**, *123*, 11917–11924; (c) Grotjahn, D. B.; Incarvito, C. D.; Rheingold, A. L. *Angew. Chem.* **2001**, *113*, 4002–4005; *Angew. Chem. Int. Ed.* **2001**, *40*, 3884–3887; (d) Chevallier, F.; Breit, B. *Angew. Chem.* **2006**, *118*, 1629–1632; *Angew. Chem. Int. Ed.* **2006**, *45*, 1599–1602. (e) Labonne, A.; Kribber, T.; Hintermann, L. *Org. Lett.* **2006**, *8*, 5853–5856. (f) Hintermann, L.; Kribber, T.; Labonne, A.; Paciok, E. *Synlett* **2009**, 2412–2416.

(21) (a) Rotem, M.; Shvo, Y. *Organometallics* **1983**, *2*, 1689–1691. (b) Mitsudo, T.; Hori, Y.; Yamakawa, Y.; Watanabe, Y. *J. Org. Chem.* **1987**, *52*, 2230–2239. (c) Ruppin, C.; Dixneuf, P. H. *Tetrahedron Lett.* **1986**, *27*, 6323–6324. (d) Philippot, K.; Devanne, D.; Dixneuf, P. H. *J. Chem. Soc. Chem. Commun.* **1990**, 1199–1200. (e) Neveux, M.; Seiller, B.; Hagedorn, F.; Bruneau, C.; Dixneuf, P. H. *J. Organomet. Chem.* **1993**, *451*, 133–138. (f) Goossen, L. J.; Paetzold, J.; Koley, D. *Chem. Commun.* **2003**, 706–707.

(22) (a) Uchimaru, Y. *Chem. Commun* **1999**, 1133–1134; (b) Tokunaga, M.; Eckert, M.; Wakatsuki, Y. *Angew. Chem.* **1999**, *111*, 3416–3419; *Angew. Chem. Int. Ed.* **1999**, *38*, 3222–3225. (c) Kondo, T.; Okada, T.; Suzuki, T.; Mitsudo, T.-a. *J. Organomet. Chem.* **2001**, *622*, 149–154. (d) Fukumoto, Y.; Dohi, T.; Masaoka, H.; Chatani, N.; Murai, S. *Organometallics* **2002**, *21*, 3845–3847. (e) Shimada, T.; Yamamoto, Y. *J. Am. Chem. Soc.* **2003**, *125*, 6646–6647. (f) Yi, C. S.; Yun, S. Y.; Guzei, I. A. *J. Am. Chem. Soc.* **2005**, *127*, 5782–5783. (g) Li, Y.; Marks, T. J. *Organometallics* **1996**, *15*, 3770–3772. (h) Li, Y.; Marks, T. J. *J. Am. Chem. Soc.* **1998**, *120*, 1757–1771.

(23) Koelle, U.; Rietmann, C.; Tjoe, J.; Wagner, T.; Englert, U. *Organometallics* **1995**, *14*, 703–704.
(24) (a) Gemel, C.; Trimmel, G.; Slugovc, C.; Kremel, S.; Mereiter, K.; Schmid, R.; Kirchner, K. *Organometallics* **1996**, *15*, 3998–4004. (b) Varela-Fernández, A.; González-Rodríguez, C.; Varela, J. A.; Castedo, L.; Saá, C. *Org. Lett.* **2009**, *11*, 5350–5353. (c) Liu, P. N.; Su, F. H.; Wen, T. B.; Sung, H. H.-Y. *Chem.—Eur. J.* **2010**, *16*, 7889–7897.
(25) Goossen, L. J.; Rauhaus, J. E.; Deng, G. *Angew. Chem.* **2005**, *117*, 4110–4113; *Angew. Chem. Int. Ed.* **2005**, *44*, 4042–4045.
(26) Goossen, L. J.; Arndt, M.; Blanchot, M.; Rudolphi, F.; Menges, F.; Niedner-Schatteburg, G. *Adv. Synth. Catal.* **2008**, *350*, 2701–2707.
(27) Goossen, L. J.; Blanchot, M.; Salih, K. S. M.; Karch, R.; Rivas-Nass, A. *Org. Lett.* **2008**, *10*, 4497–4499.
(28) Goossen, L. J.; Blanchot, M.; Brinkmann, C.; Goossen, K.; Karch, R.; Rivas-Nass, A. *J. Org. Chem.* **2006**, *71*, 9506–9509.
(29) (a) Goossen, L. J.; Salih, K. S. M.; Blanchot, M. *Angew. Chem.* **2008**, *120*, 8620–8623; *Angew. Chem. Int. Ed.* **2008**, *47*, 8492–8495. (b) Goossen, L. J.; Blanchot, M.; Salih, K. S. M.; Goossen, K. *Synthesis* **2009**, 2283–2282.
(30) Buba, A. E.; Arndt, M.; Goossen, L. J. *J. Organomet. Chem.* **2010**, *696*, 170–178.
(31) Goossen, L. J.; Blanchot, M.; Arndt, M.; Salih, K. S. M. *Synlett* **2010**, 1685–1687.
(32) (a) Bruneau, C.; Dixneuf, P. H. *Angew. Chem.* **2006**, *118*, 2232–2260; *Angew. Chem. Int. Ed.* **2006**, *45*, 2176–2203. (b) Rigaut, S.; Touchard, D.; Dixneuf, P. H. *Coord. Chem. Rev.* **2004**, *248*, 1585–1601.
(33) Oliván, M.; Clot, E.; Eisenstein, O.; Caulton, K. G. *Organometallics* **1998**, *17*, 3091–3100.
(34) DFT calculations confirmed that the reaction of 2-pyrrolidinone (**1a**) and deprotonated *N*-((*E*)-hex-1-enyl)pyrrolidin-2-one, leading to the 2-pyrrolidinyl anion and the corresponding enamide (**6a**), is both exotherm ($\Delta_r E_{tot} = -30.88$ kcal mol^{-1}) and exergonic ($\Delta_r G_{298} = -30.02$ kcal mol^{-1}).
(35) Although there is no experimental proof in literature that the rehybridisation from sp to sp^2 causes an inverse isotope effect, it must be expected based on the analogy to sp^2/sp^3 rehybridizations. See for example: Carey, F. A.; Sundberg, R. J. *Advanced Organic Chemistry*, Third edition; Plenum Press: New York, London, 1990; pp 216−218. The same assumption was made, e.g., in: Ipaktschi, J.; Mohsseni-Ala, J.; Uhlig, S. *Eur. J. Inorg. Chem.* **2003**, 4313−4320.
(36) Maegawa, T.; Fujiwara, Y.; Inagaki, Y.; Monguchi, Y.; Sajiki, H. *Adv. Synth. Catal.* **2008**, *350*, 2215–2218.
(37) Rigaut, S.; Perruchon, J.; Guesmi, S.; Fave, C.; Touchard, D.; Dixneuf, P. H. *Eur. J. Inorg. Chem.* **2005**, 447–460.
(38) Ryabov, A. D. *Chem. Rev.* **1990**, *90*, 403–424.
(39) Ciardi, C.; Reginato, G.; Gonsalvi, L.; de los Ríos, I.; Romerosa, A.; Peruzzini, M. *Organometallics* **2004**, *23*, 2020–2026.
(40) Choe, J.-I.; Choi, H.-S.; Kuczkowski, R. L. *Magn. Reson. Chem.* **1986**, *24*, 1044–1047.
(41) Touchard, D.; Haquette, P.; Pirio, N.; Toupet, L.; Dixneuf, P. H. *Organometallics* **1993**, *12*, 3132–3139.
(42) (a) Bruneau, C.; Dixneuf, P. H. *Acc. Chem. Res.* **1999**, *32*, 311–323. (b) Vijayaraj, T. A.; Sundararajan, G. *J. Mol. Catal. A* **1995**, *99*, 47–54.
(43) Caballero, A.; Jalón, F. A.; Manzano, B. R. *Chem. Commun* **1998**, 1879–1880.
(44) (a) Guerchais, V.; Lapinte, C.; Thepot, J. Y.; Toupet, L. *Organometallics* **1988**, *7*, 604–612. (b) Maurer, J.; Linseis, M.; Sarkar, B.; Schwederski, B.; Niemeyer, M.; Kaim, W.; Zli, S.; Anson, C.; Zabel, M.; Winter, R. F. *J. Am. Chem. Soc.* **2008**, *130*, 259–268. (c) Jung, S.; Ilg, K.; Brandt, C. D.; Wolf, J.; Werner, H. *Eur. J. Inorg. Chem.* **2004**, 469–480. (d) Bassetti, M.; Cadierno, V.; Gimeno, J.; Pasquini, C. *Organometallics* **2008**, *27*, 5009–5016.
(45) Cabeza, J. A.; Riera, V. *J. Organomet. Chem.* **1989**, *376*, C23–C25.
(46) (a) Hinderling, C.; Adlhart, C.; Chen, P. *Angew. Chem.* **1998**, *110*, 2831–2835; *Angew. Chem. Int. Ed.* **1998**, *37*, 2685–2689. (b) Adlhart, C.; Hinderling, C.; Baumann, H.; Chen, P. *J. Am. Chem. Soc.* **2000**, *122*, 8204–8214. (c) Frech, C. M.; Blacque, O.; Schmalle, H. W.; Berke, H.; Adlhart, C.; Chen, P. *Chem.—Eur. J.* **2006**, *12*, 3325–3338.
(47) (a) Markert, C.; Pfaltz, A. *Angew. Chem.* **2004**, *116*, 2551–2554; *Angew. Chem. Int. Ed.* **2004**, *43*, 2498–2500; (b) Markert, C.; Neuburger, M.; Kulicke, K.; Meuwly, M.; Pfaltz, A. *Angew. Chem.* **2007**, *119*, 5996–5999; *Angew. Chem. Int. Ed.* **2007**, *46*, 5892–5895; (c) Markert, C.; Rosel, P.; Pfaltz, A. *J. Am. Chem. Soc.* **2008**, *130*, 3234–3235; (d) Teichert, A.; Pfaltz, A. *Angew. Chem.* **2008**, *120*, 3408–3410; *Angew. Chem. Int. Ed.* **2008**, *47*, 3360–3362. (e) di Lena, F.; Matyjaszewski, K. *Chem. Commun.* **2008**, 6306–6308. (f) di Lena, F.; Matyjaszewski, K. *Dalton Trans.* **2009**, 8884–8890.
(48) Kuran, W.; Musco, A. *Inorg. Chim. Act.* **1975**, *12*, 187–193.
(49) Reinhardt, B. M.; Niedner-Schatteburg, G. *J. Phys. Chem. A* **2002**, *106*, 7988–7992.
(50) Six, C.; Gabor, B.; Görls, H.; Mynott, R.; Philipps, P.; Leitner, W. *Organometallics* **1999**, *18*, 3316–3326.
(51) (a) Gaussian 03, Revision E.01, Gaussian, Inc.: Wallingford CT, 2004. (b) Gaussian 09, Revision A.02, Gaussian, Inc.: Wallingford CT, 2009; for full citations see the Supporting Information.
(52) (a) Lee, C.; Yang, W.; Parr, R. G. *Phys. Rev. B* **1988**, *37*, 785–789. (b) Becke, A. D. *J. Chem. Phys.* **1993**, *98*, 5648–5652. (c) Stephens, P. J.; Devlin, J. F.; Chabalowski, C. F.; Frisch, M. J. *J. Phys. Chem.* **1994**, *98*, 11623–11627.
(53) Krishnan, R.; Binkley, J. S.; Seeger, R.; Pople, J. A. *J. Chem. Phys.* **1980**, *72*, 650–654.
(54) Hariharan, P. C.; Pople, J. A. *Theor. Chim. Acta* **1973**, *28*, 213–222.
(55) Andrae, D.; Häussermann, U.; Dolg, M.; Stoll, H.; Preuss, H. *Theor. Chim. Acta* **1990**, *77*, 123–141.
(56) Wong, M. W. *Chem. Phys. Lett.* **1996**, *256*, 391–399.

Nachdem die Ursache der Regioselektivität der Hydroamidierung geklärt werden konnte, beschäftigten sich Gooßen und Koley et al. mit dem Ursprung der Kontrolle der Stereoselektivität.[90] Aus Experimenten ist bekannt, dass der Katalysator (cod)Ru(met)$_2$ in Gegenwart von Tri-*n*-butylphosphin und 4-(Dimethylamino)-pyridin (DMAP) *E*-konfigurierte Enamide liefert, während bei Zugabe von Bis-(dicyclohexylphosphino)-methan (dcypm) *Z*-konfigurierte Enamide gebildet werden. Mit Hilfe von DFT-Rechnungen wurden nun ausgehend von Ru(P^{n}Bu$_3$)$_2$(DMAP)$_2$ und Ru(dcypm)$_2$ jeweils zwei Katalysezyklen inklusive aller Übergangszustände berechnet. Beide Reaktionspfade ausgehend von Ru(P^{n}Bu$_3$)$_2$(DMAP)$_2$ führten zum *E*-Enamid. Dies war auch für einen der Reaktionspfade ausgehend von Ru(dcypm)$_2$ der Fall. Der zweite Katalysezyklus, welcher das flachere Energieprofil aufwies, führte jedoch zum *Z*-Enamid. Diese Erkenntnisse stehen in sehr guter Übereinstimmung mit den experimentellen Befunden und sollen nun als Basis für die zukünftige rationale Entwicklung effizienterer Hydroamidierungskatalysatoren dienen.

In den letzten Jahren wurde eine Vielzahl neuer Reaktionsprotokolle von Hydroaminierungs- und Hydroamidierungsreaktionen veröffentlich. Diese wurden von Gooßen et al. in einem Übersichtsartikel zusammengefasst, der gerade zur Veröffentlichung angenommen wurde.[91]

3.4 Pd-katalysierte Synthese von Enolestern aus Allylestern

Die Entwicklung neuer Synthesemethoden für Enolester stellt ein attraktives Forschungsziel dar, da Enolester wichtige Vorstufen für eine Reihe verschiedener organischer Reaktionen sind.[92–103] Die katalytische Isomerisierung von Allylestern **3.4-3** zu Enolestern **3.4-4** (Schema 11) ist eine attraktive Alternative gegenüber bestehenden Verfahren, da Allylester einfach durch die Veresterung von Carbonsäuren **3.4-1** mit Allylalkohol (**3.4-2**) gewonnen werden können.

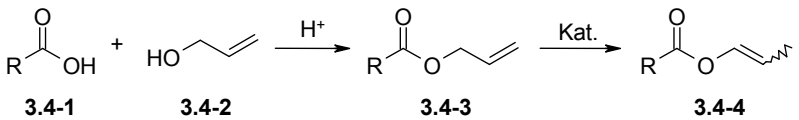

3.4-1 **3.4-2** **3.4-3** **3.4-4**

Schema 11. *Synthese von Enolester durch katalytische Isomerisierung*.

Aufgrund der schwachen thermodynamischen Triebkraft der Doppelbindungsisomerisierung und der Tendenz vieler Übergangsmetallkatalysatoren, in die C(allyl)–O-Bindung zu insertieren,[104] sind die meisten Isomerisierungskatalysatoren jedoch nicht in der Lage, diese

Reaktion zu bewerkstelligen. Arbeiten, von Mingos, Vilar und Hartwig zeigten, dass der homodinukleare Palladiumkatalysator $[Pd(\mu\text{-Br})(P^tBu_3)]_2$ unter besonders milden Bedingungen Palladium(II)hydrid-Komplexe bilden kann.[105–107] Da bekannt ist, dass Metall-Hydrid-Spezies in Hydrometallierungsreaktionen an Doppelbindungen addieren können,[108–111] wurde $[Pd(\mu\text{-Br})(P^tBu_3)]_2$ von uns in der Isomerisierung von Allylestern untersucht. Es gelang, mit diesem Katalysator eine effiziente Synthesemethode zu entwickeln, deren breite Anwendbarkeit in der Darstellung einer Vielzahl an Enolestern demonstriert werden konnte (Table 1 in *OrgLett*). In 1-Position verzweigte Enolester konnten weiterhin als Substrate für enantioselektive Hydrierungen zur Synthese chiraler enantiomerenreiner Ester eingesetzt werden (Scheme 3 in *OrgLett*).[112]

Das Ziel meines Beitrags zu diesem Forschungsprojekt war es, Einsichten in den Reaktionsmechanismus der Palladium-katalysierten Isomerisierung von Allylestern zu Enolestern zu erlangen und die katalytisch aktive Spezies der Reaktion zu identifizieren. Aufgrund der Vermutung, dass ein Palladiumhydrid-Komplex die katalytisch aktive Spezies darstellt, wurden freie Standardreaktionsenthalpien für die Bildung verschiedener Palladiumhydrid-Spezies ausgehend vom homodinuklearen Palladiumkatalysator $[Pd(\mu\text{-Br})(P^tBu_3)]_2$ (**3.4-5**) berechnet (Schema 12). Keine der betrachteten Reaktionen war exergonisch. Die geringste freie Standardreaktionsenthalpie wurde für die Bildung der Palladiumhydrid-Spezies **3.4-6** zusammen mit dem Palladiumkomplex **3.4-7** berechnet (14.9 kcal mol^{-1}). Die Dimerisierung von zwei Molekülen **3.4-7** zum homodinuklearen Palladiumkomplex **3.4-9** ist exergonisch (–18.0 kcal mol^{-1}), was die Bildung von **3.4-6** + ½ **3.4-9** auf 5.9 kcal mol^{-1} reduziert.

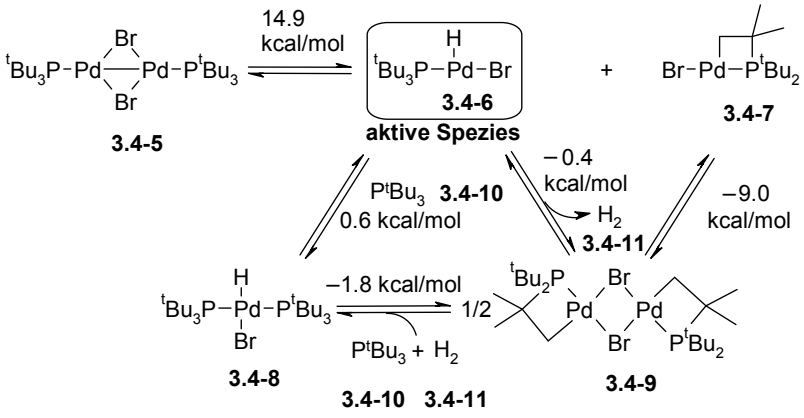

Schema 12. *Vorgeschlagene Aktivierung des homodinuklearen Palladiumkatalysators*.

Dies legte die Vermutung nahe, dass **3.4-6** die katalytisch aktive Spezies darstellt. Beim Versuch, diese mit *in situ* ^{1}H- und ^{31}P-NMR-Spektroskopie in einer Reaktionsmischung nachzuweisen, konnten nur Resonanzsignale für den oxidierten Komplex **3.4-9** gefunden werden, vermutlich weil **3.4-6** aufgrund seiner hohen Aktivität sehr schnell weiterreagiert. Bei der Zugabe von zusätzlichem Tri-*tert*-butylphosphin im Überschuss konnte der Bis(*tert*-butylphosphino)palladiumhydrid-Komplex **3.4-8** abgefangen und durch ein Triplet bei –15.6 ppm im ^{1}H-NMR nachgewiesen werden,[105] was die Vermutung von **3.4-6** als katalytisch aktive Spezies unterstützt.

Ein möglicher Reaktionsmechanismus der Isomerisierung ausgehend von Palladiumhydrid-Spezies **3.4-6** würde mit der Insertion des Allylesters **3.4-3** in die Pd–Hydrid-Bindung des Katalysators beginnen. Eine folgende *β*-Hydrideliminierung würde den Enolester **3.4-4** freisetzen und den Pd–Hydrid-Katalysator regenerieren.

Die Ergebnisse der Palladium-katalysierten Synthese von Enolestern aus Allylestern wurden in *Organic Letters* veröffentlicht. Sämtliche Ergebnisse können dem englischsprachigen Originaltext der Veröffentlichung entnommen werden, die im Folgenden abgedruckt ist.

Die Veröffentlichung entstand im Rahmen eines Kooperationsprojekts. Hierbei wurden die Optimierung des Katalysatorsystems, die Ermittlung der Anwendungsbreite der Reaktion, die experimentellen mechanistischen Untersuchungen sowie die asymmetrischen Hydrierungsreaktionen von Frau Dr. Patrizia Mamone durchgeführt. Herr Dr. Matthias F. Grünberg entdeckte die Reaktivität von $[Pd(\mu\text{-}Br)(P^tBu_3)]_2$ in der Doppelbindungs-isomerisierung. Er synthetisierte drei Ausgangsverbindungen, führte damit die Isomerisierungsreaktionen durch und isolierte die entsprechenden Enolester. Herr Dr. Bilal A. Khan synthetisierte zwei chirale Ester durch asymmetrische Hydrierung der entsprechenden verzweigten Enolester. Alle DFT-Rechnungen zum mechanistischen Verständnis und zur Identifizierung der katalytisch aktiven Spezies wurden von mir durchgeführt.

„Reprinted with permission from P. Mamone, M. F. Grünberg, A. Fromm, B. A. Khan, L. J. Gooßen, *Org. Lett.* **2012**, *14*, 3716−3719: *[Pd(μ-Br)(P^tBu_3)]$_2$ as a Highly Active Isomerization Catalyst: Synthesis of Enol Esters from Allylic Esters*. DOI: 10.1021/ol301563g. Copyright 2012 American Chemical Society."

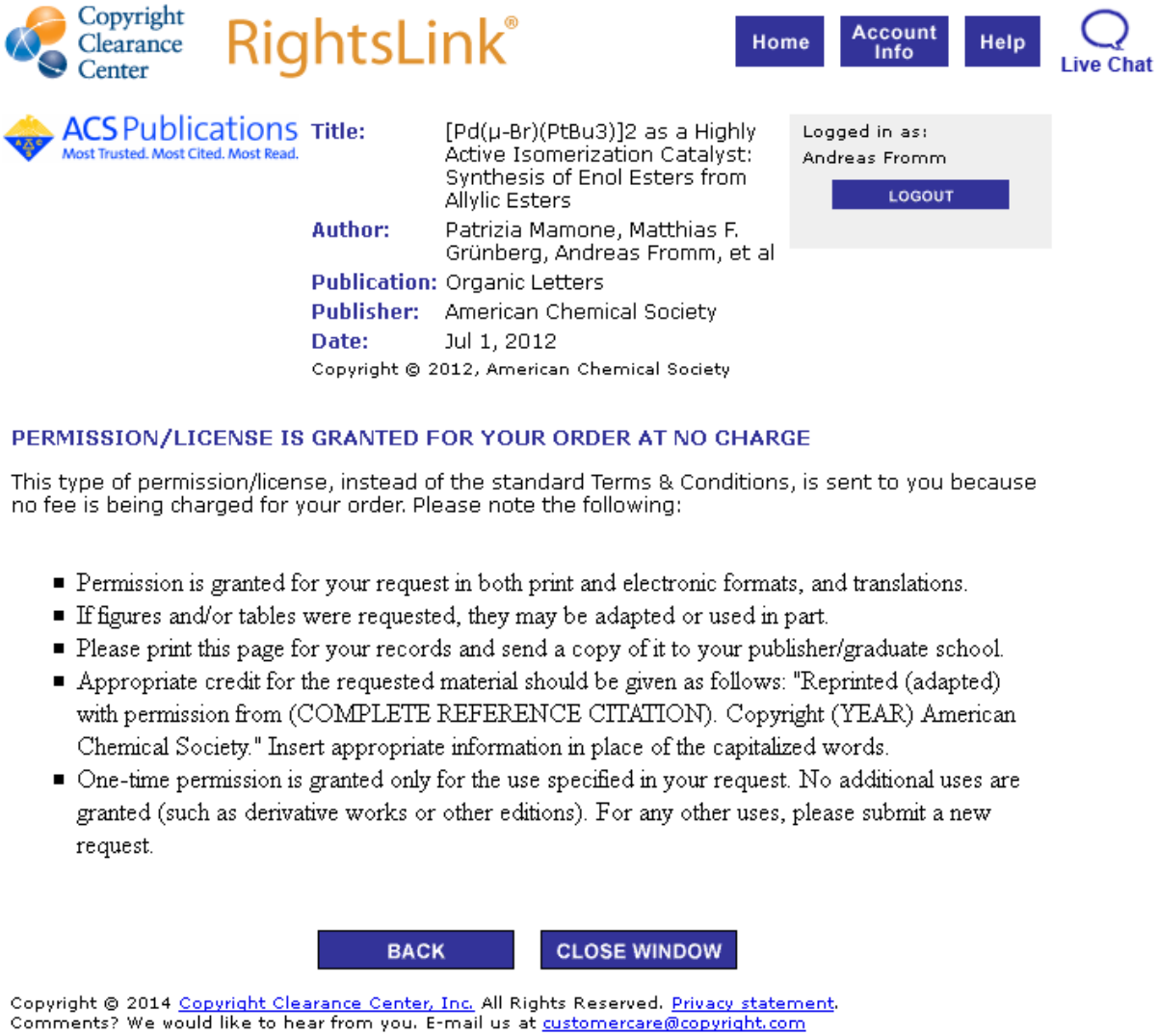

Copyright Clearance Center RightsLink®

Home | Account Info | Help | Live Chat

ACS Publications Most Trusted. Most Cited. Most Read.

Title: [Pd(μ-Br)(PtBu3)]2 as a Highly Active Isomerization Catalyst: Synthesis of Enol Esters from Allylic Esters

Author: Patrizia Mamone, Matthias F. Grünberg, Andreas Fromm, et al

Publication: Organic Letters

Publisher: American Chemical Society

Date: Jul 1, 2012

Copyright © 2012, American Chemical Society

Logged in as: Andreas Fromm

LOGOUT

PERMISSION/LICENSE IS GRANTED FOR YOUR ORDER AT NO CHARGE

This type of permission/license, instead of the standard Terms & Conditions, is sent to you because no fee is being charged for your order. Please note the following:

- Permission is granted for your request in both print and electronic formats, and translations.
- If figures and/or tables were requested, they may be adapted or used in part.
- Please print this page for your records and send a copy of it to your publisher/graduate school.
- Appropriate credit for the requested material should be given as follows: "Reprinted (adapted) with permission from (COMPLETE REFERENCE CITATION). Copyright (YEAR) American Chemical Society." Insert appropriate information in place of the capitalized words.
- One-time permission is granted only for the use specified in your request. No additional uses are granted (such as derivative works or other editions). For any other uses, please submit a new request.

BACK | CLOSE WINDOW

Copyright © 2014 Copyright Clearance Center, Inc. All Rights Reserved. Privacy statement.
Comments? We would like to hear from you. E-mail us at customercare@copyright.com

ORGANIC LETTERS

2012
Vol. 14, No. 14
3716–3719

$[Pd(\mu\text{-}Br)(P^tBu_3)]_2$ as a Highly Active Isomerization Catalyst: Synthesis of Enol Esters from Allylic Esters

Patrizia Mamone, Matthias F. Grünberg, Andreas Fromm, Bilal A. Khan, and Lukas J. Gooßen*

FB Chemie – Organische Chemie, TU Kaiserslautern, Erwin-Schrödinger-Str. Geb. 54, 67663 Kaiserslautern, Germany

goossen@chemie.uni-kl.de

Received June 6, 2012

ABSTRACT

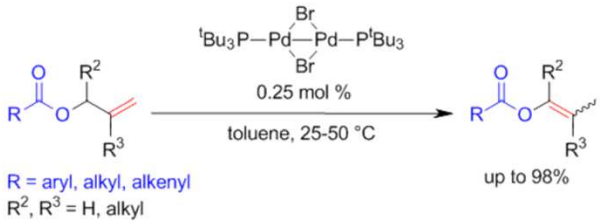

The dimeric Pd(I)-complex $[Pd(\mu\text{-}Br)(P^tBu_3)]_2$ was found to be highly active for catalyzing double-bond migration in various substrates such as unsaturated ethers, alcohols, amides, and arenes, under mild conditions. It efficiently mediates the conversion of allylic esters into enol esters, rather than inserting into the allylic C–O bond. The broad applicability of this reaction was demonstrated with the synthesis of 22 functionalized enol esters.

Enol esters are important precursors in a variety of organic transformations such as aldol- and Mannich type reactions,[1] asymmetric hydrogenations,[2] cycloadditions,[3] or other cyclization reactions to afford, e.g., heterocycles or chromones.[4] They are employed as auxiliary reagents in the desymmetrization of alcohols,[5] as well as in the synthesis of vinylic amino alcohols and diols.[6]

Classical approaches to their synthesis involve transesterification between alkyl esters and enol acetates, or *O*-acylation of enolates.[7] However, these require stoichiometric amounts of bases, acids, or toxic mercury salts. Modern, catalytic syntheses of enol esters include the Zr-catalyzed methylalumination of alkynes,[8] the Cu-catalyzed oxidative esterification of aldehydes with β-dicarbonyl compounds,[9] the Au-catalyzed intramolecular rearrangements of propargylic esters and alcohols,[10] the Fe-catalyzed asymmetric coupling of ketenes with aldehydes,[11] and the addition of carboxylic acids to alkynes catalyzed by Ru,[12] Ru–Re,[13] or Rh complexes.[14]

(1) (a) Yanagisawa, A.; Matsumoto, Y.; Asakawa, K.; Yamamoto, H. *J. Am. Chem. Soc.* **1999**, *121*, 892. (b) Isambert, N.; Cruz, M.; Arévalo, M. J.; Gómez, E.; Lavilla, R. *Org. Lett.* **2007**, *9*, 4199.

(2) (a) Tang, W.; Zhang, X. *Chem. Rev.* **2003**, *103*, 3029. (b) Minnaard, A. J.; Feringa, B. L.; Lefort, L.; De Vries, J. G. *Acc. Chem. Res.* **2007**, *40*, 1267. (c) Erre, G.; Enthaler, S.; Junge, K.; Gladiali, S.; Beller, M. *Coord. Chem. Rev.* **2008**, *252*, 471.

(3) Urabe, H.; Suzuki, D.; Sasaki, M.; Sato, F. *J. Am. Chem. Soc.* **2003**, *125*, 4036.

(4) (a) Basso, A; Banfi, L.; Galatini, A.; Guanti, G.; Rastrelli, F.; Riva, R. *Org. Lett.* **2009**, *11*, 4068. (b) Széll, T. *J. Chem. Soc. C* **1967**, 2041.

(5) Trost, B. M.; Malhotra, S.; Mino, T.; Rajapaksa, N. S. *Chem.—Eur. J.* **2008**, *14*, 7648.

(6) (a) Keinicke, L.; Fristrup, P.; Norrby, P.-O.; Madsen, R. *J. Am. Chem. Soc.* **2005**, *127*, 15756. (b) Lombardo, M.; Morganti, S.; Trombini, C. *J. Org. Chem.* **2003**, *68*, 997. (c) Liu, M.; Sun, X.-W.; Xu, M.-H.; Lin, G.-Q. *Chem.—Eur. J.* **2009**, *15*, 10217.

(7) Smith, M. B.; March, J. *Advanced Organic Chemistry*, 5th ed.; John Wiley & Sons, New York, 2001; p 486.

(8) DeBergh, J. R.; Spivey, K. M.; Ready, J. M. *J. Am. Chem. Soc.* **2008**, *130*, 7828.

(9) Yoo, W.-J.; Li, C.-J. *J. Org. Chem.* **2006**, *71*, 6266.

(10) (a) Wang, S.; Zhang, L. *Org. Lett.* **2006**, *8*, 4585. (b) Marion, N.; Nolan, S. P. *Angew. Chem., Int. Ed.* **2007**, *46*, 2750. (d) *Angew. Chem.* **2007**, *119*, 2806. (c) Peng, Y.; Cui, L.; Zhang, G.; Zhang, L. *J. Am. Chem. Soc.* **2009**, *131*, 5062.

(11) Schaefer, C.; Fu, G. C. *Angew. Chem, Int. Ed.* **2005**, *44*, 4606. *Angew. Chem.* **2005**, *117*, 4682.

(12) (a) Gooßen, L. J.; Gooßen, K.; Rodríguez, N.; Blanchot, M.; Linder, C.; Zimmermann, B. *Pure Appl. Chem.* **2008**, *80*, 1725. (b) Dragutan, V.; Dragutan, I.; Delaude, L.; Demonceau, A. *Coord. Chem. Rev.* **2007**, *251*, 765. (c) Dixneuf, P. H.; Bruneau, C.; Dérien, S. *Pure Appl. Chem.* **1998**, *70*, 1065.

10.1021/ol301563g
Published on Web 07/02/2012

Scheme 1. Synthesis of Enol Esters via Catalytic Isomerization

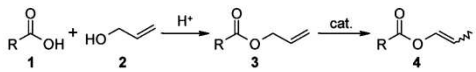

The catalytic isomerization of allylic esters to enol esters would be an attractive alternative to the above approaches, because the starting materials are easily accessible by esterification of carboxylic acids (Scheme 1). However, because of the weak thermodynamic driving force for the double-bond migration and the tendency of many metal catalysts to insert into the C(allyl)−O bond with formation of stable carboxylate complexes,[15] this reaction is beyond the performance limit of most isomerization catalysts. Even for unsubstituted allyl esters, only two reports of double-bond migrations exist. Iranpoor et al. found that stoichiometric amounts of $Fe_3(CO)_{12}$ promote this reaction when irradiated with UV light.[16] Krompiec et al. achieved up to eight catalytic turnovers for the double-bond migration, along with C(allyl)−O bond cleavage, using the ruthenium hydride complex $RuClH(CO)(PPh_3)_3$.[17] Mechanistic studies by Tokunaga et al. confirmed the low catalytic activity of Ru complexes for this type of substrate.[18]

In the context of our research on isomerizing functionalizations of fatty acids,[19] we had thoroughly investigated the activity of various isomerization methods involving acid[20] or base mediators,[21] as well as metal catalysts reported for the isomerization of alkenes,[22] allylic benzenes,[23] allylic ethers,[15,24] allylic silyl ethers,[25] alkenyl alcohols,[26] allylic amines and amides.[27] However, none of these systems permitted to convert our test substrate, oleic acid, into an equilibrium mixture of isomers within a few hours at catalyst loadings below 1%.[19]

In our search for new lead structures for highly active isomerization catalysts, reports by Mingos/Vilar and Hartwig on the dimeric palladium complex $[Pd(\mu\text{-Br})(P^tBu_3)]_2$ caught our attention.[28] They discovered that this unusual, dimeric Pd^I species, which has found applications in catalytic cross-coupling reactions,[29] can be converted into hydridopalladium(II) complexes under remarkably mild conditions. We reasoned that a metal complex with such strong tendency to form Pd−H species, which are known to add across C−C double-bonds,[22,30] should also be an excellent catalyst for alkene isomerization. Indeed, oleic acid was converted to an equilibrium mixture of double-bond isomers with only 0.5 mol % of $[Pd(\mu\text{-Br})(P^tBu_3)]_2$ within less than an hour.[31]

The high activity of this one-component system led us to evaluate the catalytic activity of the Pd^I dimer as the catalyst for double-bond migrations in a range of standard test substrates. As a reference system, we used a mixture of $Pd(dba)_2$, isobutyryl chloride, and tri(*tert*-butyl)-phosphine. This catalyst has been shown by Lindhardt and Skrydstrup to set new standards with regard to catalytic activity and functional group tolerance for single-carbon migrations of various double bonds.[32] The examples in Scheme 2 demonstrate that the Pd^I dimer is an effective catalyst for double-bond migrations in allylic arenes (**5**), amides (**7**), ethers (**9**), and alcohols (**11** and **13**). In each case, the catalyst loading was reduced to the minimum effective level, in order to differentiate between the systems. For all substrate classes, the Pd^I dimer compared favorably even to the state-of-the-art Pd-catalyst for single-carbon migration of the double-bond. It is also able to move the bond over longer alkyl chains. Thus, hexanal (**14**) was obtained from 5-hexen-1-ol (**13**) in high yield and selectivity.

The most striking result obtained in this series of test reactions was that allyl benzoate (**3a**) was cleanly converted to the corresponding enol ester **4a**. Using only 0.25 mol % of Pd^I in toluene, near-quantitative conversion to 1-propenyl benzoate (**4a**) was achieved within 2 h at 50 °C, with a product (*E*/*Z*)-ratio of 1:2. The only other component detected in the reaction mixture was 2% of the

(13) Ye, S.; Leong, W. K. *J. Organomet. Chem.* **2006**, *691*, 1216.
(14) Lumbroso, A.; Koschker, P.; Vautravers, N. R.; Breit, B. *J. Am. Chem. Soc.* **2011**, *133*, 2386.
(15) Kuźnik, N.; Krompiec, S. *Coord. Chem. Rev.* **2007**, *251*, 222.
(16) (a) Iranpoor, N.; Imanieh, H.; Iran, S.; Forbes, E. J. *Synth. Commun.* **1989**, *19*, 2955. (b) Iranpoor, N.; Mottaghinejad, E. *J. Organomet. Chem.* **1992**, *423*, 399.
(17) Krompiec, S.; Kuznik, N.; Krompiec, M.; Penczek, R.; Mrzigod, J.; Torz, A. *J. Mol. Catal. A: Chem.* **2006**, *253*, 132.
(18) Four days at 80 °C were required to achieve 92% conversion of allyl benzoate: Nakamura, A.; Hamasaki, A.; Goto, S.; Utsunomiya, M.; Tokunaga, M. *Adv. Synth. Catal.* **2011**, *353*, 973.
(19) Ohlmann, D. M.; Gooßen, L. J.; Dierker, M. *Chem.—Eur. J.* **2011**, *17*, 9508.
(20) Lee, P. H.; Kang, D.; Choi, S.; Kim, S. *Org. Lett.* **2011**, *13*, 3470.
(21) For examples, see: (a) Sagoet, O.; Monteux, D.; Langlois, Y.; Riche, C.; Chiaroni, A. *Tetrahedron Lett.* **1996**, *37*, 7019. (b) Su, C.; Williard, P. G. *Org. Lett.* **2010**, *12*, 5378.
(22) For examples, see: (a) Harrod, J. F.; Chalk, A. J. *J. Am. Chem. Soc.* **1966**, *88*, 3491. (b) Casey, C. P.; Cyr, C. R. *J. Am. Chem. Soc.* **1973**, *95*, 2248. (c) Grotjahn, D. B.; Larsen, C. R.; Gustafson, J. L.; Nair, R.; Sharma, A. *J. Am. Chem. Soc.* **2007**, *129*, 9592.
(23) For examples, see: (a) Lastra-Barreira, B.; Francos, J.; Crochet, P.; Cadierno, V. *Green Chem.* **2011**, *13*, 307. (b) Golborn, P.; Scheinmann, F. *J. Chem. Soc., Perkin Trans. 1* **1973**, 2870. (c) Mayer, M.; Welther, A.; von Wangelin, A. J. *ChemCatChem* **2011**, *3*, 1567.
(24) For examples, see: (a) Yamamoto, Y.; Fujikawa, R.; Miyaura, N. *Synth. Commun.* **2000**, *30*, 2383. (b) Carless, H. A.; Haywood, D. J. *J. Chem. Soc., Chem. Commun.* **1980**, 980. (c) Crivello, J. V.; Kong, S. *J. Org. Chem.* **1998**, *63*, 6745.
(25) Sodeoka, M.; Yamada, H.; Shibasaki, M. *J. Am. Chem. Soc.* **1990**, *112*, 4906.
(26) (a) Van der Drift, R. C.; Bouwman, E.; Drent, E. *J. Organomet. Chem.* **2002**, *650*, 1. (b) Uma, R.; Crévisy, C.; Grée, R. *Chem. Rev.* **2003**, *103*, 27.
(27) (a) Krompiec, S.; Krompiec, M.; Penczek, R.; Ignasiak, H. *Coord. Chem. Rev.* **2008**, *252*, 1819. (b) Escoubet, S.; Gastaldi, S.; Bertrand, M. *Eur. J. Org. Chem.* **2005**, *18*, 3855.
(28) (a) Durà-Vilà, V.; Mingos, D. M. P.; Vilar, R.; White, A. J.P.; Williams, D. J. *J. Organomet. Chem.* **2000**, *600*, 198. (b) Durà-Vilà, V.; Mingos, D. M. P.; Vilar, R.; White, A. J.P.; Williams, D. *Chem. Commun.* **2000**, 1525. (c) Barrios-Landeros, F.; Carrow, B. P.; Hartwig, J. F. *J. Am. Chem. Soc.* **2008**, *130*, 5842.
(29) (a) Colacot, T. J. *Platinum Met. Rev.* **2009**, *53*, 183. (b) Johansson, C. C. C.; Colacot, T. J. *Angew. Chem., Int. Ed.* **2010**, *49*, 676. *Angew. Chem.* **2010**, *122*, 686. (c) Proutiere, F; Aufiero, M; Schoenebeck, F *J. Am. Chem. Soc.* **2012**, *134*, 606.
(30) Hartley, F. R. *Chem. Rev.* **1969**, *69*, 799.
(31) This reactivity has also been exploited in isomerizing olefin metatheses: Ohlmann, D. M.; Tschauder, N.; Stockis, J.-P.; Gooßen, K.; Dierker, M.; Gooßen, L. J. submitted for publication (2012).
(32) Gauthier, D.; Lindhardt, A. T.; Olsen, E. P. K.; Overgaard, J.; Skrydstrup, T. *J. Am. Chem. Soc.* **2010**, *132*, 7998.

Scheme 2. Double-Bond Migration with the Pd^{I} Catalyst[33]

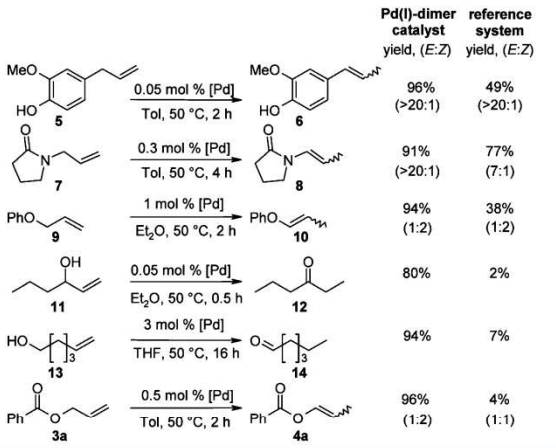

starting material **3a**, which did not disappear even after a prolonged reaction time, indicating that the equilibrium had been reached. In view of the rich chemistry of allylic acetate activation by palladium catalysts, it was surprising that no trace of benzoic acid arising from C(allyl)−O bond cleavage was observed.[34,15]

Encouraged by the observation that equilibration occurs so rapidly and that its position lies so far on the side of the enol esters, we optimized the catalyst loading and reaction conditions[33] and then explored the scope of the reaction protocol. As can be seen from the examples in Table 1, the reaction is broadly applicable with regard both to the carboxylate and allyl alcohol side of the esters.[35]

Allylic esters of electron-rich and electron-deficient aromatic (**4a**−**i**), heteroaromatic (**4j**,**k**), aliphatic (**4l**−**o**), and cinnamic (**4p**) carboxylates were successfully converted.

A variety of functionalities including alkoxy (**4c**,**d**), hydroxy (**4g**), amino (**4h**), nitro (**4i**), and keto groups (**4o**) were tolerated. Even halogen-containing substrates reacted smoothly without any indication of competing Heck-type reactions (**4e**,**f**). In all cases, (*E*:*Z*)-ratios between 1:2 and 1:5 were obtained.

The allyl residue can be linear or branched in the 1- and/or 2-positions (**4q**−**v**). Enol esters branched in the 1-position are of considerable interest as substrates for

Table 1. Isomerization of Allylic Esters to Enol Esters[f]

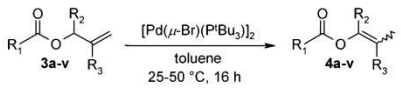

product	yield [%]/ (*E*:*Z*)	product	yield [%]/ (*E*:*Z*)
4a	90 (1:2)	**4l**	97[a,c] (1:2)
4b	98 (1:2)	**4m**	89 (1:2)
4c	90 (1:2)	**4n**	80 (1:2)
4d	91 (1:2)	**4o**	88 (1:2)
4e	73 (1:2)	**4p**	96 (1:2)
4f	91[a] (1:2)	**4q**	83[a] (1:3)
4g	98[b] (1:2)	**4r**	93[a] (1:3)
4h	91[b] (1:2)	**4s**	95[a] (1:3)
4i	87[b] (1:1)	**4t**	87[a,d] (1:5)
4j	56[b] (1:2)	**4u**	88[a,d] (1:5)
4k	76 (1:2)	**4v**	77[e]

[a] $[Pd(\mu\text{-Br})(P^tBu_3)]_2$ (0.50 mol %). [b] $[Pd(\mu\text{-Br})(P^tBu_3)]_2$ (2.50 mol %). [c] Yield and (*E*/*Z*)-selectivity was determined by NMR with anisole as internal standard. [d] 25 °C, 10% of other isomers. [e] $[Pd(\mu\text{-Br})(P^tBu_3)]_2$ (1.00 mol %). [f] Reaction conditions: Allylic esters **1a**−**v** (1.00 mmol), $[Pd(\mu\text{-Br})(P^tBu_3)]_2$ (0.25 mol %), 2 mL of toluene, 50 °C, 16 h, isolated yields. (*E*/*Z*)-selectivity was determined by GC.

enantioselective hydrogenations, but because of their limited availability, there are only few reports on such reactions.[2,36] We were thus pleased to find that compounds **4q**−**u** can be hydrogenated in high yields and enantiomeric excess (Scheme 3).[37] This demonstrates the viability of

(33) For details, see the Supporting Information.

(34) Weaver, J. D.; Recio, A., III; Grenning, A. J.; Tunge, J. A. *Chem. Rev.* **2011**, *111*, 1846.

(35) Synthesis of 1-propenyl benzoate (**4a**): Under a nitrogen atmosphere, a 50 mL vessel was charged with di-μ-bromobis(tri-*tert*-butylphosphine)dipalladium(I) (27.2 mg, 35.0 μmol), allyl benzoate (**3a**) (1.76 g, 10.0 mmol), and toluene (20 mL). The mixture was stirred at 50 °C for 16 h, diluted with diethyl ether (40 mL), and filtered through a pad of celite (5 g), and the solvent was removed in vacuo (50 mbar, 40 °C). The crude product was purified by column chromatography (SiO_2, diethyl ether/*n*-pentane gradient) to give prop-1-enyl benzoate (**4a**) (1.65 g, 94% yield, *E*:*Z* 1:2) as colorless liquid.

(36) (a) Jiang, Q.; Xiao, D.; Zhang, Z.; Cao, P.; Zhang, X. *Angew. Chem., Int. Ed.* **1999**, *38*, 516. *Angew. Chem.* **1999**, *111*, 578. (b) Jung, H. M.; Koh, J. H.; Kim, M.-J.; Park, J. *Org. Lett.* **2000**, *2*, 2487. (c) Wu, S.; Wang, W.; Tang, W.; Lin, M.; Zhang, X. *Org. Lett.* **2002**, *4*, 4495.

(37) Reetz, M. T.; Goossen, L. J.; Meiswinkel, A.; Paetzold, J.; Jensen, J. F. *Org. Lett.* **2003**, *5*, 3099.

Scheme 3. Rh-Catalyzed Asymmetric Hydrogenation of Enol Esters

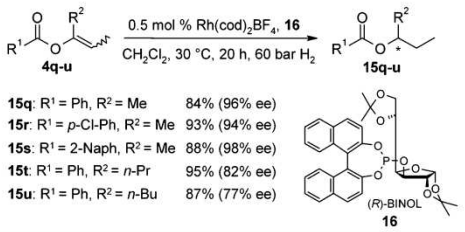

Scheme 4. Proposed Activation of the Pd^{I} Dimer

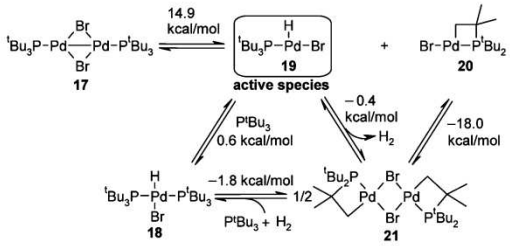

enantioselective syntheses via a double-bond isomerization/asymmetric hydrogenation sequence.

In order to evaluate how the catalytically active species may form from the Pd^{I} dimer, we calculated the standard Gibbs free energy ($\Delta_R G^{\ominus}$) for the formation of various Pd-hydride species using the B3LYP density functional.[33] The lowest energy expenditure was calculated for the formation of Pd hydride **19** along with the monomeric palladacycle **20** ($\Delta_R G^{\ominus}$ = 14.9 kcal/mol) (see Table S3 (Supporting Information) and Scheme 4). Since this reaction proceeds via an endergonic pathway, the driving force for the formation of **19** is the concomitant dimerization of **20** to the stable palladacycle **21** ($\Delta_R G^{\ominus}$ = −18 kcal/mol).

The Pd−H complex **19** likely acts as the catalytically active species, but because of its high reactivity, we were not surprised to detect the oxidized dimeric palladacycle **21** as major signal when monitoring the catalytic reaction by ^{1}H and ^{31}P NMR (^{31}P NMR: −8.6 ppm). A minor signal at −9.0 ppm also appeared, which might originate from an isomer of **21**. It is known that **21** can also form from Pd−H species **18**, with concomitant release of a phosphine and hydrogen gas.[38] Moreover, **21** may result from the decomposition of **19** after it has achieved the double bond migration. Another experimental result that supports **19** as the catalytically active species is that upon trapping with tri-*tert*-butylphosphine, the more stable bis(*tert*-butylphosphino)palladium hydride complex **18** was detected (^{1}H NMR: triplet at −15.6 ppm).[28a]

(38) Clark, H. C.; Goel, A. B.; Goel, S *J. Organomet. Chem.* **1979**, *166*, C29.

Starting from **19**, a possible mechanism for the isomerization reaction would involve an insertion of the alkene into the Pd−hydride **19** followed by β-hydride elimination with formation of the isomerized olefin and regeneration of the initial Pd−hydride **19**. Further mechanistic investigations to elucidate the origin of the high isomerization activity of $[Pd(\mu\text{-Br})(P^{t}Bu_3)]_2$ are underway.

In conclusion, the Pd^{I} dimer $[Pd(\mu\text{-Br})(P^{t}Bu_3)]_2$ possesses a new level of reactivity for catalyzing double bond migrations in a wide range of unsaturated substrate classes. It even catalyzes the isomerization of allylic esters to the corresponding enol esters, which are valuable starting materials, e.g., for asymmetric hydrogenation.

Acknowledgment. We thank D. Halter and Dr. W. Dzik (TU Kaiserslautern) for technical assistance, NanoKat, the DFG (SFB-TRR 88 "3MET"), the Landesgraduiertenstiftung Rheinland-Pfalz (fellowships to P.M., M.F.G., and A.F.) and the HEC Pakistan (fellowship to B.A.K.) for financial support, and Umicore for the donation of catalyst metals.

Supporting Information Available. Screening table, experimental procedures, characterization of all new compounds, and data of DFT calculations. This material is available free of charge via the Internet at http://pubs.acs.org.

The authors declare no competing financial interest.

Die mechanistischen Untersuchungen sind aufgrund verbleibender offener Fragen noch nicht abgeschlossen. Zum einen wurden mit Hilfe der DFT-Rechnungen lediglich Intermediate und keine Übergangszustände berechnet, so dass nur die freien Standardreaktionsenthalpien, nicht aber die freien Standardaktivierungsenthalpien für die Bildungen verschiedener potenzieller katalytisch aktiver Spezies berechnet werden konnten, was Voraussagen über die relativen Geschwindigkeiten konkurrierender Reaktionen erlauben würde.

Bisher ungeklärt ist auch die einzigartige Reaktivität des homodinuklearen Palladiumkatalysators $[Pd(\mu\text{-}Br)(P^tBu_3)]_2$. In Kontrollexperimenten konnte Frau Dr. Patrizia Mamone zeigen, dass *in situ* gebildete Koordinationsverbindungen monometallischer Palladiumpräkatalysatoren mit Tri-*tert*-butylphosphin nur äußerst geringe Ausbeuten in der Isomerisierungsreaktion liefern (Table S1 in der 'supporting information' von *OrgLett*). Somit stellt sich die Frage, ob tatsächlich ein monometallischer oder doch ein bimetallischer Palladium–Hydrid-Komplex die katalytisch aktive Spezies darstellt. Letztlich wäre auch noch denkbar, dass eine Palladiumspezies, die überhaupt kein Hydrid trägt, die katalytisch aktive Spezies darstellt.[113]

Aufgrund dieser ungeklärten Fragen planen Gooßen und Koley, die mechanistischen Untersuchungen, bei denen unter anderem wieder DFT-Rechnungen zum Einsatz kommen sollen, in einem Kooperationsprojekt fortzusetzen.

In nachfolgenden Arbeiten von Gooßen et al. bildete die Palladium-katalysierte Doppelbindungsisomerisierung die Grundlage für die Entwicklung des Konzepts der isomerisierenden Olefinmetathese. Dies konnte für die Synthese von Olefinverschnitten mit definierten Kettenlängenverteilungen aus Fettsäuren,[114] von Styrolen aus natürlich vorkommenden Allylbenzolen[115] und von Tsetsefliegenlockstoffen aus Cashewnussschalenextrakt eingesetzt werden.[116] Auch Schoenebeck et al. untersuchten weiter die katalytischen Eigenschaften des homodinuklearen Palladiumkatalysators $[Pd(\mu\text{-}Br)(P^tBu_3)]_2$. Sie beschrieben mechanistische Studien von Suzuki-Kupplungen[117,118] sowie Halogenaustauschreaktionen[119,120] und fassten ihre Ergebnisse in einem Übersichtsartikel zusammen.[121]

4 Zusammenfassung und Ausblick

Im Rahmen dieser Arbeit wurden DFT-Rechnungen zum mechanistischen Verständnis und zur rationalen Entwicklung homogenkatalytischer Reaktionen eingesetzt.

Im ersten Projekt konnten mit Hilfe von DFT-Rechnungen effizientere Katalysatorsysteme für Protodecarboxylierungsreaktionen und decarboxylierende Kreuzkupplungen durch rationale Katalysatorentwicklung identifiziert werden. Hierzu wurde die Decarboxylierung von 2- und 4-Fluorbenzoesäure mit DFT-Rechnungen untersucht. Zunächst sagten die Rechnungen keine deutlich erhöhten Reaktionsgeschwindigkeiten für Katalysatorsysteme bestehend aus Kupfer(I) und verschiedenen 4,7-disubstituierten 1,10-Phenanthrolinliganden voraus. Weitere Berechnungen prognostizierten hingegen stark erhöhte Effizienz für Silber-basierte Katalysatoren in der Decarboxylierung von *ortho*-substituierten Benzoesäuren. Tatsächlich konnte daraufhin für diese Carbonsäuren ein Katalysatorsystem bestehend aus AgOAc und K_2CO_3 in NMP entwickelt werden, welches die Protodecarboxylierung bereits bei 120 °C ermöglicht, 50 °C niedriger als die des Kupfer-basierten Systems.

Die Erkenntnisse ließen sich in der Arbeitsgruppe Gooßen weiterhin auf die decarboxylierende Kreuzkupplung übertragen. Es gelang die Entwicklung eines Ag/Pd-basierten Katalysatorsystems für die Biarylsynthese ausgehend von Benzoesäuren und Aryltriflaten bei Reaktionstemperaturen von nur 130 °C.

Im Folgenden war es möglich, durch den Einsatz von DFT-Rechnungen den Reaktionsmechanismus der decarboxylierenden Kreuzkupplung aufzuklären und Voraussagen für ein effizienteres Cu/Pd-basiertes Katalysatorsystem zu treffen. Nachdem durch experimentelle Beobachtungen klar wurde, dass der Decarboxylierungsschritt nicht notwendigerweise geschwindigkeitsbestimmend sein muss, wurde der komplette Katalysezyklus der decarboxylierenden Kreuzkupplung eingehend mit Hilfe von DFT-Rechnungen untersucht. In Abhängigkeit des Benzoats wurde die Decarboxylierung oder die Transmetallierung als geschwindigkeitsbestimmend identifiziert. Da in der Transmetallierung zunächst die Bildung eines bimetallischen Cu−Pd-Addukts erforderlich ist, wurde gefolgert, dass die Verwendung von verbrückenden, bidentaten Liganden die Reaktion begünstigen sollte. In der Tat konnte durch Einsatz eines *P*,*N*-Liganden eine Cu/Pd-katalysierte decarboxylierende Kreuzkupplung von aromatischen Carboxylaten mit

Aryltriflaten bei nur 100 °C entwickelt werden, was einer Absenkung der Reaktionstemperatur um 50 °C entspricht.

Zukünftige Weiterentwicklungen der Cu/Pd-katalysierten decarboxylierenden Kreuzkupplung zielen auf die Überwindung der Beschränkung auf *ortho*-substituierte Benzoate und den Ersatz der teuren Aryltriflate durch günstigere Arylhalogenide. Arbeiten hierzu sind bereits im Gange.

Im zweiten Projekt wurde der Reaktionsmechanismus der Ruthenium-katalysierten Hydroamidierung terminaler Alkine eingehend untersucht. Nachdem durch Isotopenmarkierungsexperimente, Bestimmungen von kinetischen Isotopeneffekten mittels *in situ* IR-Spektroskopie und verschiedene *in situ* NMR- sowie ESI-MS-Experimente drei von fünf potentiellen Reaktionsmechanismen ausgeschlossen werden konnten, erlaubten die experimentellen Ergebnisse die Eingrenzung auf einen der verbliebenen Katalysezyklen.

Mit Hilfe von DFT-Rechnungen wurde daraufhin bestätigt, dass es sich bei den postulierten Intermediaten um stabile Minima handelt. Das Auftreten einer Ru–Hydrid–Vinylidenspezies lieferte die Erklärung, warum die Hydroamidierung auf terminale Alkine beschränkt ist. Der nukleophile Angriff des Amidliganden an das Vinylidenkohlenstoffatom erklärt die *anti*-Markovnikov-Selektivität der Reaktion. Nachdem Gooßen und Koley et al. in einer weiteren Untersuchung den Einfluss der Liganden auf die Stereoselektivität der Hydroamidierung aufklären konnten, ist nun der Grundstein für die zukünftige rationale Entwicklung effizienterer Hydroamidierungskatalysatoren gelegt.

Im dritten Projekt konnten Erkenntnisse zum Reaktionsmechanismus der Palladium-katalysierten Isomerisierung von Allylestern zu Enolestern und Hinweise auf die katalytisch aktive Spezies der Reaktion erlangt werden. Zunächst gelang mit dem homodinuklearen Palladiumkatalysator $[Pd(\mu\text{-}Br)(P^tBu_3)]_2$ die Entwicklung einer effizienten Synthese zur Darstellung einer großen Bandbreite diverser Enolester. In 1-Position verzweigte Enolester dienten anschließend als Substrate für enantioselektive Hydrierungen zur Synthese enantiomerenreiner chiraler Ester.

Aufgrund experimenteller Beobachtungen, die nahelegten, dass ein Palladiumhydrid-Komplex die katalytisch aktive Spezies darstellt, wurde die Bildung verschiedener Palladiumhydrid-Spezies ausgehend vom homodinuklearen Palladiumkatalysator

$[Pd(\mu\text{-}Br)(P^tBu_3)]_2$ mit Hilfe von DFT-Rechnungen untersucht. Hierbei konnte der Palladiumhydrid-Komplex $[Pd(Br)(H)(P^tBu_3)]$ als die vermutlich katalytisch aktive Spezies identifiziert werden. Aufgrund seiner hohen Reaktivität konnten in *in situ* NMR-Experimenten lediglich ein oxidiertes Dimer und ein Abfangprodukt mit überschüssigem Tri-*tert*-butylphosphin nachgewiesen werden.

In zukünftigen Arbeiten soll durch kinetische Untersuchungen die Reaktionsordnung der Isomerisierung ermittelt werden. Dies soll dazu beitragen, Aufschluss darüber zu gewinnen, ob tatsächlich ein monometallischer oder ein bimetallischer Komplex die katalytisch aktive Spezies darstellt.

5 Theoretischer Teil

5.1 Die Theorie der DFT-Rechnungen

5.1.1 Die Hohenberg-Kohn-Theoreme

Schon 1964 erbrachten Hohenberg und Kohn den Beweis, dass die Elektronendichte eines molekularen Systems eindeutig den Hamiltonoperator bestimmt und somit auch alle anderen Eigenschaften des Systems vorgibt.[122] Sie konnten zeigen, dass das attraktive Wechselwirkungspotential zwischen Elektronen und Kernen, welches auch als externes Potential $V_{\mathrm{ext}}(\boldsymbol{r})$ bezeichnet wird, bis auf eine Konstante ein eindeutiges Funktional der Elektronendichte $\rho(\boldsymbol{r})$ des Grundzustandes ist. Da $V_{\mathrm{ext}}(\boldsymbol{r})$ wiederum eindeutig den Hamiltonoperator bestimmt, ist der Vielteilchen-Grundzustand ebenfalls ein eindeutiges Funktional der Elektronendichte $\rho(\boldsymbol{r})$. Dieser Beweis wird als erstes Hohenberg-Kohn-Theorem bezeichnet.

Weiterhin konnten Hohenberg und Kohn zeigen, dass das Funktional $F_{\mathrm{HK}}[\rho]$, welches die Grundzustandsenergie des Systems beschreibt, nur genau dann die niedrigste Energie liefert, wenn ρ die wahre Grundzustandselektronendichte ρ_0 ist. Dieses Variationsprinzip wird zweites Hohenberg-Kohn-Theorem genannt. Es gilt allerdings nur für das exakte, wahre Funktional $F_{\mathrm{HK}}[\rho]$. Dieses ist aber genauso unzugänglich wie die exakte Lösung der Vielteilchen-Schrödingergleichung. Hohenberg und Kohn geben jedoch in ihrer Veröffentlichen keine Anhaltspunkte, wie das Funktional $F_{\mathrm{HK}}[\rho]$ zur Berechnung der Energie konstruiert werden könnte. Ziel ist es folglich, Näherungen für das Funktional $F_{\mathrm{HK}}[\rho]$ zu finden.

5.1.2 Die Kohn-Sham-Gleichung

Bereits 1965 unterbreiteten Kohn und Sham einen Vorschlag, wie die Hohenberg-Kohn-Theoreme in die Praxis umgesetzt werden können.[123] Ausgangspunkt ihrer Überlegungen war ein System aus N nicht-wechselwirkenden Elektronen, die sich in einem effektiven, zunächst unbekannten Potential $V_{\mathrm{eff}}(\boldsymbol{r})$ bewegen. Es gelang ihnen, eine Gleichung herzuleiten, die der Hartree-Fock-Gleichung sehr ähnlich ist:

$$f^{\mathrm{KS}}\,\phi_i = \varepsilon_i\,\phi_i$$

Diese Gleichung wird Kohn-Sham-Gleichung genannt. Dabei ist f^{KS} der Einelektronen-Kohn-Sham-Operator:

$$f^{\mathrm{KS}} = -\frac{1}{2}\nabla^2 + V_{\mathrm{eff}}(\boldsymbol{r})$$

ϕ_i sind die sogenannten Kohn-Sham-Orbitale und ε_i deren Eigenenergien. Obwohl die Kohn-Sham-Orbitale nicht den traditionellen Molekülorbitalen entsprechen, können sie qualitativ als solche interpretiert werden.[124–127] Die Elektronendichte des Grundzustandes ist als Summe der Betragsquadrate der Kohn-Sham-Orbitale definiert:

$$\rho_{\mathrm{S}}(\boldsymbol{r}) = \sum_{i}^{N}\sum_{S} |\, \phi_i(\boldsymbol{r}, s)^2| = \rho_0(\boldsymbol{r})$$

Das Potential lässt sich als Ableitung der Energie nach der Elektronendichte ausdrücken. Die Energie liefert das Funktional $F[\rho]$:

$$V_{\mathrm{eff}}(\boldsymbol{r}) = \frac{\partial F[\rho]}{\partial \rho}$$

Das Funktional $E[\rho(\boldsymbol{r})]$, welches den Zusammenhang zwischen der Energie und der Elektronendichte herstellt, wenn man die Wechselwirkung der Elektronen wieder berücksichtigt, lautet:

$$E[\rho(\boldsymbol{r})] = T_{\mathrm{S}}[\rho(\boldsymbol{r})] + J[\rho(\boldsymbol{r})] + E_{\mathrm{Ne}}[\rho(\boldsymbol{r})] + E_{\mathrm{XC}}[\rho(\boldsymbol{r})]$$

Es ist ebenso wie der Hamiltonoperator eine Summe verschiedener Terme, die hierbei durch Funktionale gebildet werden. Dabei beschreibt das Funktional $T_{\mathrm{S}}[\rho(\boldsymbol{r})]$ die kinetischen Energie, $J[\rho(\boldsymbol{r})]$ die Wechselwirkungsenergie der Elektronen untereinander und $E_{\mathrm{Ne}}[\rho(\boldsymbol{r})]$ die Kern-Elektronen-Wechselwirkungsenergie. Das Funktional $E_{\mathrm{XC}}[\rho(\boldsymbol{r})]$ enthält die nicht-klassische Austausch- (engl. 'exchange') und Korrelationswechselwirkung (engl. 'correlation') sowie den Anteil der kinetischen Energie, welcher nicht durch das nicht-wechselwirkende System berücksichtigt ist. Während für die ersten drei Funktionale mathematisch exakte Ausdrücke existieren, ist das exakte Austausch-Korrelations-Funktional unbekannt.

Bis zu diesem Punkt ist noch keine Näherung erfolgt. Während die Hartree-Fock-Gleichungen auf der MO-Näherung beruhen, welche die Wellenfunktion als eine einzige Slater-

Determinante ansetzt, ist dagegen die Kohn-Sham-Gleichung so exakt wie die unlösbare Vielteilchen-Schrödingergleichung. Erst durch eine Näherung für das Austausch-Korrelations-Funktional $E_{\mathrm{XC}}[\rho(\boldsymbol{r})]$ wird eine Näherung eingeführt. Setzt man dann die vier Terme für die vier Funktionale ein, erhält man einen Satz gekoppelter Integrodifferentialgleichungen, die sich wie die Hartree-Fock-Gleichungen iterativ durch eine SCF-Prozedur lösen lassen. Ziel der Dichtefunktionaltheorie ist folglich, eine möglichst gute Näherung der Schrödingergleichung zu bilden. Zu diesem Zweck sind immer bessere Näherungen für das Austausch-Korrelations-Funktional erforderlich.

5.1.3 Näherungen für das Austausch-Korrelations-Funktional

Die erste Näherung, die für das Austausch-Korrelations-Funktional gemacht wurde, ist der Fall des hypothetischen einheitlichen Elektronengases, bei dem die Elektronendichte überall denselben Wert hat. Diese Näherung wird 'local density approximation' (LDA) genannt. Hier lässt sich das Austausch-Korrelations-Funktional in eine Summe aus einem Austauschfunktional und einem Korrelationsfunktional zerlegen. Für das Austauschfunktional ist ein exakter Ausdruck bekannt. Er wird als Slater-Austausch bezeichnet und mit S abgekürzt. Für das Korrelationsfunktional entwickelten Vosko, Wilk und Nusair 1980 eine Näherung, die mit VWN[128] abgekürzt wird. Kombiniert man diese beiden Funktionale, so erhält man das Austausch-Korrelations-Funktional SVWN.

Es ist eine sehr drastische Näherung, die Elektronendichte als konstant anzunehmen, da molekulare Systeme dem Fall des einheitlichen Elektronengases nicht im Entferntesten Nahe kommen. Erstaunlicherweise liefert diese Näherung Energien, die denen aus Hartree-Fock (HF)-Rechnungen recht ähnlich sind, letztere aber auch nicht in ihrer Genauigkeit übertreffen.

Der nächste Schritt war es, für die nicht-homogene, wahre Elektronendichte nicht nur die Elektronendichte $\rho(\boldsymbol{r})$ an einem bestimmten Punkt $\boldsymbol{r}$ heranzuziehen, sondern die Dichte auch mit Informationen zu ihrem Gradienten $\nabla\rho(\boldsymbol{r})$ zu versehen. Dies wird 'generalized gradient approximation' (GGA) genannt. Diese Näherung für die Elektronendichte lässt sich als Taylorreihenentwicklung interpretieren, die im Fall von LDA nur den Term 0. Ordnung enthält und im Fall von GGA nach dem Term 1. Ordnung abgebrochen wird.

Bekannte Beispiele für GGA-Funktionale sind das 1986 von Becke veröffentlichte Austauschfunktional, das mit B oder B86[129] abgekürzt wird, und das 1988 von Lee, Yang

und Parr vorgestellte Korrelationsfunktional LYP.[130] Die Kombination dieser beiden Funktionale ergibt das Austausch-Korrelations-Funktional BLYP.

Es kann auch ein LDA-Austauschfunktional mit einem GGA-Korrelationsfunktional oder umgekehrt kombinieren werden. Es resultiert dann z.B. SLYP oder BVWN.

Da bei HF-Rechnungen die Austauschenergie der Slater-Determinante exakt berechnet werden kann, kam die Idee auf, für DFT-Methoden die exakte HF-Austauschenergie zu verwenden und nur für den Teil der Austauschenergie, der im HF-Modell fehlt, eine Näherung heranzuziehen. Dies führte allerdings zu Problemen, die ohne ins Detail zu gehen, nicht erläutert werden können, aber bei Koch und Holthausen nachgelesen werden können.[131] 1993 löste Becke dieses Problem, indem er das Austauschfunktional als eine Linearkombination aus exaktem HF-Austausch und LDA-Austausch ansetzte.[132] Derartige Funktionale werden als DFT/HF-Hybridfunktionale bezeichnet. Becke nutzte drei Parameter, die er so wählte, dass sein Funktional optimale Werte für den sogenannten Gaussian-2 (G2)-Molekülsatz lieferte. Aufgrund der Verwendung von drei Parametern wird dieses Funktional mit B3 abgekürzt. 1994 schlugen Stephens et al. vor, das B3-Austauschfunktional mit dem LYP-Korrelationsfunktional zum Austausch-Korrelations-Funktional B3LYP[133] zu kombinieren.

5.2 Die Wahl der Rechenmodelle

Unter einem Rechenmodell versteht man eine eindeutig definierte und universell einsetzbare Methode, um Eigenschaften von chemischen Systemen zu berechnen.[134] Ein Rechenmodell setzt sich generell aus einer Rechenmethode und einem Basissatz zusammen. Jede derartige einzelne Paarung von Rechenmethode und Basissatz repräsentiert eine andere Näherung der Schrödingergleichung. Deshalb ist die Wahl des Rechenmodells immer ein Kompromiss aus ihrer Genauigkeit und ihrem zeitlichen Rechenaufwand.

Da eine Geometrieoptimierung viel mehr Zeit in Anspruch nimmt als das Berechnen der Energie einer vorgegebenen Geometrie (SPE-Rechnung, engl. 'single point energy calculation'), ist es sinnvoll, zunächst die Geometrie mit einem weniger genauen Rechenmodell zu optimieren und anschließend die Energie der optimierten Struktur noch einmal mit einem besseren Modell zu berechnen, da davon auszugehen ist, dass sich die Geometrie einer Struktur beim Wechsel von einem weniger genauen Rechenmodell zu einem

besseren nur geringfügig ändert, die 'single point energy' jedoch stärker vom Rechenmodell abhängt. Die Konvention für die Angabe der Rechenmodelle ist wie folgt:

Energie-Methode/Energie-Basissatz//Geometrie-Methode/Geometrie-Basissatz.

Beispielsweise bedeutet B3LYP/6-311+G(2d,p)//B3LYP/6-31G(d), dass zuerst die Geometrieoptimierung mit B3LYP und dem Basissatz 6-31G(d) durchgeführt und danach die Energie mit B3LYP und der Basis 6-311+G(2d,p) berechnet wird.

5.2.1 Die Wahl der Rechenmethode

Die in dieser Arbeit betrachteten Systeme bestehen aus bis zu 150 Atomen. Hartree-Fock (HF)-Rechnungen wären zwar mit relativ geringem Rechenaufwand durchführbar, allerdings wären die Ergebnisse nicht zufriedenstellend, da die HF-Methode die Korrelationsenergie nicht berücksichtigt, was zu falschen Geometrien und Energien führt. Coupled-cluster (CC)-, quadratic configuration interaction (QCI)- oder Møller-Plesset Störungstheorie (MP*n*)-Rechnungen sind zwar in der Lage, einen Teil der Korrelationsenergie zu erfassen, ihr Rechenaufwand wäre jedoch viel zu hoch. Einzelne Rechnungen würden Wochen oder Monate dauern. Die Methode der Wahl stammt daher aus der Dichtefunktionaltheorie (DFT). Dichtefunktionalmethoden können ebenfalls einen Teil der Korrelationsenergie erfassen, ihr Rechenaufwand ist jedoch wesentlich geringer.

Aus den vielen verfügbaren Dichtefunktionalmethoden wurde das Hybridfunktional B3LYP[130,132,133,135] gewählt. Hybridfunktionale konnten seit ihrer Einführung einen beispiellosen Erfolg verzeichnen.[136] Insbesondere entwickelte sich B3LYP zum einem der beliebtesten und weitest verbreiteten Funktionale. Gerechtfertigt wurde dieser erstaunliche Erfolg durch überraschend gute Leistungen von B3LYP bei zahllosen chemischen Anwendungen, einschließlich solcher auf dem schwierigen Gebiet der offenschaligen Übergangsmetallchemie.[131] Auch in Untersuchungen von Gooßen und Thiel, die der vorliegenden Arbeit vorangegangen waren, konnten Berechnungen mit B3LYP experimentelle Befunde bestätigen.[56]

5.2.2 Die Wahl der Basissätze für die Geometrieoptimierungen

Der kleinste Basissatz, mit welchem bei Geometrieoptimierungen vernünftige Strukturen berechnet werden können, ist 6-31G(d).[134,137–142] Zu Beginn dieser Arbeiten wurden mit B3LYP/6-31G(d) erste Geometrieoptimierungen durchgeführt. Damals stand für Rechnungen

ausschließlich der Linux-Cluster des Rechenzentrums der TU Kaiserslautern (siehe Kapitel 5.4 Verwendete Hardware, Seite 107) zur Verfügung. Die Moleküle, die im ersten Projekt dieser Arbeit untersucht wurden, bestanden aus etwa bis zu 40 Atomen. Für Strukturen, die ein Minimum darstellen, belief sich die Rechenzeit auf ein bis zwei Tage, bei denen, die einen Übergangszustand darstellen, auf akzeptable zwei bis vier Tage. Da in folgenden Projekten auch größere Moleküle berechnet werden sollten und zur Vergleichbarkeit der Ergebnisse der Basissatz beibehalten werden sollte, wurde kein größerer Basissatz als 6-31G(d) gewählt, da die Rechenzeit nicht linear mit der Anzahl der Atome ansteigt.

Ist N die Zahl der Basisfunktionen, so steigt die Rechenzeit mit N^x, wobei x je nach Rechenmethode zwischen 3 und 7 liegt. Da die Zahl der Basisfunktionen mit größerem Basissatz und steigender Zahl der Elektronen, die wiederum von der Zahl und Art der Atome abhängt, zunimmt, steigt folglich die Rechenzeit überproportional mit der Zahl der Atome an. Beispielsweise würde bei der Berechnung eines Moleküls mit 60 statt 40 Atomen die Rechenzeit nicht um das Eineinhalbfache, sondern mindestens um das Dreifache ansteigen. Dies war für 6-31G(d) gerade noch vertretbar. Bei einem größeren Basissatz wäre die Rechenzeit viel zu stark angestiegen. Auf dem Linux-Cluster des Rechenzentrums hätten Geometrieoptimierung dann bereits Wochen in Anspruch nehmen können. Die rasante Weiterentwicklung der Rechenleistung von Hochleistungsclustern in den letzten Jahren und insbesondere die Möglichkeit der parallelen Nutzung etlicher Rechenknoten für nur eine einzige Rechnung waren zu Beginn dieser Arbeit noch nicht abzusehen. Heutzutage könnte man für Geometrieoptimierungen dieser Molekülgröße problemlos auch größere Basissätze wählen.

Bei der Berechnung von anionischen Strukturen, wie sie nur in *JACS* 2014 vorkommen, wurde der Basissatz 6-31+G(d)[141,143,144] verwendet, da bekannt ist, dass bei negativ geladenen Systemen eine diffuse Basisfunktion wichtig ist, um korrekte Geometrien zu erhalten.[134] Für die Übergangsmetalle Kupfer, Silber, Palladium und Ruthenium wurde anstelle des Pople-Basissatzes der jeweilige Pseudobasissatz Stuttgart RSC 1997 ECP[145,146] verwendet. Hierbei wird für die inneren Elektronen (Cu: 10, Ag, Pd, Ru: 28) ein skalar-relativistisches effektives Kernpotential (engl. 'effective core potential', ECP) verwendet, während nur die äußeren Elektronen mit einem double-ζ-Basissatz beschrieben werden. Der Einsatz der Pseudobasissätze mit ECP hat zwei Gründe: Erstens führt dies zu einer Rechenzeitersparnis, da die kernnahen Elektronen nicht explizit berechnet werden, und

zweitens ermöglicht die Verwendung von Pseudobasissätzen, parametrisch relativistische Effekte zu erfassen. Dies ist bei den Metallen der 2. und 3. Übergangsmetallreihe besonders von Bedeutung, da hier aufgrund der hohen Kernladung die innersten Elektronen im Bohrschen Atommodell mit Bahngeschwindigkeiten kreisen, die der Lichtgeschwindigkeit so nahe kommen, dass relativistische Effekte nicht mehr vernachlässigt werden können. Da der Valenzbasissatz bereits diffuse Funktionen enthält, musste er für die Berechnungen von Anionen in *JACS* 2014 nicht mehr verändert werden.

5.2.3 Die Wahl der Basissätze für die 'single point energy'-Rechnungen

Die Genauigkeit von Rechenmodellen wurde von Curtiss, Raghavachari, Trucks und Pople am sogenannten Gaussian-2 (G2)-Molekülsatz untersucht und quantifiziert.[147] Hierzu wurden 125 Rechnungen thermochemischer Größen durchgeführt und mit experimentell ermittelten Werten verglichen. Die wichtigste Größe, um die Genauigkeit eines Rechenmodells zu charakterisieren, ist die mittlere absolute Abweichung (engl. 'mean absolute deviation', MAD). Sie gibt den Mittelwert der Beträge der Differenzen zwischen den berechneten und experimentell ermittelten Werten an. Die Standardabweichung (engl. 'standard deviation', SD) der Differenzen zwischen den berechneten und experimentell ermittelten Werten ist ein Maß dafür, wie stark die Werte um den Mittelwert streuen. Diese beiden Größen sowie die größte positive Abweichung (engl. 'largest positive error', LPE) und die größte negative Abweichung (engl. 'largest negative error', LNE) sind in Tabelle 1 für ausgewählte Rechenmodelle aufgeführt.

Tabelle 1. *Genauigkeiten verschiedener Rechenmodelle: MAD, SD, LPE und LNE in kcal / mol*.[147]

Rechenmodell	MAD	SD	LPE	LNE
B3LYP/6-31G(d)//B3LYP/6-31G(d)	7.9	9.5	12.2	–54.2
B3LYP/6-31+G(d,p)//B3LYP/6-31G(d)	4.0	4.2	17.6	–33.9
B3LYP/6-311+G(2d,p)//B3LYP/6-31G(d)	3.2	3.0	13.6	–20.1
B3LYP/6-311+G(3df,2df,2p)//B3LYP/6-31G(d)	2.7	2.6	12.5	–9.3
MP2/6-311+G(2d,p)//B3LYP/6-31G(d)	8.9	7.8	29.7	–39.2
HF/6-311+G(2d,p)//B3LYP/6-31G(d)	46.6	40.5	9.1	–174.6

Bei allen in Tabelle 1 aufgeführten Beispielen wurde die Geometrieoptimierung mit B3LYP/6-31G(d) durchgeführt. Die Genauigkeit der Rechenmodelle steigt mit wachsendem

Basissatz für die 'single point energy'-Rechnungen mit B3LYP an. Sie ist mit 6-311+G(2d,p) wesentlich höher (MAD = 3.2 kcal / mol) als mit 6-31G(d) (MAD = 7.9 kcal / mol). Zu Beginn dieser Arbeit wurde der zeitliche Rechenaufwand einer SPE-Rechnung mit B3LYP/6-311+G(2d,p) auf einem SMP-Rechenknoten mit zwei Prozessorkernen des Linux-Clusters des Rechenzentrums der TU Kaiserslautern (siehe Kapitel 5.4 Verwendete Hardware, Seite 107) ermittelt, indem mit diesem Modell eine Rechnung an einem Testmolekül mit 22 Atomen durchgeführt wurde. Die Rechenzeit belief sich nur auf eine halbe Stunde. Die Rechnung an einem weiteren Testmolekül mit 61 Atomen dauerte hingegen schon einen Tag, was noch als akzeptabel eingestuft werden kann. Um zu ermitteln, ob eine Rechnung mit 6-311+G(3df,2df,2p) auch noch in akzeptablem zeitlichen Rahmen durchführbar ist, wurde die Rechnung mit diesem Basissatz am Testmolekül mit 22 Atomen wiederholt. Die Rechnung dauerte mit einer Stunde etwa doppelt so lang. Die entsprechende Rechnung an dem Testmolekül mit 61 Atomen würde wegen des 'non linear scalings' nicht das Doppelte, sondern ein Vielfaches von einem Tag in Anspruch nehmen. Da dies für eine SPE-Rechnung einen sehr langen Zeitraum darstellt und nicht in Relation mit der Steigerung der Genauigkeit von 6-311+G(2d,p) zu 6-311+G(3df,2df,2p) steht, wurden alle 'single point energy'-Rechnungen mit dem Basissatz 6-311+G(2d,p)[148–150] durchgeführt.

In Tabelle 1 sind zum Vergleich auch die Genauigkeiten der Rechenmethoden MP2 und HF in Kombination mit dem Basissatz 6-311+G(2d,p) aufgeführt. Die MP2-Methode liefert wesentlich schlechtere Ergebnisse als B3LYP, obwohl sie einen höheren Rechenaufwand besitzt. Die HF-Methode versagt auch mit diesem großen Basissatz völlig, da sie die Korrelationsenergie nicht berücksichtigt.

Da 6-311+G(2d,p) bereits diffuse Funktionen enthält, musste der Basissatz für die Berechnungen von Anion in *JACS* 2014 nicht mehr erweitert werden. Für die Übergangsmetalle Kupfer, Silber, Palladium und Ruthenium wurde wieder anstelle des Pople-Basissatzes der entsprechende Pseudobasissatz Stuttgart RSC 1997 ECP verwendet. Für die Rechnungen in *JACS* 2014 wurde für Kupfer und Palladium die Qualität des Valenzanteils des Basissatzes von double-ζ- auf triple-ζ-Niveau erhöht. Hierzu wurden die *d*-Funktionen des ursprünglichen Basissatzes von [411] zu [3111] leicht dekontrahiert, und es wurde ein einzelner Satz von *f*-Funktionen (aus der def2-TZVP-Basis,[151] η_f(Cu) = 2.233, η_f(Pd) = 1.24629) für beide Elemente hinzugefügt.

5.2.4 Die Wahl der Skalierungsfaktoren für die Frequenzrechnungen

Die meisten Rechenmodelle machen bei der Berechnung der IR-Schwingungsfrequenzen und der thermischen Korrekturen zur Berechnung der Gesamtenergie inklusive Nullpunktsschwingungsenergie sowie der freien Enthalpie systematische Fehler. Wong[152] sowie Scott und Radom[153] berechneten von 122 Molekülen jeweils die IR-Frequenzen. Anhand des Mittelwerts der Abweichungen der 1066 berechneten IR-Frequenzen im Vergleich zu den experimentellen Werten ermittelten sie einen Skalierungsfaktor. Für B3LYP/6-31G(d) berechnete Wong $f = 0{,}9613$, Scott und Radom fanden $f = 0{,}9614$. Für 24 bzw. 25 Moleküle führten sie entsprechende Rechnungen für die thermischen Korrekturen durch, welche Skalierungsfaktoren von $f = 0{,}9804$ bzw. $f = 0{,}9806$ ergaben. Die ermittelten Skalierungsfaktoren liegen jeweils sehr dicht beieinander. Auch weitere Skalierungsfaktoren sind in der Literatur zu finden.[154–156] Jedoch konnten keine Skalierungsfaktoren für B3LYP/6-31+G(d) gefunden werden. Die Skalierungsfaktoren für HF/6-31G(d) und HF/6-31+G(d) sind allerdings nahezu identisch.[153] Scheinbar hat die diffuse Basisfunktion keinen großen Einfluss auf die Skalierungsfaktoren. Deshalb wurden für B3LYP/6-31+G(d) dieselben Skalierungsfaktoren wie für B3LYP/6-31G(d) verwendet.

In den Rechnungen zu den Publikationen *ChemComm*, *ChemCatChem*, *JACS* 2011 und *OrgLett* wurden in Gaussian (siehe Kapitel 5.5 Verwendete Software, Seite 108) keine Skalierungsfaktoren spezifiziert. Deshalb wurden die IR-Schwingungsfrequenzen nachträglich mit Wongs Skalierungsfaktor $f = 0{,}9613$ und die thermischen Korrekturen mit dem Skalierungsfaktor $f = 0{,}9804$ skaliert. In den Rechnungen von *JACS* 2014 wurden die IR-Frequenzen direkt in Gaussian mit Wongs Skalierungsfaktor $f = 0{,}9613$ skaliert. Da Gaussian die thermischen Korrekturen dann mit den bereits skalierten IR-Frequenzen berechnet, ist ein nachträgliches Skalieren der thermischen Korrekturen nicht mehr notwendig.

5.2.5 Die Wahl des Lösungsmittels

In den Publikationen *ChemComm*, *ChemCatChem*, *JACS* 2011 und *OrgLett* wurden die Geometrien und Energien aller Strukturen lediglich in der Gasphase berechnet. In *JACS* 2014 sollten die Rechnungen den experimentellen Bedingungen noch genauer entsprechen. Deshalb wurden hier zusätzlich Rechnungen mit unverändertem Basissatz durchgeführt, in denen der Einfluss des Lösungsmittels als polarisierbares Kontinuum berücksichtigt wurde.

Als Lösungsmittel wurde *N*-Methyl-2-pyrrolidon (NMP) gewählt, da es sich in der decarboxylierenden Kreuzkupplung als bestes Lösungsmittel herausgestellt hat.[54,55] Als Lösungsmittelmodell wurde das 'conductor-like screening solvation model'[157,158] (COSMO) gewählt, da es besonders gut für sehr polare Lösungsmittel wie NMP ($\varepsilon = 32.55$) geeignet ist. COSMO ist in Gaussian 09 (siehe Kapitel 5.5 Verwendete Software, Seite 108) als 'conductor-like polarizable continuum model'[159,160] (CPCM) implementiert.

Zunächst wurden Geometrieoptimierungen mit diesem Lösungsmittelmodell ausgehend von den optimierten Gasphasenstrukturen gestartet. Bei kleineren Molekülen verliefen diese problemlos, bei größeren Strukturen und vor allem bei Übergangszuständen konvergierten die Geometrieoptimierungen jedoch häufig nicht. Da aber alle Strukturen mit dem gleichen Rechenmodell berechnet werden müssen, wurde beschlossen, die Geometrieoptimierungen ohne Lösungsmitteleinfluss durchzuführen und nur zusätzliche 'single point energy'-Rechnungen mit dem Lösungsmittelmodell an den optimierten Gasphasenstrukturen durchzuführen.

5.2.6 Die Wahl der Temperaturen und Konzentrationen

Die Ergebnisse der 'single point energy'-Rechnungen hängen nur von den Geometrien der berechneten Strukturen und nicht von Temperatur oder Druck (in der Gasphase) beziehungsweise Konzentration (in Lösung) ab, die thermischen Korrekturen zur Berechnung der freien Enthalpien hingegen schon. Diese werden unter den Näherungen des idealen Gases, des harmonischen Oszillators und des starren Rotators berechnet.

Alle Rechnungen in *ChemComm*, *JACS* 2011 und *OrgLett* wurden in Gaussian (siehe Kapitel 5.5 Verwendete Software, Seite 108) in der Gasphase unter Standardbedingungen für Temperatur und Druck durchgeführt. Diese sind $T = 298.15$ K und $p = 101\,325$ Pa. Der angegebene Druck entspricht nach dem idealen Gasgesetz einer Konzentration $c = n / V = p / (R\,T)$ von 40.9 mmol / L. In *ChemCatChem* wurden die Kupfer-katalysierten Decarboxylierungsreaktionen sowohl bei 298.15 K (25 °C) als auch bei der Reaktionstemperatur von 443.15 K (170 °C) und die Silber-katalysierten Decarboxylierungsreaktionen bei 298.15 K (25 °C) sowie der Reaktionstemperatur von 393.15 K (120 °C) berechnet. Bei diesen Gasphasenrechnungen wurde der Standarddruck verwendet. In *JACS* 2014 wurden alle Rechnungen bei der Reaktionstemperatur von 443.15 K (170 °C) durchgeführt. Da typische Experimente, wie sie in den Rechnungen untersucht

wurden, etwa 1 mmol Reaktand in 2 mL Lösungsmittel enthalten, wurde eine Konzentration von 0.5 mol / L, die einem Druck von 1 844 115 Pa entspricht, gewählt. Da die Katalysatorkonzentration etwa um einen Faktor 20 geringer ist, wurde ein Druck von 101 325 Pa für alle Spezies, die Kupfer und/oder Palladium enthalten, verwendet. Experimentell bestimmte Löslichkeiten von CO_2 in NMP[161] zeigen, dass unter den Reaktionsbedingungen der Stoffmengenanteil von CO_2 / NMP deutlich unter 0.01, wahrscheinlich bei etwa 0.001 liegt, wenn man Temperatur und Druck extrapoliert. Dies bedeutet, dass ein Großteil des CO_2 die NMP-Lösung verlässt. Die verbleibende CO_2-Konzentration in der Reaktionslösung entspricht etwa einem Partialdruck von 101 325 Pa für ein ideales Gas. Deshalb wurde dieser Druck für CO_2 in den Rechnungen in *JACS* 2014 gewählt.

5.2.7 Empirische Dispersionskorrekturen

Es ist bekannt, dass Dichtefunktional-Methoden Dispersionswechselwirkung (London-Kräfte) vernachlässigen oder stark unterschätzen.[162] Eine Methode, diese zu berechnen, stand zu den Zeitpunkten der Entstehungen von *ChemComm*, *ChemCatChem*, *JACS* 2011 und *OrgLett* auf den Linux-Clustern an der TU Kaiserslautern (siehe Kapitel 5.4 Verwendete Hardware, Seite 107) noch nicht zur Verfügung. In *JACS* 2014 wurden die Dispersionswechselwirkungen durch Hinzufügen von empirischen Dispersionskorrekturen, welche die Beiträger aller Atompaare aufsummieren, in den 'single point energy'-Rechnungen einberechnet. Hierbei wurden Grimmes D3-Parameter[163] für alle Minima und Übergangszustände verwendet. Es zeigte sich, dass die für verschiedene Moleküle unterschiedlichen Dispersionswechselwirkungen großen Einfluss auf die berechneten freien Aktivierungs- und Reaktionsenthalpien haben. Durch deren Berücksichtigung wird die Energie eines Übergangszustands oder Begegnungskomplexes gegenüber der von zwei einzelnen Fragmenten stark abgesenkt. Auch wird die Energie eines kompakten Übergangszustandes im Vergleich zu einem losen Begegnungskomplex erniedrigt.

5.3 Identifizierung von Minima und Übergangszuständen

5.3.1 Identifizierung durch Frequenzrechnungen

Mit Hilfe einer Frequenzrechnung kann nachgewiesen werden, ob die optimierte Geometrie einer Struktur ein Minimum oder einen Übergangszustand darstellt. Enthält das IR-Spektrum keine einzige imaginäre Schwingungsfrequenz, so ist die berechnete Struktur ein Minimum

auf der Potentialhyperfläche (PES, engl. 'potential energy surface'). Enthält das IR-Spektrum genau eine imaginäre Schwingungsfrequenz, so ist die berechnete Struktur ein Übergangszustand (Sattelpunkt 1. Ordnung auf der PES). Die Elongation der Normalmode der imaginären Schwingungsfrequenz entlang der Reaktionskoordinate kann Aufschluss darüber geben, ob der Übergangszustand zur betrachteten Reaktion gehört, also Reaktand und Produkt miteinander verbindet. Enthält das IR-Spektrum mehr als eine imaginäre Schwingungsfrequenz, so handelt es sich um einen Sattelpunkt höherer Ordnung. Treten für die Struktur (Minimum oder Übergangszustand) mehr imaginäre Schwingungsfrequenzen auf, als erwartet wurde, muss die Geometrieoptimierung mit veränderter Startgeometrie wiederholt werden.

Zu beachten ist, dass diese Identifizierung von Minima und Übergangszuständen nur dann funktioniert, wenn die Frequenzrechnung mit demselben Rechenmodell wie die Geometrieoptimierung durchgeführt wird. Wird für die Frequenzrechnung ein anderer Basissatz verwendet, so treten fast immer mehrere imaginäre Schwingungsfrequenzen mit niedrigen Wellenzahlen auf.

5.3.2 Verifizierung der Übergangszustände durch IRC-Rechnungen

Ob ein Übergangszustand zur betrachteten Reaktion gehört, kann anhand der Normalmode der imaginären Schwingungsfrequenz aus der Frequenzrechnung nur grob abgeschätzt werden. Am zuverlässigsten kann diese Frage mit einer IRC (engl. 'intrinsic reaction coordinate')-Rechnung[164–167] beantwortet werden. Dabei wird der vom Übergangszustand hinunterführende Reaktionspfad auf der Potentialhyperfläche untersucht. Die Rechnung beginnt beim Sattelpunkt und folgt dem Pfad in beide Richtungen. Hierbei wird die Geometrie an jedem Punkt des Pfades bei festgehaltener Reaktionskoordinate optimiert. Auf diese Art werden schließlich Geometrien für einen Reaktanden und ein Produkt erhalten, die mit den erwarteten Strukturen verglichen werden können. Die IRC-Rechnung verbindet folglich definitiv diese zwei Minima durch einen Reaktionspfad, der durch den Übergangszustand auf der PES verläuft.

Die IRC-Rechnung kann somit bestätigen, dass der Übergangszustand den Reaktanden und das Produkt miteinander verbindet. Es ist jedoch nicht auszuschließen, dass noch ein weiterer Pfad auf der PES existiert, der Reaktand und Produkt über einen anderen Übergangszustand miteinander verbindet, welcher eine niedrigere Energie besitzt.

5.4 Verwendete Hardware

Alle Rechnungen wurden entweder auf Rechenknoten des Linux-Clusters des Rechenzentrums, der insgesamt 86 Prozessorkerne bereitstellt oder auf Rechenknoten der Linux-Cluster „lc“ mit 196 oder „theo“ mit 896 Prozessorkernen der Fachrichtung Theoretische Chemie der Technischen Universität Kaiserslautern durchgeführt. Die Architektur des Linux-Clusters des Rechenzentrums ist in Tabelle 2 dargestellt, die der Linux-Cluster der Fachrichtung Theoretische Chemie in Tabelle 3 und Tabelle 4.

Tabelle 2. *Architektur des Linux-Clusters des Rechenzentrums*.

Rechenknoten	CPU-Kerne	Hauptspeicher / GB	CPU-Takt / GHz
29	2	2	2.2
9	2	4	2.2
1	2	16	2.2
2	4	32	3.0

Tabelle 3. *Architektur des Linux-Clusters „lc“ der Fachrichtung Theoretische Chemie*.

Rechenknoten	CPU-Kerne	Hauptspeicher / GB	CPU-Takt / GHz
5	4	16	2.6
2	8	32	2.3
1	8	32	3.0
2	8	48	2.7
1	8	64	3.0
4	12	72	2.9
1	16	256	2.6
2	32	128	2.4

Tabelle 4. *Architektur des Linux-Clusters „theo“ der Fachrichtung Theoretische Chemie*.

Rechenknoten	CPU-Kerne	Hauptspeicher / GB	CPU-Takt / GHz
24	8	64	2.8
2	32	32	2.4
4	32	64	2.6
7	64	256	2.3
1	64	512	2.3

Die meisten Rechnungen wurden als Mehrprozessorrechnungen auf einem einzelnen SMP-Knoten (Symmetrisches Multiprozessorsystem) durchgeführt. In seltenen Fällen wurden Rechnungen über MPI (engl. 'Message Passing Interface') über mehrere Rechenknoten verteilt.

5.5 Verwendete Software

Alle Rechnungen dieser Arbeit wurden mit der 64 bit-Version von Gaussian 03[168] oder Gaussian 09[169] durchgeführt. Alle 'single point energy'-Rechnungen in *JACS* 2014, in denen die Lösungsmittelbeiträge und die empirischen Dispersionskorrekturen mitberechnet wurden, wurden ausschließlich mit Gaussian 09 durchgeführt. Zum Erstellen der Startgeometrien wurde das Programm MOLDEN[170] und zum Darstellen der optimierten Geometrien das Programm GaussView[171] verwendet.

5.6 Durchführung der Rechnungen

In folgenden Unterkapiteln sind die Durchführungen der verschiedenen Rechnungen beschrieben. Detaillierte Angaben sind auch in den entsprechenden 'supporting informations' zu den jeweiligen Publikationen zu finden (siehe Kapitel Struktur der Dissertation, Seite v).

5.6.1 Geometrieoptimierungen

Alle Geometrieoptimierungen von Intermediaten (Minima) und Übergangszuständen (Sattelpunkte) wurden mit B3LYP und den in Kapitel 5.2.2 genannten Basissätzen unter Verwendung von sphärische Basisfunktionen (5 *d*- und 7 *f*-Funktionen) in der Gasphase durchgeführt. Dabei wurden grundsätzlich alle Bindungslängen und Winkel optimiert. Zum Auffinden der Übergangszustände wurde zuerst ein „relaxed potential energy surface scan“

durchgeführt, bei dem die Reaktionskoordinate an verschiedenen definierten Punkten konstant gehalten wurde, während alle anderen Freiheitsgrade optimiert wurden. In diesen Scans wurde eine Serie von Strukturen optimiert, in welchen die Reaktionskoordinate schrittweise verändert wurde. Die Struktur mit der höchsten Energie wurde anschließend als Startpunkt für die STQN ('synchronous transit-guided quasi-Newton')-Methode[172,173] verwendet, um den Überganszustand zu lokalisieren.

5.6.2 Frequenzrechnungen

Alle Frequenzrechnungen wurden grundsätzlich in der Gasphase mit demselben Rechenmodell wie die zugehörigen Geometrieoptimierungen durchgeführt. Für die einzelnen Atome wurde jeweils das in der Natur am häufigsten vertretene Isotop gewählt. Die Skalierungsfaktoren sind in Kapitel 5.2.4 angegeben. Die Werte für Temperatur und Druck sind in Kapitel 5.2.6 zu finden.

5.6.3 'Single point energy'-Rechnungen

Alle 'single point energy'-Rechnungen wurde mit B3LYP und den in Kapitel 5.2.3 genannten Basissätzen unter Verwendung von sphärische Basisfunktionen (5 *d*- und 7 *f*-Funktionen) in der Gasphase durchgeführt. In *JACS* 2014 wurde für jede Struktur eine zweite 'single point energy'-Rechnung durchgeführt, welche die Lösungsmittelbeiträge (siehe Kapitel 5.2.5) und die empirischen Dispersionskorrekturen (siehe Kapitel 5.2.6) berücksichtigt.

5.6.4 IRC-Rechnungen

Alle IRC-Rechnungen[164–167] wurden grundsätzlich in der Gasphase mit demselben Rechenmodell wie die zugehörigen Geometrieoptimierungen durchgeführt. Sie verfolgten den Reaktionspfad generell in beide Richtungen. Ausgehend von den beiden erhaltenen Strukturen wurde anschließend jeweils eine Geometrieoptimierung gestartet. Falls hierbei neue Intermediate auftraten, wurden die diese verbindenden Übergangszustände nach der in Kapitel 5.6.1 beschriebenen Vorgehensweise lokalisiert und neue IRC-Rechnungen durchgeführt, solange bis der Reaktionspfad komplettiert war.

5.7 Energien und Geometrien der berechneten Strukturen

Die Gesamtenergien aus den 'single point energy'-Rechnungen sowie die unskalierten thermischen Korrekturen aus den Frequenzrechnungen sind für alle Minima und Übergangszustände in den 'supporting informations' der Publikationen angegeben (siehe

Kapitel Struktur der Dissertation, Seite v). Alle Energien sind in Hartree aufgeführt (E_h = 627,509391 kcal / mol). Die optimierten Geometrien aller Minima und Übergangszustände sind jeweils als kartesische Koordinaten in den 'supporting informations' der Publikationen angegeben.

6 Literaturverzeichnis

[1] L. J. Goossen, C. Linder, N. Rodríguez, P. P. Lange, *Chem. – Eur. J.* **2009**, *15*, 9336–9349.

[2] G. W. V. Cave, C. L. Raston, J. L. Scott, *Chem. Commun.* **2001**, 2159–2169.

[3] A. Kirschning, W. Solodenko, K. Mennecke, *Chem. – Eur. J.* **2006**, *12*, 5972–5990.

[4] D. J. C. Constable, P. J. Dunn, J. D. Hayler, G. R. Humphrey, J. L. Leazer Jr., R. J. Linderman, K. Lorenz, J. Manley, B. A. Pearlman, A. Wells, A. Zaks, T. Y. Zhang, *Green Chem.* **2007**, *9*, 411–420.

[5] J.-C. Hierso, M. Beaupérin, P. Meunier, *Eur. J. Inorg. Chem.* **2007**, 3767–3780.

[6] A. de Meijere, *Metal-Catalyzed Cross-Coupling Reactions*, Wiley-VCH, Weinheim, **2004**.

[7] R. A. Sheldon, *Pure Appl. Chem.* **2000**, *72*, 1233–1246.

[8] H. Davy, *Philos. Trans. R. Soc. Lond.* **1817**, *107*, 77–85.

[9] H. Hartley, *Studies in the History of Chemistry*, Clarendon Press, Oxford, **1971**.

[10] W. Ostwald, *Der Werdegang Einer Wissenschaft*, Akademische Verlagsgesellschaft, **1908**.

[11] G. Rothenberg, *Catalysis: Concepts and Green Applications*, Wiley-VCH, Weinheim, **2008**.

[12] A. Behr, *Angewandte Homogene Katalyse*, Wiley-VCH, Weinheim, **2008**.

[13] G. Ertl, H. Knözinger, F. Schüth, J. Weitkamp, Eds., *Handbook of Heterogeneous Catalysis*, Wiley-VCH, Weinheim, **2008**.

[14] J. M. Thomas, *Principles and Practice of Heterogeneous Catalysis*, VCH, Weinheim, **1997**.

[15] M. Sinnott, Ed., *Comprehensive Biological Catalysis: A Mechanistic Reference*, Academic Press, San Diego, **1998**.

[16] P. Grunwald, *Biocatalysis:Biochemical Fundamentals and Applications*, ICP, **2009**.

[17] S. Roberts, *Introduction to Biocatalysis Using Enzymes and Microorganisms*, Cambridge University Press, Cambridge ; New York, **2010**.

[18] P. D. A. Behr, P. D. D. W. Agar, P. D. J. Jörissen, in *Einführ. Tech. Chem.*, Spektrum Akademischer Verlag, **2010**, pp. 155–168.

[19] W. Langenbeck, *Die Organischen Katalysatoren Und Ihre Beziehungen Zu Den Fermenten*, Springer, Berlin, **1949**.

[20] D. Steinborn, *Grundlagen der metallorganischen Komplexkatalyse*, Vieweg + Teubner, Wiesbaden, **2010**.

[21] "The Nobel Prize in Chemistry 1909". Nobelprize.org. Nobel Media AB 2014, *http://www.nobelprize.org/nobel_prizes/chemistry/laureates/1909/*, **2014**.

[22] "The Nobel Prize in Chemistry 1963". Nobelprize.org. Nobel Media AB 2014, *http://www.nobelprize.org/nobel_prizes/chemistry/laureates/1963/*, **2014**.

[23] "The Nobel Prize in Chemistry 1973". Nobelprize.org. Nobel Media AB 2014, *http://www.nobelprize.org/nobel_prizes/chemistry/laureates/1973/*, **2014**.

[24] "The Nobel Prize in Chemistry 2001". Nobelprize.org. Nobel Media AB 2014, *http://www.nobelprize.org/nobel_prizes/chemistry/laureates/2001/*, **2014**.

[25] "The Nobel Prize in Chemistry 2005". Nobelprize.org. Nobel Media AB 2014, *http://www.nobelprize.org/nobel_prizes/chemistry/laureates/2005/*, **2014**.

[26] "The Nobel Prize in Chemistry 2010". Nobelprize.org. Nobel Media AB 2014, *http://www.nobelprize.org/nobel_prizes/chemistry/laureates/2010/*, **2014**.

[27] M. Lancaster, *Green Chemistry an Introductory Text*, Royal Society Of Chemistry, Cambridge, **2002**.
[28] I. Chorkendorff, *Concepts of Modern Catalysis and Kinetics*, Wiley-VCH, Weinheim, **2007**.
[29] F. Schüth, *Chem. Unserer Zeit* **2006**, *40*, 92–103.
[30] Acmite Market Intelligence, *Market Report: Global Catalyst Market*, **2011**.
[31] R. Dittmmeyer, K. Winnacker, *Methodische Grundlagen*, Wiley-VCH, Weinheim, **2004**.
[32] L. Lloyd, *Handbook of Industrial Catalysts*, Springer, New York, **2007**.
[33] J. J. Spivey, Y.-F. Han, K. M. Dooley, Eds., *Catalysis*, Royal Society Of Chemistry, Cambridge, **2013**.
[34] B. Cornils, W. A. Herrmann, C.-H. Wong, H.-W. Zanthoff, Eds., *Catalysis from A to Z: A Concise Encyclopedia*, Wiley-VCH, Weinheim, **2013**.
[35] E. Negishi, A. de Meijere, Eds., *Handbook of Organopalladium Chemistry for Organic Synthesis*, Wiley-Interscience, New York, **2002**.
[36] L. S. Hegedus, *Transition Metals in the Synthesis of Complex Organic Molecules*, University Science Books, Sausalito, CA, **2010**.
[37] M. Beller, C. Bolm, Eds., *Transition Metals for Organic Synthesis: Building Blocks and Fine Chemicals*, Wiley-VCH, Weinheim, **2004**.
[38] President's Information Technology Advisory Committee, *Computational Science: Ensuring America's Competitiveness*, Arlington, VA, **2005**.
[39] H. Eyring, *J. Chem. Phys.* **1935**, *3*, 107–115.
[40] C. Amatore, A. Jutand, *J. Organomet. Chem.* **1999**, *576*, 254–278.
[41] S. Kozuch, S. Shaik, *Acc. Chem. Res.* **2011**, *44*, 101–110.
[42] L. J. Goossen, D. Koley, H. L. Hermann, W. Thiel, *J. Am. Chem. Soc.* **2005**, *127*, 11102–11114.
[43] L. J. Goossen, D. Koley, H. L. Hermann, W. Thiel, *Organometallics* **2006**, *25*, 54–67.
[44] K. Nagayama, F. Kawataka, M. Sakamoto, I. Shimizu, A. Yamamoto, *Chem. Lett.* **1995**, *24*, 367–368.
[45] R. Kakino, H. Narahashi, I. Shimizu, A. Yamamoto, *Bull. Chem. Soc. Jpn.* **2002**, *75*, 1333–1345.
[46] A. S. Dudnik, Y. Xia, Y. Li, V. Gevorgyan, *J. Am. Chem. Soc.* **2010**, *132*, 7645–7655.
[47] G. Mpourmpakis, D. G. Vlachos, *MRS Bull.* **2011**, *36*, 211–215.
[48] L. J. Gooßen, N. Rodríguez, K. Gooßen, *Angew. Chem.* **2008**, *120*, 3144–3164.
[49] L. J. Gooßen, N. Rodríguez, K. Gooßen, *Angew. Chem. Int. Ed.* **2008**, *47*, 3100–3120.
[50] L. J. Gooßen, K. Gooßen, N. Rodríguez, M. Blanchot, C. Linder, B. Zimmermann, *Pure Appl. Chem.* **2009**, *80*, 1725–1733.
[51] L. J. Goossen, F. Collet, K. Goossen, *Isr. J. Chem.* **2010**, *50*, 617–629.
[52] N. Rodríguez, L. J. Goossen, *Chem. Soc. Rev.* **2011**, *40*, 5030–5048.
[53] W. I. Dzik, P. P. Lange, L. J. Gooßen, *Chem. Sci.* **2012**, *3*, 2671–2678.
[54] L. J. Gooßen, G. Deng, L. M. Levy, *Science* **2006**, *313*, 662–664.
[55] L. J. Goossen, N. Rodríguez, B. Melzer, C. Linder, G. Deng, L. M. Levy, *J. Am. Chem. Soc.* **2007**, *129*, 4824–4833.
[56] L. J. Gooßen, W. R. Thiel, N. Rodríguez, C. Linder, B. Melzer, *Adv. Synth. Catal.* **2007**, *349*, 2241–2246.
[57] A. Fromm, *Rationale Entwicklung Eines Decarboxylierungskatalysators*, Technische Universität Kaiserslautern, **2008**.
[58] L. J. Gooßen, P. P. Lange, N. Rodríguez, C. Linder, *Chem. – Eur. J.* **2010**, *16*, 3906–3909.

[59] S. Dupuy, F. Lazreg, A. M. Z. Slawin, C. S. J. Cazin, S. P. Nolan, *Chem. Commun.* **2011**, *47*, 5455–5457.
[60] S. Dupuy, S. P. Nolan, *Chem. – Eur. J.* **2013**, *19*, 14034–14038.
[61] L. J. Goossen, F. Manjolinho, B. A. Khan, N. Rodríguez, *J. Org. Chem.* **2009**, *74*, 2620–2623.
[62] L. J. Gooßen, F. Rudolphi, C. Oppel, N. Rodríguez, *Angew. Chem.* **2008**, *120*, 3085–3088.
[63] L. J. Gooßen, F. Rudolphi, C. Oppel, N. Rodríguez, *Angew. Chem. Int. Ed.* **2008**, *47*, 3043–3045.
[64] L. J. Gooßen, B. Zimmermann, T. Knauber, *Angew. Chem.* **2008**, *120*, 7211–7214.
[65] L. J. Gooßen, B. Zimmermann, T. Knauber, *Angew. Chem. Int. Ed.* **2008**, *47*, 7103–7106.
[66] L. J. Goossen, N. Rodríguez, C. Linder, *J. Am. Chem. Soc.* **2008**, *130*, 15248–15249.
[67] L. J. Gooßen, C. Linder, *Unveröffentlichte Ergebnisse*, Technische Universität Kaiserslautern, **2009**.
[68] D. Hackenberger, *Bimetallisch-Katalysierte Decarboxylierende Kreuzkupplung Mit Bidentaten Liganden*, Technische Universität Kaiserslautern, **2013**.
[69] B. Song, T. Knauber, L. J. Gooßen, *Angew. Chem.* **2013**, *125*, 3026–3030.
[70] B. Song, T. Knauber, L. J. Gooßen, *Angew. Chem. Int. Ed.* **2013**, *52*, 2954–2958.
[71] D. Hackenberger, B. Song, M. F. Grünberg, S. Farsadpour, L. Taghizadeh Ghoochany, F. Menges, H. Kelm, L. Burkhardt, G. Niedner-Schatteburg, W. R. Thiel, L. J. Gooßen, *Manuskript in Vorbereitung*, **2014**.
[72] J. Tang, L. J. Gooßen, *Org. Lett.* **2014**, *16*, 2664–2667.
[73] L. Yet, *Chem. Rev.* **2003**, *103*, 4283–4306.
[74] Y. Sugie, K. A. Dekker, H. Hirai, T. Ichiba, M. Ishiguro, Y. Shioni, A. Sugiura, L. Brennan, J. Duignan, L. H. Huang, J. Sutcliffe, Y. Kojima, *J. Antibiot. (Tokyo)* **2001**, *54*, 1060–1065.
[75] D. Davyt, W. Entz, R. Fernandez, R. Mariezcurrena, A. W. Mombrú, J. Saldaña, L. Domínguez, J. Coll, E. Manta, *J. Nat. Prod.* **1998**, *61*, 1560–1563.
[76] J. P. Vidal, R. Escale, J. P. Girard, J. C. Rossi, J. M. Chantraine, A. Aumelas, *J. Org. Chem.* **1992**, *57*, 5857–5860.
[77] K. L. Erickson, J. A. Beutler, J. H. Cardellina, M. R. Boyd, *J. Org. Chem.* **1997**, *62*, 8188–8192.
[78] R. Jansen, P. Washausen, B. Kunze, H. Reichenbach, G. Höfle, *Eur. J. Org. Chem.* **1999**, *5*, 1085–1089.
[79] L. A. McDonald, J. C. Swersey, C. M. Ireland, A. R. Carroll, J. C. Coll, B. F. Bowden, C. R. Fairchild, L. Cornell, *Tetrahedron* **1995**, *51*, 5237–5244.
[80] M. R. Boyd, C. Farina, P. Belfiore, S. Gagliardi, J. W. Kim, Y. Hayakawa, J. A. Beutler, T. C. McKee, B. J. Bowman, E. J. Bowman, *J. Pharmacol. Exp. Ther.* **2001**, *297*, 114–120.
[81] D. R. Carbery, *Org. Biomol. Chem.* **2008**, *6*, 3455.
[82] P. J. Stevenson, I. Graham, *ARKIVOC* **2003**, *7*, 139–144.
[83] C. Gaulon, R. Dhal, T. Chapin, V. Maisonneuve, G. Dujardin, *J. Org. Chem.* **2004**, *69*, 4192–4202.
[84] G. J. Roff, R. C. Lloyd, N. J. Turner, *J. Am. Chem. Soc.* **2004**, *126*, 4098–4099.
[85] C. E. Willans, J. M. C. A. Mulders, J. G. de Vries, A. H. M. de Vries, *J. Organomet. Chem.* **2003**, *687*, 494–497.
[86] R. Matsubara, Y. Nakamura, S. Kobayashi, *Angew. Chem.* **2004**, *116*, 1711–1713.

[87] R. Matsubara, Y. Nakamura, S. Kobayashi, *Angew. Chem. Int. Ed.* **2004**, *43*, 1679–1681.
[88] M. van den Berg, A. J. Minnaard, R. M. Haak, M. Leeman, E. P. Schudde, A. Meetsma, B. L. Feringa, A. H. M. de Vries, C. E. P. Maljaars, C. E. Willans, D. Hyett, J. A. F. Boogers, H. J. W. Henderickx, J. G. de Vries, *Adv. Synth. Catal.* **2003**, *345*, 308–323.
[89] H.-U. Blaser, C. Malan, B. Pugin, F. Spindler, H. Steiner, M. Studer, *Adv. Synth. Catal.* **2003**, *345*, 103–151.
[90] B. Maity, L. J. Gooßen, D. Koley, *Chem. Sci.* **2014**, *Manuskript akzeptiert*.
[91] L. Huang, M. Arndt, K. Gooßen, H. Heydt, L. J. Gooßen, *Chem. Soc. Rev.* **2014**, *Manuskript akzeptiert*.
[92] A. Yanagisawa, Y. Matsumoto, K. Asakawa, H. Yamamoto, *J. Am. Chem. Soc.* **1999**, *121*, 892–893.
[93] N. Isambert, M. Cruz, M. J. Arévalo, E. Gómez, R. Lavilla, *Org. Lett.* **2007**, *9*, 4199–4202.
[94] W. Tang, X. Zhang, *Chem. Rev.* **2003**, *103*, 3029–3070.
[95] A. J. Minnaard, B. L. Feringa, L. Lefort, J. G. de Vries, *Acc. Chem. Res.* **2007**, *40*, 1267–1277.
[96] G. Erre, S. Enthaler, K. Junge, S. Gladiali, M. Beller, *Coord. Chem. Rev.* **2008**, *252*, 471–491.
[97] H. Urabe, D. Suzuki, M. Sasaki, F. Sato, *J. Am. Chem. Soc.* **2003**, *125*, 4036–4037.
[98] A. Basso, L. Banfi, A. Galatini, G. Guanti, F. Rastrelli, R. Riva, *Org. Lett.* **2009**, *11*, 4068–4071.
[99] T. Széll, *J. Chem. Soc. C Org.* **1967**, 2041–2044.
[100] B. M. Trost, S. Malhotra, T. Mino, N. S. Rajapaksa, *Chem. – Eur. J.* **2008**, *14*, 7648–7657.
[101] L. Keinicke, P. Fristrup, P.-O. Norrby, R. Madsen, *J. Am. Chem. Soc.* **2005**, *127*, 15756–15761.
[102] M. Lombardo, S. Morganti, C. Trombini, *J. Org. Chem.* **2003**, *68*, 997–1006.
[103] M. Liu, X.-W. Sun, M.-H. Xu, G.-Q. Lin, *Chem. – Eur. J.* **2009**, *15*, 10217–10224.
[104] N. Kuźnik, S. Krompiec, *Coord. Chem. Rev.* **2007**, *251*, 222–233.
[105] V. Durà-Vilà, D. M. P. Mingos, R. Vilar, A. J. P. White, D. J. Williams, *J. Organomet. Chem.* **2000**, *600*, 198–205.
[106] V. Durà-Vilà, D. M. P. Mingos, R. Vilar, A. J. P. White, D. J. Williams, *Chem. Commun.* **2000**, 1525–1526.
[107] F. Barrios-Landeros, B. P. Carrow, J. F. Hartwig, *J. Am. Chem. Soc.* **2008**, *130*, 5842–5843.
[108] J. F. Harrod, A. J. Chalk, *J. Am. Chem. Soc.* **1966**, *88*, 3491–3497.
[109] C. P. Casey, C. R. Cyr, *J. Am. Chem. Soc.* **1973**, *95*, 2248–2253.
[110] D. B. Grotjahn, C. R. Larsen, J. L. Gustafson, R. Nair, A. Sharma, *J. Am. Chem. Soc.* **2007**, *129*, 9592–9593.
[111] F. R. Hartley, *Chem. Rev.* **1969**, *69*, 799–844.
[112] M. T. Reetz, L. J. Goossen, A. Meiswinkel, J. Paetzold, J. F. Jensen, *Org. Lett.* **2003**, *5*, 3099–3101.
[113] P. Mamone, *Nachhaltige Katalytische Transformationen von Carbonsäuren Und Ihren Derivaten*, Technische Universität Kaiserslautern, **2014**.
[114] D. M. Ohlmann, N. Tschauder, J.-P. Stockis, K. Gooßen, M. Dierker, L. J. Gooßen, *J. Am. Chem. Soc.* **2012**, *134*, 13716–13729.
[115] S. Baader, D. M. Ohlmann, L. J. Gooßen, *Chem. – Eur. J.* **2013**, *19*, 9807–9810.

[116] S. Baader, P. E. Podsiadly, D. J. Cole-Hamilton, L. J. Goossen, *Green Chem.* **2014**, DOI 10.1039/C4GC01269K.
[117] F. Proutiere, M. Aufiero, F. Schoenebeck, *J. Am. Chem. Soc.* **2012**, *134*, 606–612.
[118] M. Aufiero, F. Proutiere, F. Schoenebeck, *Angew. Chem. Int. Ed.* **2012**, *51*, 7226–7230.
[119] K. J. Bonney, F. Proutiere, F. Schoenebeck, *Chem. Sci.* **2013**, *4*, 4434–4439.
[120] I. Kalvet, K. J. Bonney, F. Schoenebeck, *J. Org. Chem.* **2014**, DOI 10.1021/jo501889j.
[121] K. J. Bonney, F. Schoenebeck, *Chem. Soc. Rev.* **2014**, *43*, 6609.
[122] P. Hohenberg, W. Kohn, *Phys. Rev.* **1964**, *136*, B864–B871.
[123] W. Kohn, L. J. Sham, *Phys. Rev.* **1965**, *140*, A1133–A1138.
[124] W. Kohn, A. D. Becke, R. G. Parr, *J. Phys. Chem.* **1996**, *100*, 12974–12980.
[125] E. J. Baerends, O. V. Gritsenko, *J. Phys. Chem. A* **1997**, *101*, 5383–5403.
[126] R. Stowasser, R. Hoffmann, *J. Am. Chem. Soc.* **1999**, *121*, 3414–3420.
[127] E. J. Baerends, *Theor. Chem. Acc.* **2000**, *103*, 265–269.
[128] S. H. Vosko, L. Wilk, M. Nusair, *Can. J. Phys.* **1980**, *58*, 1200–1211.
[129] A. D. Becke, *J. Chem. Phys.* **1986**, *84*, 4524–4529.
[130] C. Lee, W. Yang, R. G. Parr, *Phys. Rev. B* **1988**, *37*, 785–789.
[131] W. Koch, M. C. Holthausen, *A Chemist's Guide to Density Functional Theory*, Wiley-VCH, Weinheim, **2001**.
[132] A. D. Becke, *J. Chem. Phys.* **1993**, *98*, 5648–5652.
[133] P. J. Stephens, F. J. Devlin, C. F. Chabalowski, M. J. Frisch, *J. Phys. Chem.* **1994**, *98*, 11623–11627.
[134] J. B. Foresman, Ae. Frisch, *Exploring Chemistry with Electronic Structure Methods*, Gaussian, Inc., Pittsburgh, PA, **1996**.
[135] A. D. Becke, *Phys. Rev. A* **1988**, *38*, 3098–3100.
[136] K. Raghavachari, *Theor. Chim. Acta* **2000**, *103*, 361–363.
[137] R. Ditchfield, *J. Chem. Phys.* **1971**, *54*, 724.
[138] W. J. Hehre, *J. Chem. Phys.* **1972**, *56*, 2257.
[139] P. C. Hariharan, J. A. Pople, *Theor. Chim. Acta* **1973**, *28*, 213–222.
[140] V. A. Rassolov, J. A. Pople, M. A. Ratner, T. L. Windus, *J. Chem. Phys.* **1998**, *109*, 1223.
[141] R. C. Binning, L. A. Curtiss, *J. Comput. Chem.* **1990**, *11*, 1206–1216.
[142] T. H. Dunning, *J. Chem. Phys.* **1977**, *66*, 1382.
[143] T. Clark, J. Chandrasekhar, G. W. Spitznagel, P. v. R. Schleyer, *J. Comput. Chem.* **1983**, *4*, 294–301.
[144] G. W. Spitznagel, T. Clark, P. v. R. Schleyer, W. J. Hehre, *J. Comput. Chem.* **1987**, *8*, 1109–1116.
[145] M. Dolg, U. Wedig, H. Stoll, H. Preuss, *J. Chem. Phys.* **1987**, *86*, 866.
[146] D. Andrae, U. Häußermann, M. Dolg, H. Stoll, H. Preuß, *Theor. Chim. Acta* **1990**, *77*, 123–141.
[147] L. A. Curtiss, K. Raghavachari, G. W. Trucks, J. A. Pople, *J. Chem. Phys.* **1991**, *94*, 7221.
[148] R. Krishnan, J. S. Binkley, R. Seeger, J. A. Pople, *J. Chem. Phys.* **1980**, *72*, 650–654.
[149] L. A. Curtiss, M. P. McGrath, J.-P. Blaudeau, N. E. Davis, R. C. Binning Jr., L. Radom, *J. Chem. Phys.* **1995**, *103*, 6104–6113.
[150] J.-P. Blaudeau, M. P. McGrath, L. A. Curtiss, L. Radom, *J. Chem. Phys.* **1997**, *107*, 5016–5021.
[151] F. Weigend, R. Ahlrichs, *Phys. Chem. Chem. Phys.* **2005**, *7*, 3297–3305.

[152] M. W. Wong, *Chem. Phys. Lett.* **1996**, *256*, 391–399.
[153] A. P. Scott, L. Radom, *J. Phys. Chem.* **1996**, *100*, 16502–16513.
[154] G. Rauhut, P. Pulay, *J. Phys. Chem.* **1995**, *99*, 3093–3100.
[155] C. W. Bauschlicher Jr., H. Partridge, *J. Chem. Phys.* **1995**, *103*, 1788–1791.
[156] J. Jaramillo, G. E. Scuseria, *Chem. Phys. Lett.* **1999**, *312*, 269–276.
[157] A. Klamt, G. Schüürmann, *J. Chem. Soc. Perkin Trans. 2* **1993**, 799–805.
[158] A. Schäfer, A. Klamt, D. Sattel, J. C. W. Lohrenz, F. Eckert, *Phys. Chem. Chem. Phys.* **2000**, *2*, 2187–2193.
[159] V. Barone, M. Cossi, *J. Phys. Chem. A* **1998**, *102*, 1995–2001.
[160] M. Cossi, N. Rega, G. Scalmani, V. Barone, *J. Comput. Chem.* **2003**, *24*, 669–681.
[161] F. Murrieta-Guevara, A. Romero-Martinez, A. Trejo, *Fluid Phase Equilibria* **1988**, *44*, 105–115.
[162] E. R. Johnson, I. D. Mackie, G. A. DiLabio, *J. Phys. Org. Chem.* **2009**, *22*, 1127–1135.
[163] S. Grimme, J. Antony, S. Ehrlich, H. Krieg, *J. Chem. Phys.* **2010**, *132*, 154104.
[164] K. Fukui, *Acc. Chem. Res.* **1981**, *14*, 363–368.
[165] H. P. Hratchian, H. B. Schlegel, *Theory and Applications of Computational Chemistry: The First Forty Years*, Elsevier Science Ltd, Amsterdam ; Boston, **2005**.
[166] H. P. Hratchian, H. B. Schlegel, *J. Chem. Phys.* **2004**, *120*, 9918–9924.
[167] H. P. Hratchian, H. B. Schlegel, *J. Chem. Theory Comput.* **2005**, *1*, 61–69.
[168] M. J. Frisch, G. W. Trucks, H. B. Schlegel, G. E. Scuseria, M. A. Robb, J. R. Cheeseman, J. A. Montgomery, Jr., T. Vreven, K. N. Kudin, J. C. Burant, J. M. Millam, S. S. Iyengar, J. Tomasi, V. Barone, B. Mennucci, M. Cossi, G. Scalmani, N. Rega, G. A. Petersson, H. Nakatsuji, M. Hada, M. Ehara, K. Toyota, R. Fukuda, J. Hasegawa, M. Ishida, T. Nakajima, Y. Honda, O. Kitao, H. Nakai, M. Klene, X. Li, J. E. Knox, H. P. Hratchian, J. B. Cross, V. Bakken, C. Adamo, J. Jaramillo, R. Gomperts, R. E. Stratmann, O. Yazyev, A. J. Austin, R. Cammi, C. Pomelli, J. W. Ochterski, P. Y. Ayala, K. Morokuma, G. A. Voth, P. Salvador, J. J. Dannenberg, V. G. Zakrzewski, S. Dapprich, A. D. Daniels, M. C. Strain, O. Farkas, D. K. Malick, A. D. Rabuck, K. Raghavachari, J. B. Foresman, J. V. Ortiz, Q. Cui, A. G. Baboul, S. Clifford, J. Cioslowski, B. B. Stefanov, G. Liu, A. Liashenko, P. Piskorz, I. Komaromi, R. L. Martin, D. J. Fox, T. Keith, M. A. Al-Laham, C. Y. Peng, A. Nanayakkara, M. Challacombe, P. M. W. Gill, B. Johnson, W. Chen, M. W. Wong, C. Gonzalez, J. A. Pople, *Gaussian 03, Revision E.01*, Gaussian, Inc., Wallingford CT, **2003**.
[169] M. J. Frisch, G. W. Trucks, H. B. Schlegel, G. E. Scuseria, M. A. Robb, J. R. Cheeseman, G. Scalmani, V. Barone, B. Mennucci, G. A. Petersson, H. Nakatsuji, M. Caricato, X. Li, H. P. Hratchian, A. F. Izmaylov, J. Bloino, G. Zheng, J. L. Sonnenberg, M. Hada, M. Ehara, K. Toyota, R. Fukuda, J. Hasegawa, M. Ishida, T. Nakajima, Y. Honda, O. Kitao, H. Nakai, T. Vreven, J. A. Montgomery, Jr., J. E. Peralta, F. Ogliaro, M. Bearpark, J. J. Heyd, E. Brothers, K. N. Kudin, V. N. Staroverov, R. Kobayashi, J. Normand, K. Raghavachari, A. Rendell, J. C. Burant, S. S. Iyengar, J. Tomasi, M. Cossi, N. Rega, J. M. Millam, M. Klene, J. E. Knox, J. B. Cross, V. Bakken, C. Adamo, J. Jaramillo, R. Gomperts, R. E. Stratmann, O. Yazyev, A. J. Austin, R. Cammi, C. Pomelli, J. W. Ochterski, R. L. Martin, K. Morokuma, V. G. Zakrzewski, G. A. Voth, P. Salvador, J. J. Dannenberg, S. Dapprich, A. D. Daniels, Ö. Farkas, J. B. Foresman, J. V. Ortiz, J. Cioslowski, D. J. Fox, *Gaussian 09, Revision D.01*, Gaussian, Inc., Wallingford CT, **2009**.
[170] G. Schaftenaar, J. H. Noordik, *J. Comput.-Aided Mol. Design* **2000**, *14*, 123–134.

[171] R. Dennington, T. Keith, J. Millam, *GaussView, Version 5*, Semichem Inc., Shawnee Mission, KS, **2009**.
[172] C. Peng, H. B. Schlegel, *Isr. J. Chem.* **1993**, *33*, 449–454.
[173] C. Peng, P. Y. Ayala, H. B. Schlegel, M. J. Frisch, *J. Comput. Chem.* **1996**, *17*, 49–56.

Lebenslauf

Persönliche Daten

Name	Andreas Fromm

Hochschulstudium und Promotion

Seit 07.2008	Promotion an der TU Kaiserslautern am Fachbereich Chemie in der Arbeitsgruppe von Prof. Dr. Lukas J. Gooßen
10.2001 – 05.2008	Studium der Chemie an der TU Kaiserslautern, Abschluss: Diplom in Chemie
03.2005 – 05.2005	Forschungspraktikum in organischer Chemie an der University of Edinburgh

Schulausbildung und Zivildienst

09.2000 – 07.2001	Zivildienst beim Landesamt für Umweltschutz in Saarbrücken
1991 – 2000	Gymnasium am Schloss, Saarbrücken, Abschluss: Abitur

Auszeichnungen und Stipendien

10.2009 – 09.2011	Promotionsstipendium des Landes Rheinland-Pfalz
03.2005 – 05.2005	Sokrates/Erasmus-Stipendium zum Auslandsaufenthalt in Edinburgh
2004	Förderpreis der Firma Procter & Gamble und Preis des Verlags Wiley-VCH für das beste Vordiplom in Chemie
10.2001 – 09.2002	Anfängerstipendium der Förderungsabteilung der TU Kaiserslautern, gestiftet vom 1. FC Kaiserslautern
2000	Buchpreis des Fonds der Chemischen Industrie (VCI) als bester Abiturient im Fach Chemie